NASA Conference Publication 10008

1987 Ground Vortex Workshop

Proceedings of a Meeting
held at NASA Ames Research Center
Moffett Field, California
April 22-23, 1987

NASA

NASA Conference Publication 10008

1987 Ground Vortex Workshop

Edited by
Richard J. Margason
NASA Ames Research Center
Moffett Field, California

Proceedings of a Meeting
held at NASA Ames Research Center
Moffett Field, California
April 22-23, 1987

National Aeronautics and
Space Administration

Ames Research Center
Moffett Field, California 94035
1988

INTRODUCTION

A Ground Vortex Workshop was held at NASA Ames Research Center on April 22-23, 1987, and was sponsored by the Center's Powered-Lift Group of the Fixed Wing Aerodynamics Branch.

The purpose of the workshop was to discuss the current understanding of the ground vortex phenomena and their effects on aircraft, and to establish directions for further research on advanced, high-performance aircraft designs, particularly those concepts utilizing powered-lift systems; e.g., V/STOL, ASTOVL, and STOL aircraft. A total of 9 papers covering a survey of early work on the ground vortex, recent experimental and theoretical studies, and the effect of the ground vortex flow field on the aircraft were presented on the first day. This publication presents 8 of the 9 papers given at the workshop. These papers are printed from photo-ready originals supplied by the authors, who are responsible for the content and the technical accuracy of their respective papers.

A panel discussion was held on the morning of the second day to summarize the papers presented and to discuss the direction that future work should take. A synopsis of that discussion is presented at the end of this publication.

NASA AMES RESEARCH CENTER
GROUND VORTEX RESEARCH WORKSHOP
SPACE SCIENCES AUDITORIUM
APRIL 22-23, 1987

PROGRAM

WEDNESDAY - APRIL 22, 1987

9:00	**WELCOME:**	C. Thomas Snyder Director of Aerospace Systems
9:15	**OVERVIEW:**	L. Kerry Mitchell Fixed Wing Aerodynamics Branch
9:30	The Characteristics of the Ground Vortex and its Effects on the Aerodynamics of the STOL Configuration	Stewart (Consultant)
10:00	Summary of an Experimental Investigation of the Ground Vortex	Billet (Pennsylvania State University)
10:30	**BREAK**	
10:45	Ground Vortex Flowfield Investigation	Kuhn (Consultant) Del Frate (NASA Ames-Dryden Flight Research Facility) Eshleman (Lockheed California Company)
11:15	F-15 SMTD Low Speed Jet Effects: Wind Tunnel Tests Results	Blake (U.S. Air Force Wright Aeronautical Laboratory)
11:45	**LUNCH**	
1.00	An Assessment of Ground Effects Determined by Static and Dynamic Testing Techniques	Paulson (NASA Langley Research Center)
1:30	The Effect of a Ground Vortex on the Aerodynamics of an Airfoil	Krothapalli (Florida State University)
2:00	**BREAK**	
2:15	Noise of the Harrier in Vertical Landing and Takeoff	Soderman (NASA Ames Research Center) Foster (NASA Ames Research Center)

2:45	Numerical Investigation of a Jet in Ground Effect Using the Fortified Navier Stokes Scheme	Van Dalsem (NASA Ames Research Center) Steger (NASA Ames Research Center)
3:15	Unsteady Three-Dimensional Simulations of a VTOL Upwash Fountain (oral presentation only)	Childs (Nielsen Engineering and Research) Nixon (Nielsen Engineering and Research)

3:45 **ADJOURN**

THURSDAY - APRIL 23, 1987

9:00 Panel discussion, moderated by Richard J. Margason (Fixed Wing Aerodynamics Branch)

Panel Members
- Vearl R. Stewart (Consultant)
- Michael L. Billet (Pennsylvania State University)
- Richard E. Kuhn (Consultant)
- William B. Blake (U.S. Air Force Wright Aeronautical Laboratory)
- John W. Paulson (NASA Langley Research Center)
- A. Krothapalli (Florida State University)
- Paul T. Soderman (NASA Ames Research Center)
- William R. Van Dalsem (NASA Ames Research Center)
- Robert Childs (Nielson Engineering and Research)

11:30 **LUNCH**

CONTENTS

THE CHARACTERISTICS OF THE GROUND VORTEX AND ITS EFFECT ON THE AERODYNAMICS OF THE STOL CONFIGURATION

V. R. Stewart

ABSTRACT

The interaction of the free stream velocity on the wall jet formed by the impingement of deflected engine thrust results in a rolled up vortex which exerts sizable forces on a STOL airplane configuration. Some data suggests that the boundary layer under the free stream ahead of the configuration may be important in determining the extent of travel of the wall jet into the oncoming stream. This paper examines and discusses the early studies of the ground vortex and compares those results to some later data obtained with a moving model over a fixed ground board. The effect of the ground vortex on the aerodynamic characteristics is also discussed.

SYMBOLS

BP	Butt Plane
C_L	Lift Coefficient Lift/$q_0 S$
C_p	Pressure Coefficient $\Delta P/q_0 S$
C_μ	Blowing Coefficient $\dot{M}V_j/qS$
d	Nozzle diameter
e_x	Longitudinal distance between jet centerlines
e_y	Lateral distance between jet centerlines
h	Height above ground
$\dot{M}$	Jet mass flow
q_n	Jet dynamic pressure
q_0	Freestream dynamic pressure
S	Reference area
V_e	Equivalent velocity V_∞/V_j
V_j	Jet velocity
V_∞	Freestream velocity
x	Longitudinal distance
x'	Forward extent of ground vortex
y	Lateral distance
z	Vertical distance
$(W/\ell)_j$	Jet aspect ratio
ΔP	Local pressure - ambient pressure
δ	Jet deflection

INTRODUCTION

When a high velocity jet impinges on the ground the jet will form a wall jet. This wall jet will flow along the ground until it is stopped by some outside force. This force may be a second jet, in which case the two wall jets will be deflected off the ground and upward onto the airplane creating a fountain effect. The outside force may be only the ground friction, as in the case of a single jet with no free stream velocity. The wall jet continues along the ground until the forward energy is dissipated by friction.

The third case and the one which is of interest here is that case in which the jet is exhausted from a moving vehicle and impinges on the ground, splits into a wall jet, and spreads along the ground. A portion of the wall jet flows in the same direction as the free stream velocity and, thereby, behaves similar to the single jet without free stream case. The remainder of the jet flows forward into the oncoming free stream and interacts with the free stream to form the ground vortex. It is this portion of the jet and the interaction with the free stream which can result in very sizable suckdown loads and moments on a STOL airplane configuration. The forward extent of the wall jet into the free stream air flow can be related to the relative velocities of the two interacting airstreams. The forward extent will also depend on the angle at which the jet strikes the ground and the height at which the jet is exhausted toward the ground. The angle at which the jet is directed in reality determines the amount of the flow along any ground path. A jet directed aft of the vertical will allow most of the flow to propagate away from the oncoming air while a jet directed into the free stream, such as a thrust reverser, will direct more of the energy into the path of the oncoming stream. Most of the existing data are for the vertical jet condition and, therefore, most of this paper will deal with this condition. A simple expression to account for the angle relationship has been developed and will be discussed.

DISCUSSION

Ground Vortex Formation and Characteristics: The ground vortex is created by that portion of the wall jet which is opposed by the free stream velocity. As seen in Figure 1, the forward portion of the wall jet is rolled into a type of vortex and is directed back onto the wall jet. In truth, this flow is not a real vortex, but rather, a redirection of the flow direction, at least in the single jet configuration as pictured. A jet flap configuration, with a large span nozzle tends to form a rear boundary to the vortex and to result in a more concentrated vortex. With an axisymmetric, round nozzle and jet the vortex is not bound at the rear and is allowed to flow away from the airplane with the free stream. As demonstrated in Figure 1, a vertical (90 degree) jet is directed from the vehicle toward the ground. The jet impacts the ground and a radial wall jet is formed. The wall jet portion which is directed into the

free stream is retarded and rolled back forming the ground vortex. The reversed flow then moves with or parallel to the free stream. This flow field wills create negative pressures on the ground and on the underside of the vehicle.

A typical jet centerline pressure distribution is presented in Figure 2. The figure shows a jet at a height less than the critical height above which a vortex would not be formed. The jet from the nozzle will begin to curve into the free stream flow direction and would impact the ground at an angle slightly less than the initial jet angle depending on the height of the nozzle. The jet upon impact will form a radial wall jet as as shown in Figure 1 and flow along the ground. That portion of the wall jet directed into the oncoming airstream will form the ground vortex. The ground pressure distribution is also depicted in Figure 2. A positive pressure is seen on the ground at the point of impact and a negative ground pressure is seen in the area influenced by the ground vortex. This negative pressure will, at least at the lower heights, be reflected onto the lower surface of the airplane configuration directly above the vortex. As seen in the figure the negative pressure region attains maximum negative value at some distance ahead of the impact point and then the negative pressure decreases and, in fact, becomes slightly greater than local static pressure at some point ahead of the vortex. The point of zero delta static pressure has been established as depicting the forward edge of the vortex flow field. This zero pressure point is used in the correlations.

A third important characteristic of the ground vortex is seen in Figure 3. The radial wall jet extends into the free stream a distance related to the energy of the wall jet in that direction. The forward component of energy is reduced as the radial angle moves away from the directly ahead. The shape of the ground vortex is therefore seen as a curved or a horseshoe shaped profile. Figure 3 shows that for these particular conditions, the centerline vortex extends 2.5 nozzle diameters ahead of the nozzle while at a lateral position of three diameters away from the nozzle the forward extent of the vortex is only about one half of a diameter ahead oh the nozzle centerline. The implications of the curved vortex leading edge are significant. The most significant are the asymmetric loads induced on an airplane wings under certain yawed conditions. Since the vortex profile is seen to be symmetric about the free stream centerline, yawing of the vehicle can result in one wing in the influence of the vortex flow field while the opposite wing is forward of the that influence. This condition where one wing is in the influence of the vortex while the other is relatively unaffected can result in large rolling moments into the yawed wing.

Review of Early Data Base: There are several early studies which have investigated the extent and characteristics of the ground vortex. Many of these were done to investigate the effects of the ground flow on the dust and debris and reingestion characteristics due to the vortex. Unfortunately, the early data

base as well as some of the later data did not utilize sufficient instrumentation to link the vortex to the aerodynamic lift losses. The studies of the ground vortex tend to be limited to flow field measurements and the aerodynamic tests tend not to properly define the ground vortex. References 1 through 4 fall in the first category. These experimental studies explored the ground vortex formation and investigated the forward travel of the vortex leading edge and all four dealt with with round jets exhausting toward a fixed ground board. The test configurations primarily dealt with isolated jets. Reference 1, Colin and Olivari, investigated the effect of a single vertical jet exhausting at four nozzle diameters above a fixed ground board. Ground board pressure distributions were recorded. Figure 4 presents the ground board pressures in the region of the vortex. These data were obtained at very low nozzle pressure ratios, approximately 1.05, and with a jet velocity of about 265 feet per second. A vortex penetration of approximately 8.5 nozzle diameters is shown at a velocity ratio of 0.10. The data indicate a maximum negative pressure coefficient of approximately -1.7 on the ground at all velocity ratios.

Reference 2, by Abbott, represents a different test technique. Abbott utilized a moving model over a fixed ground board. Abbott's moving model was at the end of a rotating arm and data consisted of photographs of the dust cloud. Abbott's results indicated considerably less forward travel of the ground vortex compared to other tests with a fixed model and fixed ground board, References 3 and 4 offer other measurements of a fixed model over a fixed board and are based on ground pressure instrumentation as was Colin and Olivari. These data present extremes in ground boundary layers. Schwantes, Reference 3, simulated a wind over the ground and produced a thick ground boundary layer, while, Weber and Gay in Reference 4 appeared to utilize a relatively short ground board which would limit the boundary layer thickness. Figure 5 presents a comparison of the ground vortex forward penetration from these references. The penetration from the moving model data is approximately 30 percent less than that shown from References 1 and 3 while the short ground board data from Reference 4 is seen to be between the the data from References 1 and 3 and that of Reference 2.

The data presented in Reference 5 and extensively summarized in Reference 6 and to a lessor extent in References 7 and 8 was obtained from a wind tunnel test of a generic, deflected thrust STOL model configuration. This test provided the first data to investigate the vortex characteristics and relate these to the model loads. The model, shown in Figure 6, was tested with a fixed ground board at varying heights from very near the ground, one nozzle height to free air. The model utilized several nozzle configurations and provided comparisons for an isolated nozzle and a nozzle in presence to a blocking plate and a lifting airplane wing. Nozzle configurations consisting of round and rectangular with aspect ratios of 4 and .25 were tested. Single and multiple nozzle configurations were also tested. Instrumentation included ground board pressures and a model

force balance. From these data it is possible to determine the height at which the vortex forms and the extent of the vortex penetration into the free stream air mass. The aerodynamic forces can be related to the vortex characteristics. These tests at velocity ratios of 0.1 and 0.2 were done for a choked nozzle pressure ratio, approximately 1.80. Velocity ratios of 0.1 to 0.2 were obtained by altering tunnel velocity. In order to test a velocity ratio of 0.3, nozzle pressure ratio was reduced.

Represenative ground board pressures are presented in Figures 7 and 8 at a velocity ratio of 0.1. Figure 7 presents the isolated jet results while Figure 8 presents the results with a 10d blocking plate located at the nozzle exit and parallel to the ground. The nozzle exits at the center of the plate for these data. The results shown in Figure 8 indicate that at heights less than approximately 4 diameters the vortex is trapped under the plate and the forward travel is restricted resulting in an increased negative pressure.

The forward projection of the ground vortex has been correlated as a function of height and is reasonably accounted for by the following equation;

$$\frac{X'}{d} = \frac{h}{d}\tan(\delta-90) + \left(.75 - 1.75\left(\frac{h}{d}\right)^{2.5}\left(\frac{W}{\ell}\right)_j^{.3} V_e^{3.25}\,[1 - \sin(\delta-90)]\right)\frac{\left(\frac{\delta}{90}\right)^2}{V_e}$$

The correlation of all nozzle configuration data from Reference 5 is shown in Figure 9. The correlation utilizing the above equation to account for nozzle aspect ratio and angle shows relatively good agreement for all data including that with the blocking plates. The summary of data from Reference 5 is compared to that from References 1 through 4 in Figure 10. The penetration of the vortex on the nozzle centerline is slightly less than that from References 1 and 3 but somewhat greater than that of Weber and Gay, Reference 4, and approximately 30 percent greater than shown by Abbott's moving model data, Reference 2.

The comparison of the maximum negative pressure from References 1 and 5, Figures 4 and 7, show the data from Reference 5, taken at a nozzle pressure ratio of 1.8 are significantly higher than that from Reference 1, obtained at a nozzle pressure ratio of approximately 1.05. The pressure ratio may account for the difference in the negative pressure observed under the vortex. However, data more recently obtained at NASA, Langley Research Center (LaRC) may be indicative of another explanation for these differences in the ground board pressures.

The NASA data was obtained with a moving model and a fixed ground board. The ground board had a 4 degree ramp and a long flat section parallel to the model path. Details of this test are discussed in Paulson's paper presented in this workshop. Data were taken with a circular nozzle deflected 90 degrees to the ground. The ground board is depicted in Figure 11. Data for

the comparison was obtained utilizing time sensitive pressure transducers located along the nozzle path. Reduction of the data to ground board pressures as a function of nozzle path resulted in the pressure profiles shown in Figures 12 to 16. Comparison of the vortex from the moving model with the fixed model data from Reference 5 are shown in Figures 14 and 15. These results show that the vortex from the moving model does not extent as far forward as that from the fixed model tests, Reference 5. Also, as can be seen in Figure 17, the negative pressures under the vortex of the moving jet is greater than either that of Reference 5 or 1. The nozzle pressure ratio for the moving jet was approximately the same as that of Reference 5 so the difference in vortex characteristics would appear to be the effect of the moving vs. the fixed jet, that is the ground board boundary layer. The boundary layer does, most likely, account for the reduced penetration of the vortex into the free stream. The increase in the negative pressure does not appear to be related to the ground boundary layer but is thought to be more accurately relatable to the energy in the wall jet or to the thrust coefficient of the wall jet and to the forward extent of the vortex. This relationship, if true, would indicate that regardless of the penetration of the vortex with different ground boundary layer conditions, the lift loss will be nearly the same at the same jet conditions of angle and thrust coefficients and therefore the aerodynamic effects may be relatable to thrust coefficient. This relationship is likely to be true if the vortex is trapped under the configuration but the suckdown will be configuration dependent when related to the wings and control surfaces on most real configurations. Figure 18 presents the comparison of this moving model data with that of References 1 through 7. This moving model data appears to agree well with that of Abbott, Reference 2, and to be approximately 30 percent less than that from the fixed model and ground board tests. A possible result of the reduced penetration of the ground vortex may be an increase in the pitching moment of the system. A pitch up and a lift loss will result if a vortex is formed by an aft located nozzle such as a thrust reverser. If the lift loss in the actual airplane case, with no ground boundary layer, is the same as the fixed model tests the load center will move aft and the pitch up will be greater for the moving condition.

A second interesting variation of the ground board pressures is also seen in Figures 12 through 16. This data represents one of the few attempts to measure the dynamic characteristics of the ground vortex. As the velocity ratio of the jet, free stream velocity to jet velocity, is reduced the vortex appears to become increasingly less stable. This unsteadiness has been noted in several other studies.

Slot Nozzles and Jet Flaps: Several studies have investigated the effects of slot nozzles in near proximity to the ground. References 5 through 7 discussed one test of a slot nozzle in which the ground vortex was measured. Reference 8 presented a summary of a propulsive wing study for NASA which was later published in Reference 9. This study, Reference 9, as well

as most early jet flap tests were aerodynamic characteristic tests and did not measure or visualize the ground vortex penetration. An exception is the work of Butler, Guyett, and Moy, Reference 10. Reference 11 presented additional results of this study. Figure 19 from Reference 10 presents photography views of the development of the ground vortex as the jet impingement point is moved forward and the angle of impact increased by the increasing angle of attack of the model. At zero angle of attack the ground vortex is undefined, it may be present outboard and well aft. As the angle of attack is increased the vortex becomes well defined and is located under and eventually ahead of the wing. Figure 20, Reference 10, presents a graphic description of the vortex flow field. The cross section of the flow field shows two vortex patterns, first a large vortex under the wing and secondly a tightly rolled secondary vortex on the ground ahead of the larger vortex.

An early look at the effects of a moving ground belt on the ground effects of a jet flap was done by Butler, Moy, and Hutchins, Reference 12. This study investigated the effect of the moving belt on the aerodynamics and on the ground vortex and flow field under the jet flap wing. Figures 21 and 22 show the effect of the moving belt on the flow field. The flow field was visualized by a series of tufts attached to wires under the wing. In Figure 21 at an angle of attack of 5 degrees the moving belt appears to reduce the forward extent of the vortex. At 15 degrees angle of attack, Figure 22, the effect is less apparent. These data are both at a blowing coefficient of 4.0.

The ground effects of these configurations is seen in Figures 23 and 24. The data for the configuration of Reference 10 seen in Figure 23. The lift coefficient is seen to be unaffected by the ground at low angles of attack and at low blowing coefficients, however, at combinations of blowing coefficients and angle of attack which produce large lift coefficients, the effect of the ground is significant. The large losses in lift coefficient seen on this configuration may be attributed, in effect, to the ground vortex. If the presence of the ground boundary layer affects the vortex it will also effect the lift loss. Figure 24 shows the effect of the moving belt on the lift coefficient of the configuration of Reference 12. The lift coefficient at the higher angle of attack and blowing coefficient is greater with the moving belt.

A similar pattern is shown on the lower surface pressure distribution of a low aspect propulsive wing, Reference 8. These pressure variations, Figure 25, seem to indicate the double vortex discussed earlier. The slot jet of Reference 5 is summarized in References 6 and 8. The ground board pressures and lift losses are presented in Figures 26 and 27. Figure 26 presents pressure and lift data at a jet deflection of 90 degrees and Figure 27 presents the same data for 45 degree deflection. In the latter case, the vortex is formed aft of the wing and a positive incremental lift is seen at near proximity to the ground. The deflection of 90 degrees produces a vortex ahead of

the wing and a significant lift loss.

Unpublished data from a later test of the low aspect ratio propulsive wing did not measure the ground vortex, but as can be seen in Figure 28 a large lift loss is experienced at low heights and large blowing coefficients indicate the presence of the ground vortex.

One result of the of the ground vortex of the jet flap configurations is the requirement for a moving ground belt for near ground testing. Turner, Reference 13, established a boundary of height and lift coefficient for moving belt testing. The results of the vortex effects of References 5, 9, and 13 indicate that the requirement for the belt may be more critical than that established by Turner. Turner's data was for relatively large aspect ratio wings. The later data is for lower aspect ratios and appear to suggest that the region requiring a moving belt should be expanded. Figure 29 compares the limits set by Turner and that indicated by the ground vortex and propulsive wing tests. These data were established with a fixed ground board. There is not sufficient data to determine what, if any, effect the moving belt would have on the vortex formation or the aerodynamic characteristics of these configurations.

CONCLUSIONS

The presence of a ground vortex due to the interaction of the wall jet and the free stream is well established.

The vortex affects the aerodynamic characteristics of the airplane. A lift loss due to the negative pressures in the vortex is generally experienced. If the jet producing the vortex is well aft on the configuration, a pitch up will also be experienced.

The effect of the boundary layer on the ground ahead of the configuration appears to be significant in the development of the vortex. Approximately a thirty percent reduction in the vortex penetration is indicated when the boundary layer is eliminated.

The presence of the ground vortex and the significant effect of that vortex on the aerodynamic characteristics indicate that a moving ground board should be considered for all STOL powered model ground effects testing. A moving model technique may be preferred if the data gathering capabilities are not too restrictive.

RECOMMENDATIONS

The ground vortex characteristics need further definition. Testing should be accomplished to compare fixed and moving ground boards and to compare both with the moving model technique. These tests are needed for both concentrated jets and for slot nozzles, jet flaps.

The dynamics of the vortex should be investigated. The single piece of quantitative dynamic data available indicates that the vortex unsteadiness is a function of the forward speed.

REFERENCES

1. Colin, P. E. and Olivari, D.: "The Impingement of Circular Jet Normal to a Flat Surface with and without Cross Flow", von Karman Institute for Fluid Dynamics, Rhode-St., Genese, Belgium, Report AD688953, Jan. 1969.
2. Abbott, W. A.: "Studies of Flow Fields Created by Vertical and Inclined Jets Moving over a Horizontal Surface", ACR Cp No. 911, 1967.
3. Schwantes, E.: "The Recirculation Flow Field of a VTOL Lifting Engine", NASA TT F-14912 June 1973.
4. Weber, H. A. and Gay, A.; "VTOL Reingestiom Model Testing of Fountain Control and Wind Effects", Prediction for V/STOL Propulsion Aerodynamics, Vol. 1, NASC, 1975, pp 358-380.
5. Stewart, V. R. and Kuhn, R. E.: "A Method for Estimating the Propulsion-Induced Aerodynamic Characteristics of STOL Aircraft in Ground Effect", NADC 80226-60 Aug. 1983.
6. Stewart, V. R., Kuhn. R. E., and Walters, M. M.: "Characteristics of the Ground Vortex Developed by Various V/STOL Jets at Forward Speed", AIAA Paper 83-2494, Oct. 1983.
7. Stewart, V. R., Kuhn. R. E., and Walters, M. M.: " A Method for Estimating The Propulsion Induced Aerodynamic Characteristics of STOL Aircraft in Ground Effect", AIAA Paper 83-0169, Jan. 1983.
8. Stewart, V. R. and Kemmerly, G. T.: "Effects of Ground Proximity on a Low Aspect Ratio Propulsive Wing/Canard Configuration", NASA, Ames Research Center, Workshop on Ground Effects, Aug. 1985.
9. Stewart, V. R.: "Aerodynamic Characteristics of a Propulsive Wing/Canard Concept at STOL Speeds", NASA CR 177982 Nov. 1985.
10. Butler, S. F. J., Guyett, M. B. , and Moy,B. A.: "Six Component Low-Speed Tunnel Tests of Jet-Flap Complete Models with Variation of Aspect Ratio, Dihedral, and Sweepback, Including the Influence of Ground Proximity", R & M 3441, 1967.
11. Williams, J., Butler, S. F. J., and Wood, M. N.: "The Aerodynamics of Jet Flaps:, RAE R & m 3304, Jan. 1961.
12. Butler, S. F. J., Moy, B. A., and Hutchins, G. D., " Low-Speed Tunnel Tests of an Aspect-Ratio 9 Jet-Flap Model, With Ground Simulation by Moving-Belt Rig, C.P. 849, 1966.
13. Turner, T. R.: "Endless Belt Technique For Ground Simulation", NASA SP-116, pp 435-446, April 1966.

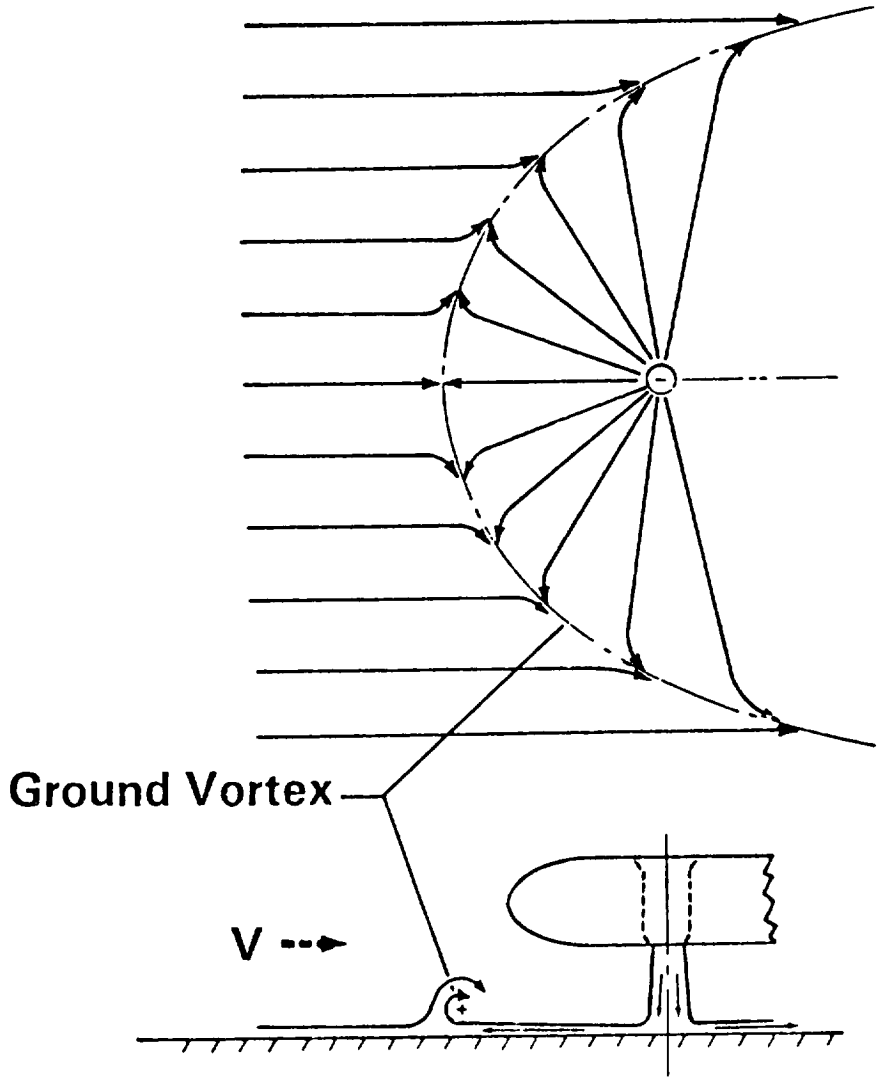

Figure 1. Formation of the Ground Vortex

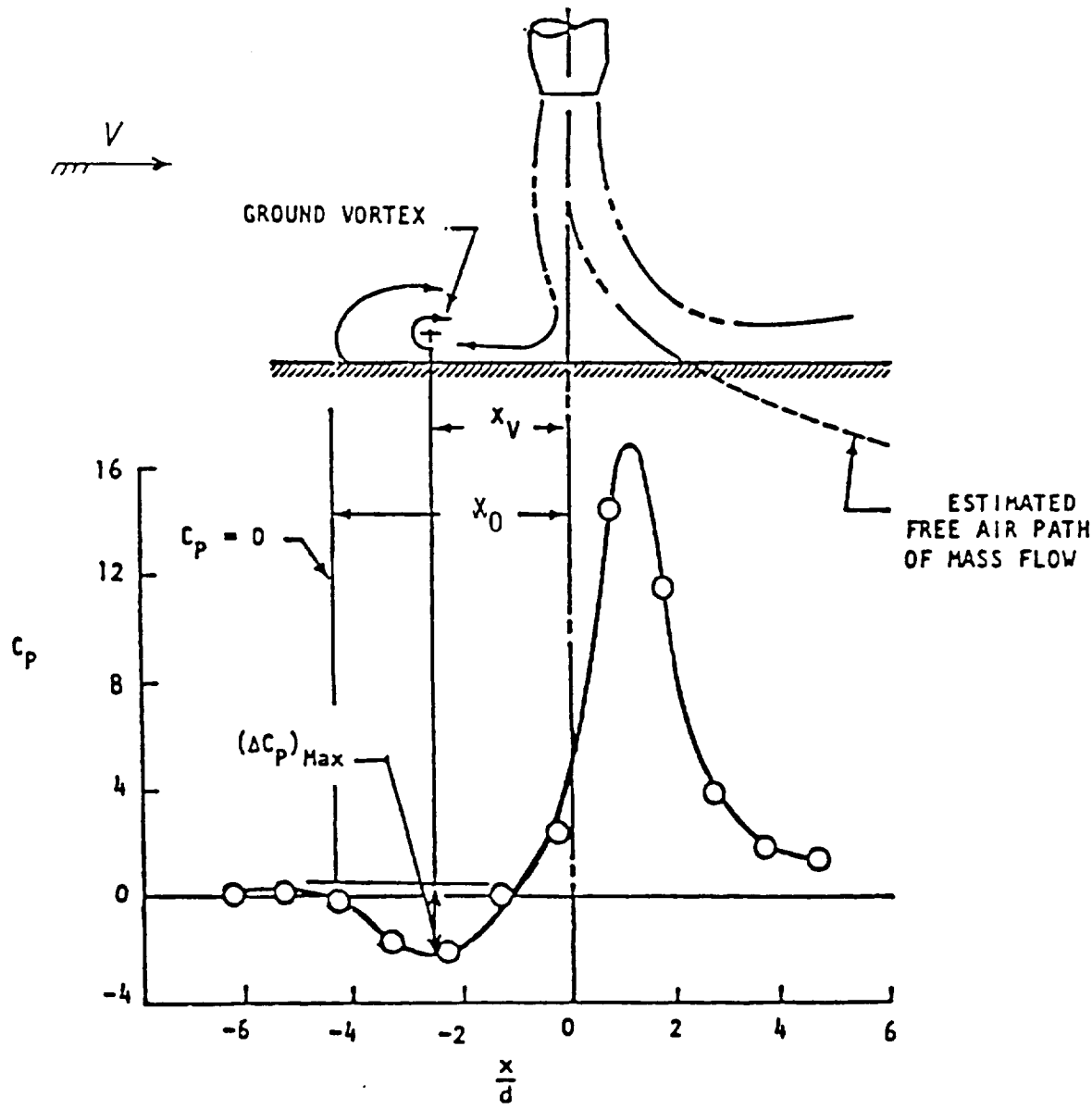

Figure 2. Typical Pressure Distribution and Definition of Terms

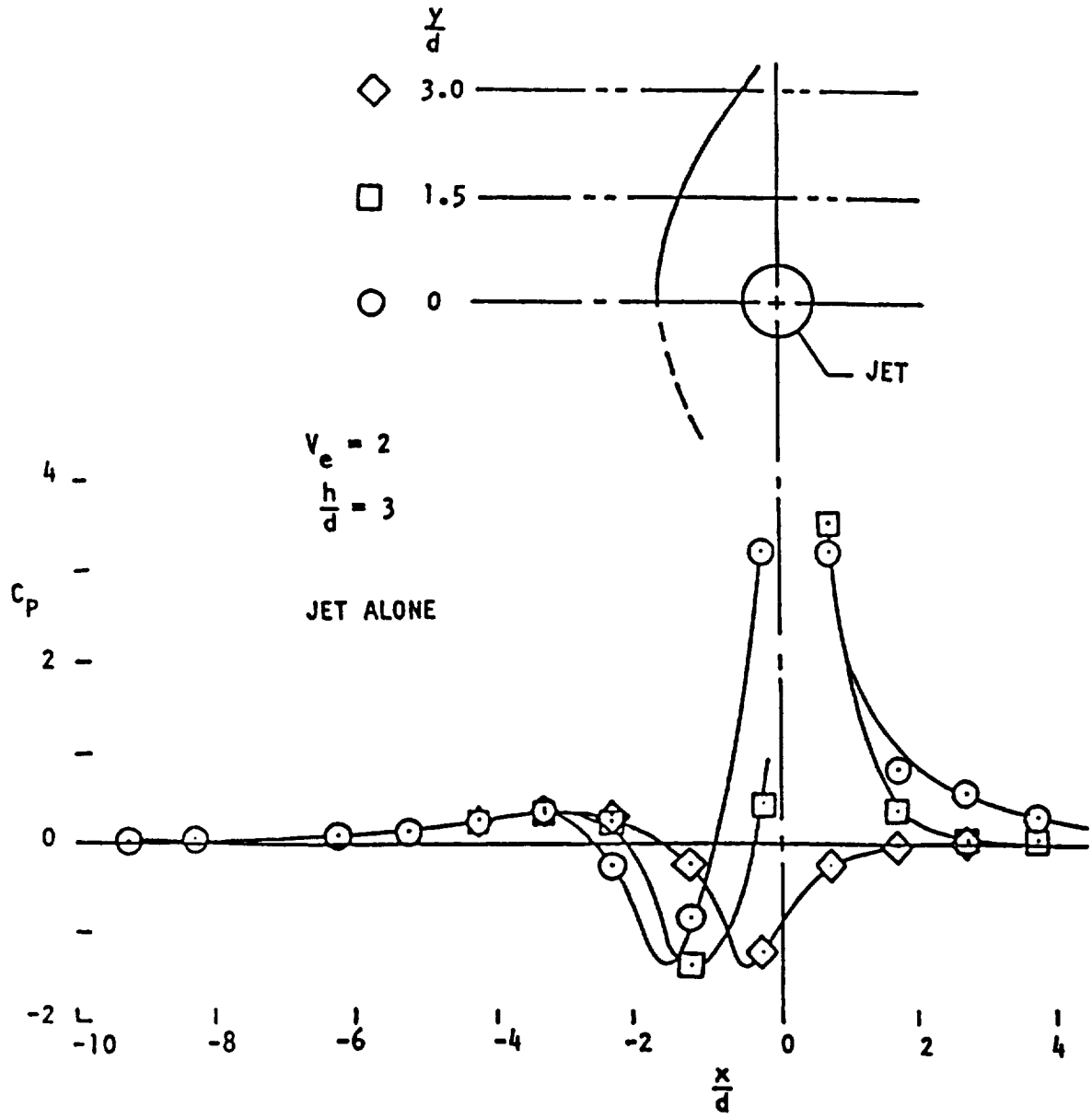

Figure 3. Ground Board Pressures Due to Jet and Vortex

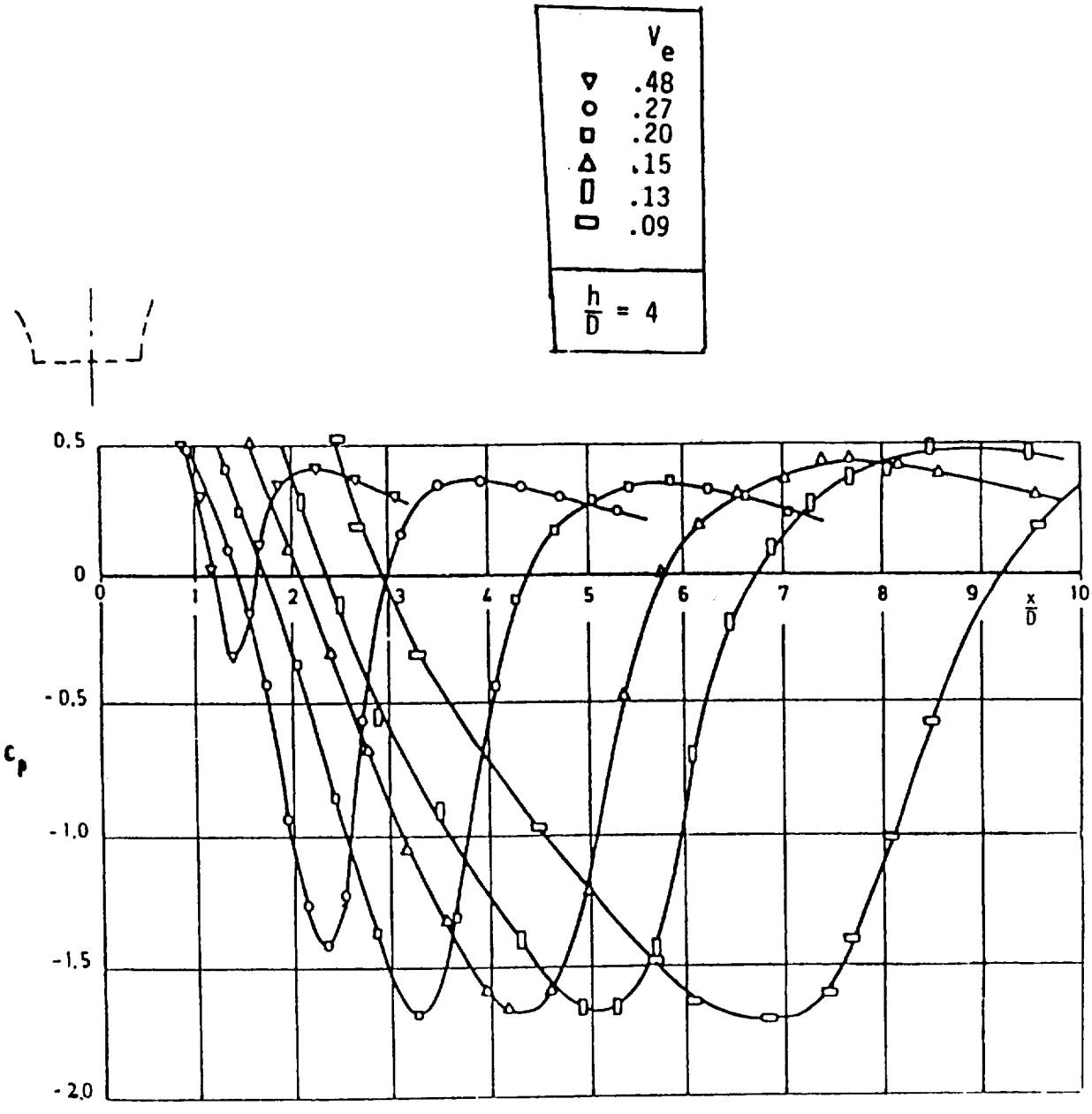

Figure 4. Wall Static Pressure Distribution (Ref.1)

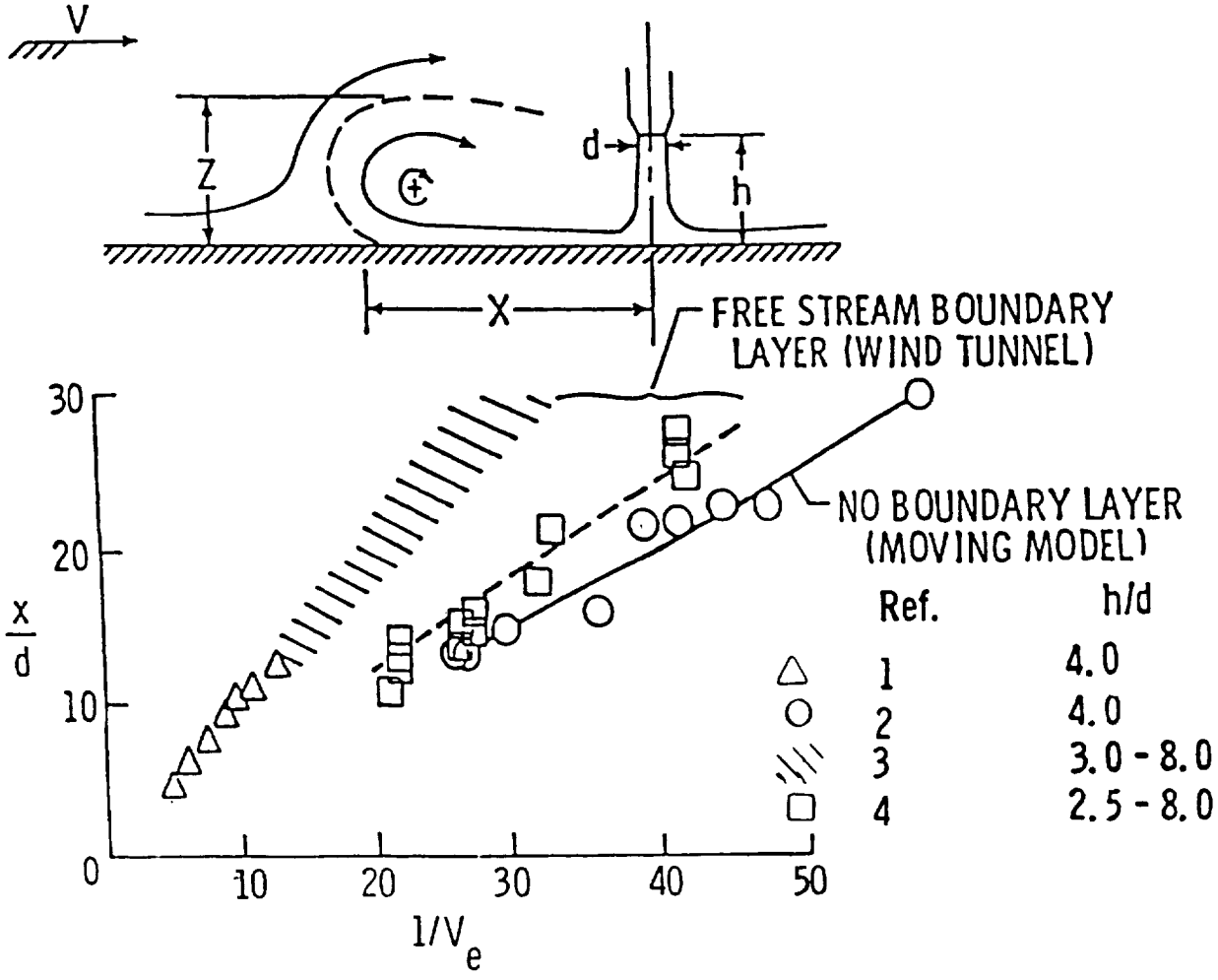

Figure 5. Forward Extent of Ground Vortex

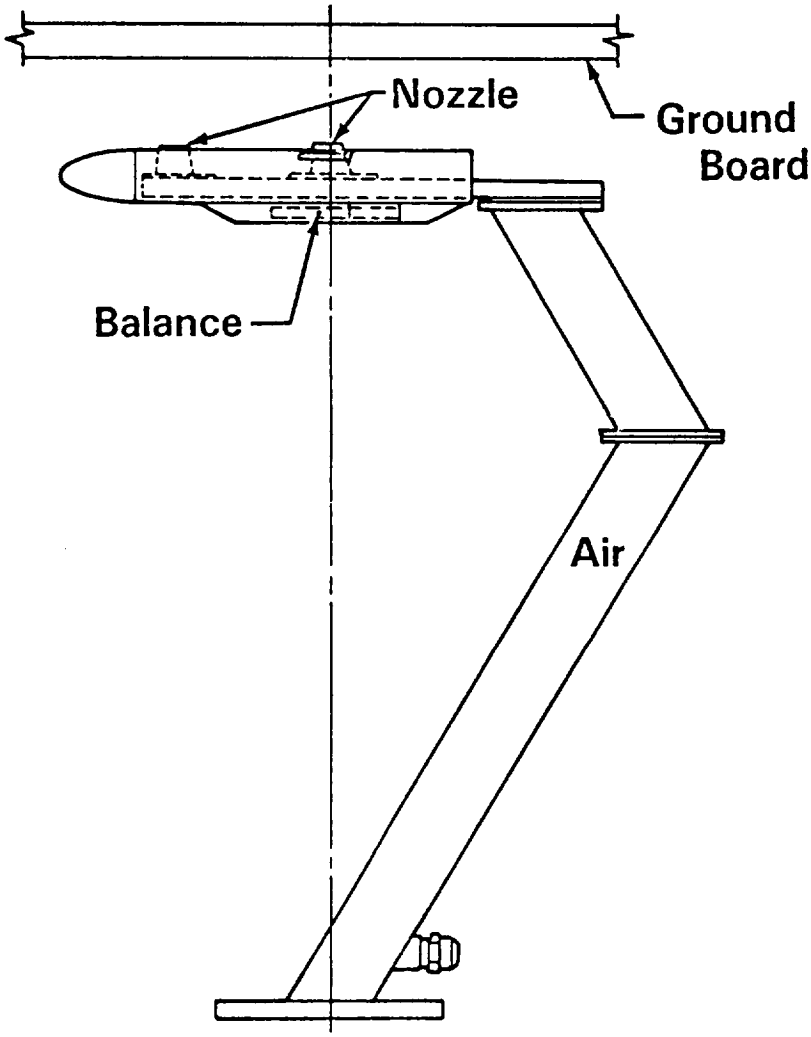

Figure 6. Model Installation

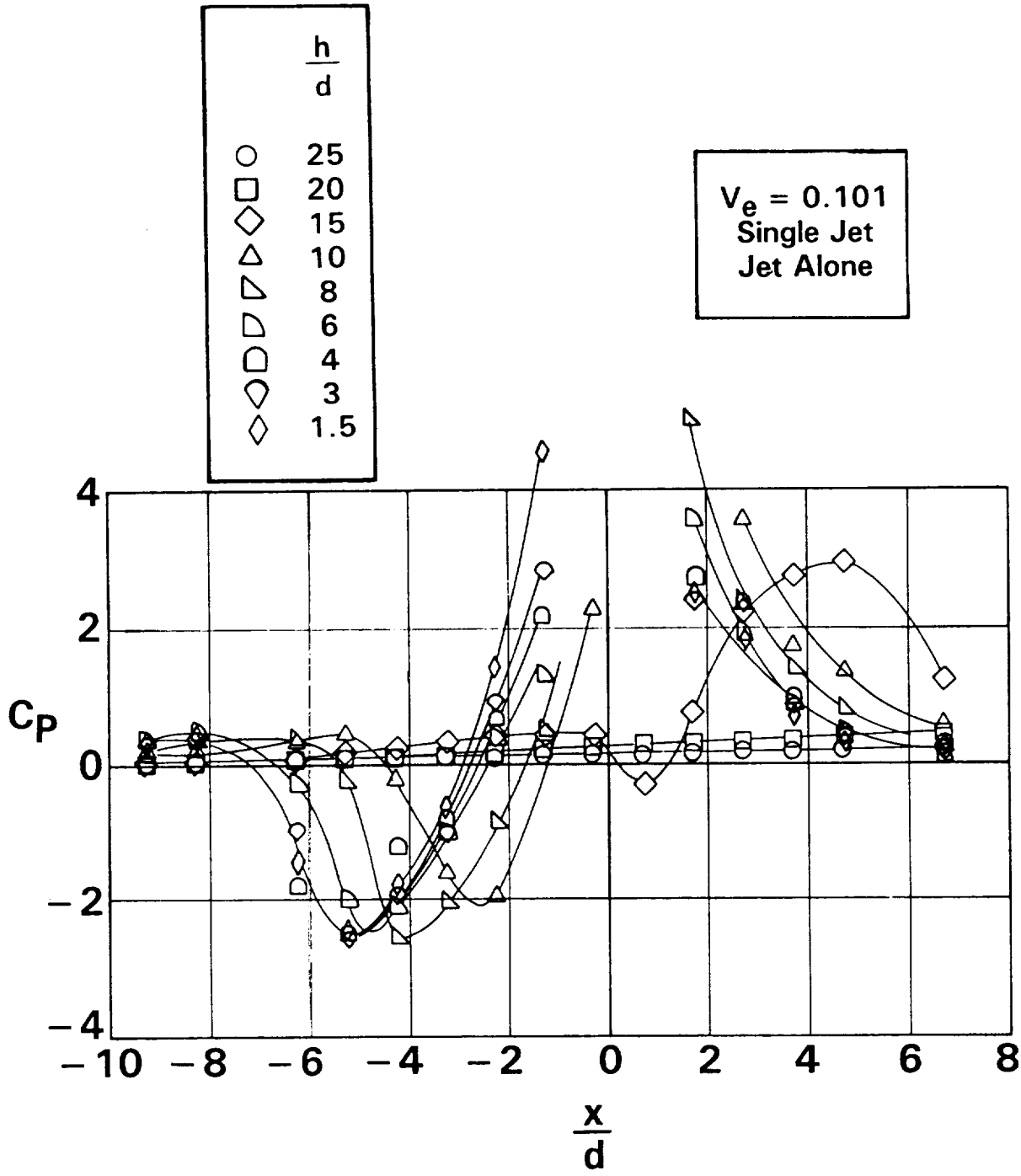

Figure 7. Effect of Height on Pressure Distribution Measured on Ground Board

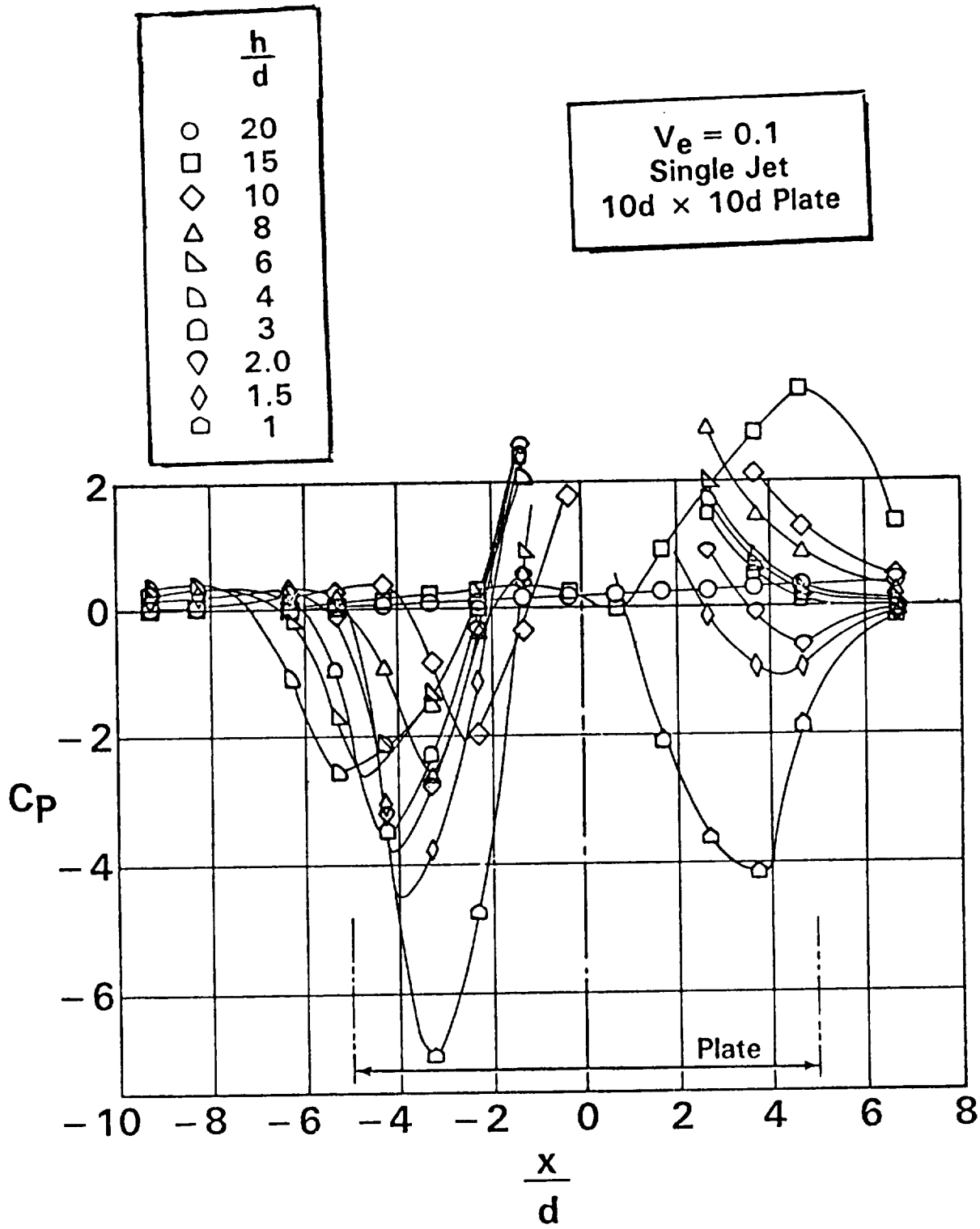

Figure 8. Effect of Height with Large Plate on Ground Board Pressures

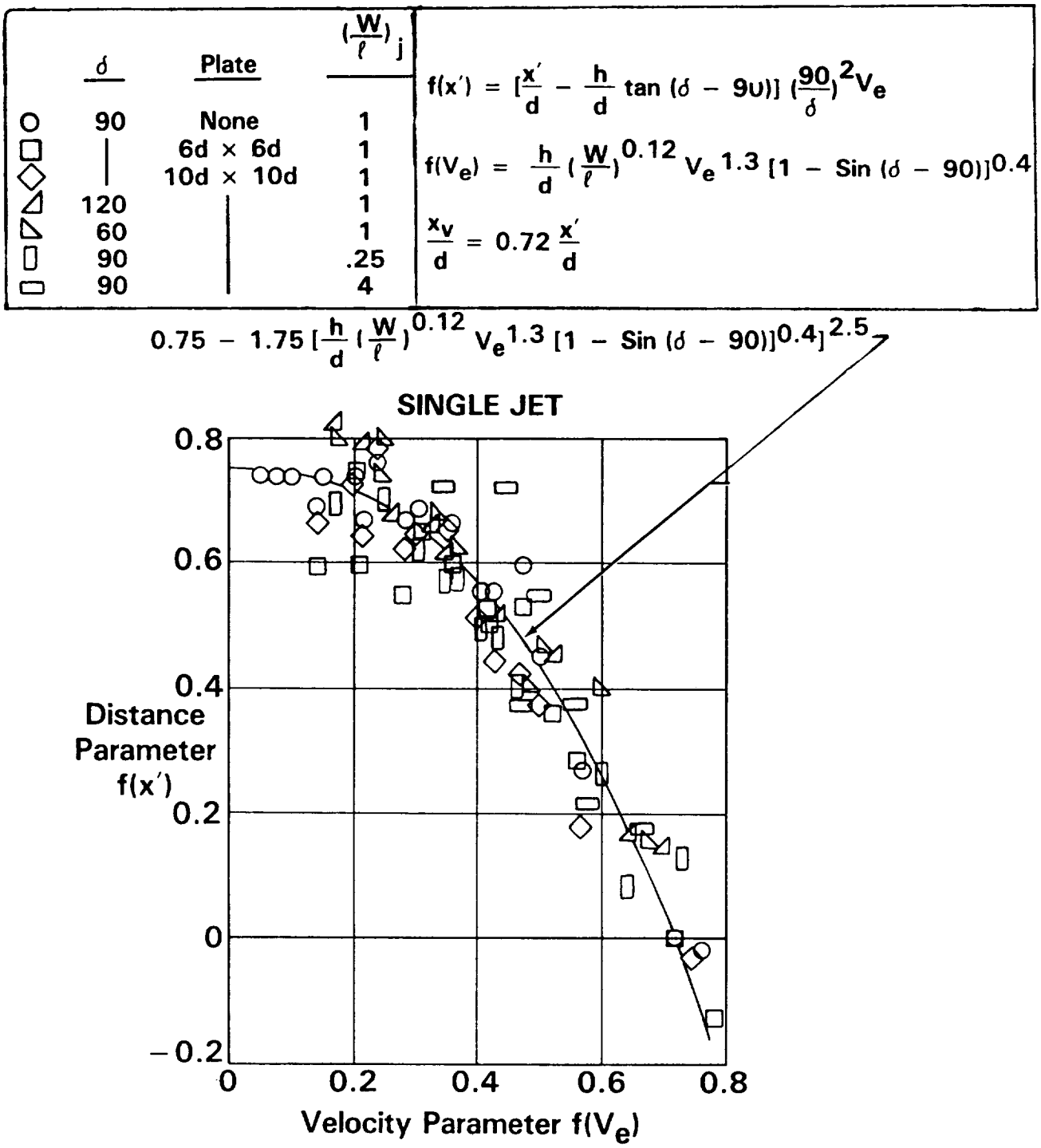

Figure 9. Correlation of Forward Extent of Vortex

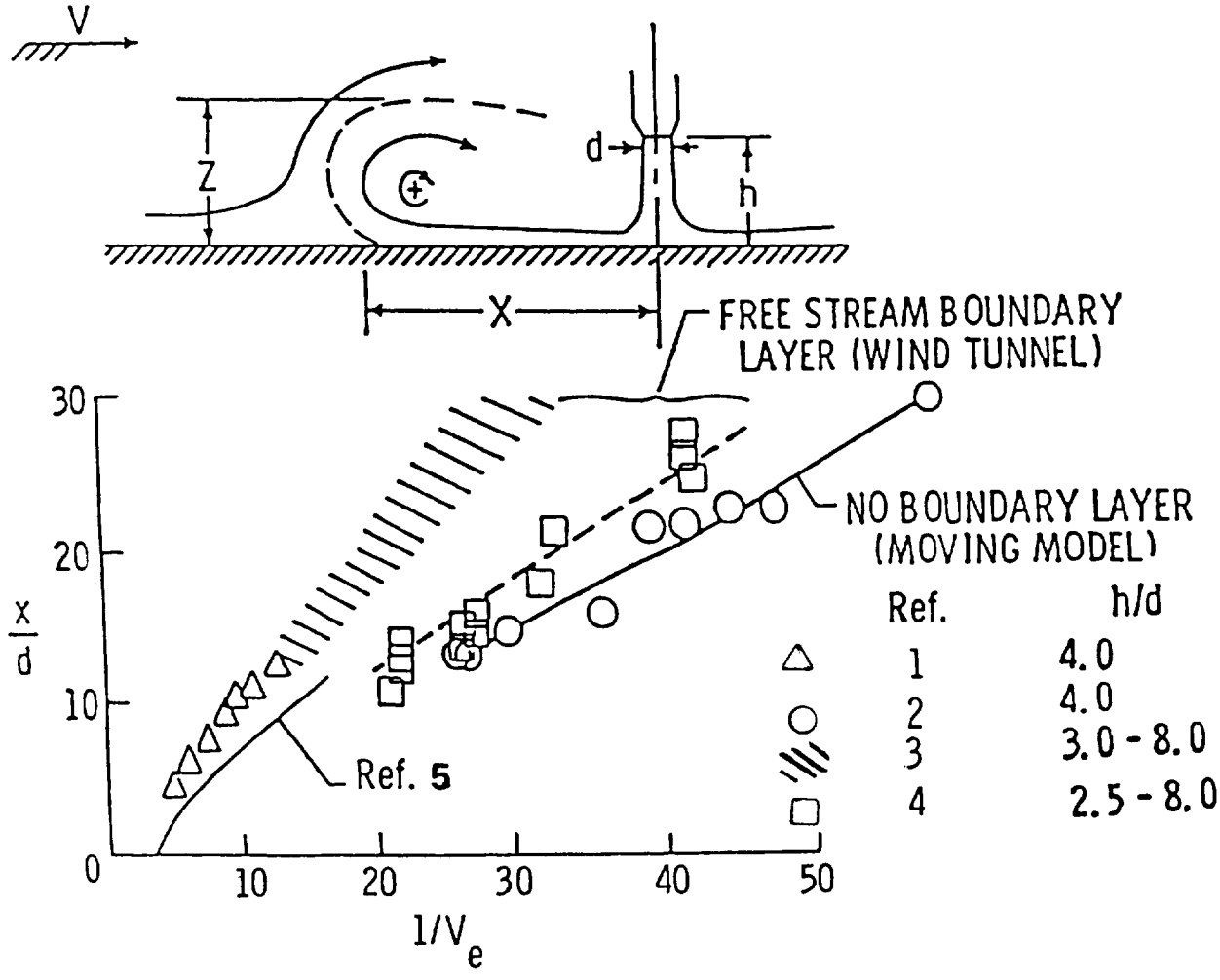

Figure 10. Forward Extent of Ground Vortex

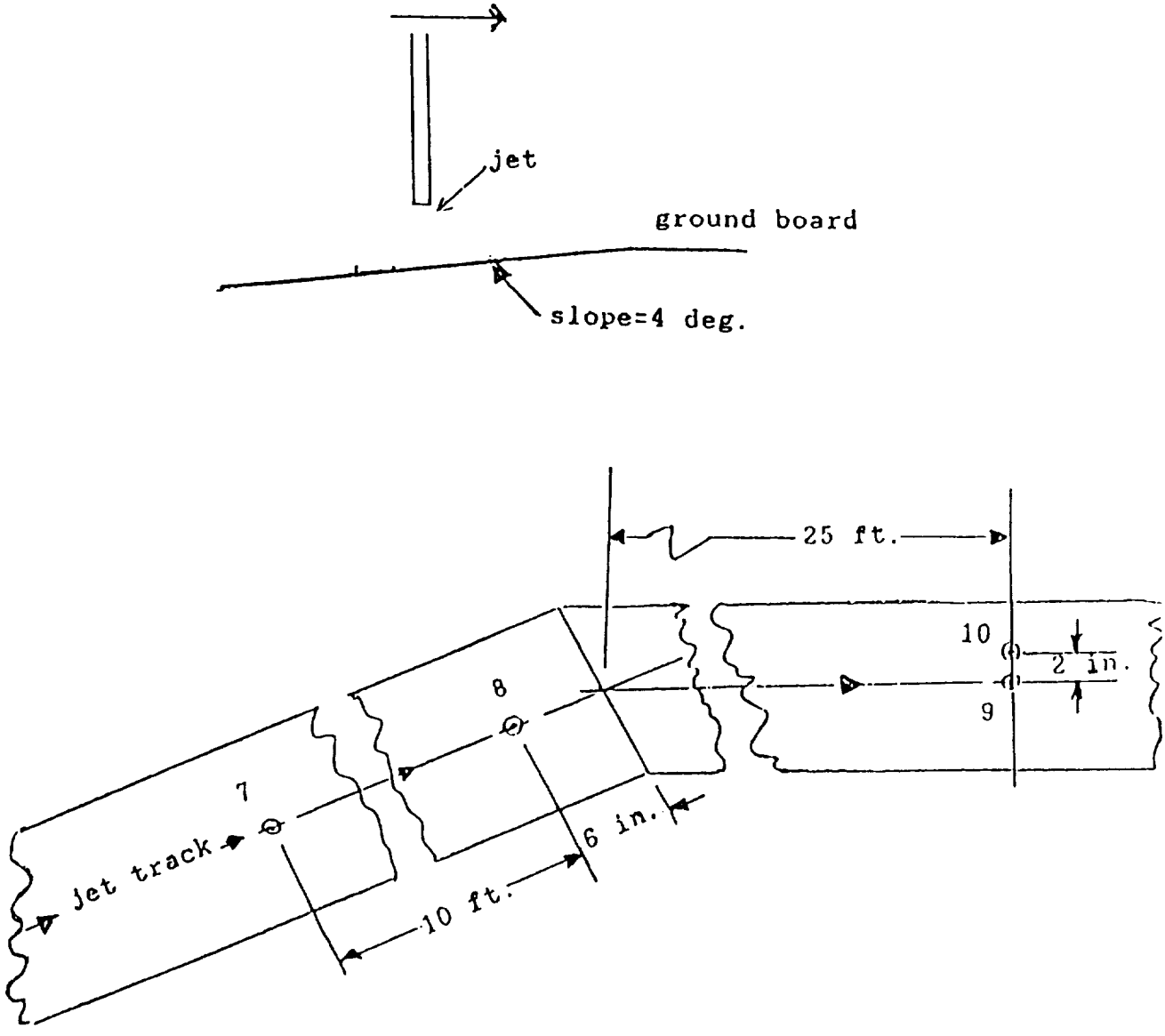

Figure 11. Moving Model Ground Board Instrumentation

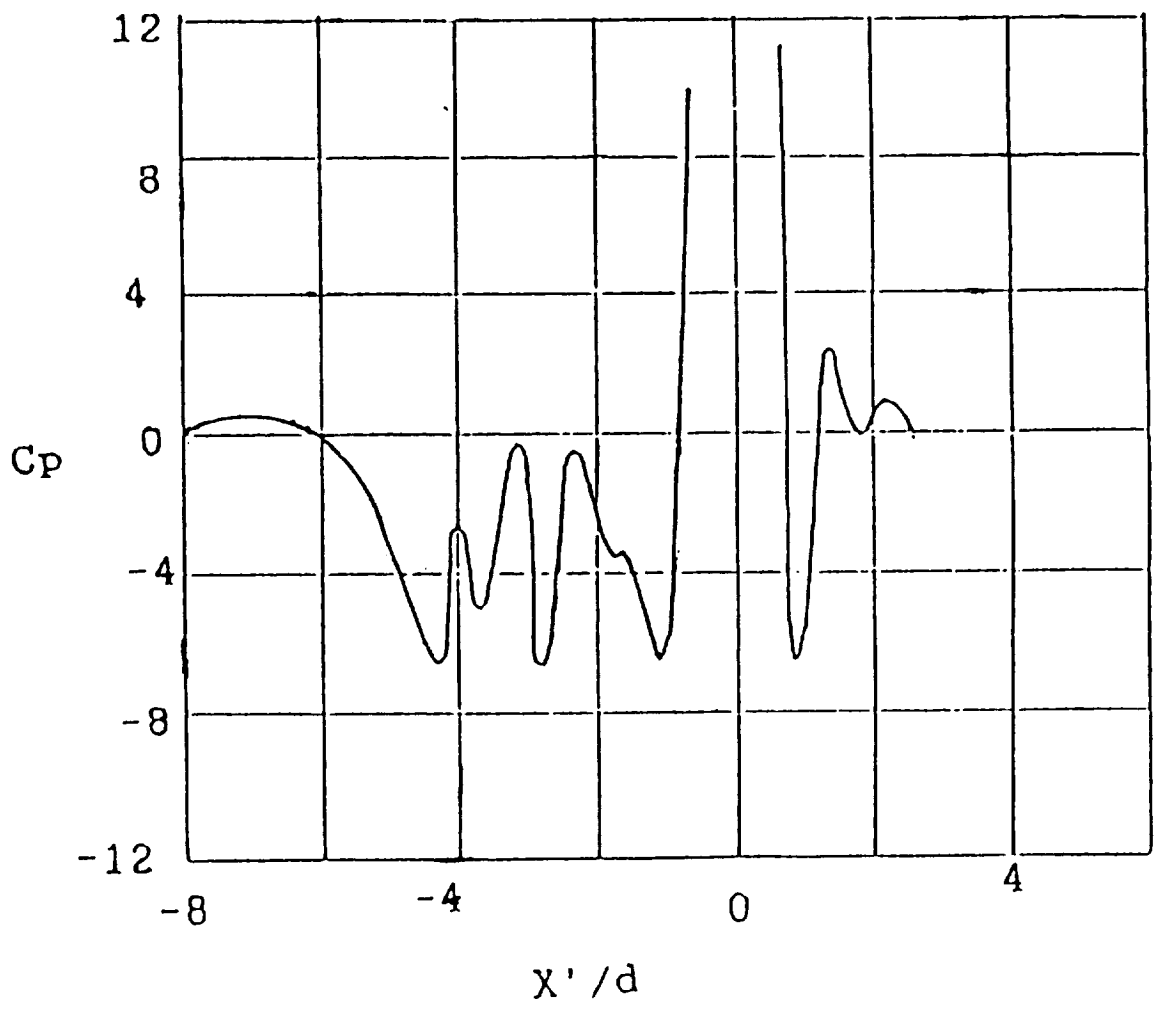

Figure 12. Moving Model Ground Board Pressures

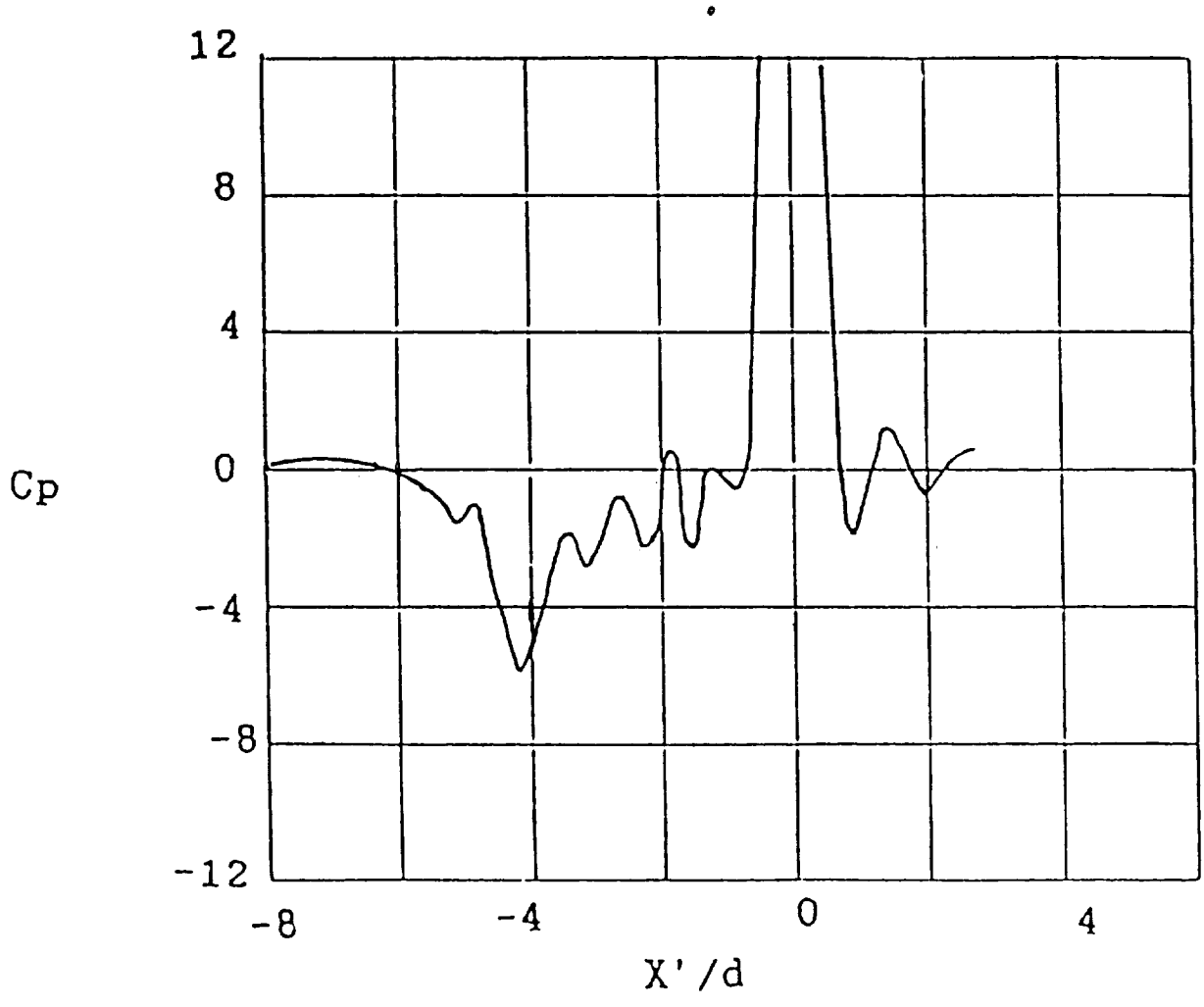

Figure 13. Moving Model Ground Board Pressures

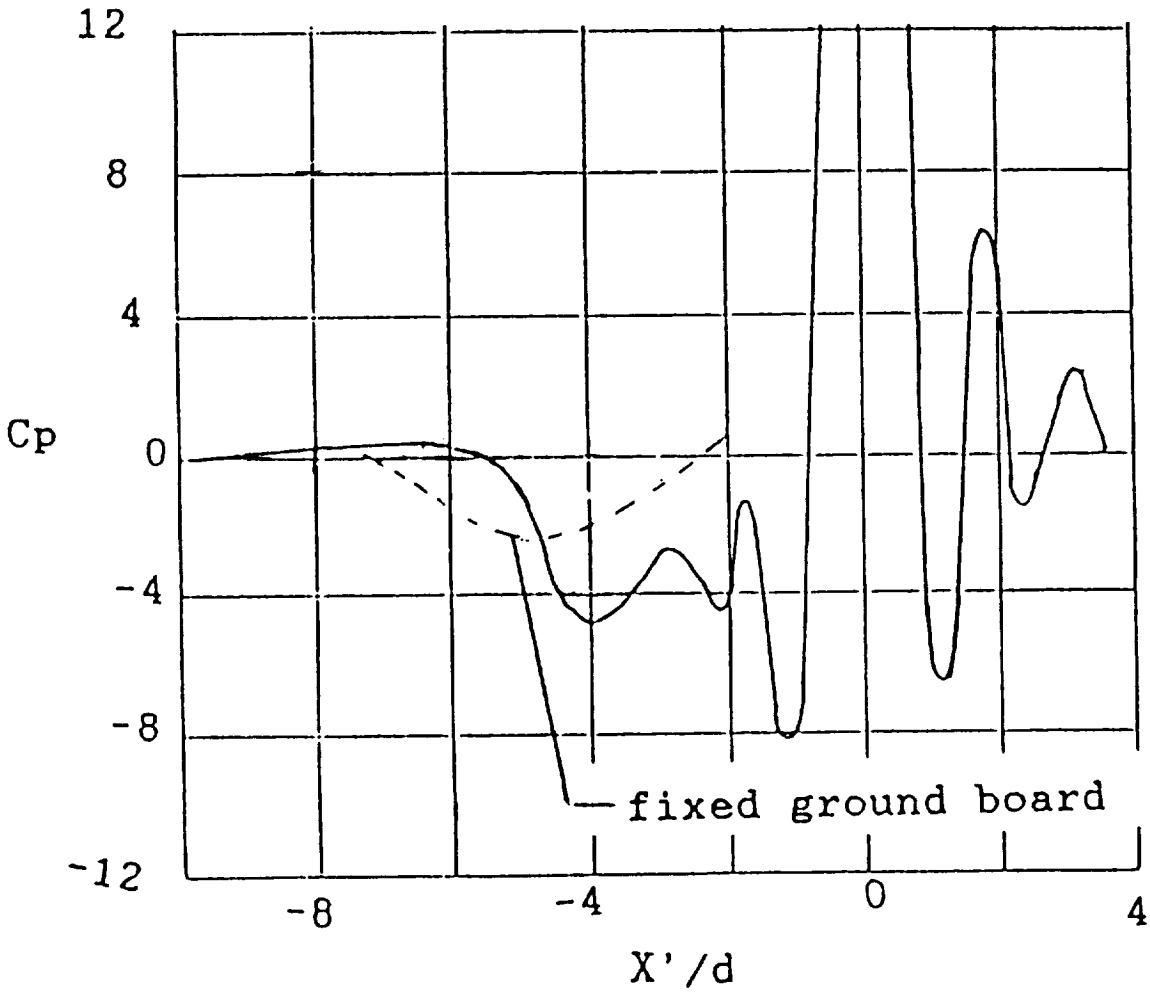

Figure 14. Moving Model Ground Board Pressures

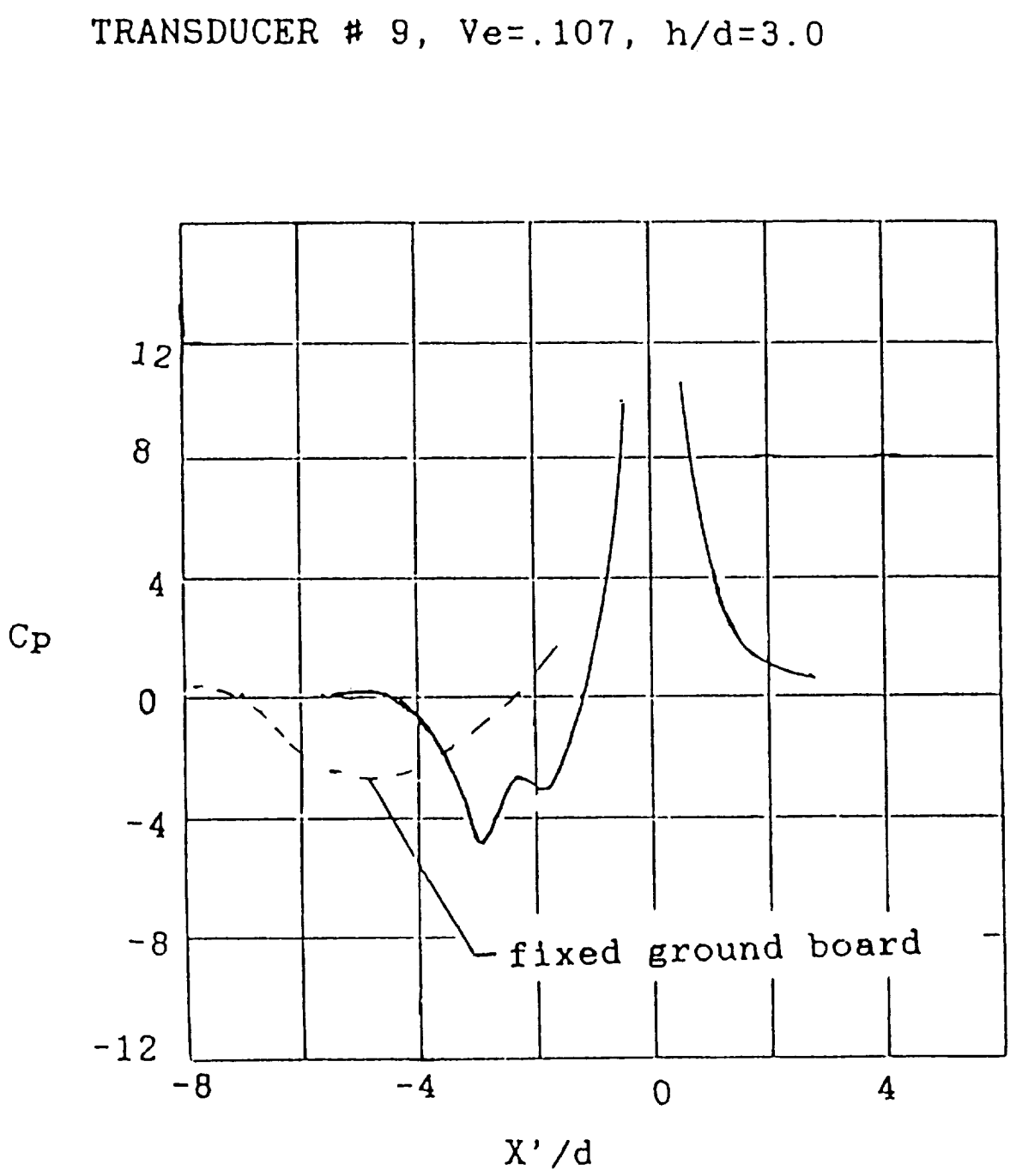

Figure 15. Moving Model Ground Board Pressures

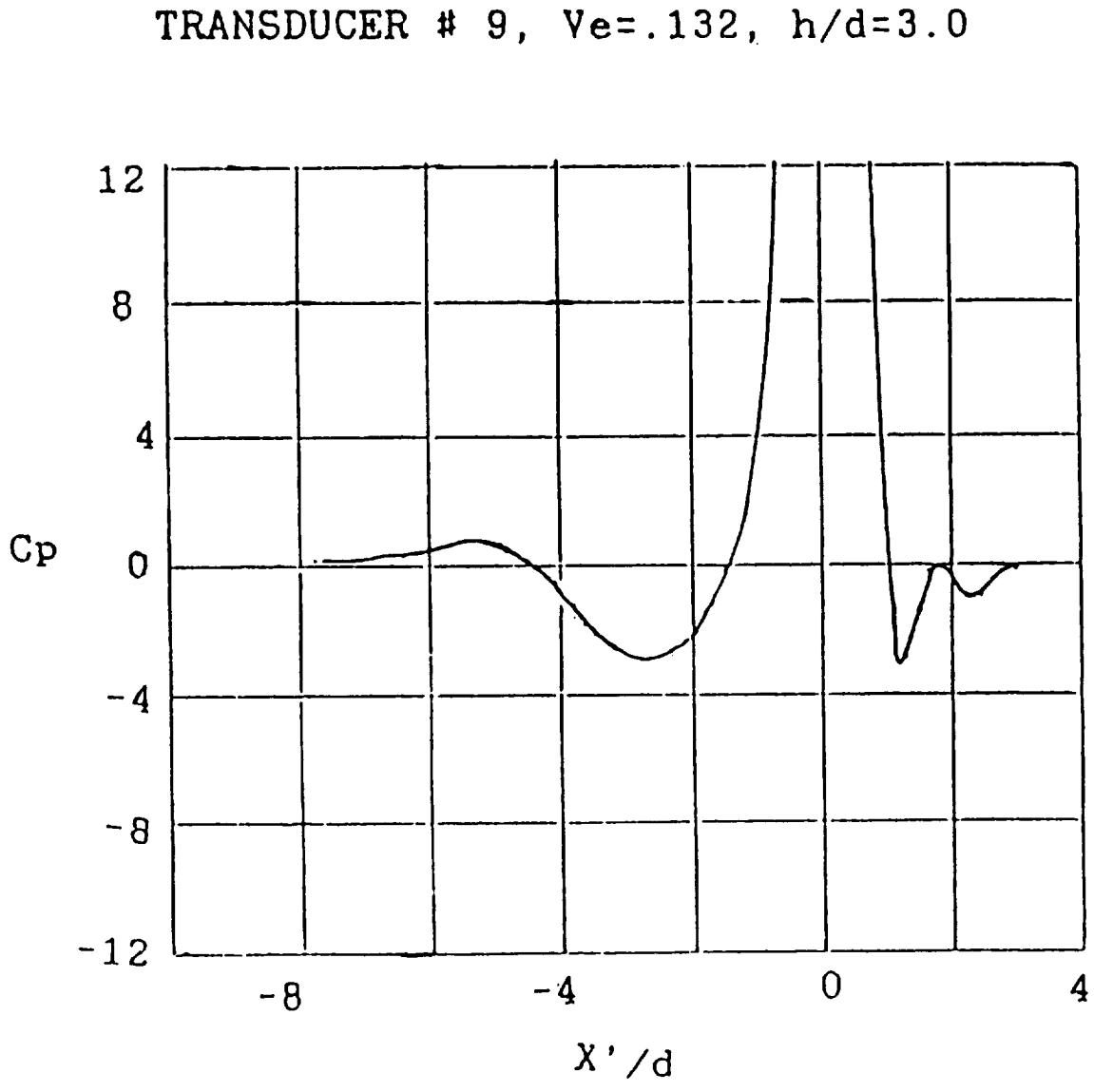

Figure 16. Moving Model Ground Board Pressures

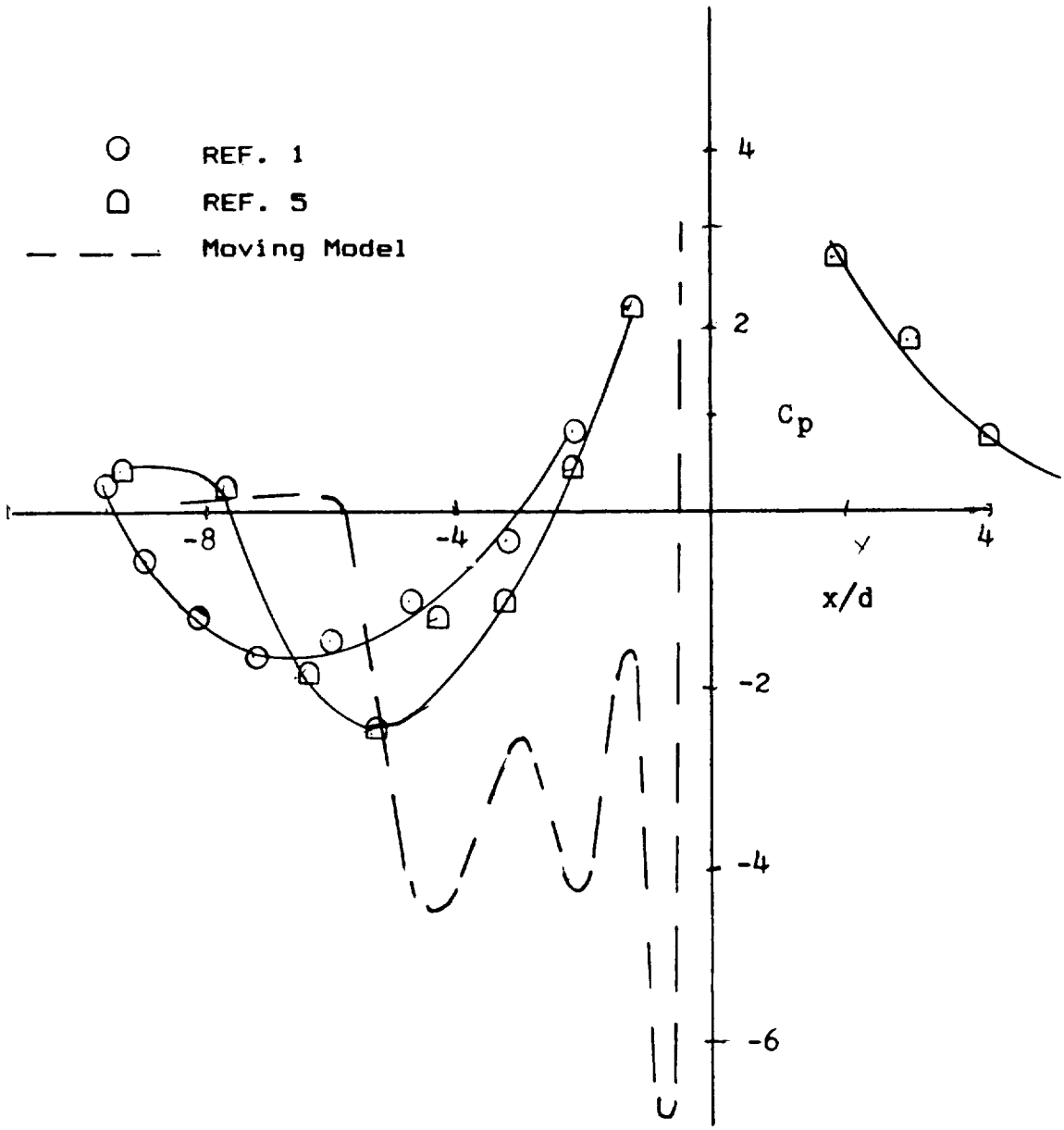

Figure 17. Comparison of Ground Vortex

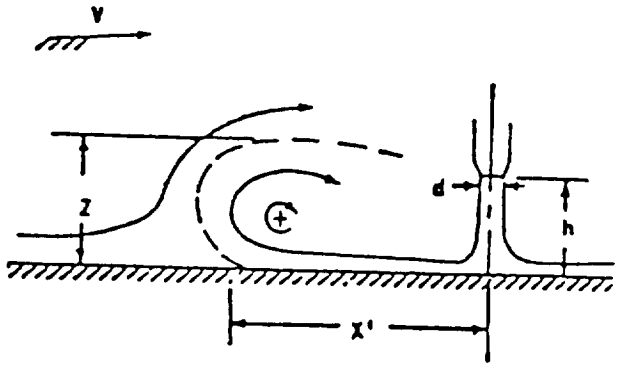

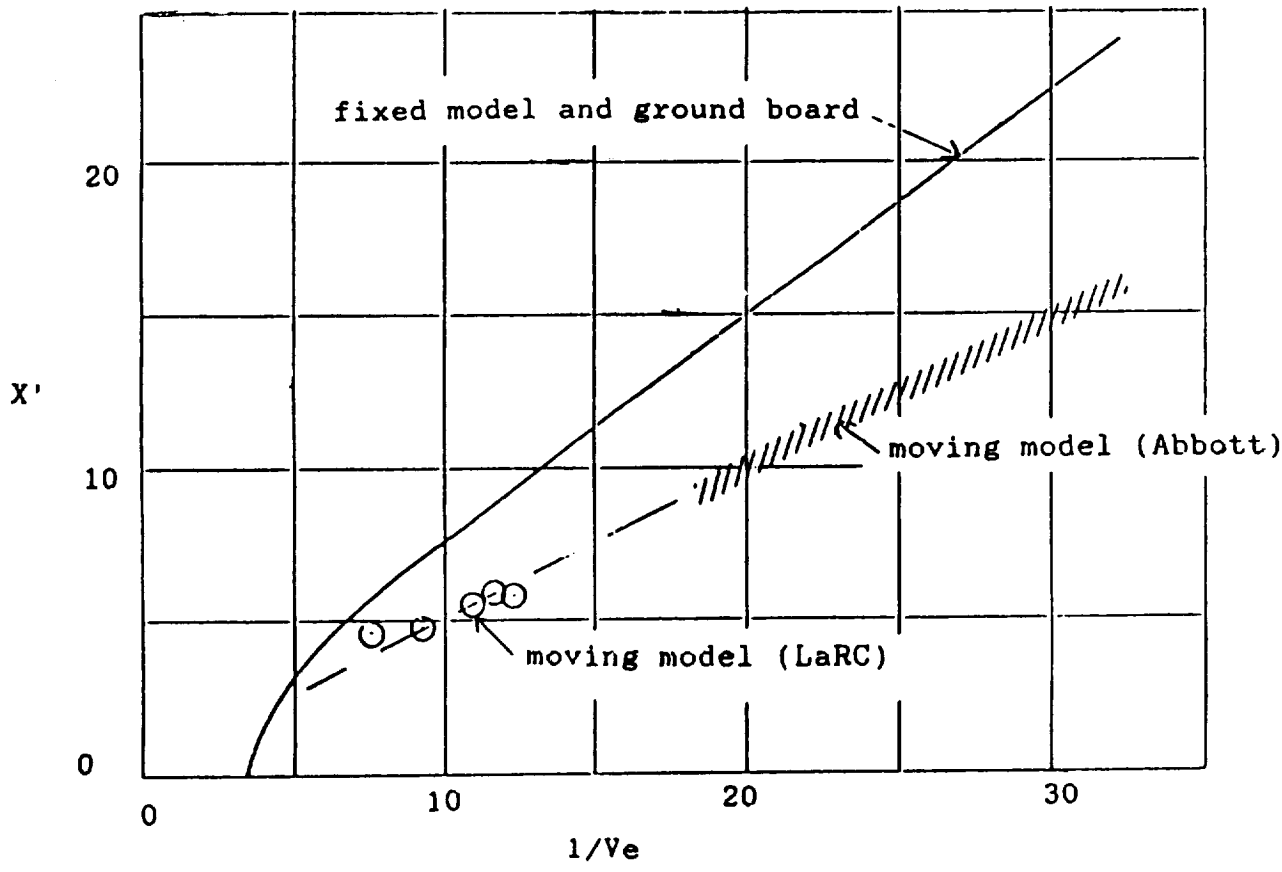

Figure 18. Effect of Moving Model of the Penetration of the Ground Vortex

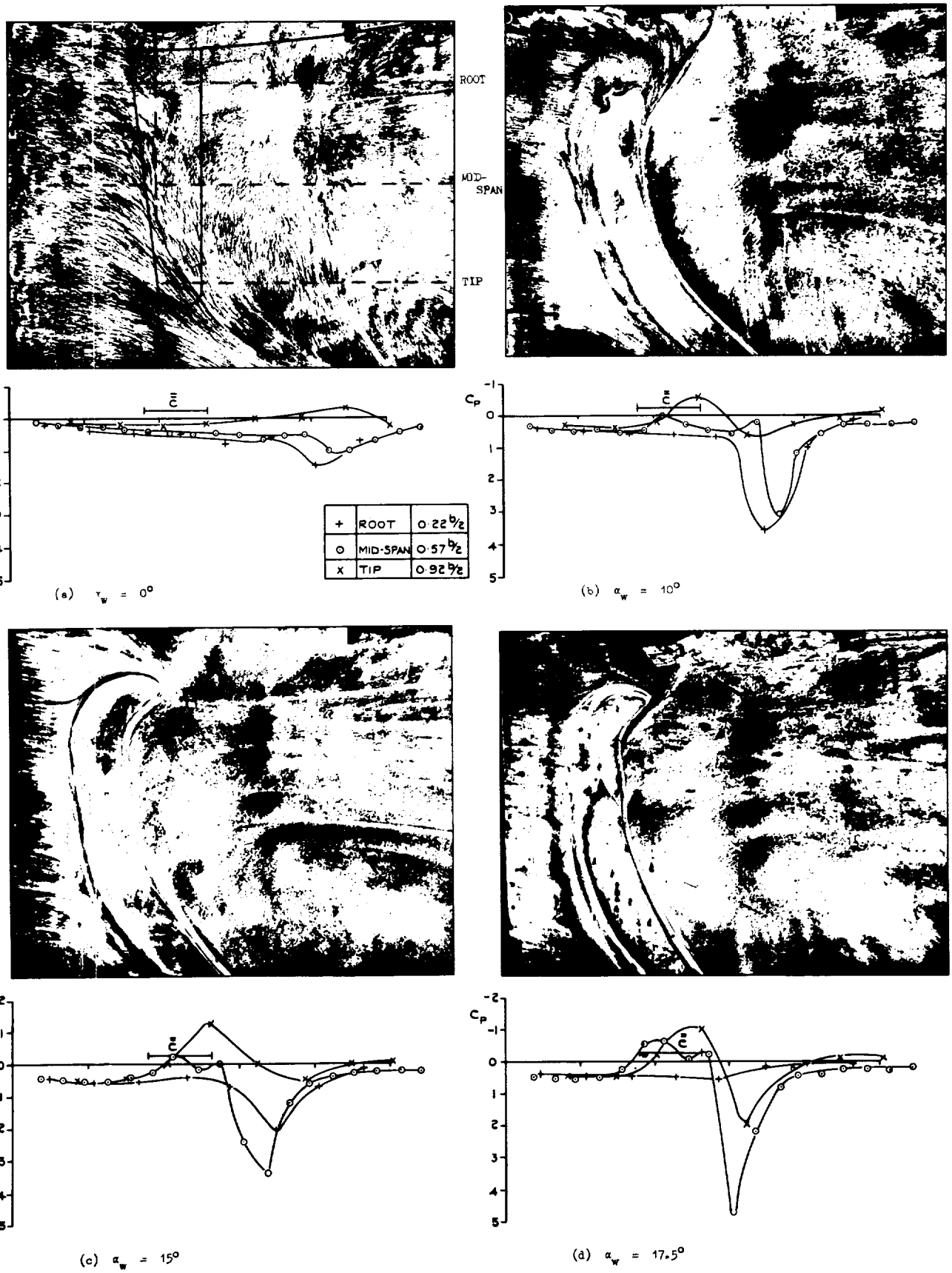

Figure 19. Ground Board Flow Patterns and Pressure Distributions

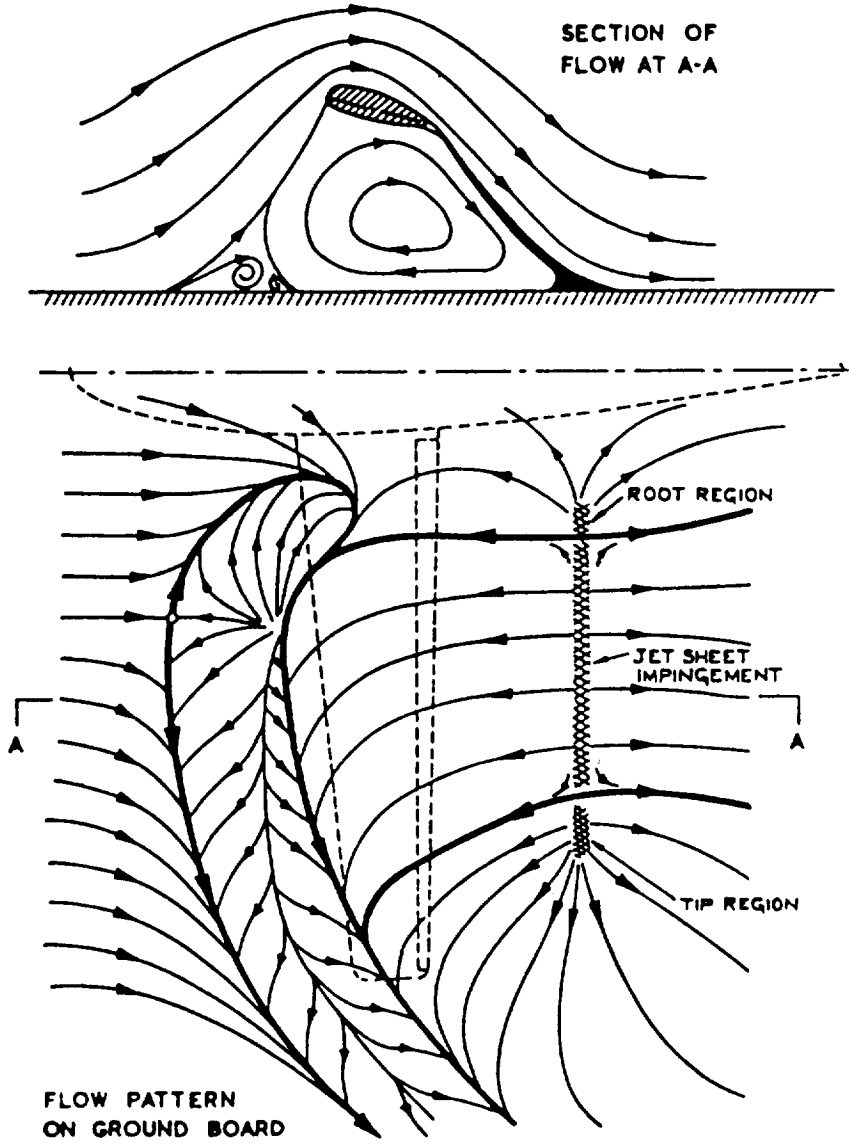

Figure 20. Jet Flap Flow (Ref. 10)

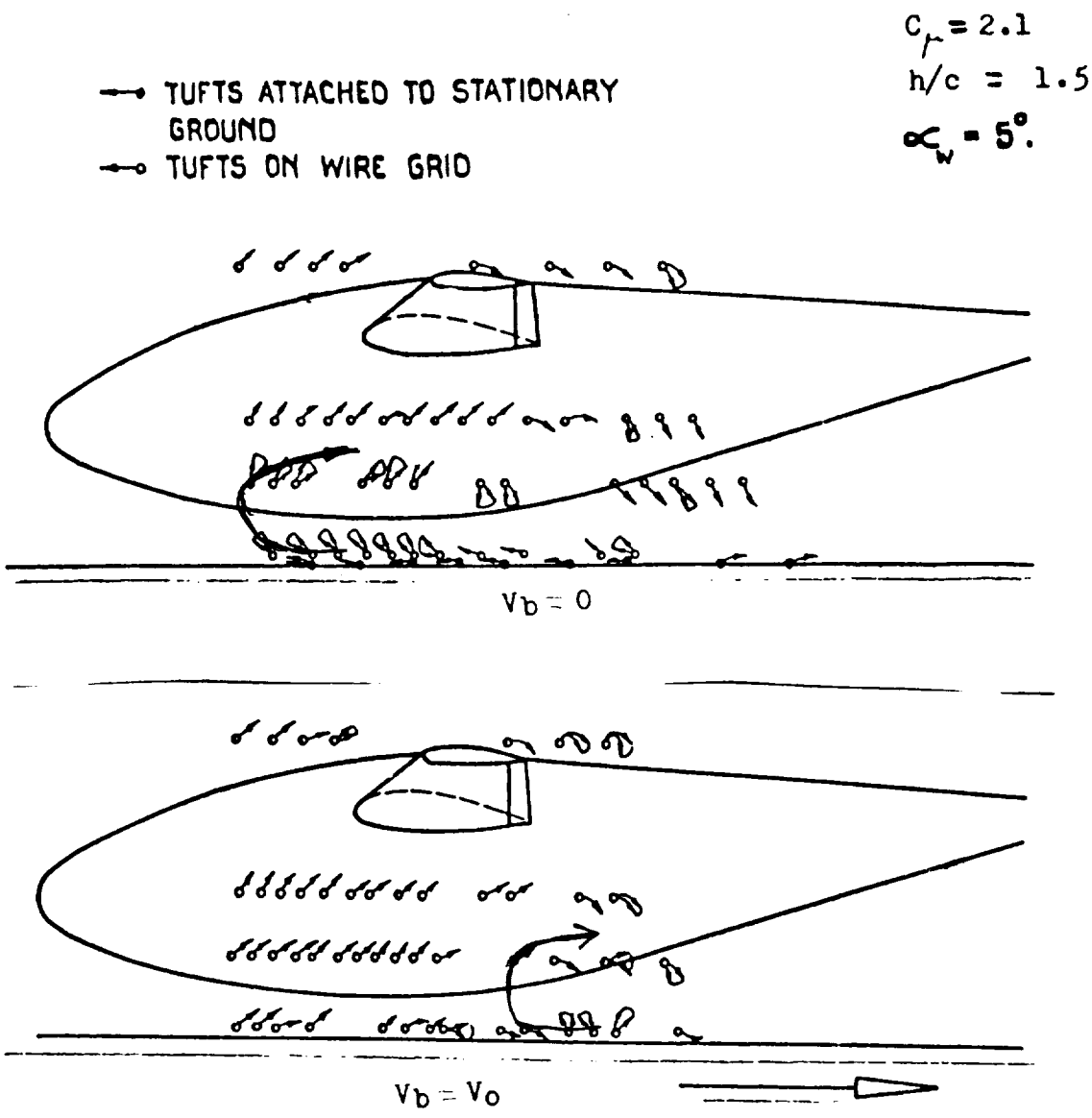

Figure 21. Effect of Moving Belt on Ground Vortex

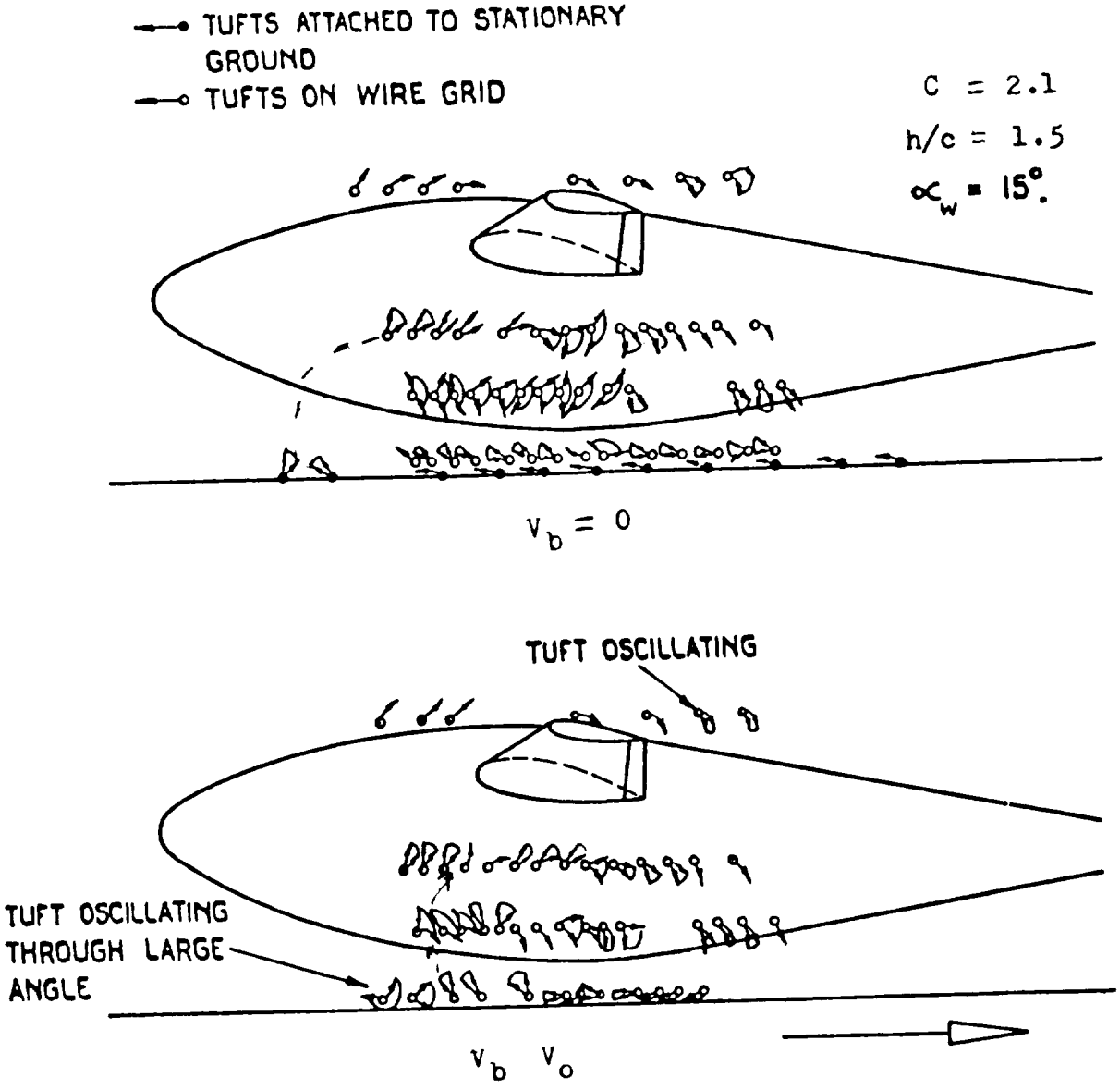

Figure 22. Effect of Moving Belt on Ground Vortex

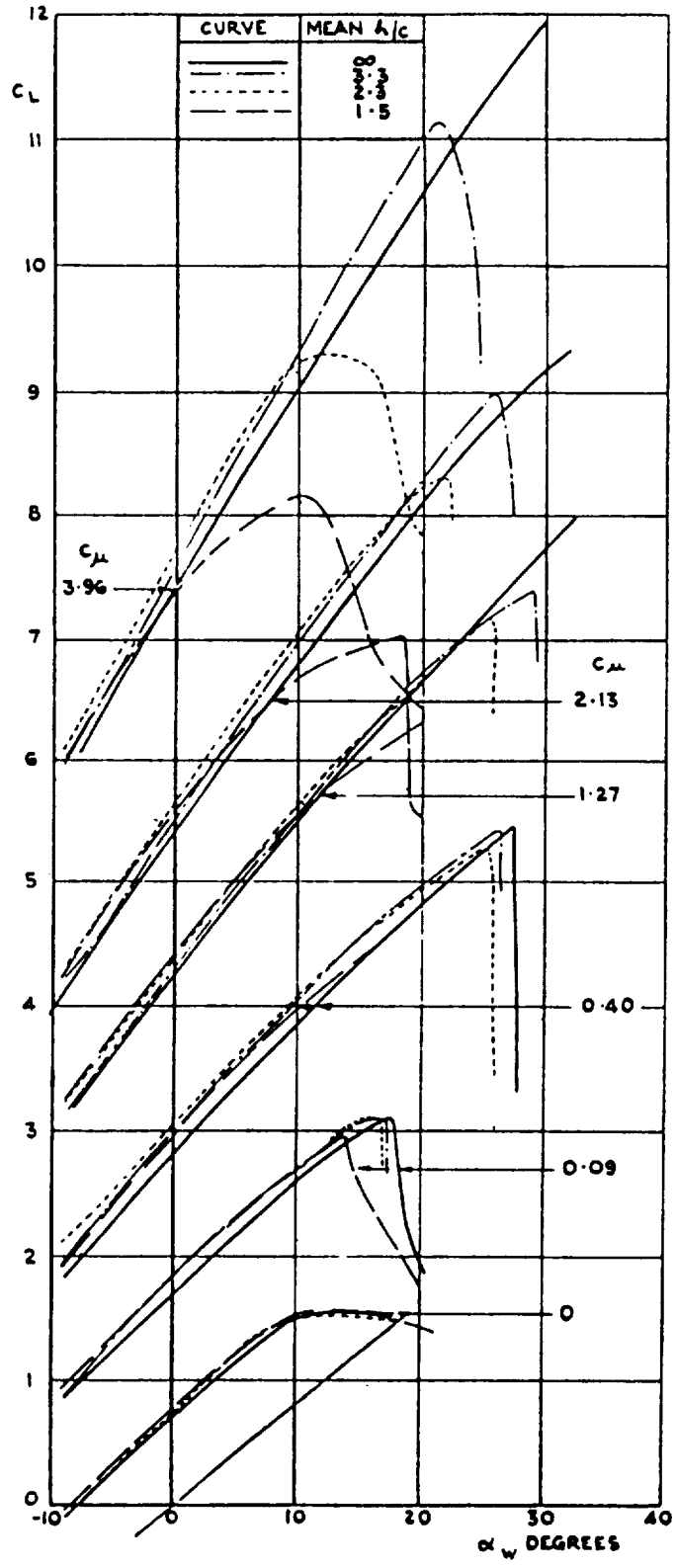

Figure 23. Effect of Ground Vortex on Lift Coefficient (Ref 10)

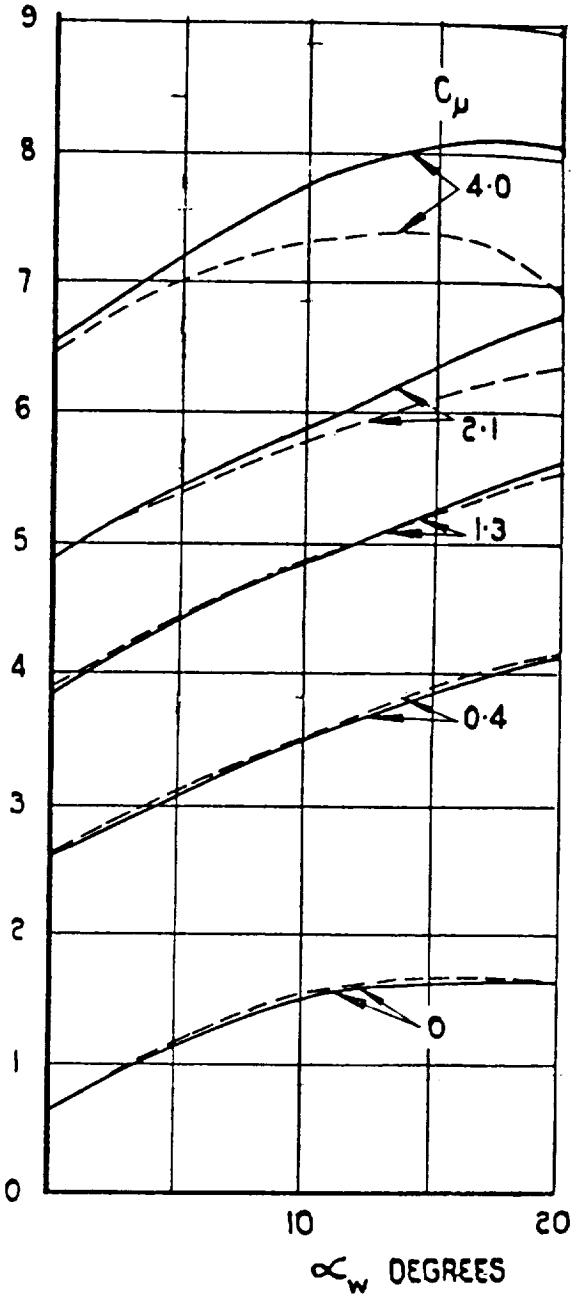

CONTROL ANGLE = 30°
(θ = 50°).

Figure 24. Effect of Moving Belt on Lift Coefficient (Ref 11)

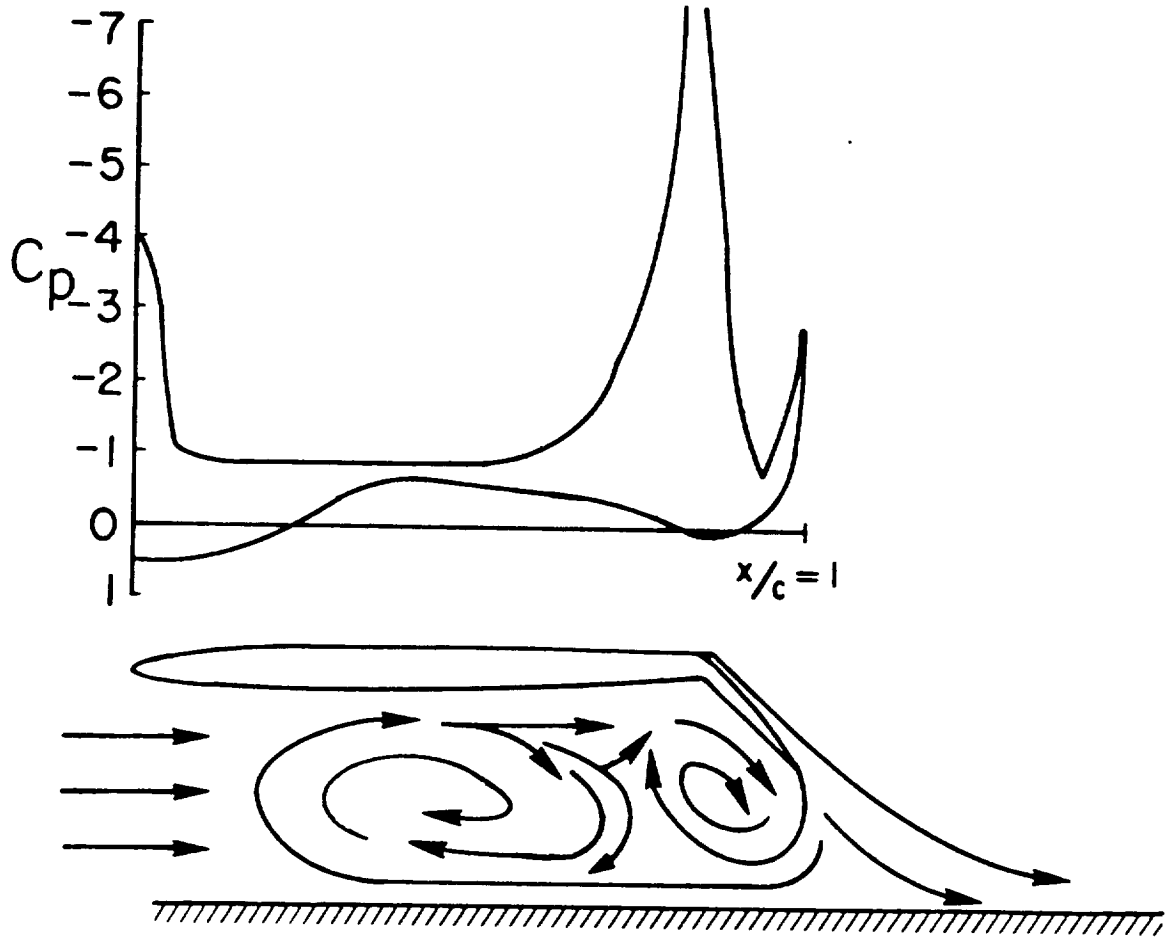

Figure 25. Pressure Distribution on a Wing with a Jet Flap

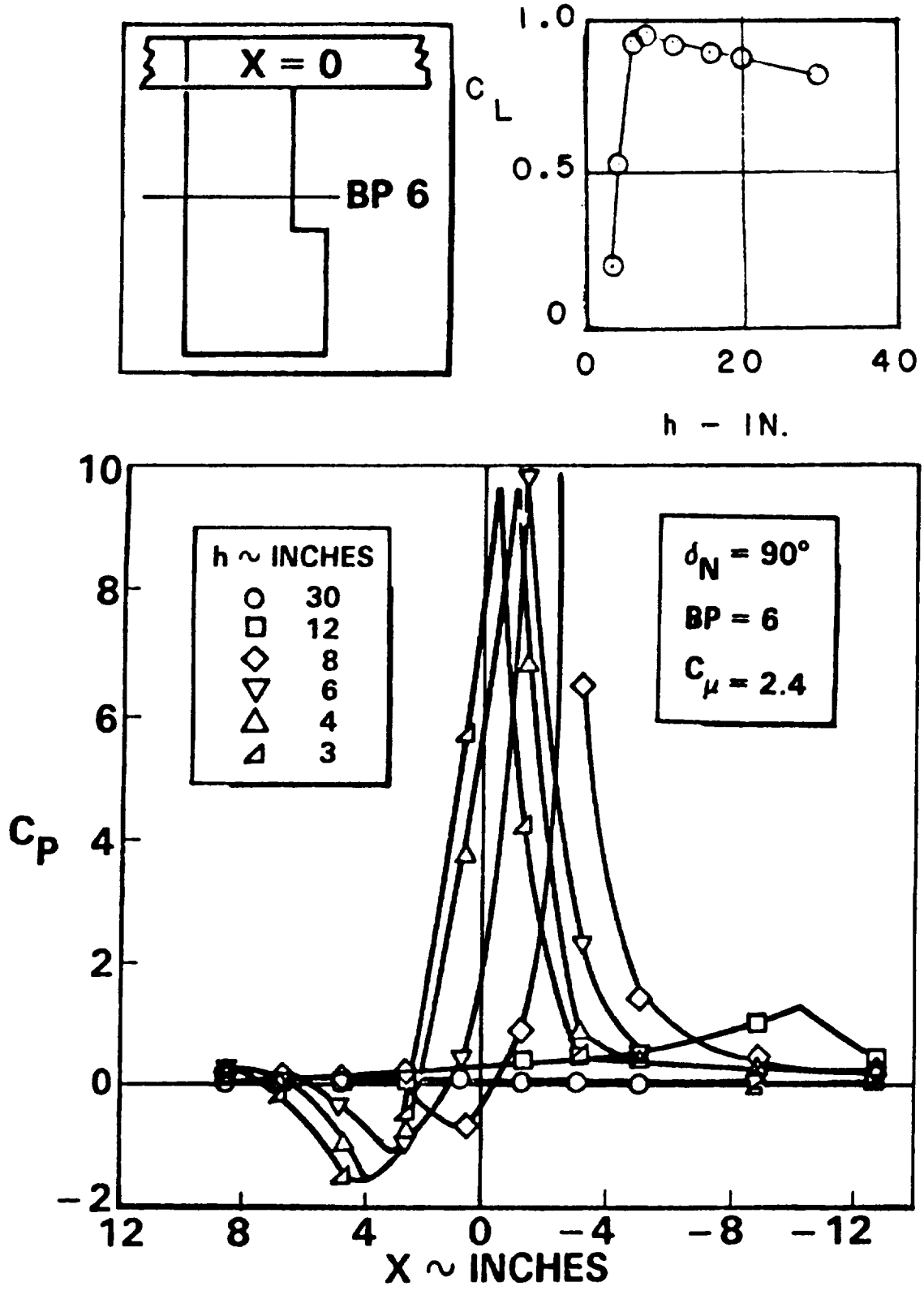

Figure 26. Ground Board Pressure Distribution, Jet Flap

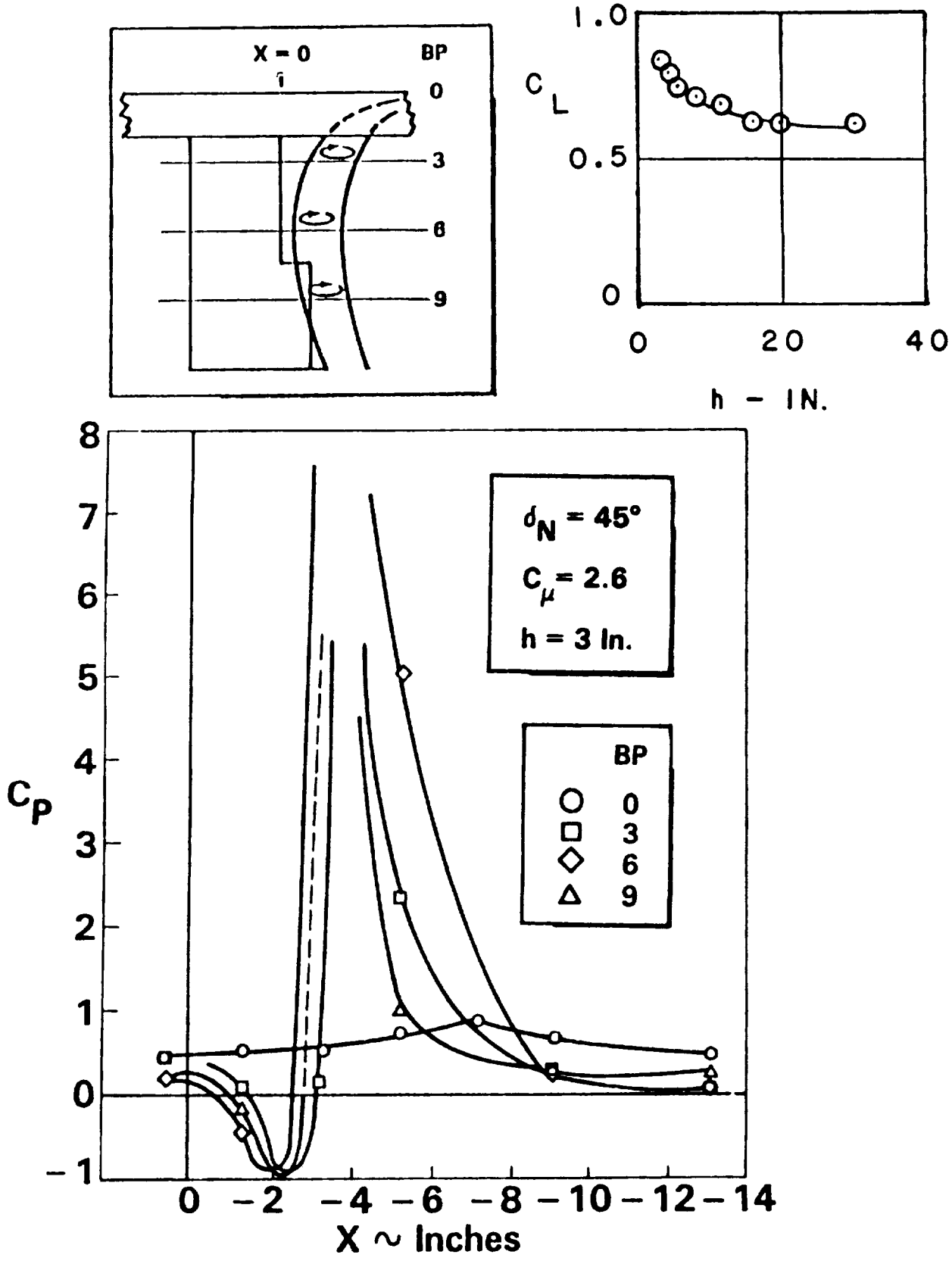

Figure 27. Ground Board Pressure Distribution, Jet Flap

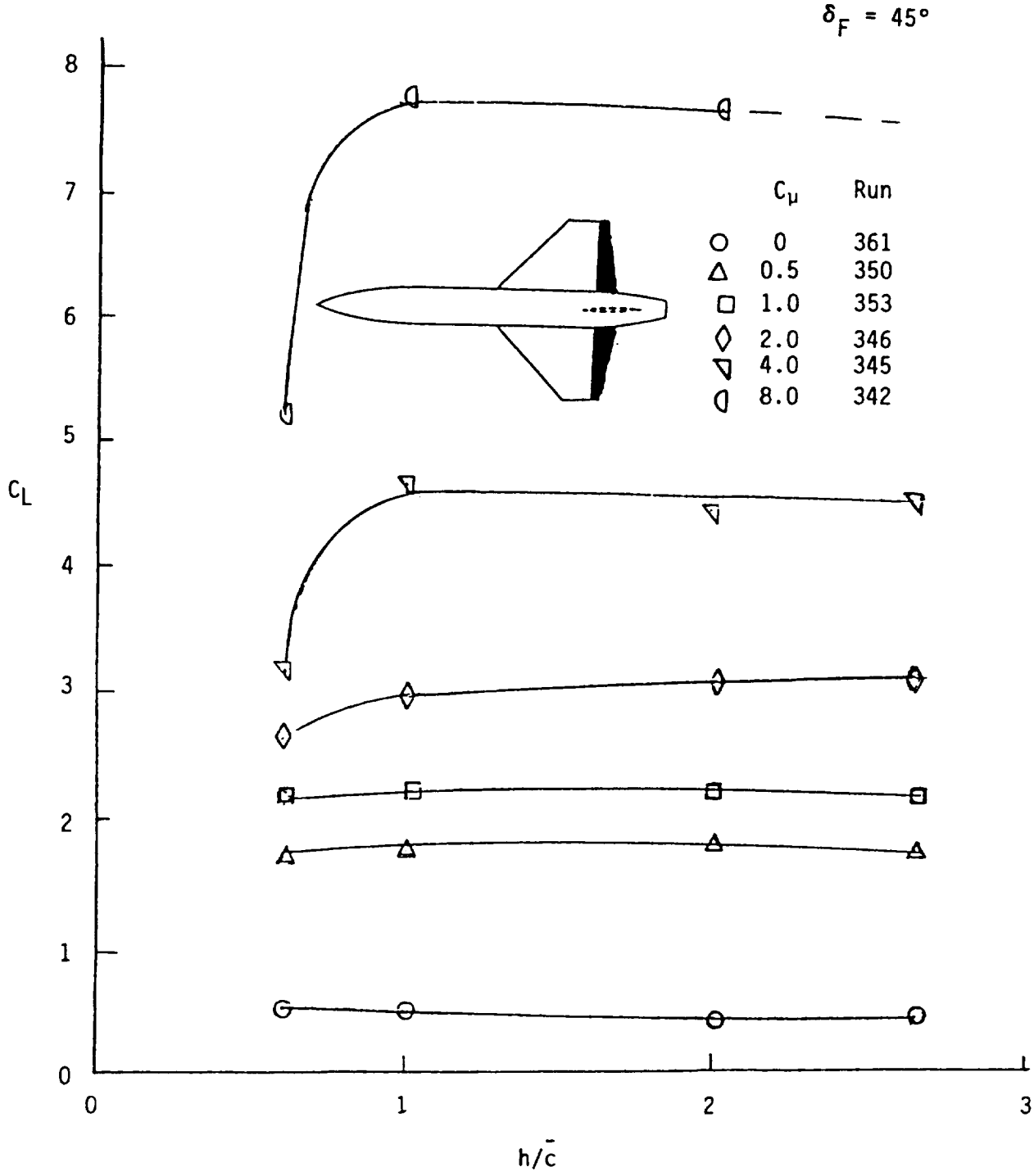

Figure 28. Effect of Ground Proximity on Lift Coefficient

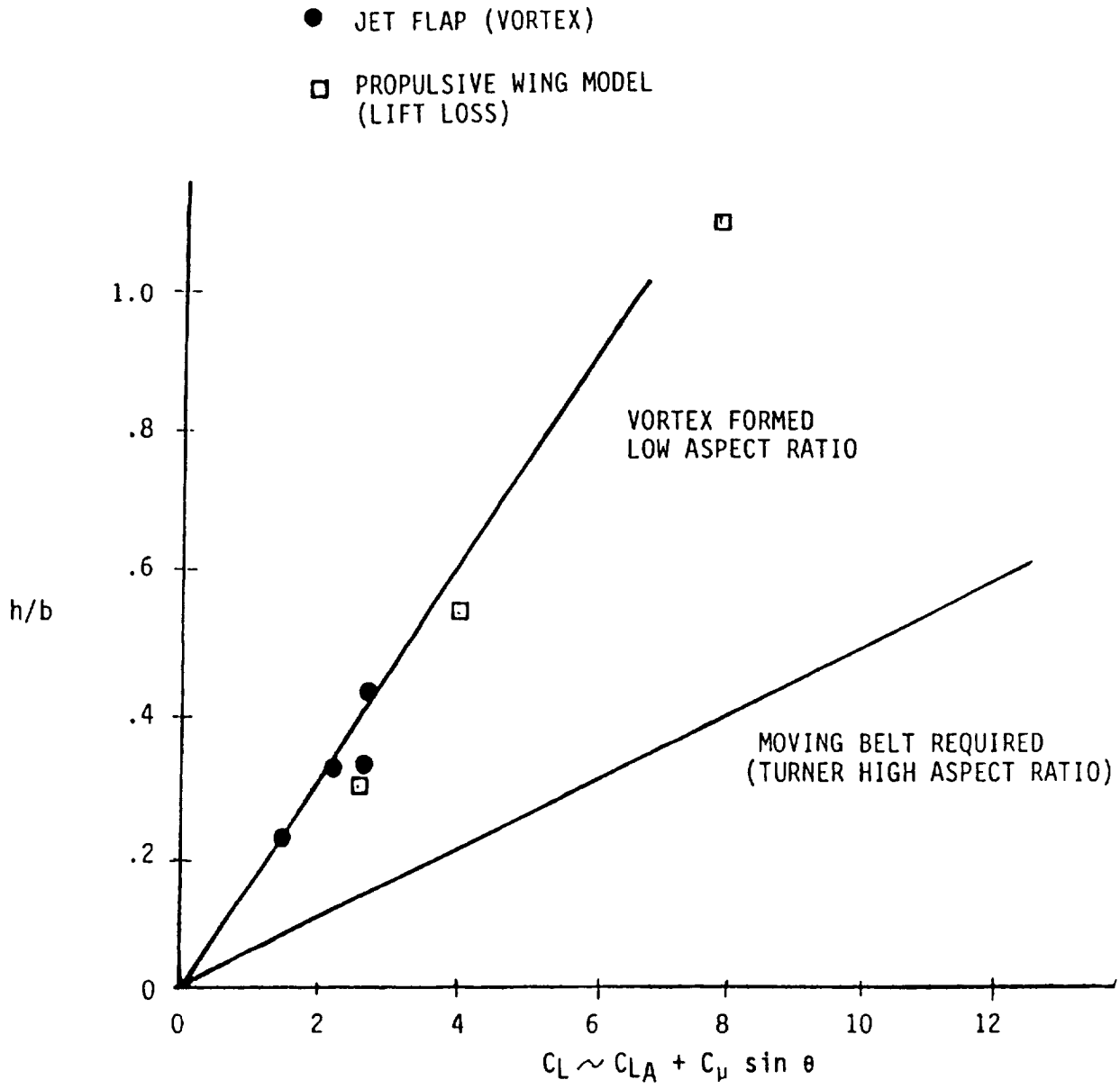

Figure 29. Requirement for a Moving Ground Board

Summary of an Experimental Investigation On the Ground Vortex

Michael L. Billet
John M. Cimbala

The Pennsylvania State University
Applied Research Laboratory
Post Office Box 30
State College, PA 16804

Introduction

The impingement of a circular jet exhaust flow on a ground plane results in the formation of a wall jet which flows radially from the point of impingement along the ground surface. Forward motion of the jet source or the introduction of a cross-flowing freestream interacts with the wall jet to create a stagnation line and tends to roll the wall jet back on itself forming a horseshoe-shaped ground vortex, as illustrated in Figure 1. Generally taking the shape of an ellipse whose major axis is aligned with the freestream flow, the location of this stagnation line is dependent on the ratio of the freestream and wall jet dynamic pressures, the distance from the jet to the ground plane, and the injection angle of the exhaust into the freestream flow. The location of the center of the vortex is downstream from this stagnation line and at a height above the ground which is also a function of the jet-to-cross-flow velocity ratio. When flow conditions are appropriate for its formation, this vortex is a major source of induced flow in the near field. Shown in Figure 2, is a side view diagram of the ground vortex and the coordinate system used.

The results of an experimental investigation into the position and characteristics of the ground vortex are summarized in this paper. The ARL/PSU 48-inch wind tunnel was modified to create a testing environment suitable for the ground vortex study. Flow visualization was used to document the jet-crossflow interaction and a two-component Laser Doppler Velocimeter (LDV) was used to survey the flowfield in detail. Measurements of the ground vortex characteristics and location as a function of freestream-to-jet velocity ratio, jet height, pressure gradient and upstream boundary layer thickness were obtained.

Test Facility

A 3.0 inch diameter open-jet facility was fabricated and inserted through one side of the test section of the 48-inch wind tunnel as shown in Figure 3. Details of the wind tunnel can be found in Reference 1. The jet features a 16:1 contraction ratio and is equipped with two wire mesh screens and honeycomb to improve the flow quality. The 150.0 ft/sec jet was powered by a variable speed 5.0 hp blower which injected air from the wind tunnel at a port far downstream from the test chamber.

The test section of the wind tunnel can be separated which permitted the horizontal jet to exhaust into the still air in the absence of any physical constraint. Velocity surveys to measure jet characteristics were conducted at 1.0, 2.0, 3.0, 4.0 and 6.0 jet diameters with V_j = 150 ft/sec. The axisymmetric jet mean velocity profiles obtained with a five-hole probe are shown in Figure 4 for the vertical plane. In addition turbulence measurements were made using a hot-wire anemometer at an axial distance of 2.0 jet diameters. The turbulence intensity at the centerline was experimentally measured to be approximately 2%.

The test chamber was formed by two 8.03 ft long wooden panels with circular arc leading edges. The jet tube extended 6.00 in. through the center of the 0.75 in. thick, 37.00 in. wide jet plane at a streamwise distance 47.0 in. downstream of its leading edge. The jet plane was at a fixed streamwise location, but could be rotated to a positive or negative angle of attack. The movable 43.0 in. wide ground plane was designed to facilitate conducting various phases of the test program. The ground plane was attached to inserts along the tunnel walls, and could be positioned at 1, 2, 3, 4 or 6 jet diameters from the jet exit plane. The ground board was also equipped with interchangeable 2.0 ft by 3.0 ft window inserts. Three windows were available for various phases of the test program, i.e., a glass flow visualization window instrumented with fluorescent mini-tufts, a glass window for LDV surveys, and a plexiglass window instrumented with static pressure taps. The leading edge of the window insert was 18.75 in. upstream of the jet centerline.

Because the wind tunnel facility is symmetric, it was possible to rotate the entire installation of Figure 3 by 90°. Both orientations (ground plane vertical and ground plane horizontal) were used in this experimental program. The vertical-ground-plane orientation was used for the preliminary measurements and surface flow visualizations, while the horizontal-ground-plane orientation was more convenient for the smoke-wire flow visualizations and detailed LDV measurements.

Wall-to-wall surveys of the velocity field between the ground plane and the jet plane were conducted with a five-hole probe to document the uniformity of the test chamber with the jet off. Figure 5 shows a typical survey at h/D_j = 2.0, and at V_∞ = 60.0 ft/s. The boundary layers on both walls can be seen from the streamwise velocity component, which is quite uniform in the core flow between the walls; the other two velocity components are negligibly small.

In addition velocity profiles of the wall jet itself were obtained with the jet on and the wind tunnel turned off. Figure 6 shows a survey obtained with the total-head boundary layer probe for V_j = 150ft/sec, h/D_j = 3.0 and the probe located 5.33 jet diameters upstream of the jet centerline. Also shown in this

figure is the theoretical wall jet profile, calculated from the semi-empirical relations found in Reference 2. The agreement between experiment and theory is excellent.

Since the entire test chamber lies within the confines of a wind tunnel test section, it is likely that when the jet is then turned on, the flow field around the jet and ground planes would be altered. This effect was studied both with flow visualization and surface static pressure measurements. These results are discussed in detail in Reference 3.

Based on these results, the following procedure was employed to establish zero pressure gradient, constant cross flow velocity between the plates upstream of the region of interest: 1). The reference cross-flow velocity was measured with a pitot-static tube located far enough upstream, between the jet and ground planes, and outside of any side wall boundary layers so as to be well within the region of zero pressure gradient (i.e. upstream of any jet effects). The probe location $x/D_j = 9.67$ was found to satisfy these requirements for all test cases. 2). The wind tunnel velocity was adjusted with the jet on, so that an accurate V_∞ and p_∞ could be established and recorded. In this manner, the blockage effect of the jet was reduced.

Summary of Experimental Results

Flow Visualization

The window instrumented with the fluorescent mini-tufts was used to obtain a first-order measurement of the ground vortex location. These data were then used to facilitate the later phases of the measurements. Surface flow visualization studies were conducted at the four values of V_∞/V_j [V_∞ = 15, 30, 45, 60 ft/sec, V_j = 150 ft/sec] and the five h/D_j locations [h/D_j = 1.0, 2.0, 3.0, 4.0 and 6.0]. The primary data obtained were photographs of the resulting flow patterns and the location of the separation line and the maximum penetration line of the recirculation region on the ground board. The quantities x_s, x_i, and x_{mp} were measured from the centerline of the jet tube and were determined by both real time observation of the mini-tuft pattern and later analysis of the photographs.

The impingement point x_i was easily identified from the photographs as the point from which the tufts spread out radially. The separation line was determined from the photographs as the line where the mini-tufts change orientation from upstream to downstream. Separation point x_s is defined here as the distance upstream from the jet centerline to this separation line. The leading edge or maximum penetration line is defined as the location upstream of which the mini-tufts align themselves parallel to the cross flow. Maximum penetration point x_{mp} is defined as the streamwise distance from this line to the jet centerline.

A comparison between the location of the separation point defined from the photographs and obtained from plate pressure distribution data is shown in Figure 7. The accuracy of the photographic data is $\pm$ 0.25 jet diameters which corresponds to $\pm$ 1 mini-tuft spacing. A discussion of the pressure distribution data is given in a following section.

In addition to the surface flow visualizations, smoke-wire photographs provided instantaneous views of the ground vortex itself. Again, photographs were taken for the various combinations of h/D_j and V_∞/V_j. Figure 8 shown the smoke streakline pattern for $h/D_j = 2.0$. It is important to note that the jet tube protruded two jet diameters down from the jet plane, and therefore the total height between ground and jet planes was four jet diameters. It is clear that the ground vortex decreases in size and moves further downstream as the cross flow velocity increases. It appears that very little of the freestream fluid enters the ground vortex; the freestream apparently jumps over the vortex, much as it would over a solid body obstruction in the flow. As will be discussed below, velocity measurements have shown that the ground vortex is really not a vortex at all, but rather a region of separated recirculating flow. The "ground vortex" is thus more properly referred to as a separation bubble.

Note that photos a) and b) of Figure 8 were taken for identical test chamber conditions, but at different times (about a minute apart). Comparing the two, one can see the unsteadiness in the flow pattern. Both photos are instantaneous snap shots, and therefore have "frozen" the motion at one arbitrary point in time. The flow field captured in photo a) contains one large separation bubble, while that of photo b) appears to contain two separation bubbles.

Pressure Distributions

One of the interchangeable window inserts on the ground plate was instrumented with an array of 72 static pressure taps. The time-averaged static pressure distribution along the ground plane was measured for each combination of h/D_j and V_∞/V_j. The maximum resolution of a single pressure survey was limited to the distance between pressure taps in the array; however, the resolution was enhanced by shifting the ground plane by small amounts in the streamwise direction, with the jet location remaining fixed.

Figure 9 shows a typical smoothed static pressure distribution along the centerline of the ground plane for the case $h/D_j = 3.0$ and $V_\infty/V_j = 0.2$ The impingement point x_i of the jet is easily identified as the point of maximum C_p. Moving upstream (left to right in Figure 9) the pressure coefficient drops to a negative value, rises again above zero, and then slowly returns to zero far upstream. Colin and Olivari [2] have identified the negative C_p region as the approximate location of the ground vortex, with x_v the vortex center at the minimum C_p point. The zero-crossing point has been labeled x_s on Figure 9 and has been found to correspond to the separation point identified by the mini-tuft surface flow-visualization technique. Similar pressure distributions along the centerline of the ground plane have been taken for various values of h/D_j and V_∞/V_j. The zero-crossing point is compared in Figure 7 to the separation point determined from the mini-tuft photographs. The agreement is excellent except for the lowest velocity case ($V_\infty/v_j = 0.1$).

The static pressure tap array was also used to obtain pressure distributions along the ground plane at points away from the centerline. Seven streamwise rows of taps were instrumented, and labeled rows A-G with G being the centerline row. Each row was 1.5 in. (0.5 jet diameters) apart in the z-coordinate direction. A typical set of transverse pressure distributions is shown in Figure 10 for the

case h/D_j = 3.0 and V_∞/V_j = 0.2. The "horseshoe" shape of the separation bubble can be inferred from this figure; i.e. dip in the pressure distribution upstream of impingement shifts downstream and decreases in magnitude as one moves further and further away from the centerline.

Laser Doppler Velocimeter Measurements

A schematic of the instrumentation for the Laser Doppler Velocimetry tests is presented in Figure 11. A two-component LDV system was used to survey the region upstream of the jet perpendicular to the ground plane centerline. The system was positioned using a three-axis traversing mechanism.

A smoke generator shown in Figure 11, which burns 'Punk' incense sticks, was used to seed the flow. A sample of the smoke was collected in a millipore filter; the size of the smoke particles was under 1 μm as determined with a scanning electron microscope. The seeding smoke was introduced into the flow through four ports located along the centerline of the ground plane. Two ports were selected for introducing seeding material into the jet flow and two parts for seeding the freestream.

Histograms of the velocity distribution at each point were obtained and analyzed statistically. A representative vector plot showing mean data is given in Figure 12 for V_∞/V_j = 0.2, and h/D_j = 4.0. A sample histogram is shown in Figure 13 for a point near the center of the vortex.

As can be noted in Figure 13, the flow within the ground vortex is extremely unsteady; however, the vector plot provides a visualization of the mean flow. For all cases measured, the cross-section through the ground vortex has an elliptical shape. It can also be noted that the flow is separated upstream of the vortex. The jet flow along the plate decreases and eventually reaches zero upstream of the vortex.

Discussion

A comparison with experimental data is shown in Figure 14 with the predicted curve of Colin and Olivari [2] and the model of Abbott [4]. The best comparison is obtained with the model of Abbott [4]. Abbott [4] showed that his data collapsed universally to the simple expression that the wall jet penetrates upstream to a point where, under stationary conditions, the maximum velocity of the wall jet would be approximately twice that of the oncoming freestream.

Unsteadiness in the flow field was observed, particularly at the lower values of V_∞/V_j. As discussed above, two instantaneous snap shots of the separation bubble, taken at different times, can appear drastically different, even for identical configurations and velocities. A most striking example of this is shown in Figure 8, for h/D_j = 2.0 and V_∞/V_j = 0.1. A likely candidate for the source of this unsteadiness is the amplification of shear layer vortices shed from the lip of the jet. These shear layer vortices can be most clearly seen in photo a) of Figure 8. It appears that the vortices convect upstream along the wall, and then fold back around the separation bubble. As they convect back toward the jet, the vortices may be amplified to the point of sudden bursting, which disrupts the entire flowfield.

Conclusions

A test facility suitable for the study of the ground vortex resulting from a jet impinging on a ground plane in the presence of a cross flow has been developed. Tests have defined the aerodynamic characteristics of the test chamber, the ground plane static pressure distributions, and flow patterns associated with the ground vortex. A summary of findings is listed below, not all of which have been discussed here; further details can be found in Reference 3:

1) For a given jet-exit-to-ground-plane height h/D_j, the ground vortex moved downstream and decreased in size and strength as freestream-to-jet velocity ratio V_∞/V_j was increased.

2) The separation point x_s of the wall jet on the ground plane was measured with both fluorescent mini-tuft surface flow visualization and static pressure measurements on the ground plane; agreement between the two techniques is excellent. Namely, the separation point corresponds to the zero-crossing point of the static pressure distribution.

3) The addition of a large flat plate, flush-mounted to the jet exit plane, forced the ground vortex to move downstream significantly and to decrease in size.

4) Within the limited range of pressure gradients obtainable with the present experimental setup, only a small effect of streamwise pressure gradient was found. There was a tendency for the separation point to move upstream with increasing pressure gradient.

5) Artificial thickening of the oncoming boundary layer on the ground plane resulted in further upstream penetration of the wall jet, but the effect was not as great as anticipated. Differences in boundary layer thickness are therefore not sufficient to account for the large scatter in data from various experimenters. Further differences, such as the jet and ground plane motion need to be explored.

6) The present experimental data for separation point location do not agree with the theory or measurements of Colin and Olivari [2], but agree fairly well with the empirical relationship suggested by Abbott [4].

7) LDV surveys indicate that the ground vortex is elliptical in shape, and does not have a velocity field describable by a classical free vortex. The ground vortex is thus really not a vortex at all, but rather a recirculating separation bubble, driven by the opposing wall jet and freestream flows.

8) Unsteadiness was observed in the separation bubble, particularly at the smaller values of V_∞/V_j (~0.1). It is conjectured that these fluctuations may be related to large-scale coherent vortical structures shed from the lip of the jet. No attempt was made to quantify this phenomenon, but should be considered during future experimentation.

References

1. "Garfield Thomas Water Tunnel Test Facilities," Applied Research Laboratory, The Pennsylvania State University, January 1980.

2. Colin, P. E. and Olivari, D., "The Impingement of a Circular Jet Normal to a Flat Surface With and Without a Cross Flow," Von Karman Institute Final Technical Report, January 1969, United States Defense Technical Information Center Technical Report AD688953.

3. Cimbala, J. M., Stinebring, D. R., Treaster, A. L., and Billet, M. L., "Experimental Investigation of a Jet Impinging on a Ground Plane in the Presence of a Cross Flow," Naval Air Development Center, Contractors Report NADC-87019-60, March 1987.

4. Abbott, W. A., "Studies of Flow Fields Created by Vertical and Inclined Jet When Stationary or Moving Over a Horizontal Surface," RAE CP No. 911, 1967.

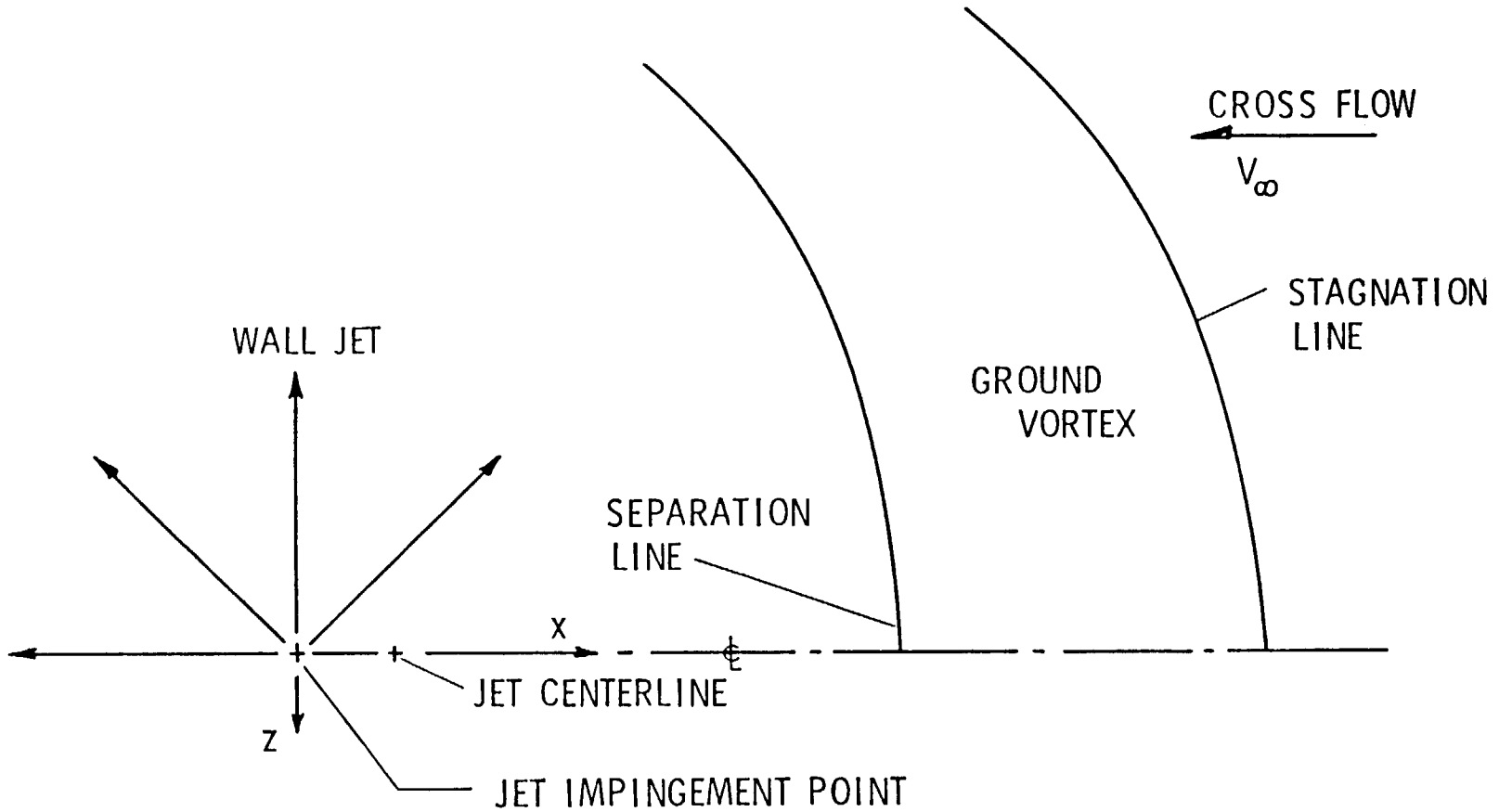

Figure 1. Horseshoe-Shaped Stagnation Line on Ground Plane (Plan View).

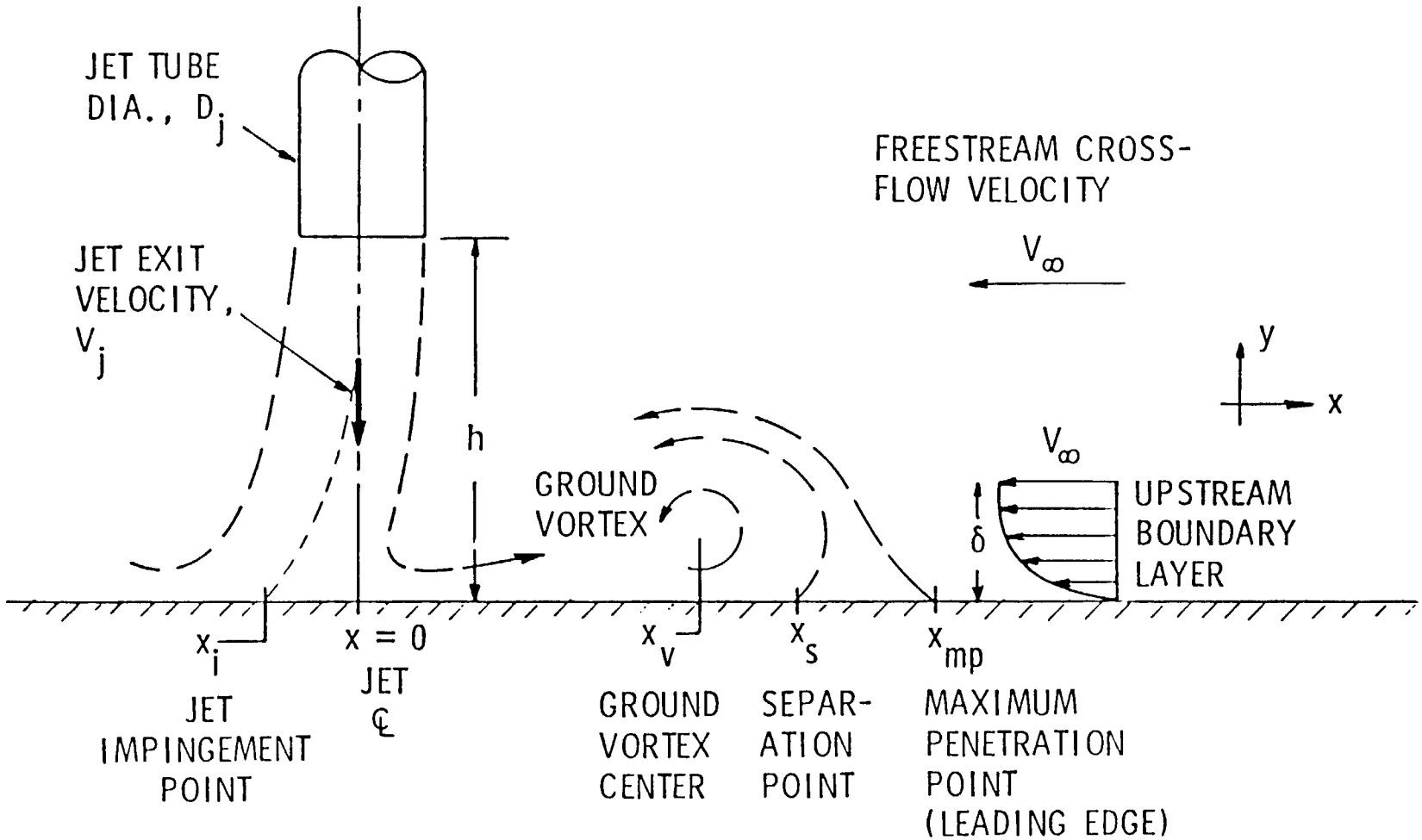

Figure 2. Ground Vortex Formed by a Jet Impinging Normally on a Flat Plate in a Cross Flow.

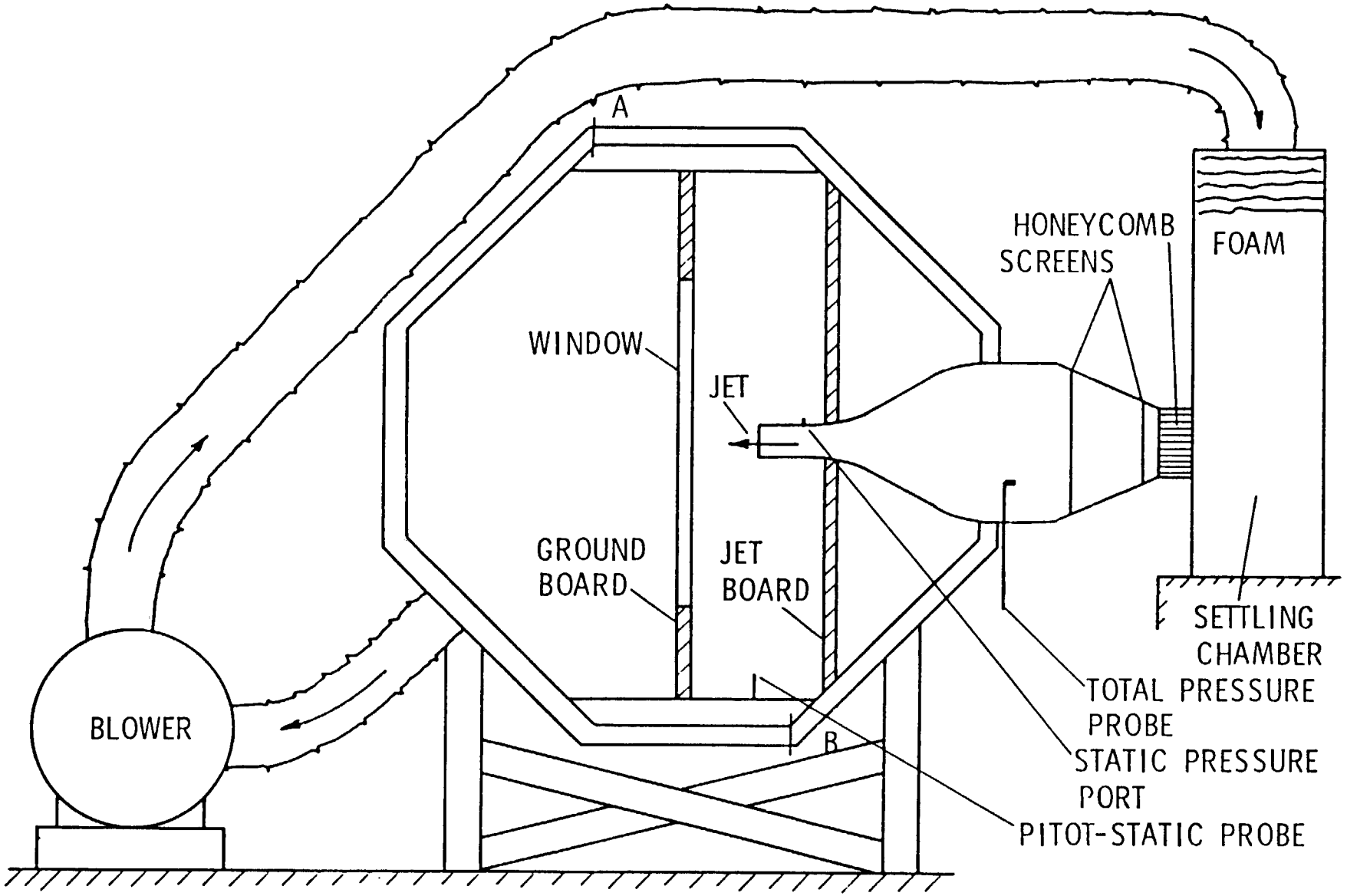

Figure 3. Jet Installation in Wind Tunnel (Vertical Ground Plane).

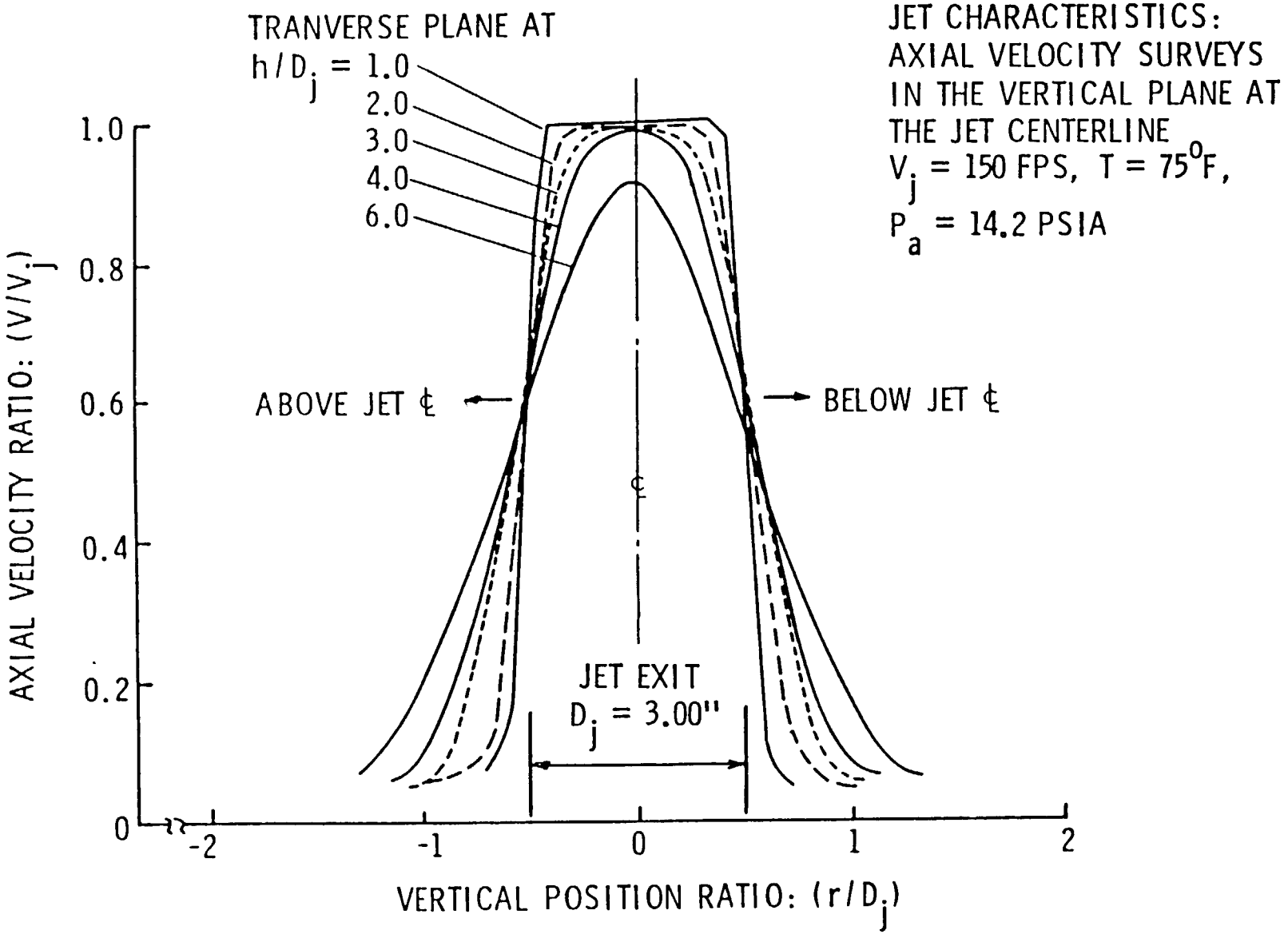

Figure 4. Jet Characteristics - Mean Velocity Surveys.

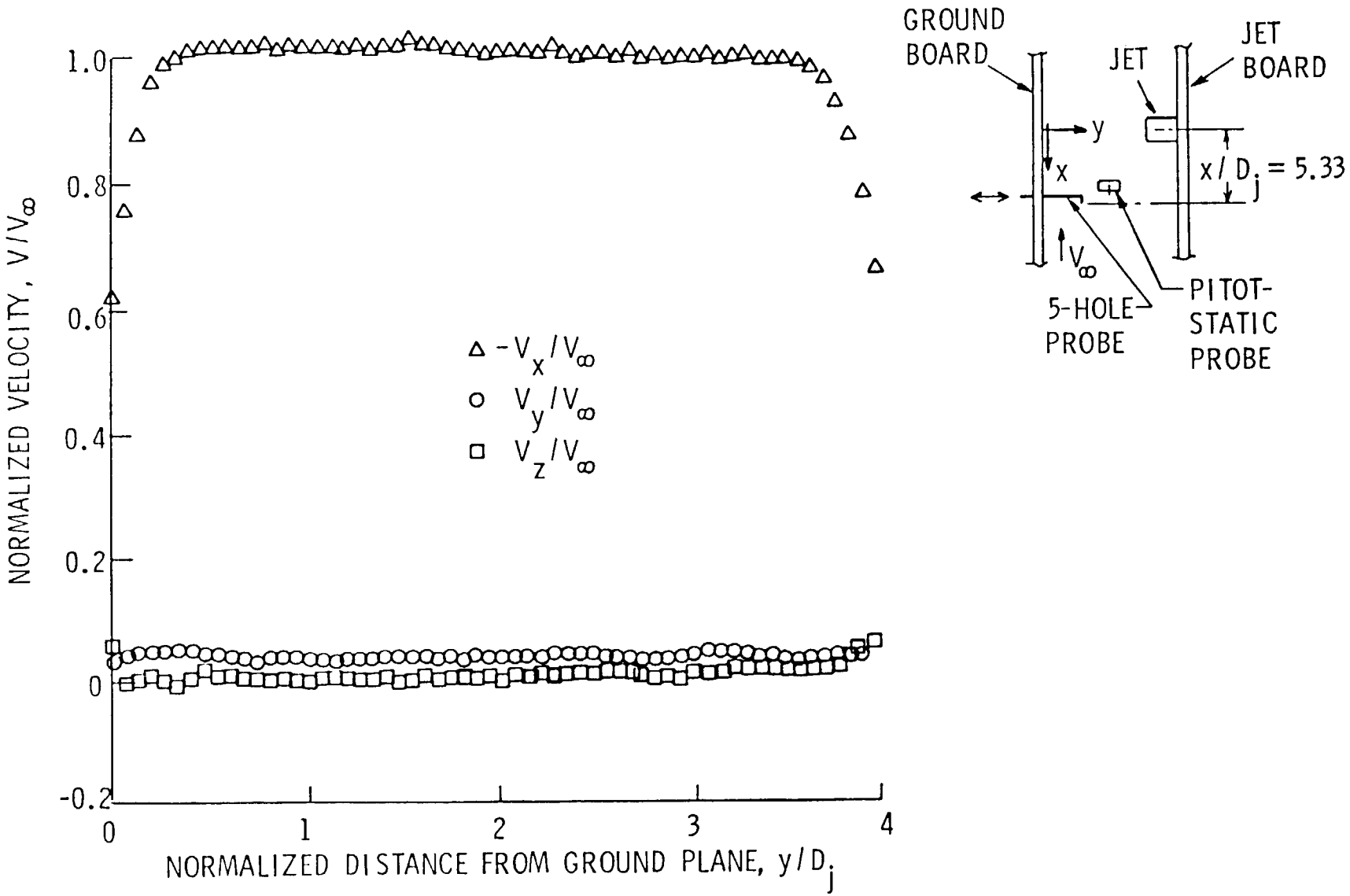

Figure 5. Test Chamber Velocity Survey at h/D_j = 2.0, and at V_∞ = 60.0 ft/s (18.3 m/s) with Jet Turned Off.

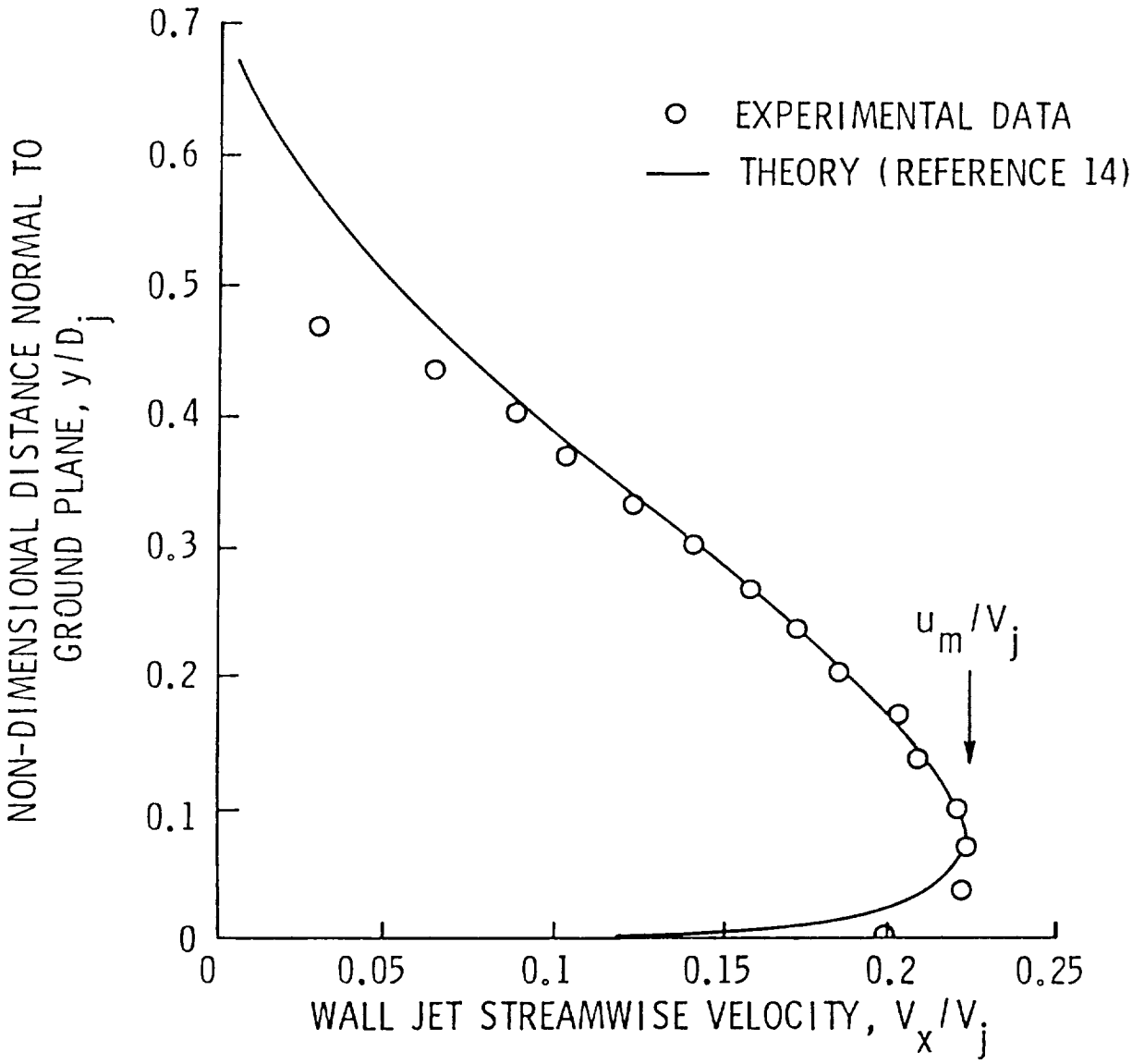

Figure 6. Wall Jet Velocity Profile at $h/D_j = 3.0$, $x/D_j = 4.8$, with Jet Velocity $V_j = 150$ ft/s (45.7 m/s), and No Cross Flow.

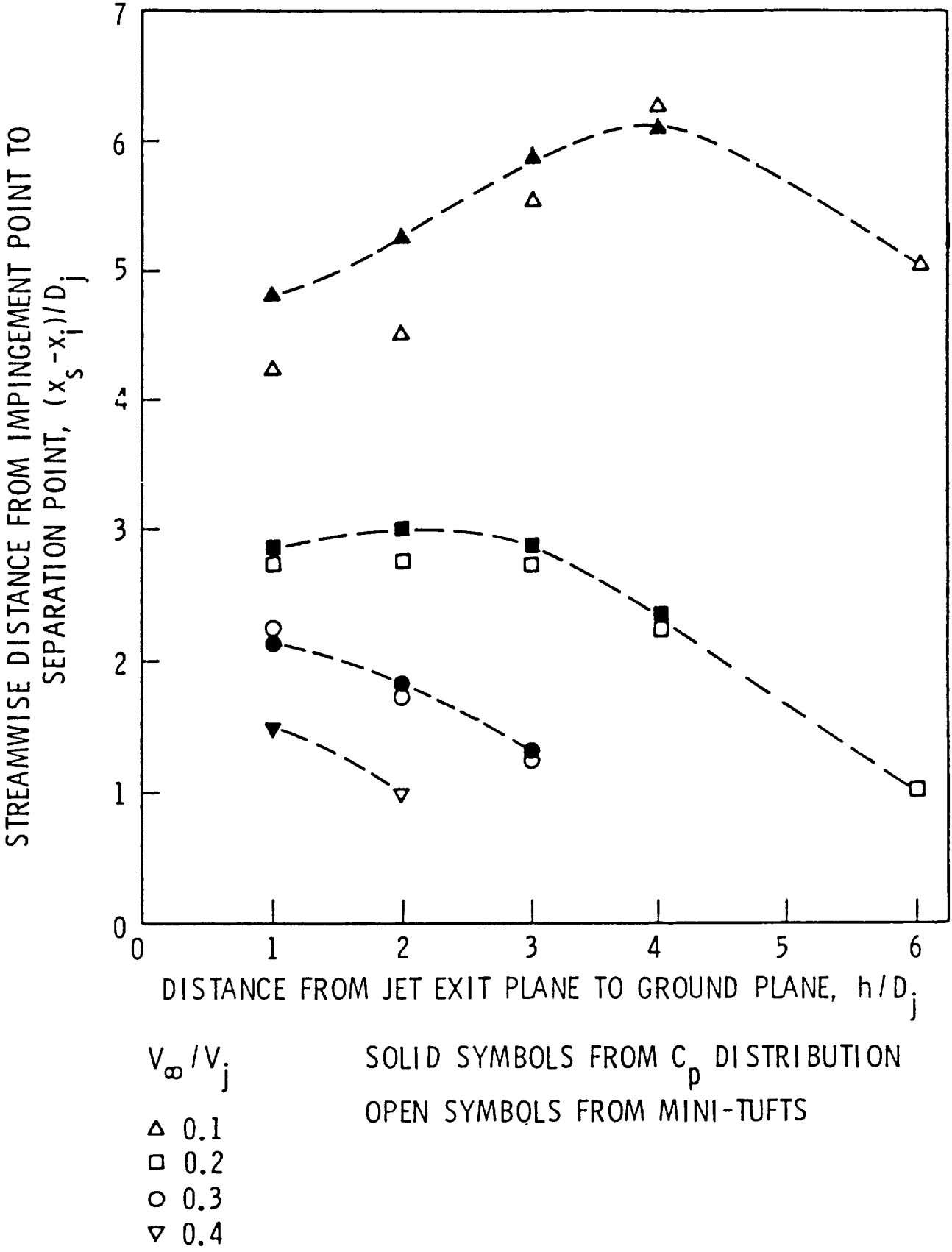

Figure 7. Measurement of Separation Point Location as a Function of Ground-Plane-to-Jet Distance for Four Velocity Ratios.

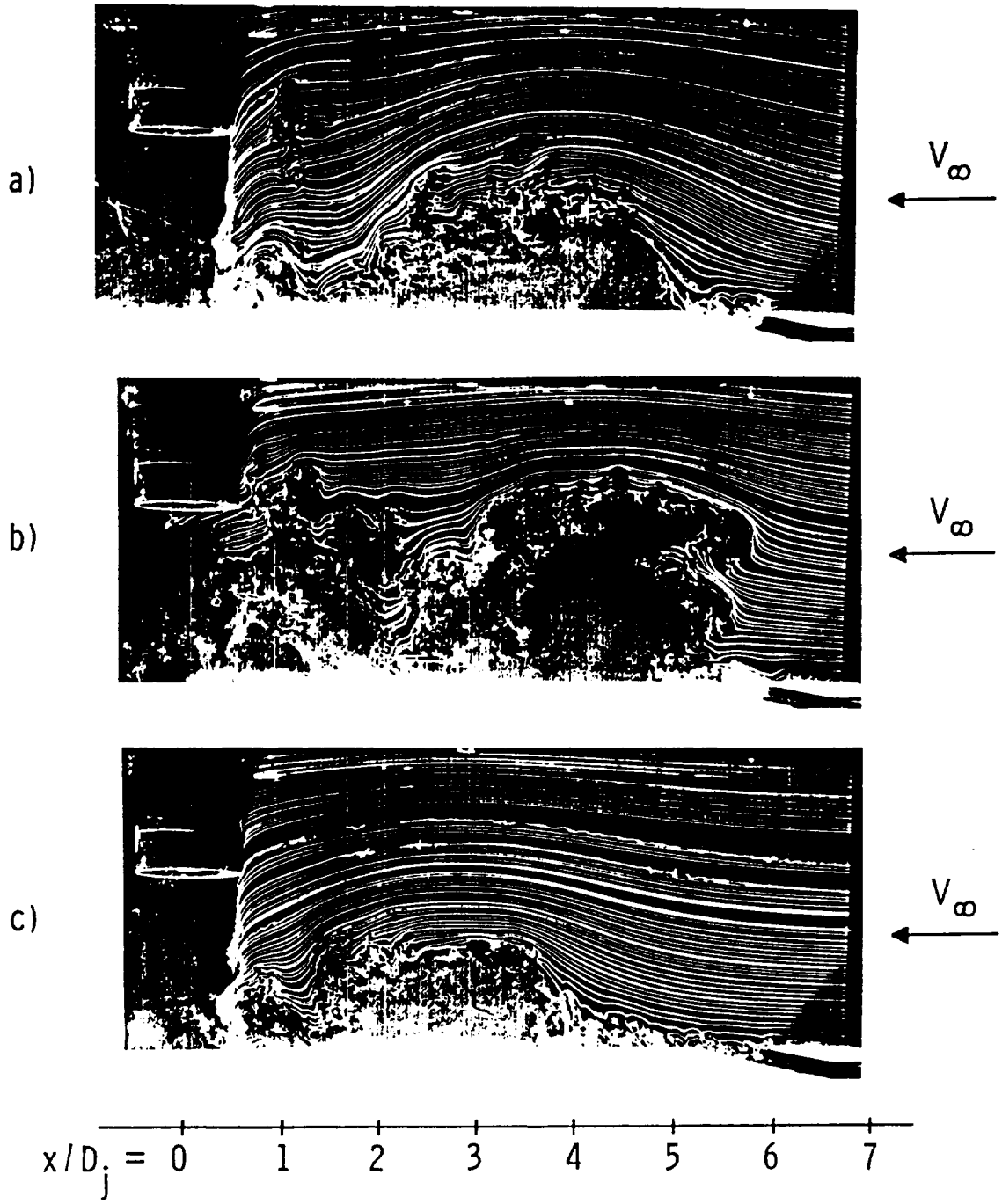

Figure 8 . Smoke-wire Photographs of Separation Bubble for h/D_j = 2.0, Standard Configuration, V_∞/V_j = a) 0.1, b) 0.1, c) 0.15, d) 2.0, e) 0.25, and f) 0.30. (Photos a) and b) are for identical conditions, but different times, and illustrate the unsteadiness.)

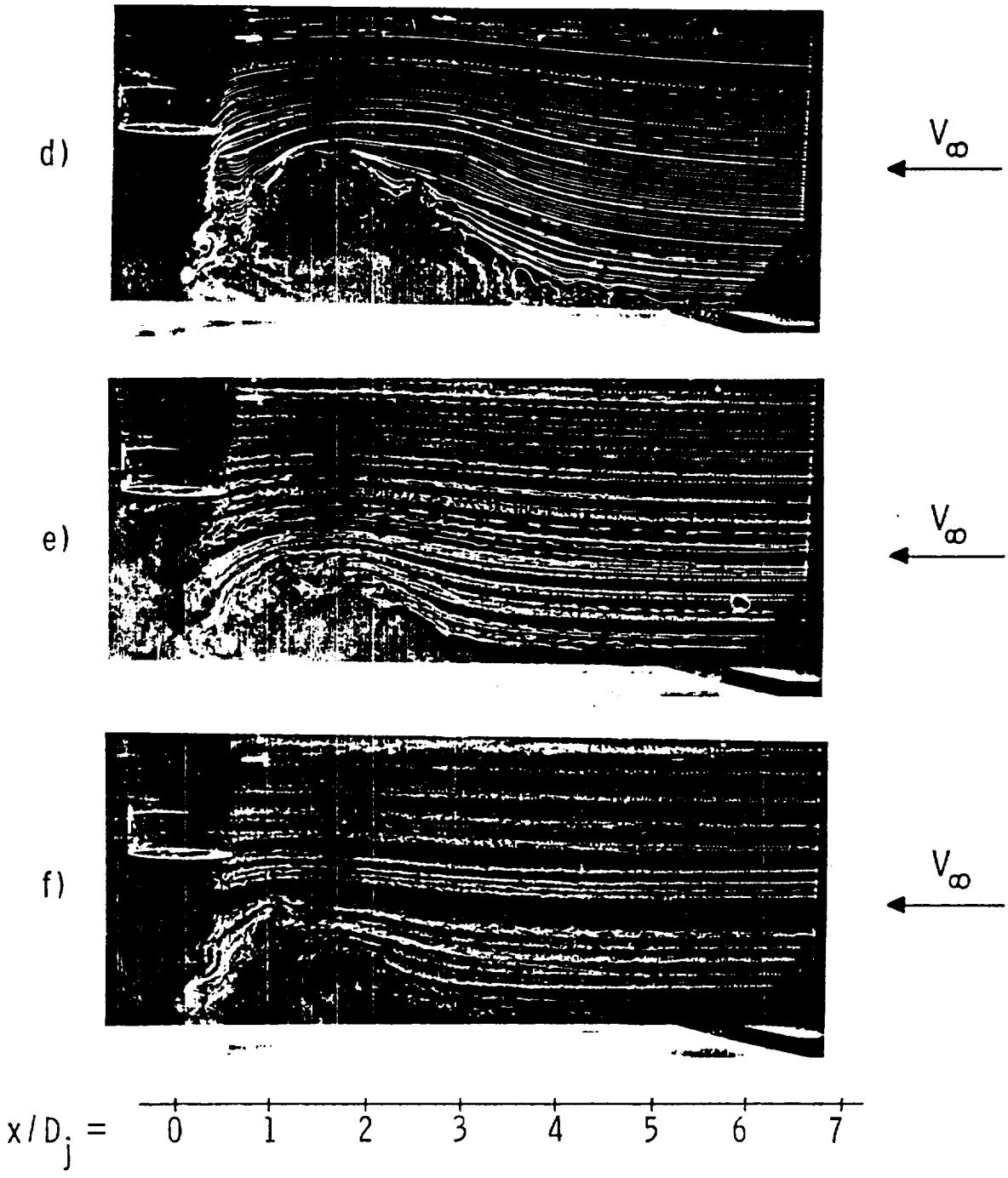

Figure 8. (Cont.)

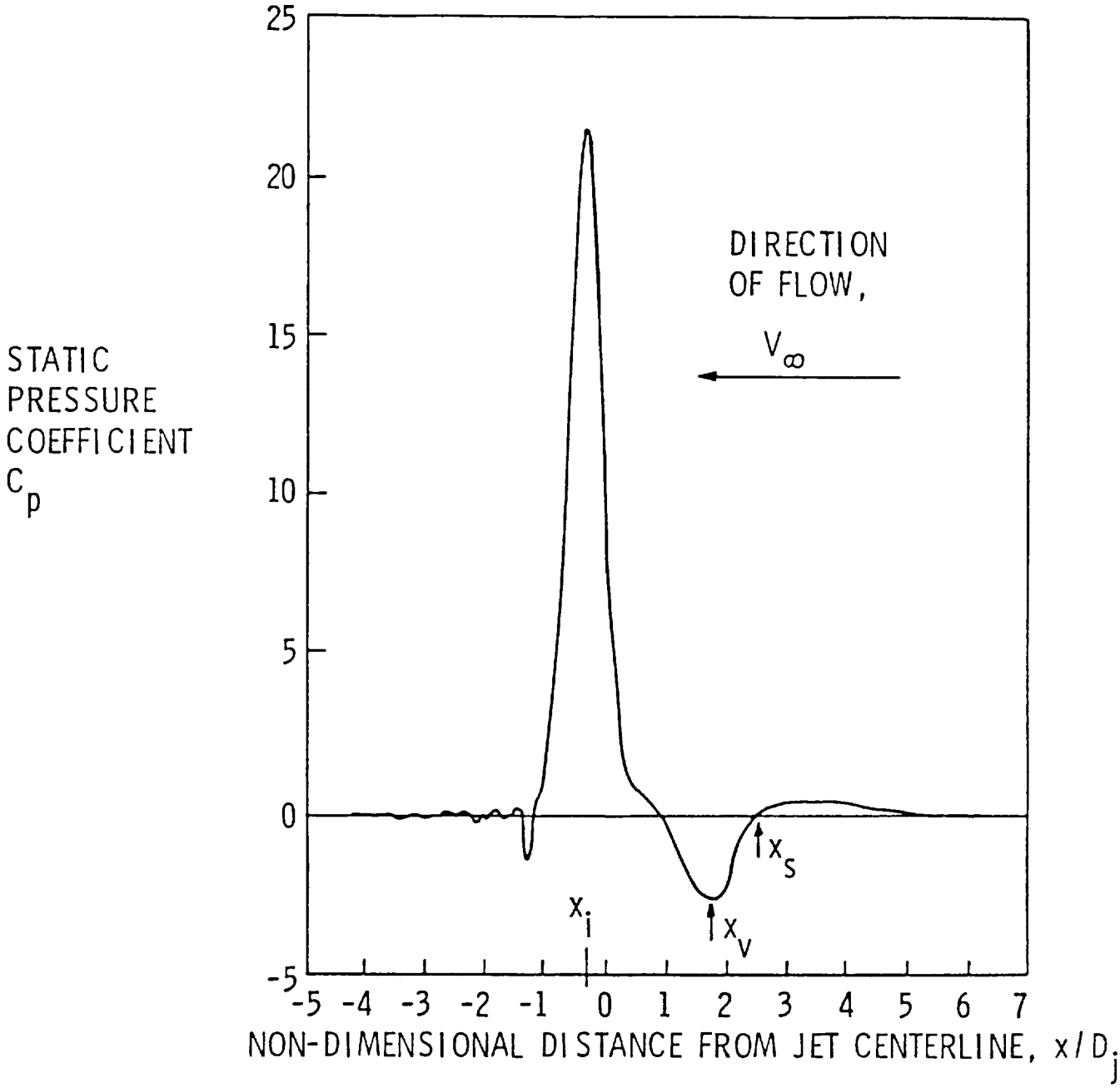

Figure 9. Static Pressure Coefficient Distribution Along Centerline of Ground Plane for $h/D_j = 3.0$, $V_\infty/V_j = 0.2$

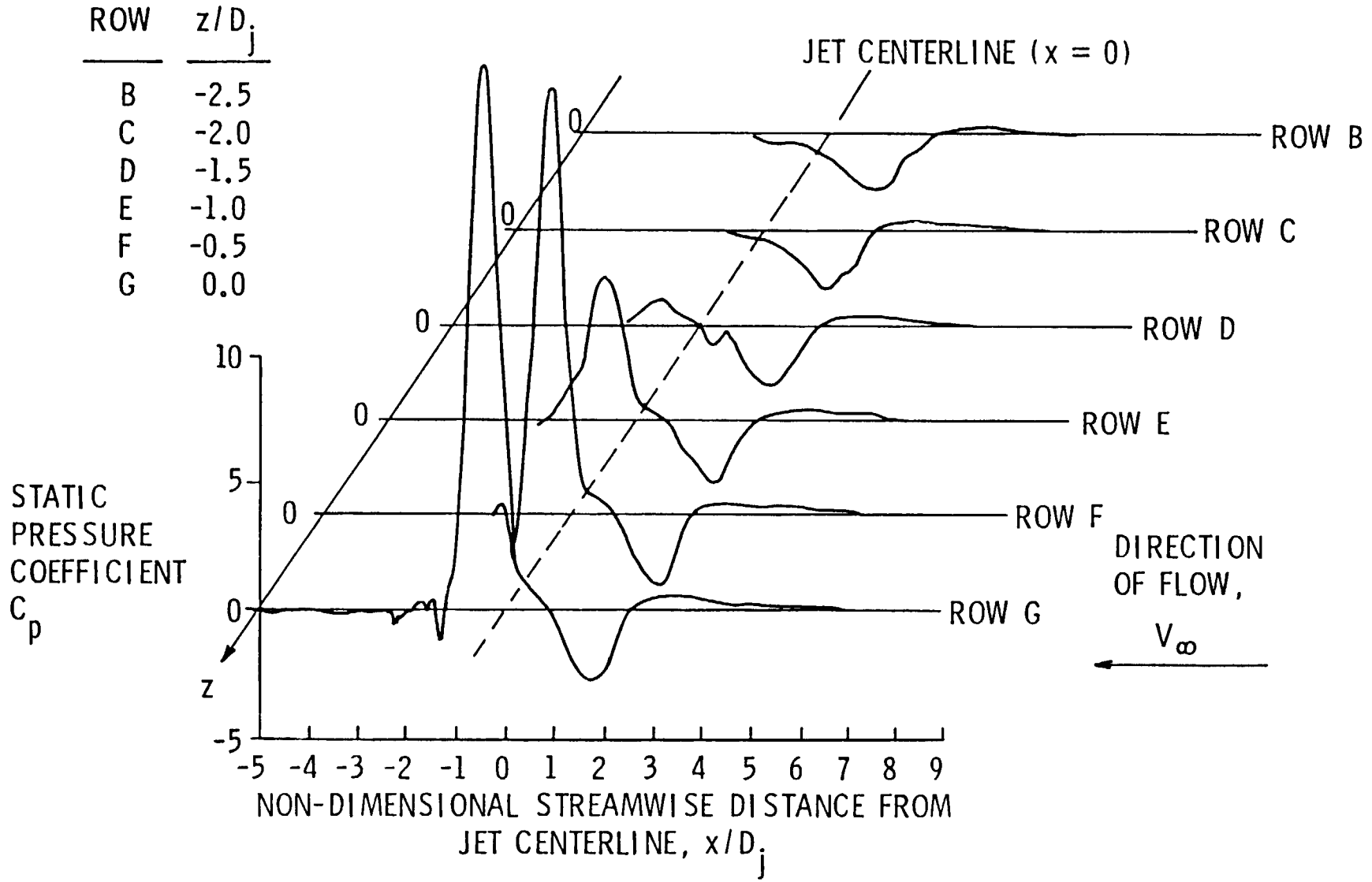

Figure 10. Static Pressure Distribution Along the Ground Plane as a Function of Streamwise and Transverse Distances from the Jet Centerline, $h/D_j = 3.0$, $V_\infty/V_j = 0.2$

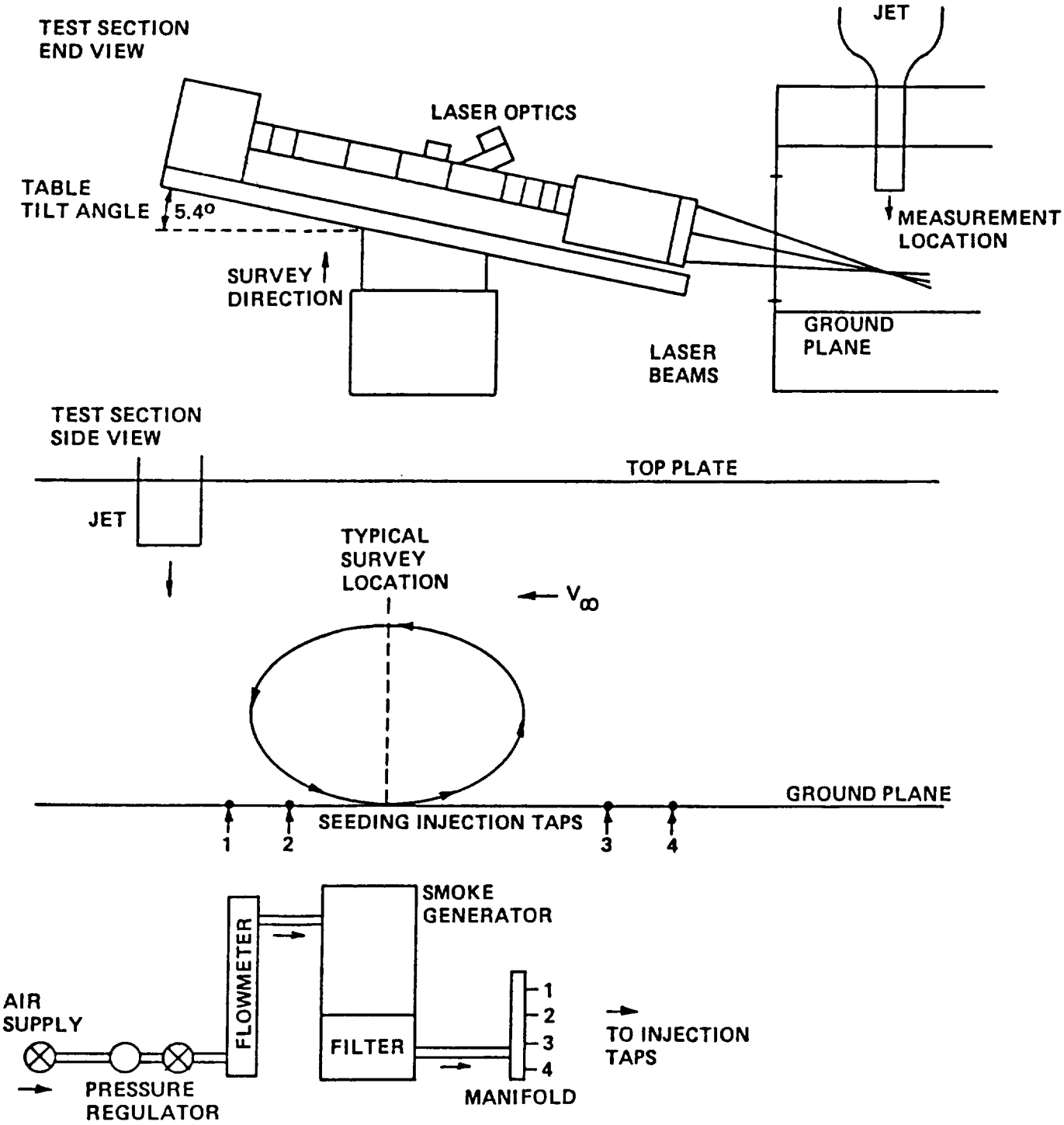

Figure 11. Schematic of Test Setup for LDV Surveys.

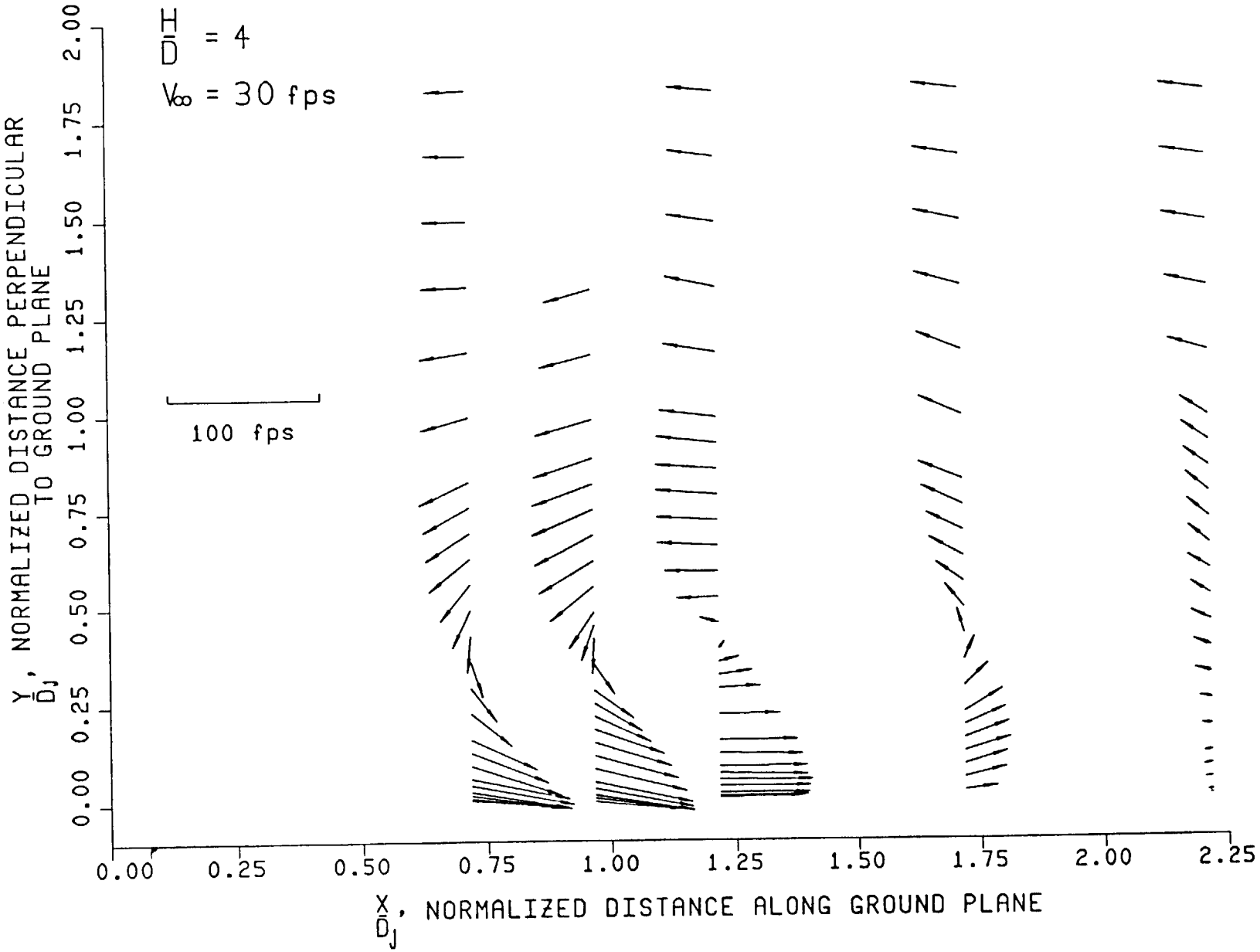

Figure 29. Vector Plot of Velocity Field for V_∞/V_j = 0.2 and h/D_j = 4.0

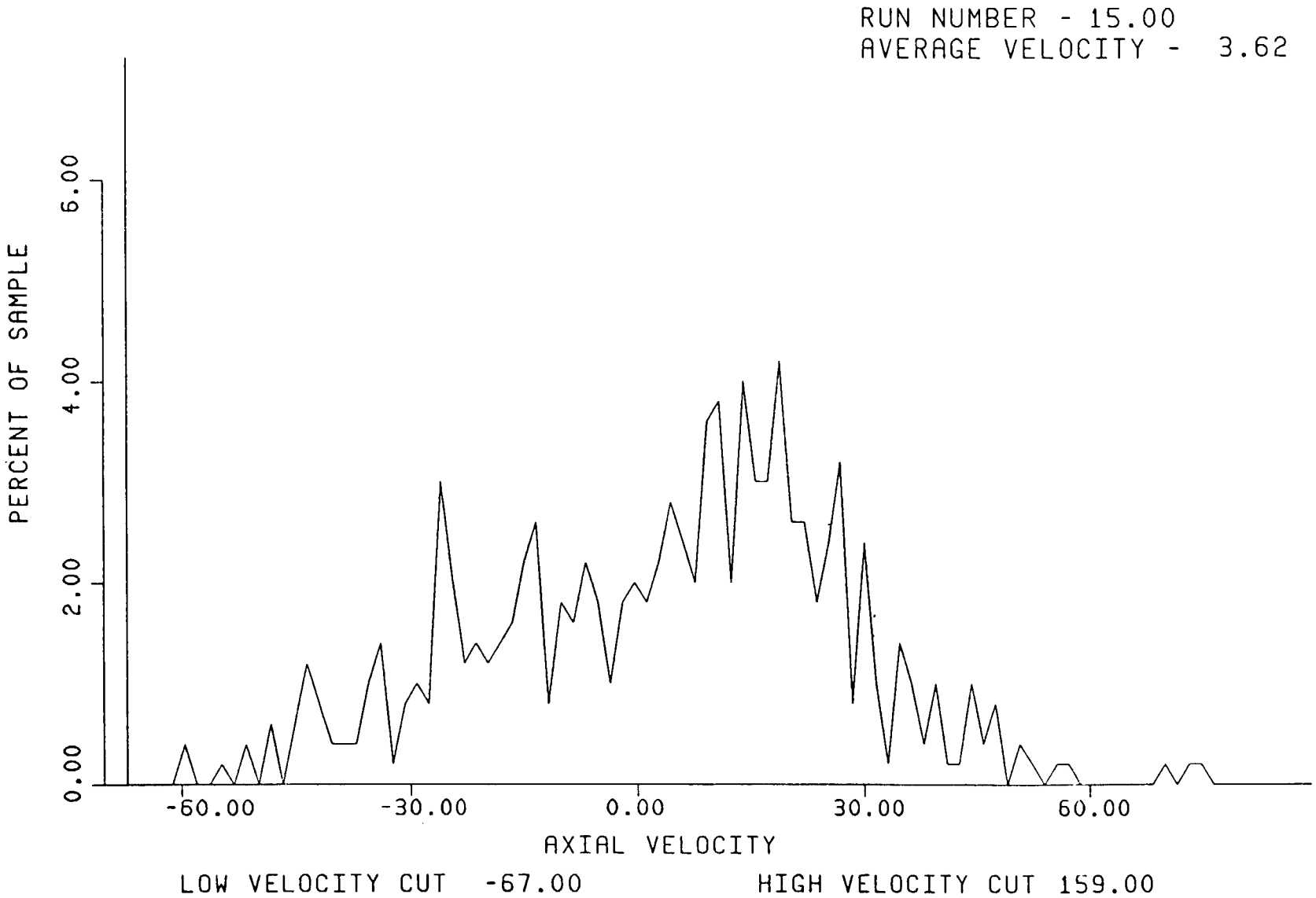

Figure 13. Velocity Probability Histogram for V_∞/V_j = 0.2 h/D_j = 4.0 x/D_j = 1.217 and y/D_j = 0.388

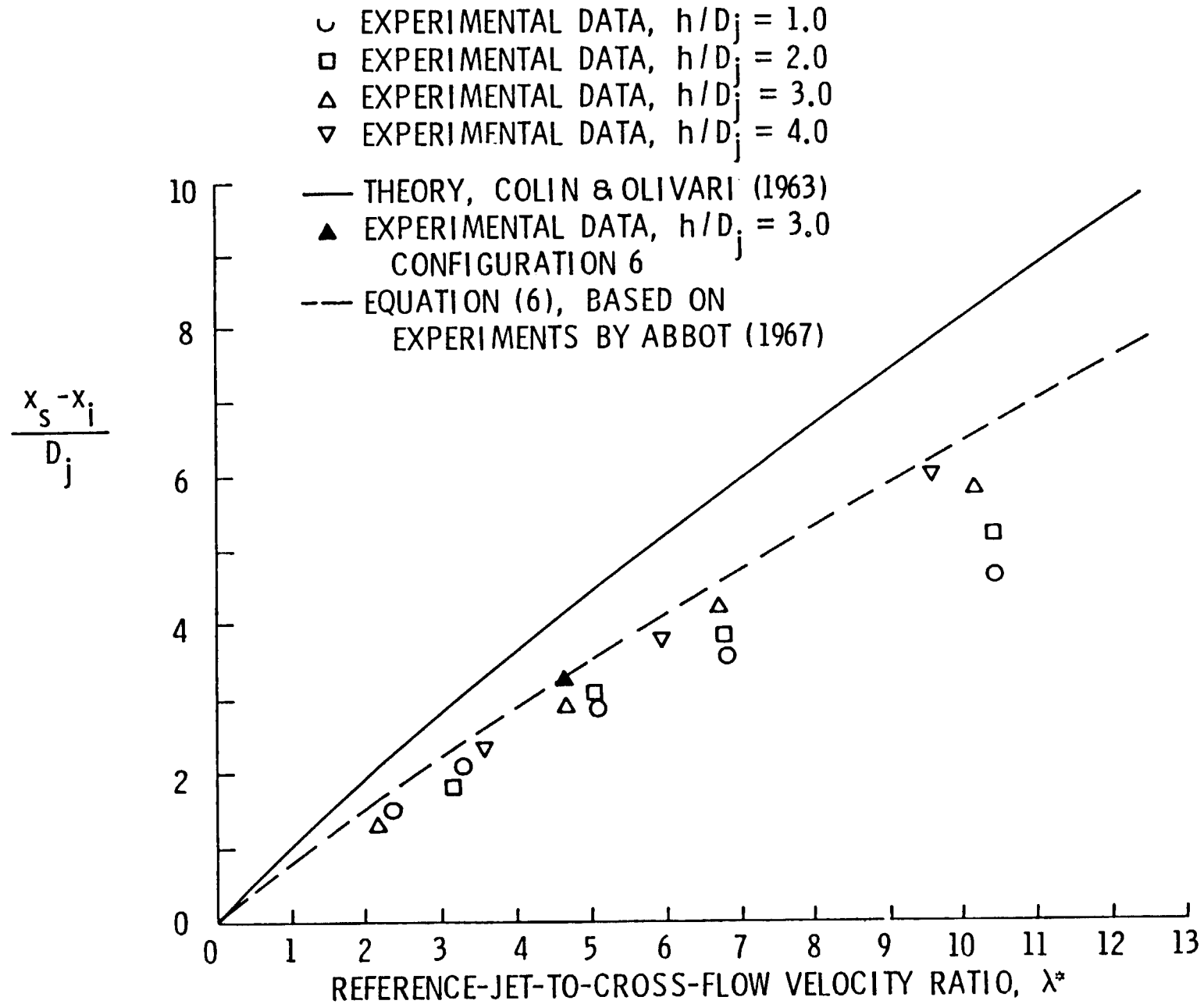

Figure 14. Comparison of Experimental and Theoretical Locations of Separation Points x_s for Various Values of h/D_j

N89-10852

GROUND VORTEX FLOW FIELD INVESTIGATION

Richard E. Kuhn
STOVL Consultant
Valencia, California

John H. Del Frate
NASA Ames Research Center
Dryden Flight Research Facility
Edwards, California

and

James E. Eshleman
Lockheed California Co.
Burbank, California

INTRODUCTION

In hover and low-speed operation the jets from a V/STOL configuration impinge on the ground and form a wall jet flowing radially outward from the impingement point of each jet. In STOL operation the forward-flowing part of the wall jet is opposed by the free stream generated by forward motion and is rolled back on itself to form a horseshoe-shaped ground vortex, as shown in figure 1. When operating over loose terrain this ground vortex creates and defines the dust cloud that can reduce visibility and damage engines. It is also one of the primary mechanisms of hot gas ingestion and can cause significant lift loss and associated pitching and rolling (in a sideslip condition) moments.

The flow field associated with the ground vortex formed in STOL operation has been studied in several investigations (refs. 1 to 5). Unfortunately, these five investigations show a wide variation in the forward projection of the ground vortex flow field, as shown in figure 2. Some of this variation may be due to the manner in which the forward edge of the flow field was defined. Some measured the position from photographs of dust clouds and some inferred the position from pressure distributions measured on the ground board. Also they were run at different jet pressure ratios and Reynolds numbers.

However, it is believed that the boundary layer present in most tests between the free stream and the ground board and the relative motion between the jet and the ground surface may be the primary factors responsible for the variations in the forward projection (fig. 2). Most of these investigations were conducted in wind tunnels with fixed ground boards. When using this test technique a boundary layer forms between the free stream and the ground board. The velocity decrement of the ground board boundary layer allows the high-velocity wall jet to penetrate further upstream than would be possible against a full free-stream velocity profile. All the wind tunnel investigations (refs. 1 to 4) show more forward penetration than the moving model investigation (ref. 5), where there was no boundary layer. Also, in the moving model case the ground surface is moving rearward relative to the wall jet flow and therefore retarding and eroding the energy of the wall jet and reducing its ability to penetrate against the free stream.

To avoid the ingestion of hot gas or dirt and debris, the inlet should be ahead of or above the recirculating flow field generated by the ground vortex. Unfortunately, the height of the recirculating flow field has received very little attention. Abbott (ref. 5) simply states that the depth of the flow field is approximately one-half the forward projection. This result was obtained from jet-alone tests. It has been speculated that the sink effect of an inlet, located slightly above or ahead of the ground vortex, may increase the height or forward extent of the flow field. Unfortunately, there have been no investigations of the sink effect of the inlet.

The investigations described in this paper had several objectives:

1. to evaluate water tunnel tests as a technique to visualize and evaluate the flow field under and ahead of a V/STOL model;

2. to investigate the effects of the boundary layer and movement relative to the ground on the forward projection of the flow field;

3. to determine the depth of the flow field;

4. to investigate the effects of inlet flow on the forward extent and depth of the flow field; and

5. to investigate the flow fields generated by twin-jet configurations.

SUMMARY

Flow field investigations were conducted at the NASA Ames-Dryden Flow Visualization Facility (water tunnel) to study the ground vortex produced by the impingement of jets from aircraft nozzles on a ground board in a STOL operation. Effects on the overall flow field with both a stationary and a moving ground board were photographed and compared with similar data found in other references. Additionally, nozzle jet impingement angles, nozzle and inlet interaction, side-by-side nozzles, nozzles in tandem, and nozzles and inlets mounted on a flat plate model were investigated. Results show that the wall jet that generates the ground vortex is unsteady and the boundary between the ground vortex flow field and the free-stream flow is unsteady. Additionally, the forward projection of the ground vortex flow field with a moving ground board is one-third less than that measured over a fixed ground board. Results also showed that inlets did not alter the ground vortex flow field.

NOMENCLATURE

d	jet diameter, ft
h	height of jet exit above ground, ft
K	factor to account for moving ground
m_i/m_j	inlet mass to jet mass flow ratio
q_0	free-stream dynamic pressure, lb/ft^2
q_j	jet dynamic pressure, lb/ft^2
V_0	free-stream velocity, ft/sec
V_j	jet velocity, ft/sec
V_b	belt velocity, ft/sec
w/ℓ	width/length ratio of jet nozzle
X	forward projection of ground vortex flow field, ft
x	longitudinal distance between jet centers in tandem pair, ft

z depth of ground vortex flow field, ft

δ jet deflection angle, measured from horizontal, deg

MODEL AND APPARATUS

The investigation was conducted in the Flow Visualization Facility (ref. 6) at the NASA Ames Research Center, Dryden Flight Research Facility. This flow visualization facility is a continuous-flow water tunnel with a vertical test section (fig. 3). The walls of the 16- by 24-in test section are made of 2-in-thick plexiglass to provide for easy visual and photographic observation of the flow. Photographs can be taken either using general lighting or using a light sheet generated by an argon laser.

The setup for the investigation is shown in figure 4. A special endless-belt ground board was built for these studies. The belt material was transparent plastic, and the belt was supported by a transparent backing plate (in the jet impingement region) so that photographs could be taken and the flow field could be illuminated by the laser light sheet through the belt. The belt assembly was installed against the 16-in side of the tunnel, and fairings were installed upstream and downstream of the belt to ensure smooth flow. A boundary layer removal system was installed at the leading edge of the belt to remove the boundary layer generated on the wall and fairing ahead of the belt. The regeneration of the boundary layer on the belt surface was eliminated by operating the belt at the free-stream velocity.

The investigation was conducted in two phases. Phase I, conducted in September 1986, used a 0.5-in-diameter jet and a 1-in-diameter inlet (fig. 4) in an investigation of the effects of jet/free-stream velocity ratio, belt speed, jet height, jet deflection angle, and inlet flow on the ground vortex flow field set up by the jet. The jet could be positioned at heights from 1 to 5 in. above the ground board. The inlet was supported from the tubing supporting the jet, and both the fore and aft position and the height of the inlet could be varied.

Phase II, conducted in December 1986, extended the investigation to cover the effects of dual jets, side-by-side or in tandem, and the effects of the proximity of a wing or body surface at the exit plane. The clipped delta configuration and the inlet and jet positions and spacings investigated are shown in figure 5.

For the phase II tests, the diameters of the two individual jets were reduced to 0.35 in each. Also, extra precautions were taken in the construction of the phase II nozzles to reduce the turbulence of the jets. As shown in figure 6, the phase II nozzles incorporated two screens and a finer honeycomb than that used in the phase I nozzle.

RESULTS AND DISCUSSION

All the data from the present investigation were obtained from still photographs and video records of the flow. The best insight into the flow is obtained from the video records; a 15-min tape was prepared to illustrate the significant findings of

the study. (This tape is available on loan and can be obtained by contacting John Del Frate at the NASA Ames Research Center, Dryden Flight Research Facility.)

Figure 7 presents a typical still photograph of the flow illuminated by the laser light sheet. In this photograph the jet is at a height of 2 diameters and the inlet is at a moderately high and forward position. This photograph was taken with the jet operating at a velocity 6.1 times the free-stream velocity, no inlet flow, and the belt stopped. The free-stream flow is from right to left. Fluorescent dye was injected into the jet flow well upstream of the nozzle to make the jet flow visible. The impingement of the jet stream on the ground and the formation of the wall jet can be seen.

At this ratio of jet velocity V_j to free-stream velocity V_0 ($V_j/V_0 = 6.1$) the ground vortex flow field is seen to project about 5 jet diameters ahead of the jet center line. However, the boundary between the ground vortex flow field and the free stream is not smooth, as is implied in figure 1, but is very irregular and unsteady. Observations during the test and posttest analysis of the video records show a significant unsteadiness of this boundary with what appear to be chunks of the ground vortex flow field being projected out through the boundary at random intervals and at random positions of the horseshoe-shaped front of the ground vortex flow field. Similar behavior was observed using smoke flow in a related investigation of ground vortex flow fields (ref. 7).

A unique feature of the flow with the belt stopped is the formation of a boundary layer wedge immediately upstream of the ground vortex flow field. This wedge is similar to that observed in the boundary layer of the free stream approaching a step on a flat plate. In the present case there appear to be vortices imbedded in this wedge, and these vortices are rotating in the same direction as the ground vortex. Visualizations and the video records show these vortices peeling off from the wedge and rolling up over the ground vortex flow field.

How much of the unsteadiness of the boundary between the ground vortex flow field and the free stream is associated with the remnants of these vortex-like flows being transported back over the ground vortex flow field cannot be determined. However, the boundary layer wedges are primarily associated with the belt-stopped testing conditions. With the belt running at free-stream velocity, the boundary layer wedge was seldom observed. At times it appeared that a wedge would form; however, some difficulty was experienced in maintaining the belt speed at the free-stream velocity, and these transient indications of boundary layer wedge formation may have been associated with belt speed significantly below free-stream velocity. Also, with the belt running, significant unsteadiness of the boundary between the ground vortex flow field and the free stream was still observed.

Effect of Velocity Ratio

The forward projection of the ground vortex flow field is determined by the energy of the forward-flowing wall jet on the ground relative to the energy of the free-stream flow close to the ground. Previous investigations of jet-induced effects, both in and out of ground effect and at operating conditions involving compressibility effects and hot jets, have shown that the induced effects are a function of the square root of the ratio of jet dynamic pressure to free-stream dynamic pressure. For the present investigation, where the flow is incompressible

and the jet and free stream are at the same temperature, this ratio reduces to the ratio of jet velocity to free-stream velocity.

Figure 8 shows, as expected, that the forward projection of the flow and the depth of the flow both increase as the ratio of jet to free-stream velocity is increased.

Effect of Inlet Flow

Some concern has been expressed that the sink effect of an inlet located slightly ahead of the ground vortex flow field may tend to pull the ground vortex flow forward and aggravate the tendency to ingest hot gas. Similarly, with the inlet slightly above the ground vortex flow field there may be a tendency for the sink effect to raise the upper boundary of the ground vortex flow field. Neither of these effects were observed in the tests. The photographs in figure 8 show comparisons of the flow field with and without inlet flow for two velocity ratios. At a velocity ratio of $V_j/V_0 = 9.1$ the forward projection of the flow field appears to actually be less with the inlet operating. At a velocity ratio of $V_j/V_0 = 11.4$ the ground vortex flow field appears to be deeper and further forward with inlet flow than without. However, these differences are within the scatter caused by the unsteadiness of the boundary between the ground vortex flow field and the free stream. Careful examinations of other photographs and, in particular, review of the video records indicate that the effects of inlet flow on the ground vortex flow field are negligible.

Unfortunately, during the phase I tests it was not always possible to have the inlet mass flow equal to the jet mass flow with the equipment available; but for those operating conditions where the inlet and exit mass flow could be matched, the effects on the ground vortex flow field, if any, were lost in the unsteadiness of the boundary layer between the ground vortex flow field and the free stream, and no effect of varying the inlet mass flow could be observed. The negligible effect of the sink effect of the inlet on the depth and forward projection of the ground vortex flow field was confirmed during the phase II tests when full inlet mass flow was simulated.

Effect of Moving Ground Plane

In considering the proper means of simulating the ground plane, two aircraft operating conditions must be considered: (1) an aircraft hovering in a wind and (2) an aircraft taking off or landing with zero wind. If the condition to be simulated is an aircraft hovering in a wind, the fixed ground board approximates the correct flow field. When hovering in a wind, the free stream approaching the aircraft includes a boundary layer between the free stream (wind) and the ground. However, the flow field in the wind tunnel may not exactly match the actual atmospheric flow field because the boundary layer profile normally available in a wind tunnel will probably have less energy deficiency near the ground than the boundary layer present under atmospheric winds. Schwantes (ref. 2) set out to simulate the boundary layer associated with atmospheric winds. His results show more forward projection of the ground vortex flow field than most other studies.

If the condition to be simulated is an aircraft taking off or landing with zero wind, the flow field generated over a conventional fixed ground board is in error on

two counts: First the forward velocity is represented by the flow approaching the model, and this flow includes a boundary layer between the free-stream flow and the fixed ground board; this boundary layer should not be present. The wall jet flowing forward from the jet impingement point can penetrate further upstream against the lower energy in this boundary layer than it could if the full energy of the free stream extended to the ground surface. A properly designed moving-belt ground board includes a boundary layer removal slot ahead of the belt to remove the free-stream boundary layer, and the belt, moving at the same speed as the free stream, prevents this boundary layer from redeveloping (left side of fig. 9).

Second, the scrubbing action of the ground surface acting on the wall jet under the moving aircraft (or model) causes the wall jet to decay faster than it would over a fixed ground board. Moving the belt at the same speed as the free stream duplicates this scrubbing effect (right side of fig. 9). This scrubbing effect reduces the energy of the wall jet, and it will not project as far forward over a moving belt or with a moving model (or aircraft) as it would over a fixed ground board.

The scrubbing effect of the moving ground surface on the wall jet was observed with zero tunnel speed in the test program, as shown in figure 10. With zero belt speed (and zero tunnel speed) the wall jet moves out radially in all directions (fig. 10(a)). However, with the belt running at about 40 percent of the jet velocity, the wall jet projects only a small distance ahead of the jet impingement point (fig. 10(b)), and the jet flow is soon carried downstream by the belt.

Wall Jet Turbulence

Sketches of the ground vortex and wall jet flows such as figure 1 imply a smooth flow in the wall jet and a steady boundary between the ground vortex flow and the free stream. However, as discussed at the beginning of the Results and Discussion section, the boundary between the free stream and the ground vortex flow is very unsteady. Figure 10 also shows that the wall jet flow is unsteady. With the belt stopped the flow appears to be a series of concentric, ever-expanding (like ripples on a pond when a rock is tossed in), irregular circles. This same unsteadiness is observed in figure 11, which shows laser light sheet sections through the wall jet flow at zero tunnel velocity.

The cause of this unsteadiness is unknown, but during phase I tests it was feared that it may be caused by an unsteady flow from the nozzle. The scale of the turbulence is large with respect to the nozzle diameter, and it was thought that the flow from the nozzle may be pulsing.

The nozzles for the phase II tests were redesigned in an attempt to minimize this problem. As shown in figure 6, the step at the entrance to the large-diameter flow section upstream of the nozzle was replaced by a diffuser section, two screens were added, and a finer and longer honeycomb section was installed. No quantitative measurements of the turbulence of the flow from the nozzle or in the wall jets were made, but the character of the wall jet flow generated by the phase II nozzle did not appear to be different than that generated by the phase I nozzle. This suggests that the unsteady nature of the wall jet flow may be associated with the type of unsteady flow observed in the shear layer of an open jet or that the unsteady flow may be a natural result of impingement and the transformation of the impinging jet into the wall jet.

Forward Projection of Ground Vortex Flow Field

As indicated in the introduction and shown in figure 2, there are large differences in measurements of the forward projection of the ground vortex flow field among several wind tunnel investigations (refs. 1 to 4) and between wind tunnel studies and the moving model investigation (ref. 5). A comparison of the results over the fixed ground board and those over the belt is presented in figure 12. Although there is considerable scatter, the results clearly show less forward projection of the flow field with the belt running at the same speed as the free stream. With the belt moving, the forward projection is in good agreement with the moving model results of reference 5.

Reference 1 presented an expression for estimating the forward projection X of the ground vortex flow field that included the effects of height h, velocity ratio, jet width/length ratio w/ℓ, and jet deflection angle δ. This expression can be written as

$$\frac{X}{d} = \frac{h}{d} \tan (\delta - 90) + 0.75\sqrt{\frac{q_j}{q_0}} \left(\frac{\delta}{90}\right)^2 K$$

$$- 1.75\left(\frac{w}{\ell}\right)_j^{0.3} \left(\frac{q_j}{q_0}\right)^{-1.12} [1 - \sin (\delta - 90)] \left(\frac{h}{d}\right)^{2.5} \left(\frac{\delta}{90}\right)^2 \qquad (1)$$

where d is jet diameter, q_j is jet dynamic pressure, q_0 is free-stream dynamic pressure, K is the moving ground factor, and X is measured from the jet center projected to the ground surface.

The first term accounts for the geometric effect of jet deflection in moving the impingement point forward or aft from the jet center. The second term accounts for the basic effects of velocity ratio as well as for the effect of jet deflection in biasing the amount of the jet flow entering the forward-flowing part of the wall jet. The last term modifies the second term for the aft deflection of the jet stream by the free stream. As the height is increased, the jet impingement point is moved aft by the rearward deflection of the jet due to interaction with the free stream. This moves the entire flow field aft and also reduces the amount of flow going into the forward-flowing part of the wall jet.

Equation (1) is presented in terms of the square root of the ratio of the jet to free-stream dynamic pressure (as it was in ref. 1, which is the source of equation (1)). The square root of the dynamic pressure ratio is used to account for the effects of compressibility and jet temperature. For the present tests where the flow is incompressible and the jet and free-stream flows are at the same temperature, this reduces to the ratio of jet to free-stream velocity, which is used in the data plots presented in this paper.

The factor K is introduced to modify the method of reference 1 to account for the effects of the belt. Figure 12 shows that with the belt operating at the free-stream velocity, a value of K = 0.67 brings the estimate into good agreement with the data. With the belt stopped (K = 1.0) the data from the phase I tests are in reasonably good agreement with the estimate; however, the phase II data depart from the estimate at the higher ratios of jet to free-stream velocity (fig. 12 (b)). The reason for this departure is not known.

The present results suggest that a value of K = 0.67 should be used for takeoff and landing with zero wind. For hover with no wind, the results of reference 2 suggest the possibility that $K \geq 1.0$; for takeoff or landing in a headwind, $0.67 \leq K \leq 1.0$ may be appropriate. However, the present data base does not permit determining the variation of K with the ratio of headwind to takeoff or landing velocity.

Depth of Ground Vortex Flow Field

As indicated in the introduction, few data were available on the depth of the ground vortex flow field. Abbott (ref. 5) merely stated that the depth of the flow field was about one-half the forward projection. Typical Z/d measurements of the present investigation are shown in figure 12. These results are in good agreement with the observation of reference 5. It is interesting that there is no discernable difference between the belt-operating and belt-stopped data. The data (including results for deflected jets, discussed in the following section) indicated that the average depth Z of the ground vortex flow field for vertically impinging jets can be estimated by

$$\frac{Z}{d} = 0.25\sqrt{\frac{q_j}{q_0}}\left(\frac{\delta}{90}\right)^2 \qquad (2)$$

Effect of Jet Deflection

When the jet impinges on the ground vertically, the flow outward from the impingement point is equal in all directions. If the jet impinges at an angle, the flow is asymmetrical. A forward-projected jet (as for thrust reversers) should project the ground vortex flow field further forward, and a rearward-deflected jet should reduce the forward projection of the flow field. These observations are born out in the photographs shown in figure 13.

The forward projection and depth of the ground vortex flow field for 120° and 60° jet deflections are presented in figure 14. The forward projection, estimated by equation (1), is in reasonable agreement with the experimental data, but there appears to be no noticeable effect of the belt. Both the belt-running and the belt-stopped data for the 120° deflection agree with the estimate for the belt-stopped case; for the 60° case, both the belt-running and belt-stopped data agree with the estimate for the belt-running case.

As expected, the depth of the flow field is greater for forward deflections and less for aft deflections. It appears that these effects are proportional to the square of the deflection angle.

Side-by-Side Jets

At zero forward speed (in hover), the wall jets from two jets will meet between the jets and form an upwash fountain flow. If jets are side by side with respect to the free-stream direction, this fountain will be aligned with the free-stream direction, and for closely spaced jets, a forward projection of the flow would be expected

at forward speed. However, if the jets are far enough apart, they will act as individual jets at relatively high forward speeds, and the forward-projecting part of the fountain will not appear until low speeds (high ratios of jet to free-stream velocity).

In the present study the ground vortex flow field for side-by-side jets was investigated only for a spacing of 10 diameters. As can be seen in figure 15, at the lowest jet to free-stream velocity ratio (upper left) the two jets are early operating independently. The fountain flow can be seen at zero forward speed ($V_j/V_0 = \infty$, hover) but does not appear until $V_j/V_0 = 9.6$ is achieved and does not project ahead of the jets until $V_j/V_0 = 16.1$.

The forward projection and depth of the flow field for side-by-side jets are compared with those for a single jet in figure 16. Within the range of the data, the jets at this spacing of 10 jet diameters produce forward projections and depths equal to those for a single jet.

Jets in Tandem

With two jets in tandem, the fountain flow generated in hover will be crosswise to the free stream, and the rear jet will be operating in the wake of the front jet. Figure 17 presents photographs of the flow for a jet spacing of 10 diameters. The fountain generated in hover can be seen at the right. This fountain grows rapidly in width as it rises from the ground and, as others have noted, is very unsteady. At high forward speed (low ratio of jet to free-stream velocity, left side of fig. 17), a ground vortex is formed ahead of each jet. As can be seen in figure 18(a) both of these ground vortices have the characteristic horseshoe shape. As the jet to free-stream velocity ratio is increased, the rear ground vortex moves forward until it reaches the midpoint between the jets, and a straight-across fountain flow is generated (fig. 18(c)).

The forward projection of the ground vortex flow field generated by the front and rear jets is compared with the same quantities generated by a single jet in figure 19. For the wide spacing (10 diameters, fig. 19(a)) and the belt running, the ground vortex flow field generated by the front jet is essentially the same as that generated by the single jet. However, as expected, the flow field created by the rear jet only progresses forward to the fountain position. The slightly more forward position shown by the data points in figure 19 is due to the width of the fountain flow.

With the belt stopped (fig. 19(b)), the flow field generated by the front jet does not progress as far forward as that of an isolated jet. In fact the flow field only progresses as far forward as it would with the belt operating at free-stream velocity. This appears to be true for both the wide (fig. 19(b)) and close (fig. 19(c)) spacing. For the more closely spaced tandem pair, the depth of the ground vortex flow field generated by both the front and rear jets appears to be less than that generated by the single jet. The reason for this behavior is unknown.

Effect of Blocking Surface

In an actual airplane the ground vortex flow field may completely fill space below the lower surfaces of the aircraft for some operating conditions. Reference 1 showed that when this occurs, the forward progression of the ground vortex flow field is reduced. Only limited data were obtained for this condition in the present investigation. The data for the tandem pair (fig. 20(a)) agree with the results of reference 1. The depth of the flow field equals the height at $V_j/V_0 \approx 16$, and the forward progression at higher velocity ratios is less than for the front jet without the blocking plate.

With the side-by-side pair, the results are less conclusive. The depth of the flow field again fills the space between the blocking surface and the ground at $V_j/V_0 \approx 16$, but there is only one data point at a higher velocity ratio, and this shows only marginally less forward projection.

CONCLUDING REMARKS

This water tunnel flow visualization of the ground vortex flow field has shown that both the wall jet that generates the ground vortex and the boundary between the ground vortex flow field and the free-stream flow are very unsteady.

The forward projection of the flow field with a fixed ground board generally validates the method of estimating this forward projection presented in reference 1. However, the fixed ground board does not properly simulate the takeoff or landing flow fields. With a moving-belt ground board, which eliminates the boundary layer between the free stream and the ground surface and also introduces the scrubbing action of the ground surface on the wall jet flowing forward from the impingement point, the forward projection of the flow field is only about two-thirds of that measured over a fixed ground board.

The depth of the flow field is proportional to the square root of the ratio of the jet dynamic pressure to the free-stream dynamic pressure and to the square of the jet deflection angle.

The size of the flow field generated by the front jet of a widely spaced tandem pair is the same as that generated by the front jet alone. However, the size of the flow field generated by the front jet appears to reduce as the jets are moved closer together.

Inlet flow did not noticeably affect the forward projection or depth of the flow field.

REFERENCES

1. Stewart, V.R.; and Kuhn, R.E.: A Method for Estimating the Propulsion Induced Aerodynamic Characteristics of STOL (short takeoff and landing) Aircraft in Ground Effect, vol. 1. NADC-80226-60, Aug. 1983.

2. Schwantes, E.: The Recirculation Flow Pattern of a VTOL Lifting Engine. NASA TT-F-14912, 1973.

3. Weber, H.A.; and Gay, A.: VTOL Reingestion Model Testing of Fountain Control and Wind Effects. Eleventh Propulsion Conference, AIAA-75-1217, Sept. 1975.

4. Colin, P.E.; and Olivari, D.: The Impingement of a Circular Jet Normal to a Flat Surface With and Without Cross Flow. AD-688953, European Research Office, United States Army, Jan. 1969.

5. Abbott, W.A.: Studies of Flow Fields Created by Vertical and Inclined Jets When Stationary or Moving Over a Horizontal Surface. ARC-CP-911, 1967.

6. Beckner, C.; and Curry, R.E.: Water Tunnel Flow Visualization Using a Laser. NASA TM-86743, 1985.

7. Cimbala, J.M.; Stinebring, D.R.; Treaster, A.L.; and Billet, M.L.: An Experimental Investigation of a Jet Impinging on a Ground Plane in the Presence of a Crossflow. NADC-87019-60, March 1987.

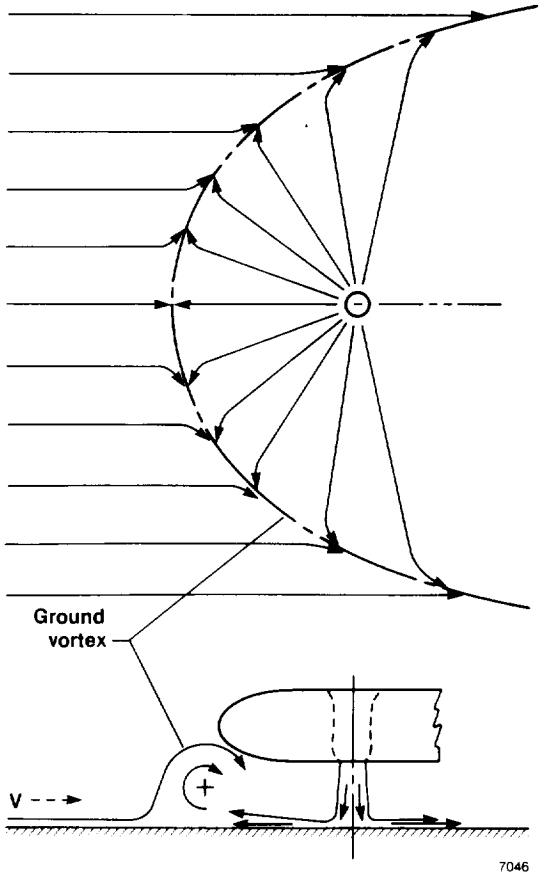

Figure 1. Formation of the ground vortex flow field.

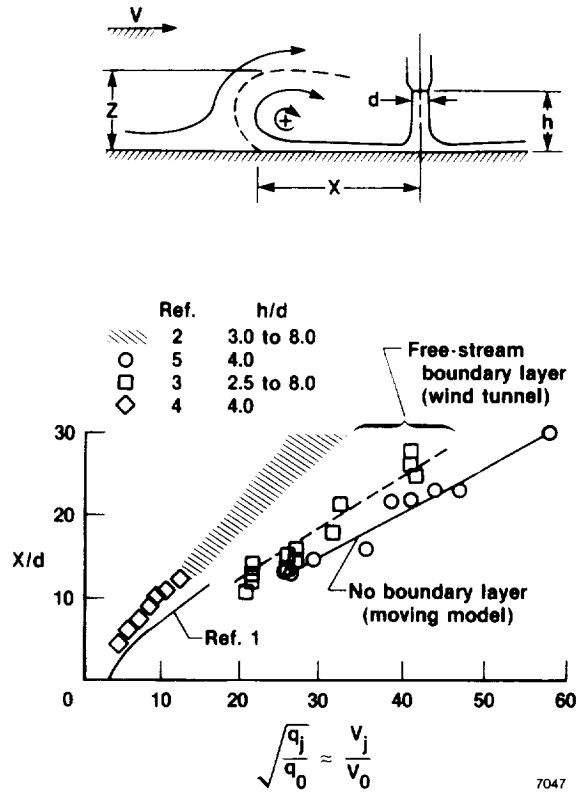

Figure 2. Forward projection of the ground vortex flow field as determined by several investigations.

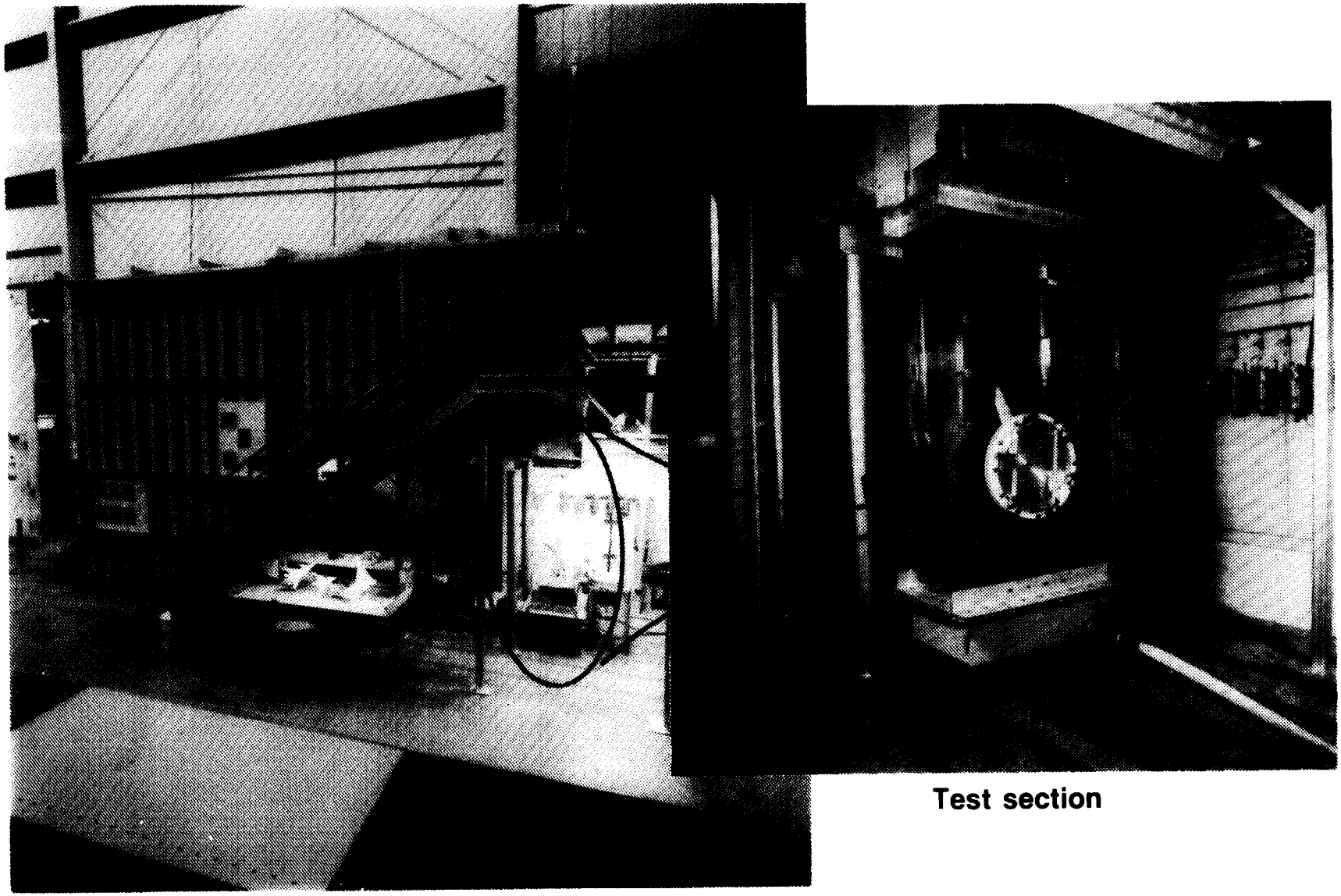

Figure 3. NASA Ames-Dryden Flow Visualization Facility.

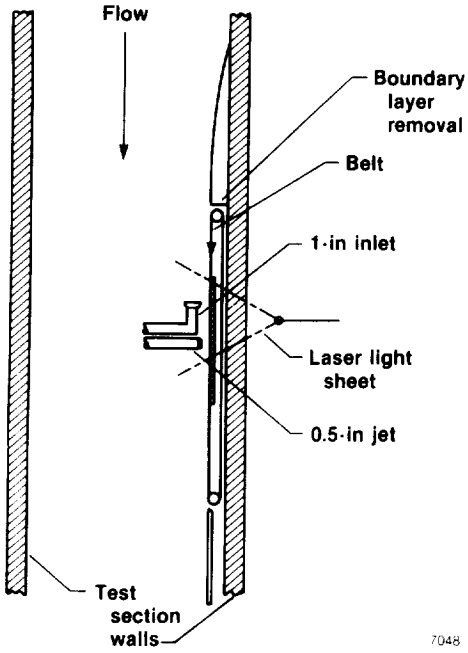

Figure 4. Installation of jet, inlet, and moving ground board in the test section.

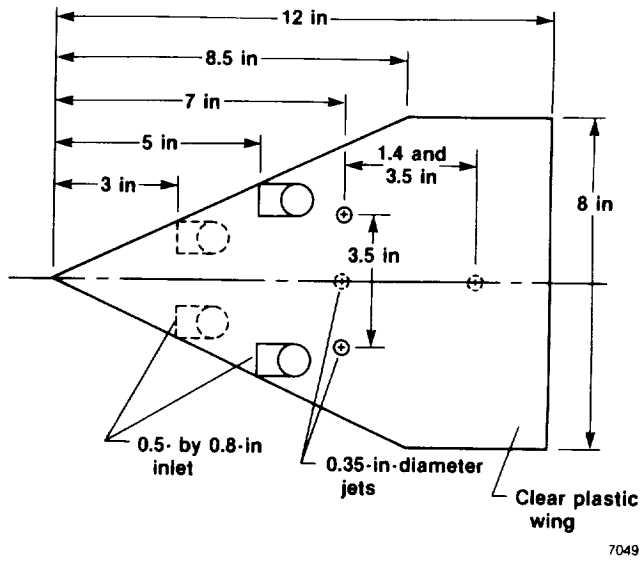

Figure 5. Phase II model.

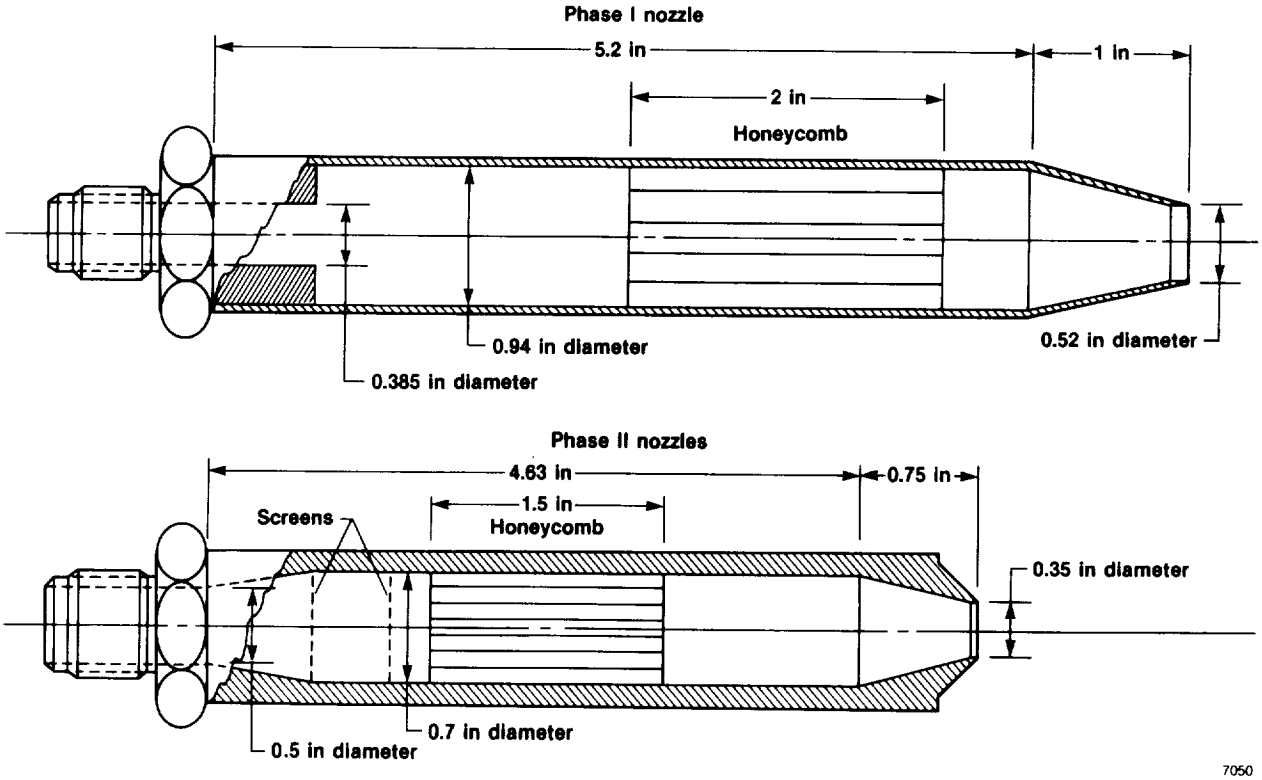

Figure 6. Flow conditioning treatment for phase I and phase II jets.

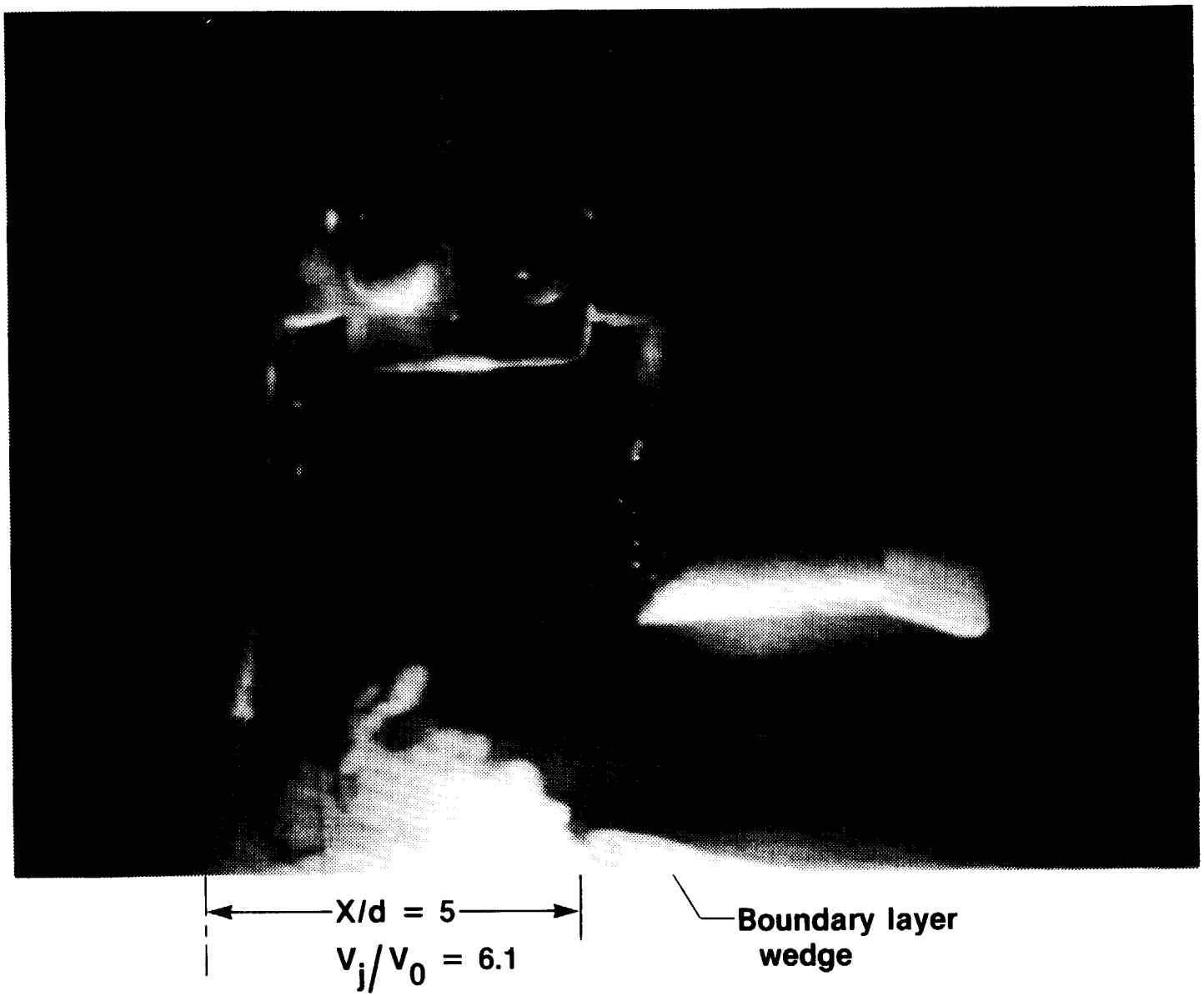

Figure 7. Experimental setup showing jet, inlet, ground vortex flow field, and boundary layer wedge; belt stopped.

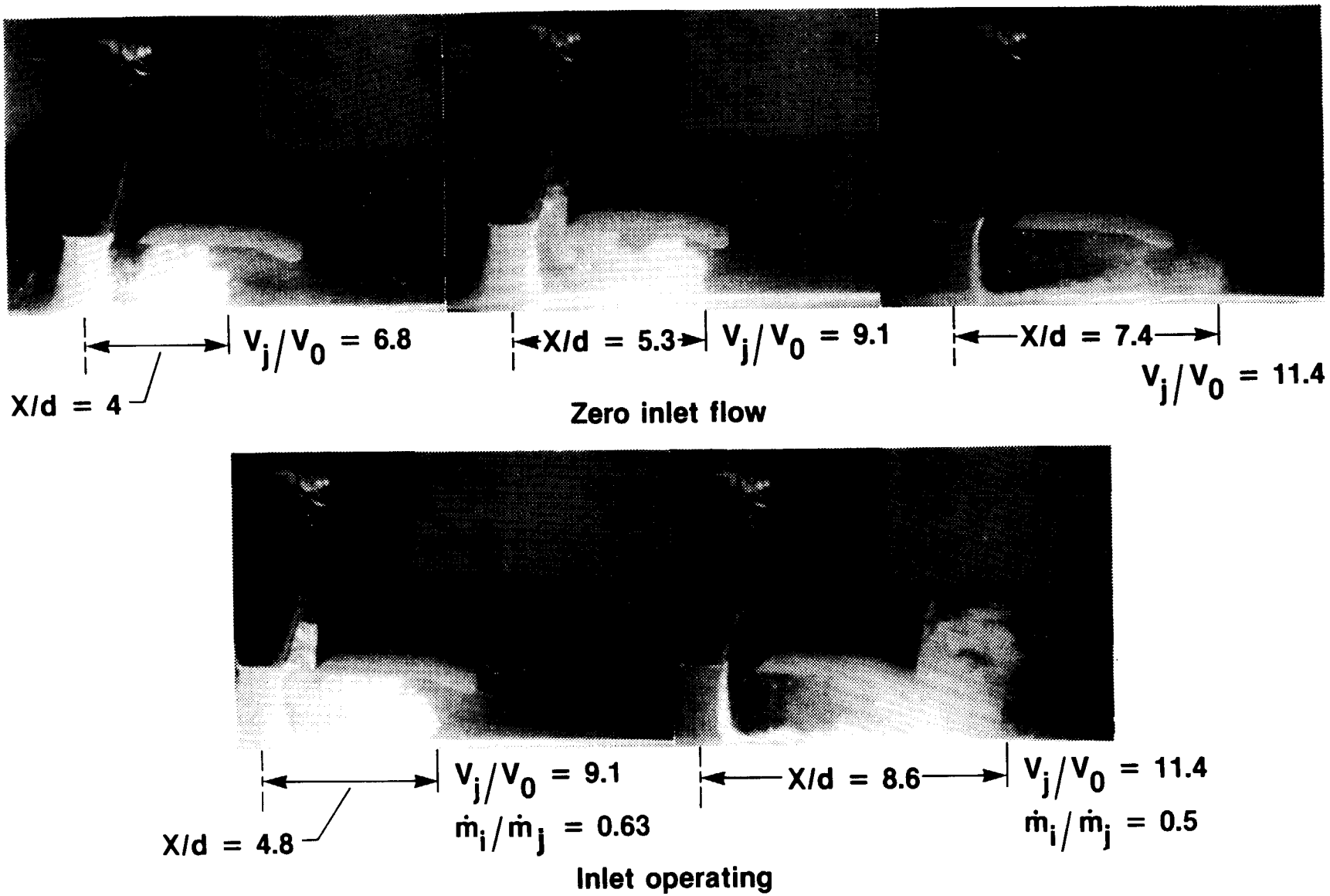

Figure 8. Effect of velocity ratio and inlet flow on forward projection and depth of the ground vortex flow field; h/d = 2, belt running.

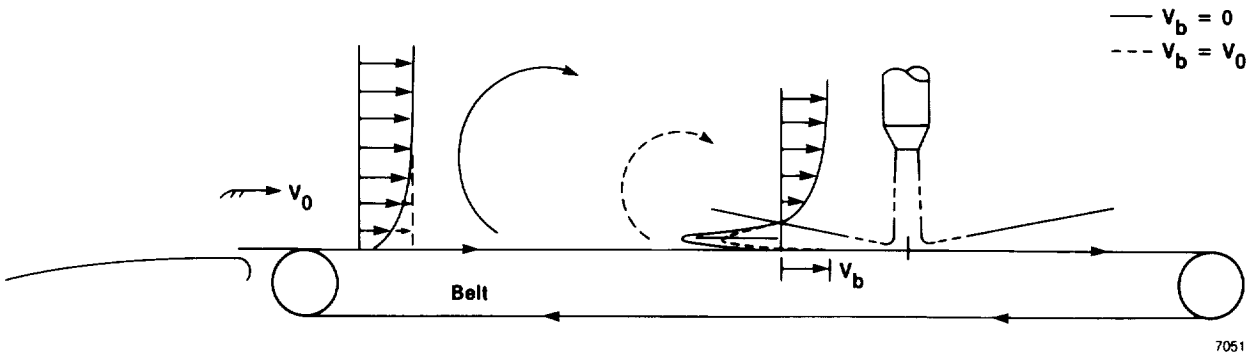

Figure 9. Effect of belt on free-stream flow, wall jet flow, and ground vortex position; V_b is belt velocity.

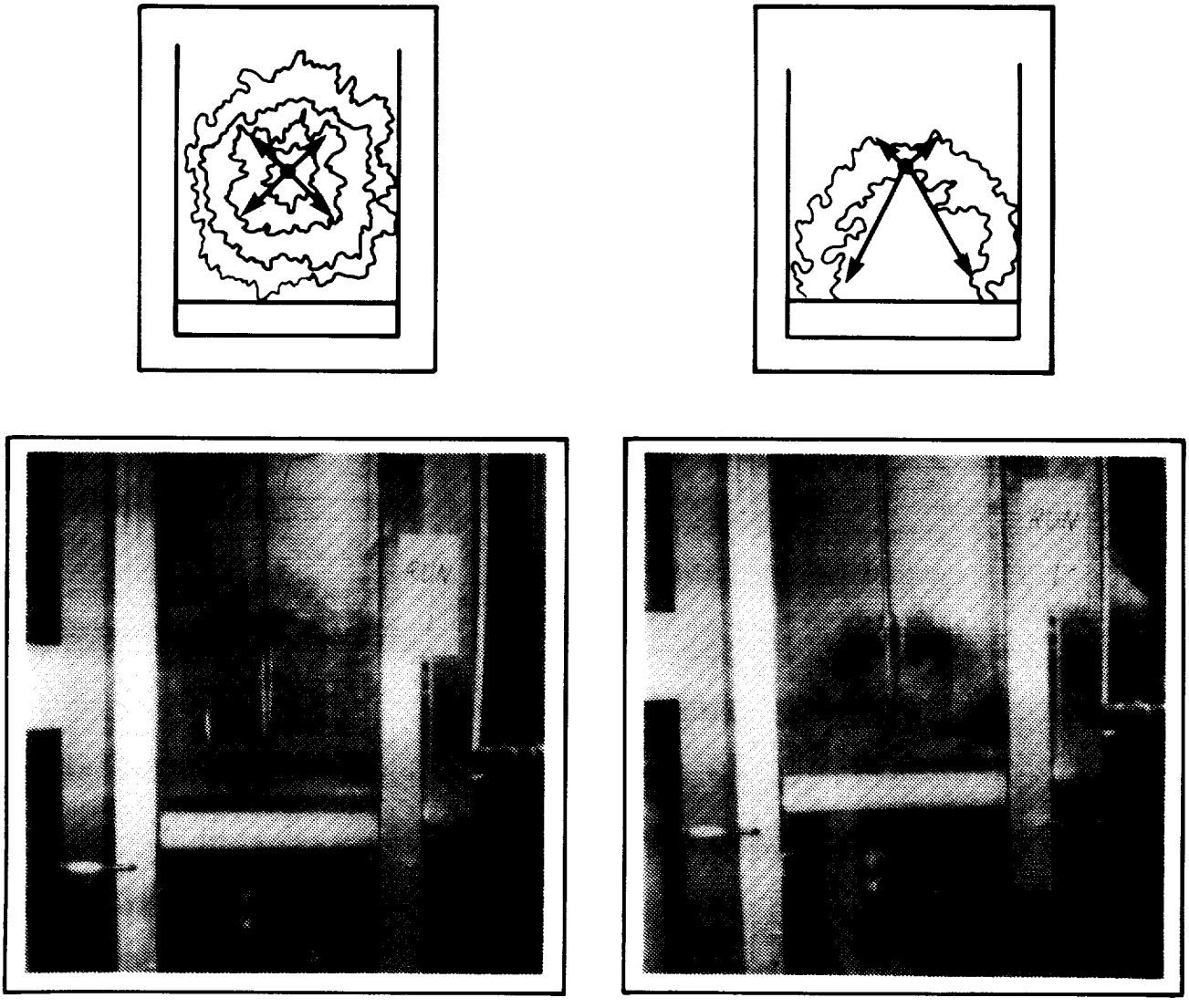

(a) Belt stopped. *(b) Belt running; $V_b = 0.4V_j$.*

Figure 10. Bottom view of wall jet flow at zero tunnel speed (hover).

AD87-178

Figure 11. Laser light sheet view of wall jet at zero tunnel speed. The two photographs show the unsteady nature of the flow.

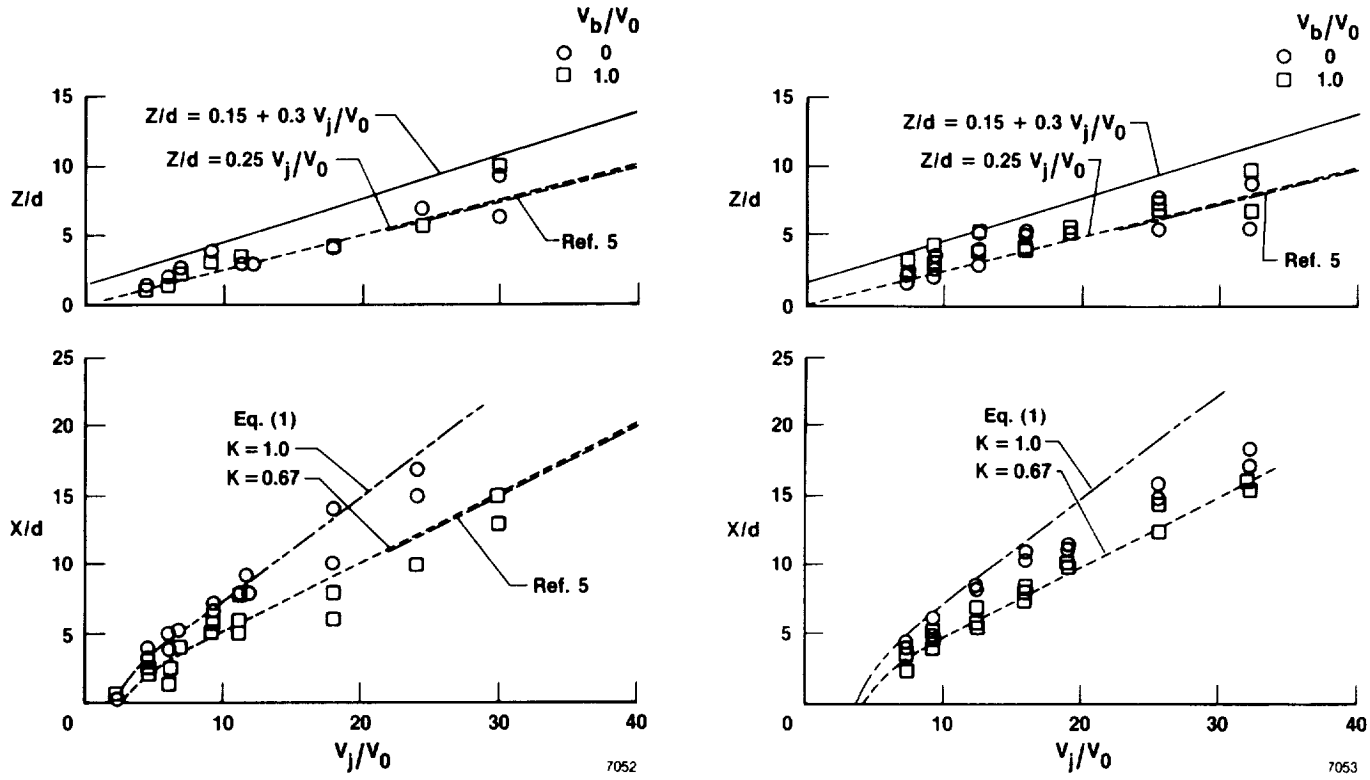

(a) h/d = 2 (phase I). *(b) h/d = 4 (phase II).*

Figure 12. Effect of velocity ratio and belt speed on forward projection and depth of the ground vortex flow field.

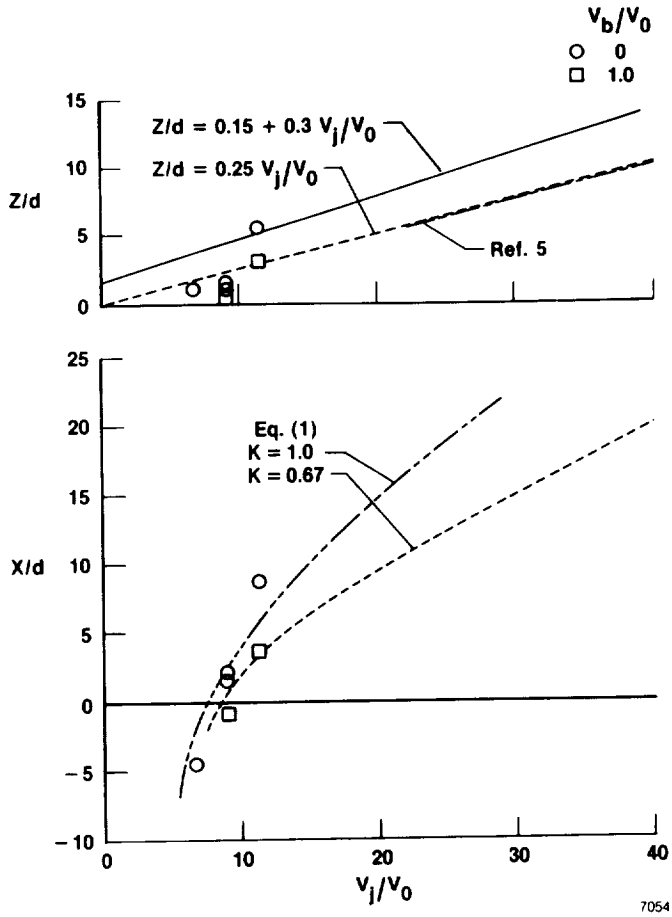

(c) h/d = 10 (phase I).

Figure 12. Concluded.

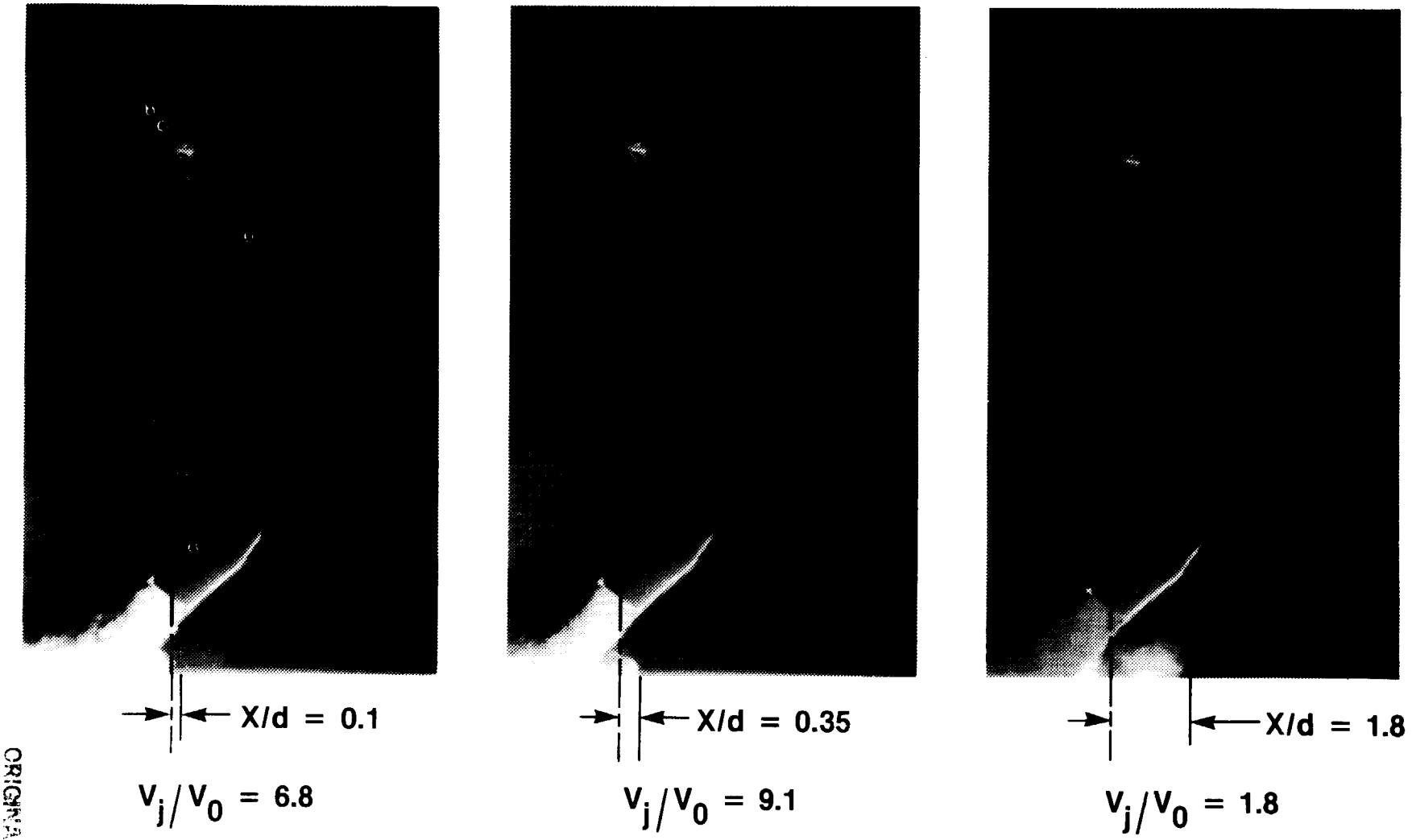

(a) δ = 60°.

Figure 13. Flow field with jet deflected; belt running.

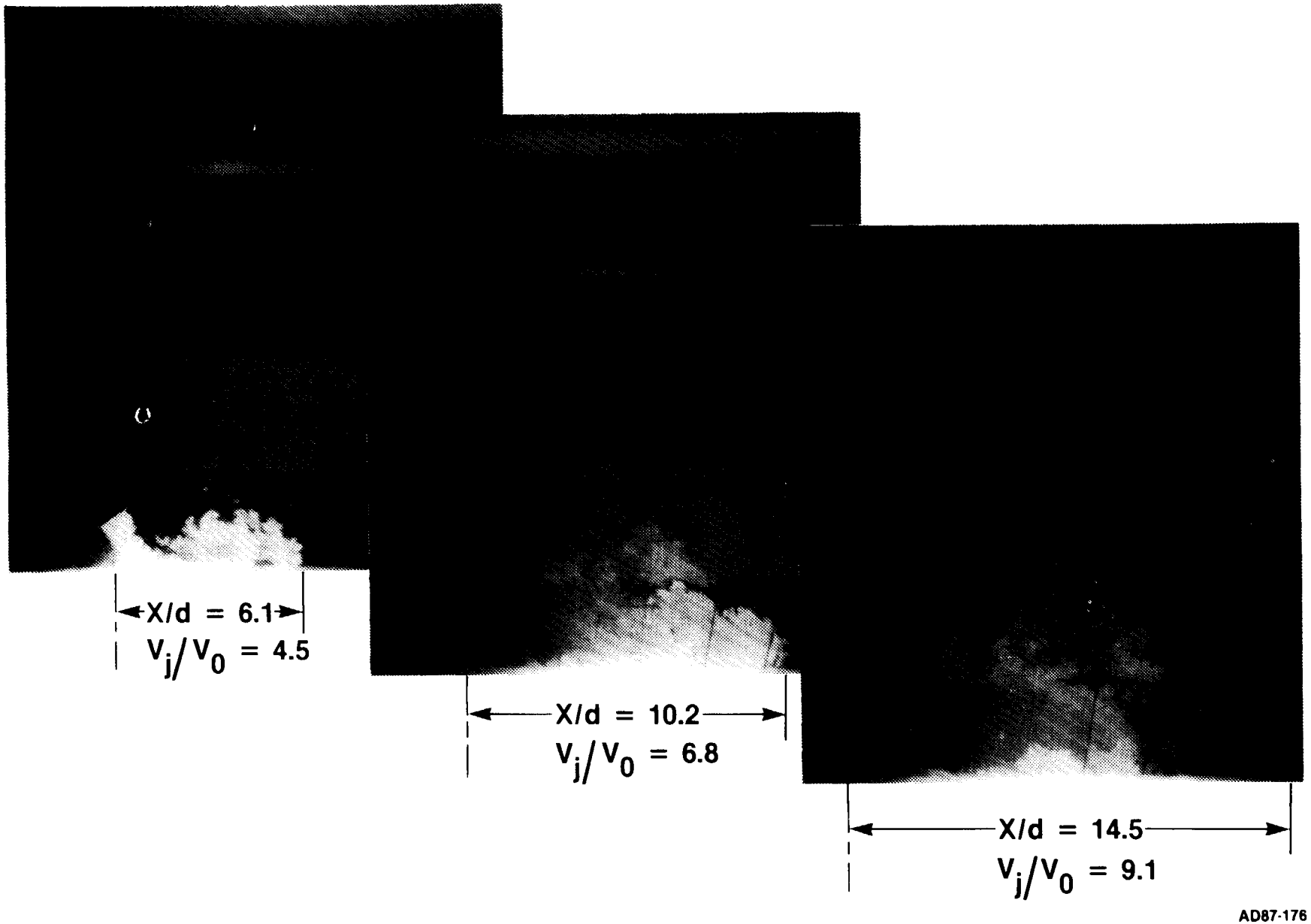

(b) $\delta = 120°$.

Figure 13. Concluded.

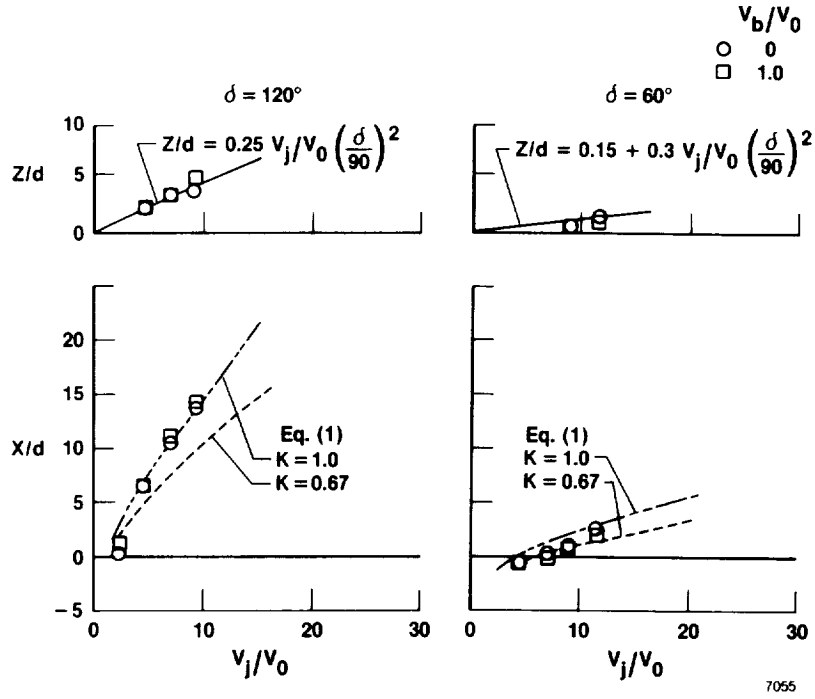

Figure 14. Effect of impingement angle on flow field size; h/d = 2.

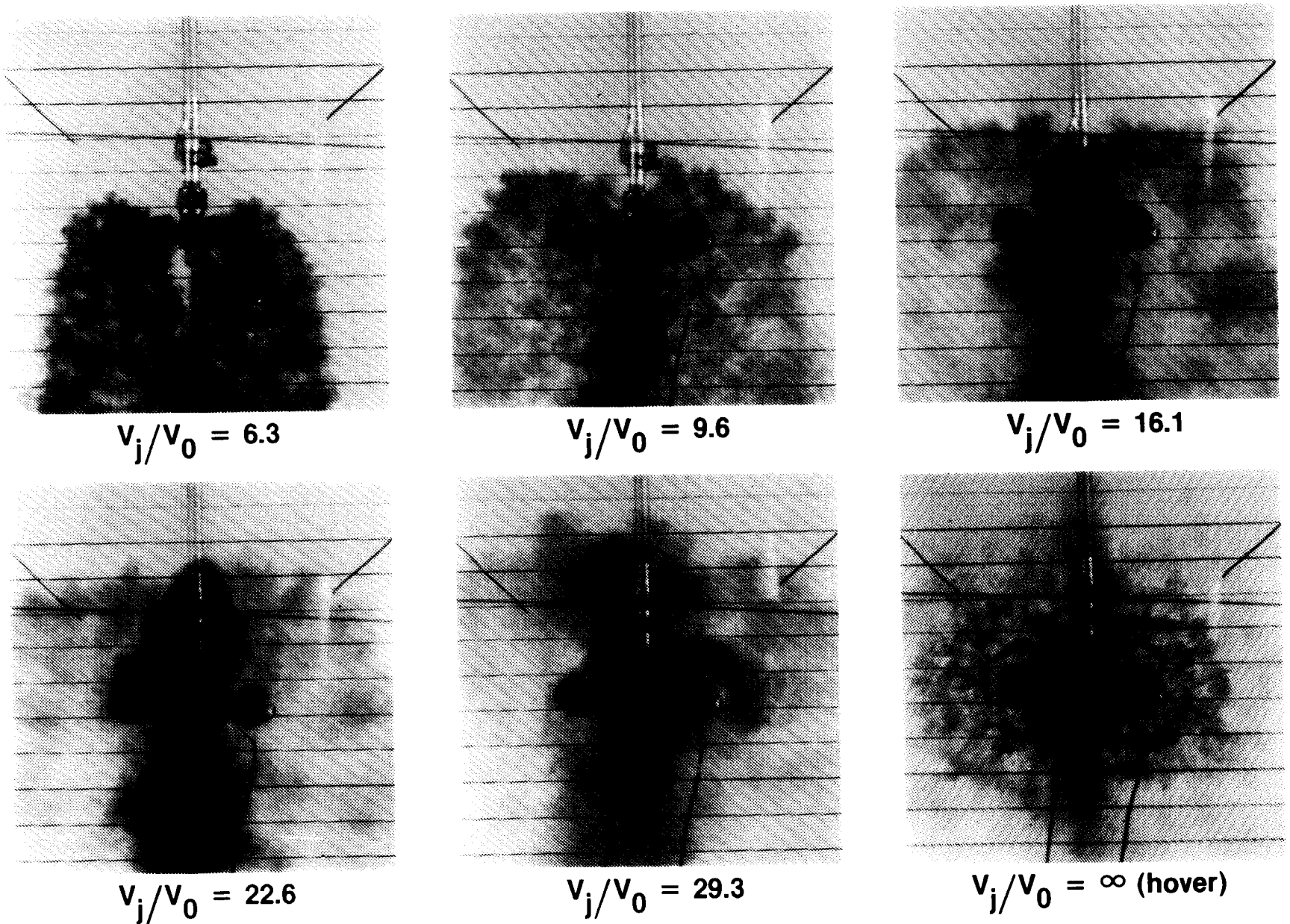

Figure 15. Bottom view of ground vortex flow fields generated by side-by-side jets.

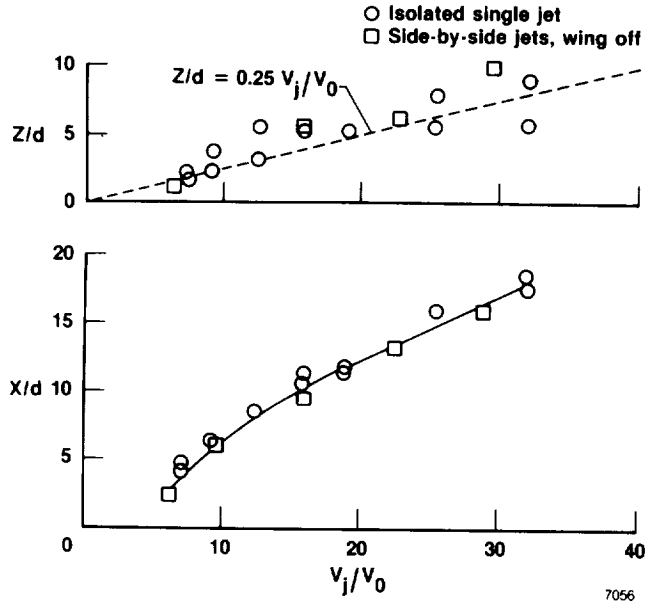

Figure 16. Comparison of sizes of flow fields generated by an isolated jet and side-by-side jets.

(a) V_j/V_0 = 6.3.

(b) V_j/V_0 = 16.1.

(c) V_j/V_0 = ∞ (hover).

Figure 17. Laser light sheet view of flow fields generated by tandem jets; X/d = 10.

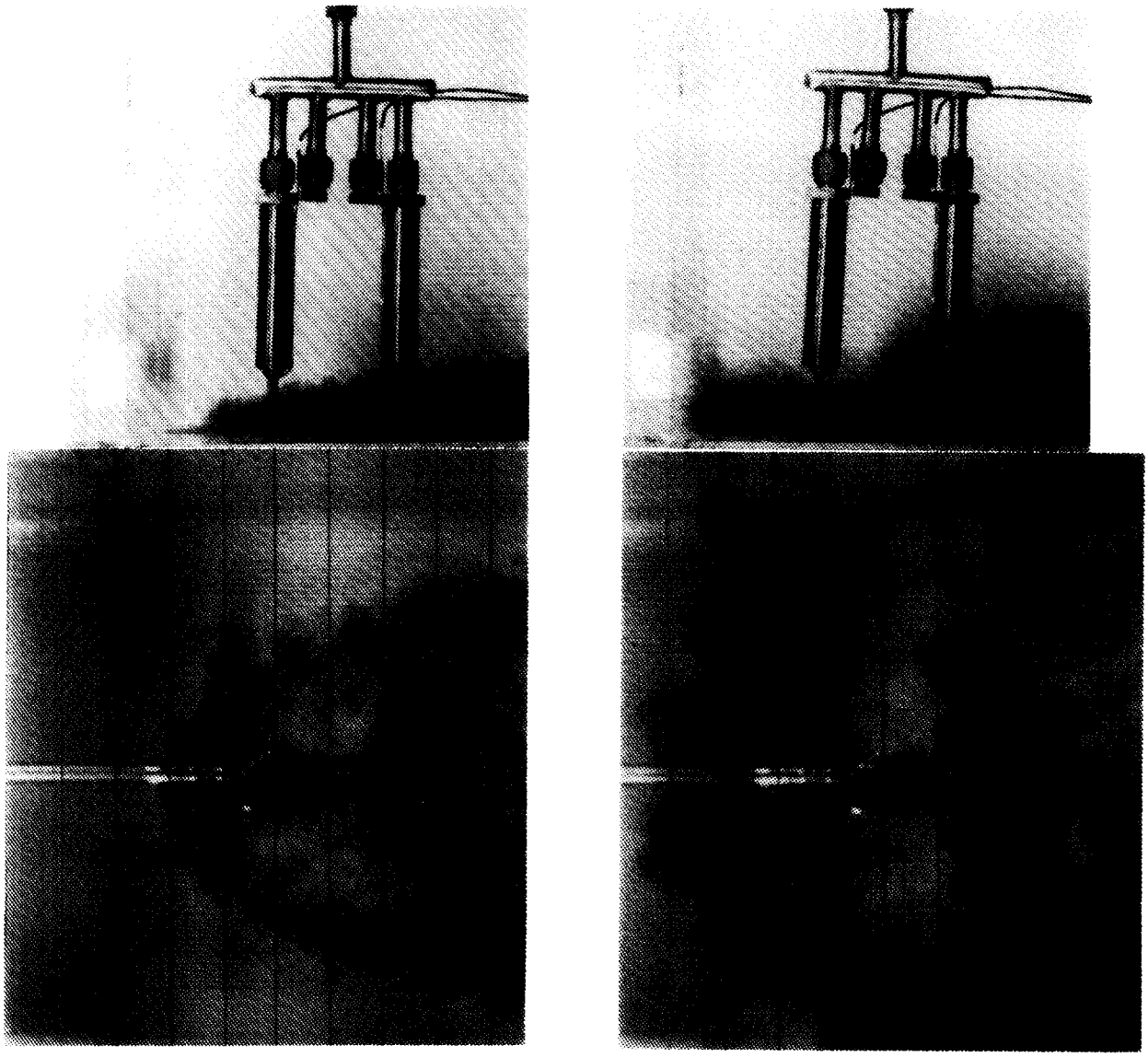

Figure 18. General lighting view of flow fields generated by tandem jets; X/d = 10.

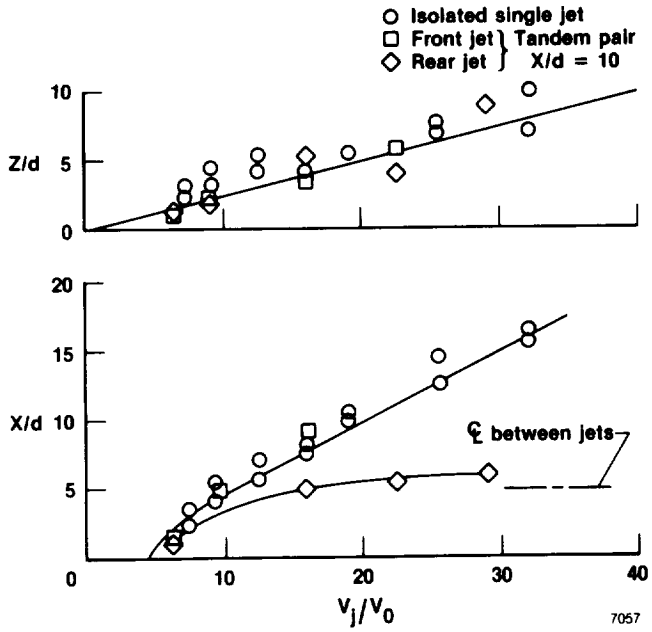

(a) Wide spacing, X/d = 10, belt running.

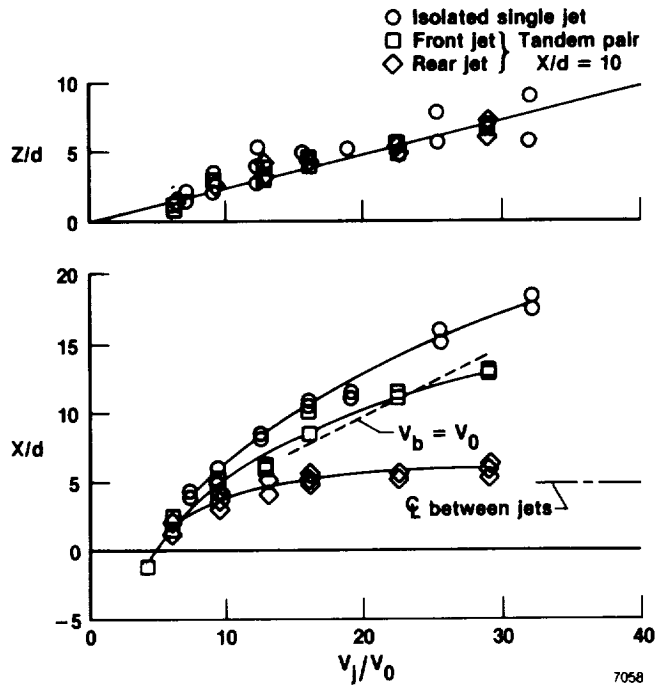

(b) Wide spacing, X/d = 10, belt stopped.

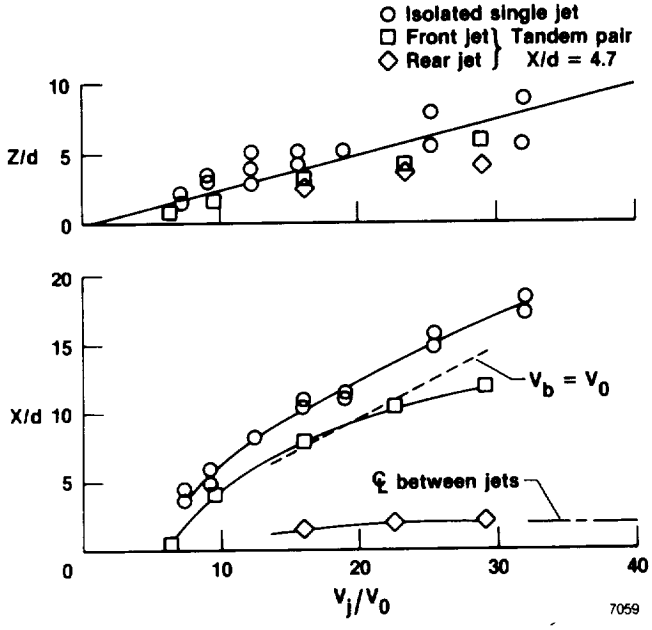

(c) Close spacing, X/d = 4.7, belt stopped.

Figure 19. Comparison of sizes of flow fields generated by an isolated jet and front and rear jets of a tandem pair.

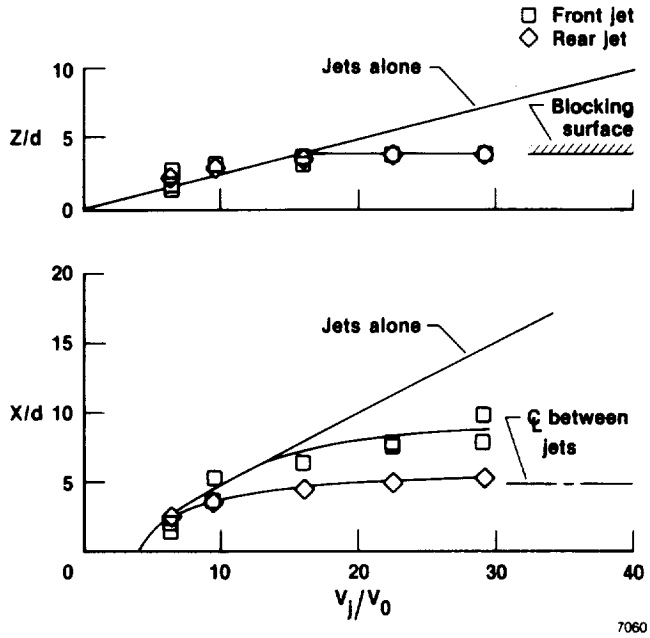

(a) Tandem jets.

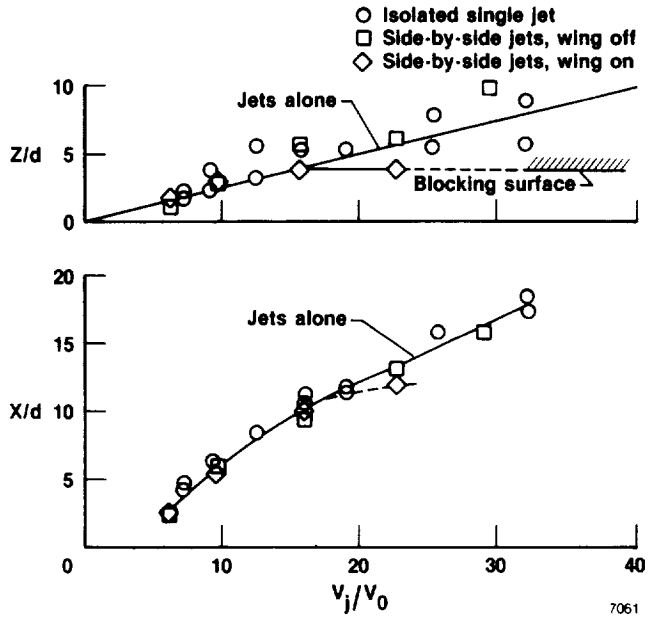

(b) Side-by-side jets.

Figure 20. Effect of a blocking surface on flow field size.

F-15 SMTD Low Speed Jet Effects Wind Tunnel Test Results

William B. Blake
Air Force Wright Aeronautical Laboratories
Wright Patterson Air Force Base, Ohio 45433

Summary

Key results from low speed wind tunnel testing of the F-15 SMTD with thrust reversers are presented. Longitudinally, the largest induced increments in the stability and control occur at landing gear height. These generally reflect an induced lift loss and a nose-up pitching moment, and vary with sideslip. Directional stability is reduced at landing gear height with full reverse thrust. Non-linearities in the horizontal tail effectiveness are found in free air and at landing gear height.

Introduction

One of the most promising means of achieving short landing capability on tactical aircraft is through the use of thrust reversal during ground rollout. Several studies have shown that thrust reversing can reduce landing rollout distances by as much as 75%. Numerous wind tunnel investigations (e.g. references 1-4) have studied the effects of thrust reversal on fighter aerodynamics at low speeds. Large changes in the stability and control characteristics of the aircraft can be induced by the reverse flow. These studies found the proximity of the reverser to the tail surfaces, the reverser efflux angle, and the reverser jet to free-stream dynamic pressure ratio to be key parameters affecting the reverser induced aerodynamics.

A full scale thrust reverser equipped aircraft, designated as the F-15 SMTD (STOL and Maneuver Technology Demonstrator), is currently being developed by McDonnell Douglas under USAF sponsorship. This aircraft is being designed for landings on a 50 x 1500 foot icy runway, in a crosswind gusting to 30 Knots. In addition its advanced STOL capability, the F-15 SMTD will be equipped with advanced rough/soft field landing gear and have a digital fly-by-wire integrated flight/propulsion control system. The objective of the program is to integrate all of these technologies with no degradation in the overall vehicle performance. As a part of the development program, wind tunnel tests were conducted to determine the jet induced effects on the aircraft during the approach and landing phases. The objective of these tests was to generate a data base for use in control law development and simulation. Key results from these tests will be presented, and where appropriate, a qualitative explanation of the phenomena in terms of the classical V/STOL flow effects will be postulated. Most of the stability and control results presented will be in terms of force and moment coefficient increments, defined as the jet-on minus the jet-off values.

Nomenclature

A_j Aspect ratio of reverser port

b Wing span ,ft

c Wing mean aerodynamic chord, ft

C_L Lift coefficient, $L/q_\infty S$

C_m Pitching moment coefficient, $M/q_\infty Sc$

C_ℓ Rolling moment coefficient, $\ell/q_\infty Sb$

C_n Yawing moment coefficient, $n/q_\infty Sb$

d Equivalent single jet diameter, ft

h Height of center of gravity above ground, ft

K_y Empirical lateral jet spacing factor, $1+1.2/(q_j/q_\infty)^{0.5}$ for the F-15 SMTD

NPR Ratio of nozzle total pressure to free-stream static pressure

q_∞ Free-stream dynamic pressure, psf

q_j Jet dynamic pressure, psf

q_j/q_∞ Dynamic pressure ratio (jet to free-stream)

S Wing area, ft^2

X Distance from jet exit to ground stagnation line

α Angle of attack

β Angle of sideslip

δ_h Horizontal tail deflection angle

δ_r Rudder deflection angle

δ_{uv} Upper reverser vane angle

δ_{lv} Lower reverser vane angle

Test Article

The Low Speed Jet Effects test was conducted in the McDonnell Aircraft 8 x 12 foot Low Speed Wind Tunnel at St. Louis. The test article was a 7.5% scale model of the three-surface F-15 SMTD (figure 1). It differs from a production F-15B through the addition of a canard mounted ahead of the wing at a 20 degree dihedral angle, as well as a set of 2-D nozzles which can be used for both thrust vectoring and reversing. The model was equipped with a six-component internal strain gauge balance for measuring the aerodynamic loads (figure 2). Each reverser port (figure 3) consists of a set of rotating vanes which can be used to provide axial as well as reverse thrust. The reversers are designed to allow a constant flow area at all deflection angles. Seven specific reverser vane angles were tested, ranging from 45 to 135 degrees The reverser ports were non-metric, so no direct jet forces and moment on the aircraft were measured by the balance. Cold high pressure air for the reverser plume simulation was routed through the twin sting which supported the model. The engine inlets were blocked, so there was no simulation of inlet mass flow. Ground simulation was achieved using a fixed ground board which had a trailing edge flap for controlling the leading edge stagnation point. This allowed for flow angularity control ahead of the ground board.

Test Approach

The test was conducted in two phases. During the first phase, testing was conducted in free air; at three intermediate ground heights (0.20, 0.35, and 0.5 h/b), at angles of attack from zero to twenty. Testing was also conducted at landing gear height (0.17 h/b), but only at zero angle of attack. The second phase of the test was conducted solely at landing gear height, at angles of attack up to six degrees. During this phase, a shortened ground board was used in order to minimize the ground board boundary layer effects. During both phases, testing was conducted at three nozzle pressure ratio settings; 1.0 (jet off), 2.2 (reduced power), and 2.7 (nominal approach power setting). The angle of sideslip and nozzle pressure ratio were held constant, while the angle of attack and tunnel speed were varied. Due to the crosswind requirement on the F-15 SMTD program, the sideslip angles tested varied from -30 to +30 degrees while on the ground. Parametric variations on all control surfaces (canard, tail, rudder, flaperon, and aileron) were tested to determine the impact of the reverser induced flow fields. The upper vanes were set at 135 degrees for all runs at landing gear height. The only exception to this was the series of differential (left/right) upper reverser runs. A matrix of lower reverser vane settings and forward velocities was tested to determine the impact of decreasing the lower vane angle during rollout on the stability and control characteristics. This reduction in lower vane angle with velocity is intended to preclude hot gas ingestion on the full scale aircraft.

Flow Field Mechanisms

Prior to the presentation of the test data, a brief summary of the basic flow field effects which are induced by thrust reverser jets will be presented. This summary is based on the results presented in references 4-7. The interpretation of the data will be in terms of these phenomena.

Free Air

In free air, the efflux from a thrust reverser can be interpreted as a growing solid body immersed in the free-stream. The jet grows as it moves along its trajectory, entraining air from around it. This entrainment action induces negative pressures, and is strongest in the wake immediately behind the jet. Upstream and around the jet, blockage is the dominant mechanism. The blockage decelerates the flow upstream, inducing positive pressures, and induces negative pressures as the flow accelerates around the jet. As the jet to free-stream dynamic pressure ratio increases, the entrainment mechanism increases, reducing the extent of the blockage induced positive pressures.

Many of the reverser vane angles tested in free air (45 to 90) represent forward thrust conditions. Here, the induced effects are analogous to those encountered with thrust vectoring. For these settings, the entrainment action of the jet can increase the local dynamic pressure at the tail surfaces, resulting in increases in the horizontal and vertical tail effectiveness. Flow will also be entrained over the upstream portion of the fuselage. This could result in a "jet flap" effect on the fuselage, if a pressure differential is established between the upper and lower body surfaces.

For reverse thrust settings (90 to 135) the jets primarily affect the flow around the tail surfaces and aft portion of the fuselage. At very high reverser angles, the jet can attach to the fuselage and move rapidly forward along the configuration through the boundary layer. The F-15 SMTD reverser was designed to avoid the possibility of jet flow attachment. For unattached jets, the induced flow fields are complex and not very well understood. It is known that the impact of the reversers on the aircraft stability and control depends largely on the relative orientation of the reverser efflux and the tail surfaces. This orientation is defined by the port location relative to the tails; the reverser vane angle; and the jet dynamic pressure ratio.

For twin vertical tail configurations, the reverser efflux can induce significant changes in directional stability. If the maximum efflux penetration is in between the tails, blockage is the predominant mechanism. The induced positive pressures will cause an outboard load on each tail. At sideslip, the free-stream shifts the efflux towards the leeward tail. The side load on the leeward tail will exceed the load on the windward tail, resulting in an increase in directional stability. If most of the vertical tail surface is aft of the efflux, the tail will experience the suction pressures associated with the entrainment action of the efflux wake. This causes inboard tail loads. At sideslip, the leeward tail will experience a greater inboard load, resulting in a decrease in directional stability.

Ground Effect

Additional flow mechanisms result from the interaction of the lower reverser and the ground. As the thrust reverser efflux impinges on the ground, a wall jet is formed which spreads radially outward from the impingement point (figure 4). This jet entrains flow around and underneath the aircraft, creating a negative pressure region which results in a suckdown (negative lift) force on the underside of the aircraft. The forward motion of the wall jet is opposed by the free stream. This eventually results in the separation of the wall jet from the ground, and a rearward deflection of the

wall jet flow. A stagnation line forms at the point where the wall jet departs from the ground. The following empirical expression, adapted from reference 5, gives the distance between the jet exit and the forward extent of the ground stagnation line:

$$(X/d) = (h/d)\tan(\delta_{1V}/90) + 0.75\,K_y(\delta_{1V}/90)^2(q_j/q_\infty)^{0.5}$$

$$- 1.75\,K_y(h/d)^{2.5}(A_j)^{0.3}(1-\sin(\delta_{1V}-90))(\delta_{1V}/90)^2(q_j/q_\infty)^{-1.125} \qquad (1)$$

A region of recirculating flow forms behind the stagnation line. Due to the rotational nature of this flow, this phenomenon is commonly referred to as a "ground vortex". It is not a vortex in the classical sense, rather, it is a point about which the free stream and wall jet flow rotate following the separation of the wall jet from the ground. Due to the deceleration of the free-stream flow as it moves up and over the ground vortex, positive pressures are induced upstream of the stagnation line. Downstream of the ground vortex, negative pressures are induced. The ground vortex defines the forward boundary of the suckdown region. As indicated by equation (1), the size of the suckdown region changes with the lower reverser angle and the jet dynamic pressure ratio. This can result in changes in the induced pitching moment, due to variations in the magnitude and center of pressure of the suckdown force.

When two or more jets are used for thrust reversal, their radial flow patterns on the ground converge, and can result in an upflow (or fountain) underneath the aircraft, which causes positive lift forces. As the distance between the jet exit and the ground impingement point increases, jets which are closely spaced tend to merge, and the fountain effect decreases. On a fighter aircraft with closely spaced reverser jets, as on the F-15 SMTD, the fountain effect is expected to be negligible for vane angles approaching 135 degrees. For nearly vertical (90 degree) lower vane angles, a fountain will form, but its impact is expected to be small compared the suckdown effect. Multiple jets can also affect the forward projection of the ground vortex. Empirical criteria for estimating the additive effect of multiple jets are given in reference 5. If the lateral spacing of the jets is sufficiently large, the jets are assumed to act independently. On the F-15 SMTD, the mutual interaction of the jets results in a more forward location of the stagnation line. This is reflected by the factor K_y in equation (1).

Longitudinal Results

Characteristics in Free Air

Effect of Reverser Vane Angle

Lift and pitching moment coefficient increments at zero angle of attack in free air are presented in figures 5 and 6 for combinations of upper and lower vane angles. When the upper and lower vane angles are equal, the lift and moment coefficient increments are both about zero. When the upper vane is deflected less than the lower vane, the induced lift is positive. Similarly, when the lower vane is deflected less than the upper vane, the induced lift is negative. One possible interpretation of this is a "jet flap" effect on the fuselage forward of the reverser ports. Differing amounts of entrainment on the upper and lower surfaces of the fuselage due to different upper/lower vane

settings could cause a pressure and hence a lift differential across the upper and lower fuselage surfaces. The moment increments are very small compared to the lift increments, which indicates that the center of pressure of the induced forces is near the center of gravity. This rules out interpretations which assume the induced effects act on the horizontal tail. It is consistent, however, with the idea of flow entrainment ahead of the ports. The induced lift forces shown in figure 5 are in the same direction as the direct jet lift forces. While the induced moment produced is small, the direct jet moment is large.

Horizontal Tail Effectiveness

As seen in figure 7, horizontal tail effectiveness is affected by reverser angle. The increase in effectiveness results for the 45 degree vanes is felt to result from an increase in the tail dynamic pressure due to increased local velocities resulting from flow entrainment. The reverser ports are located 0.45 root chords aft of the horizontal tail leading edge, (0.14 chords forward of the hinge line). With the lower reverser vane at 135 degrees, there is a reduction in the horizontal tail effectivness for negative (trailing edge up) deflections, which is not evident at the positive deflection. With this vane setting, the reverser efflux opposes the free stream flow, and significant mixing will occur. This may result in a local dynamic pressure ratio decrease. With a negative tail setting, the leading edge of the tail is in this region, and this could account for the non-linearity. A similar non-linearity was not found with the upper reverers at high settings, presumably because of the presence of the vertical tails.

Characteristics in Height Transition

Effect of Lower Vane Angle

Lift and pitching moment coefficient increments as a function of height above the ground and lower vane angle are presented in figures 8 and 9. These are jet induced effects only, jet-off aerodynamic ground effects are subtracted. Both curves show increasing increments near the ground as the lower vane angle is increased. There is a large increase in the pitching moment increment, as the height decreases, while the lift increment changes from positive to negative. As the aircraft moves into ground effect, the ground vortex and associated suckdown region begin to form, and become larger as the height above the ground decreases. The magnitude of the induced pitching moment coefficients near the ground is larger than the free air effects noted above.

Effect of Angle of Attack

Increments at zero and twelve degrees angle of attack are presented in figures 10 and 11. Twelve degrees is the current approach angle of attack for the F-15 SMTD. Near the ground, larger increments are found at the higher angles of attack. This is not suprising in that as angle of attack increases, the horizontal tail and reverser ports move closer to the ground. In addition, positive angle of attack increases the effective lower reverser angle. As a result, the suckdown region becomes larger.

Characteristics at Landing Gear Height

Effect of Ground Board Boundary Layer

The presence of a ground board boundary layer will influence the flow field induced by the lower reversers. The upstream penetration of the ground vortex and the associated suckdown region should be primarily affected. Other test techniques can be used to modify or eliminate the ground boundary layer (e.g. moving ground board, moving model), but these have additional complexities. A fixed ground board is the simplest test technique, and has been used in numerous thrust reverser studies. During the second phase of this test, runs were made on a shortened ground board (figure 12), in order to analyze the effect of the ground board boundary layer on the reverser induced flow field. The distance from the leading edge of the ground board to the nose of the model was decreased from 92" to 50". Theoretically, with a thinner ground boundary layer, and thus more kinetic energy in the boundary layer to oppose the wall jet, the forward penetration of the ground vortex should be reduced. This should result in a smaller suckdown region, with a corresponding decrease in the lift loss. The results of repeat runs made following the ground board change showed an increase in both the lift loss and the pitching moment (figures 13 and 14). The reason for the added lift loss is not clear at this time. The nozzle pressure ratio varied slightly (2.67 vs 2.86) between the repeat runs, so the minor changes that were found may not be entirely attributable to the thinner boundary layer. With the exception of horizontal tail effectiveness data, all subsequent longitudinal data at landing gear height will be from the second phase of the test, with the short ground board.

Effect of Lower Reverser Vane Angle

The effect of lower reverser vane angle and forward speed on the reverser induced lift and pitching moment is shown in figures 15 and 16. A loss in lift coefficient of about 0.7 was induced at vane angles above 110 degrees, for all velocities. The smaller lift loss as the lower vane angle decreases is due to the smaller suckdown region caused by the resultant aft movement of the ground vortex. As the lower vane angle decreases (or the forward velocity increases), both the point of reverser impingement on the ground and the ground vortex move aft, so the center of pressure of the net suckdown force moves rearward, which results in an increase in pitching moment (figure 16). The pitching moment increments begin to decrease as the ground vortex moves back to the vicinity of the wing trailing edge. As the lower reverser angle decreases, the direct jet force will give positive lift and nose down pitching moment increments (assuming a constant 135 degree upper reverser setting), both of which act to offset the induced effects.

Effect of Angle of Attack

During the second phase of testing, each reverser configuration was tested over an alpha range of zero to six degrees. The results of these runs are presented in figures 17 and 18. These are jet-induced effects only, jet-off aerodynamic ground effects are subtracted. An additional lift loss was found at six degrees angle of attack for all lower vane angles tested. This was accompanied by a decreasing moment increment back to about a 100 degree vane setting, where the moment increment then started to increase. Two key changes

happen at angle of attack: the effective reverser efflux angle increases from the vane angle to the vane angle plus the angle of attack, and the distance between the reverser ports and the ground decreases. The net effect is a forward movement of the ground vortex, so the suckdown region becomes larger. Using equation (1), each additional degree of angle of attack at 120 kts is estimated to produce a forward ground vortex movement of approximately 3% c. This forward movement results in a forward shift of the suckdown center of pressure, which gives the decreased moment increment. This is encouraging from an operational viewpoint, in that the reverser induced increments are stable.

Horizontal Tail Effectiveness

The impact of reversing on horizontal tail effectiveness as a function of the reverser jet to free-stream dynamic pressure ratio for a 110 degree vane setting is shown in figure 19. Two curves are presented, one based on the difference in pitching moment at zero and plus fifteen degrees elevator deflection, the other based on the difference at zero and minus fifteen degrees. A dynamic pressure ratio of 50 is representative of the touchdown condition. As the ground speed decreases, the dynamic pressure ratio increases (for a fixed nozzle pressure ratio). At high values of the dynamic pressure ratio, both curves show a decrease from the jet off value. At this condition, the ground vortex is far forward of the tail; the flow seen by the tail is the wake behind the ground vortex. For low dynamic pressure ratios, the tail effectiveness becomes highly nonlinear with tail deflection. At a dynamic pressure ratio of 50, the center of the ground vortex is estimated by equation (1) to be under the wing trailing edge. The complex interactions between the wing, tail, and ground vortex result in a significant loss in the tail effectiveness for the negative deflection.

Effect of Sideslip

One interesting result from this test was a large variation in the induced lift and pitching moment with sideslip angle (figures 20 and 21). As seen in figure 21 the pitching moment increments at high angles of sideslip are much higher than those found at zero sideslip for the 135 and 110 degree lower reverser settings. These increments were accompanied by a large reduction in the induced lift loss (figure 20), which indicates that the source of the additional moment is a positive lift force. In addition, a large negative increase in the rolling moment was found at positive sideslip, possibly indicating a greater lift on the windward side of the aircraft. These pieces of evidence point to the cause of the increased pitch-up being a shift of the ground vortex to the lee side of the aircraft. This moves the windward canard and forward portion of the windward wing out of the suckdown region and into the free-stream. An additional contributing factor may be induced upwash on the windward canard from the leading edge of the shifted ground vortex. The shift in the stagnation line was confirmed by flow visualization (figure 22). As the lower reverser vane angle decreases, the ground vortex and thus the induced center of pressure moves rearward, resulting in a decreased moment arm. Hence, the additional moment due to sideslip decreases with lower vane angle.

Lateral-Directional Results

Characteristics in Free Air

Effect of Upper Reverser Vane Angle

The reverser induced increment in directional stability as a function of upper vane angle is presented in figure 23. All data represent a nozzle pressure ratio of 2.7 and a lower vane angle of 110 degrees. Also included is a full reverse case (135 degree setting) taken from testing at landing gear height. For all vane angles less than 90 degrees, an increase in the directional stability is found. This may be due to an increase in the local dynamic pressure due to entrainment. Negligible changes were found in lateral stability with thrust reversers in free air.

The reverser induced rudder effectiveness increment as a function of upper vane angle is presented in figure 24. Included with the free air data is a full reverse (135 degree upper vane) case taken from testing at landing gear height. The trends are similar to the directional stability trend, the largest increase in rudder effectiveness is found with the reverser angles near vertical. It is interesting to note that the 110 degree vane results in no change compared to the jet off value, while it did result in a moderate loss in directional stability at the same flight condition.

Characteristics at Landing Gear Height

Directional Stability

For the upper reverser setting of 135 degrees, a reduction in the directional stability was found for all flight conditions representative of ground rollout. As shown in figure 25, the induced directional stability increment is negative and roughly constant over the dynamic pressure ratio range from 50 to 115. This loss is due to the reverser efflux penetrating forward (approximately two root chords) of the vertical tail leading edge. This results in negative pressures between the tails, due to entrainment. The resultant inboard tail loads act to reduce the directional stability. The dynamic pressure ratio of 50 corresponds to a nozzle pressure ratio of 2.7 at touchdown speed. Data taken at very low dynamic pressure ratios during high speed tests of the F-15 SMTD conducted at the Arnold Engineering Development Center are also presented. At these conditions, directional stability is regained, and increases slightly over the jet off value. Here, the efflux penetration does not project forward of the vertical tail, so the tails experience blockage induced positive pressures. Outboard tail loads result which act to increase the directional stability. The induced directional stability was found to be independent of the lower vane angle. This supports the belief that at landing gear height, the upper reverser interaction with the vertical tail is the dominant effect directionally.

An investigation of the effect of axial location of upper reverser ports on a YF-17 configuration is reported in reference 3. The aft-most locations (0.9 and 0.4 root chords aft of the vertical tail leading edge) yielded an increase in the directional stability for all upper vane angles and dynamic pressure ratios tested. For these locations, the efflux is in between the tails, where the blockage induced pressures increase the stability. The

forward location (0.12 chords forward of the trailing edge) showed a decrease in directional stability for high (>75) values of the dynamic pressure ratio. This is consistent with the F-15 SMTD data, since the efflux penetration increases with dynamic pressure ratio. For comparison, the F-15 SMTD ports are located 0.33 root chords forward of the vertical tail trailing edge.

Lateral Stability

The effect of jet dynamic pressure ratio on lateral stability is shown in figure 26. A large increase in lateral stability is found as the dynamic pressure ratio increases. Increasing the lower vane angle at a constant dynamic pressure ratio also increased the induced lateral stability. These increases are due to the shift in the ground vortex induced flow field towards the leeward side of the aircraft (see figure 22). This shift causes the center of pressure of the induced lift losses to move to the leeward side of the aircraft. It also causes portions of the windward wing and canard to move from the suckdown region into the free-stream. Both of these effects act to cause positive rolling moments at a negative sideslip angle, so the lateral stability is increased. It would be expected that the upper reverser/vertical tail interaction would also contribute to lateral stability changes. Due to the decreased tail effectiveness, this interaction should result in a decrease in the lateral stability. It is impossible to assess this contribution, because no vertical tail-off runs were conducted.

Differential Upper Reversing

Differential upper reversing (differing upper left/right vane settings) was tested in order to investigate the induced aerodynamic effects to determine the potential for using differential upper vanes for yaw control. Incremental yawing moment coefficient data versus sideslip angle are presented in figure 27 for a fixed left upper vane setting. For the asymmetric settings, a zero beta yawing moment increment of about -0.025 is present for all cases. This is in the same direction as the induced forces, and is equivalent to about a fifteen degree rudder deflection. Even though the trends are non-linear, all of the differential settings tested induce roughly neutral directional stability.

An asymmetric yawing moment is apparent in the symmetric 135/135 upper vane setting. It is believed that this asymmetry may arise from small differences in the left/right reverser nozzle pressure ratio settings.

The induced effect of differential upper reversing on rudder effectiveness is given in figure 28. The trend is identical to that found with symmetric upper vanes (figure 24). The magnitude of the increases with differential reversing is smaller than with symmetrical reversing. With differential reversing, the left upper reverser remains at the 135 degree setting, so only the right hand vertical tail benefits from the vane angle reduction. It should be noted that while differential upper reversing favorably impacts the stability and control characteristics, it also causes significant (possibly unacceptable) losses in reverse thrust.

Conclusions

A low speed wind tunnel test with a 0.075 scale model of the F-15 SMTD with thrust reversers has been conducted. The test was conducted in the McDonnell Aircraft 8 x 12 Low Speed Wind Tunnel, using a fixed ground board whose length was reduced in order to minimize the effect of the ground boundary layer. The thrust reversers were found to induce:

(a) Small lift and negligible pitching moment increments in free air.

(b) Increasing lift and pitching moment increments during transition into ground effect.

(c) Large lift losses and nose-up pitching moment increments at landing gear height. These increments varied with the lower vane angle, velocity, nozzle pressure ratio, and sideslip angle.

(d) Non-linear horizontal tail effectiveness characteristics in all flight regimes.

(e) Negligible changes in lateral stability in free air.

(f) Large increases in lateral stability at landing gear height.

(g) Changes in directional stability and rudder effectiveness, which were strongly affected by the upper vane angle. These changes were independent of the height above the ground.

(h) Large favorable yawing moment increments with differential upper reversing.

References

1. Tolhurst, W.H., and Kelly, M.W., "Full-Scale Wind-Tunnel Investigation of the Effects of a Target-Type Thrust Reverser on the Low-Speed Aerodynamic Characteristics of a Single-Engine Jet Airplane," NASA TN D-72, September 1959.

2. Kelly, M.W., Greif, R.K., and Tolhurst, W.H., "Full-Scale Wind-Tunnel Tests of a Swept-Wing Airplane With a Cascade-Type Thrust Reverser," NASA TN D-311, April 1960.

3. Joshi, P.B., and Compton, M., "Approach and Landing Thrust Reverser Testing in Ground Effect," AIAA 85-3075, October 1985.

4. Glezer, A., Hughes, R.V., and Hunt, B.L., "Thrust Reverser Effects on Fighter Aircraft Aerodynamics," Journal of Aircraft, Vol. 22, June 1985, pp. 455-462.

5. Stewart, V.R., and Kuhn, R.E., and Walters, M.M., "Characteristics of the Ground Vortex developed by Various V/STOL Jets at Forward Speed," AIAA 83-2492, October 1983.

6. Weston, R.P., and Thames, F.C., "Properties of Aspect-Ratio-4.0 Rectangular Jets in a Subsonic Crossflow," Journal of Aircraft, Vol. 16, October 1979, pp. 701-708.

7. Ransom, E.C.P., and Smy, J.R., "Introduction and Review of Some Jet Interference Phenomena Relevant to V/STOL Aircraft," AGARD-R-710, pp. 2-1-2-23, April 1984.

F-15 S/MTD AIRCRAFT

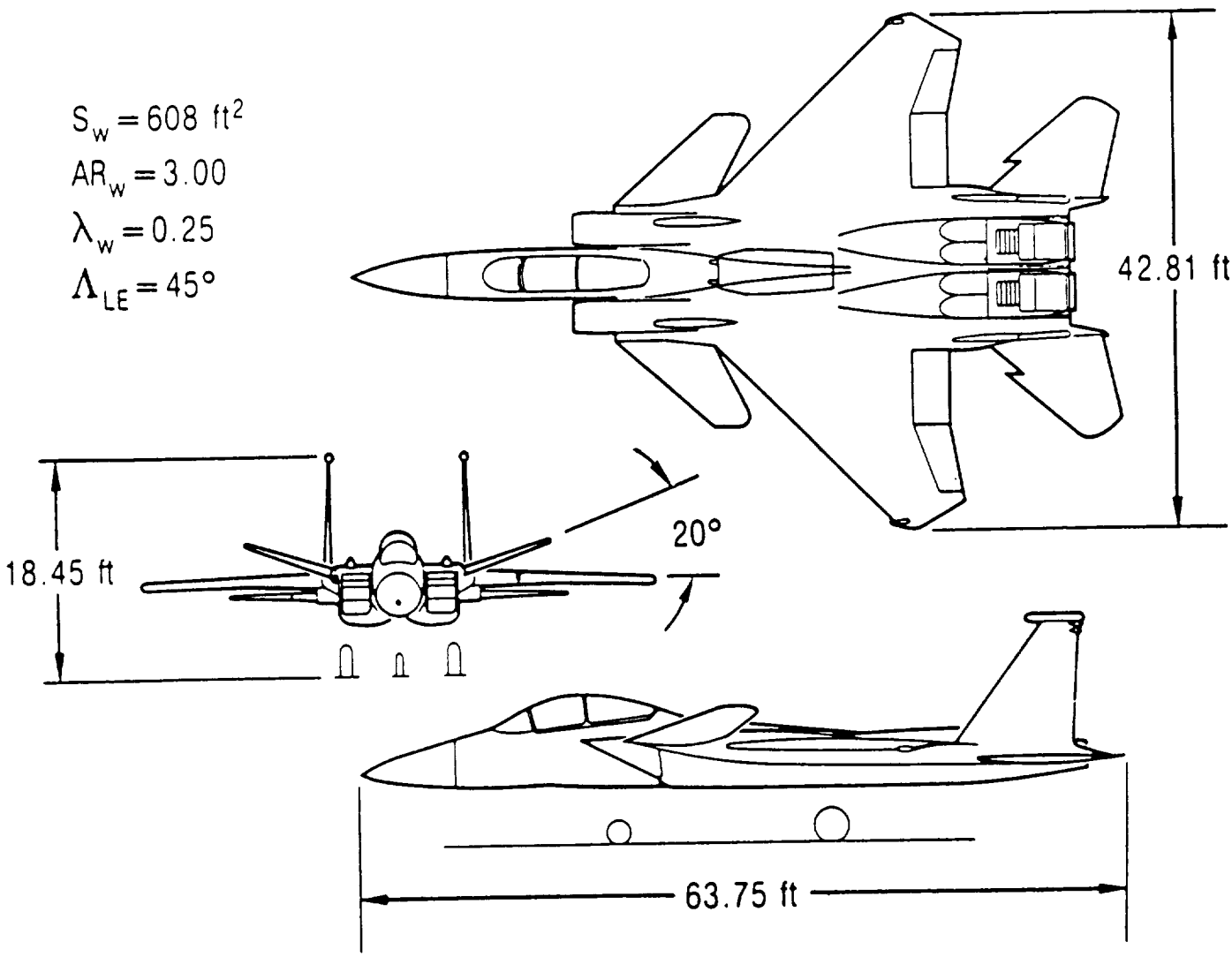

Figure 1. F-15 SMTD Three View.

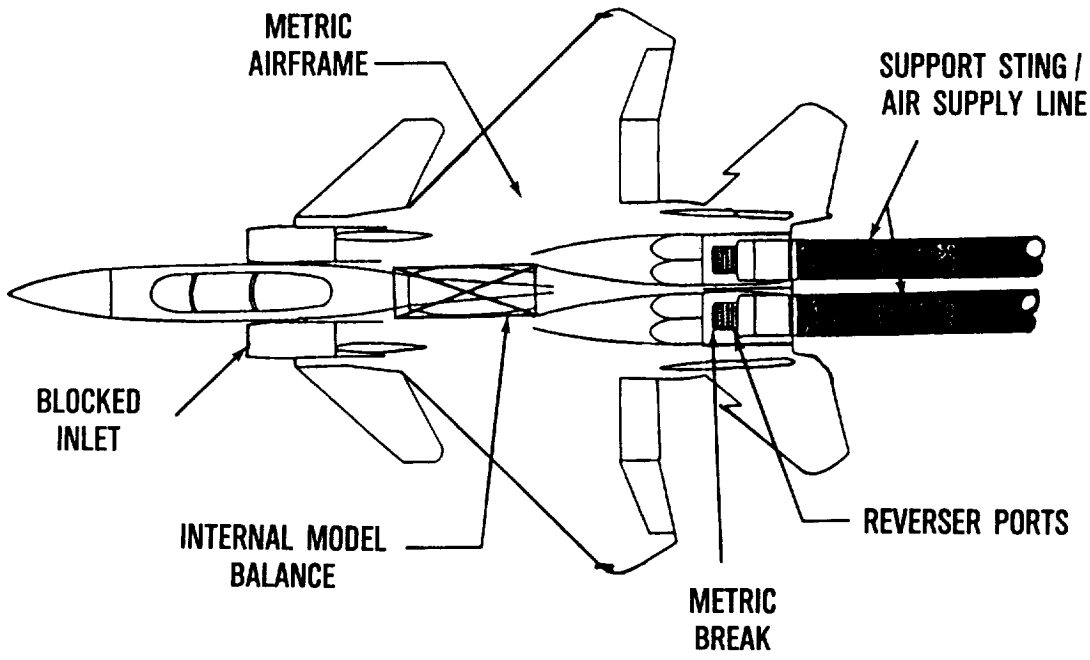

Figure 2. Jet Effects Model Schematic.

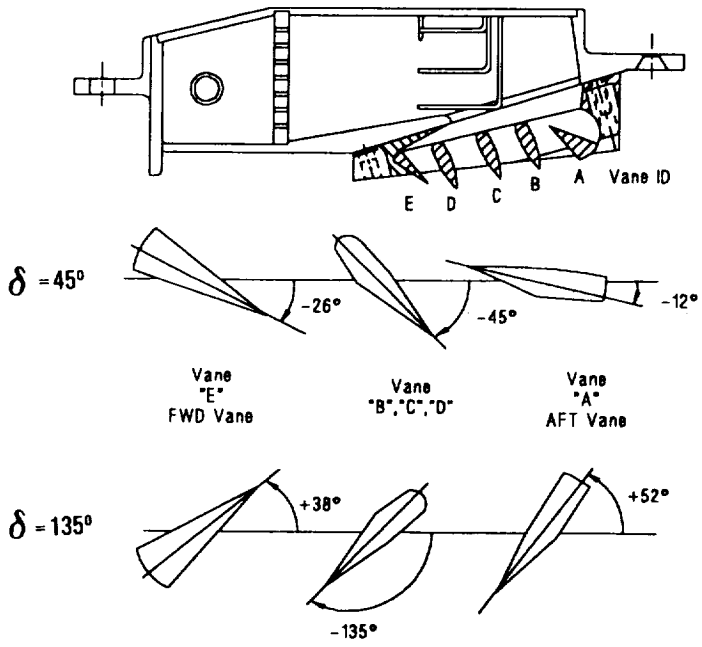

Figure 3. Reverser Vane Pack Assembly.

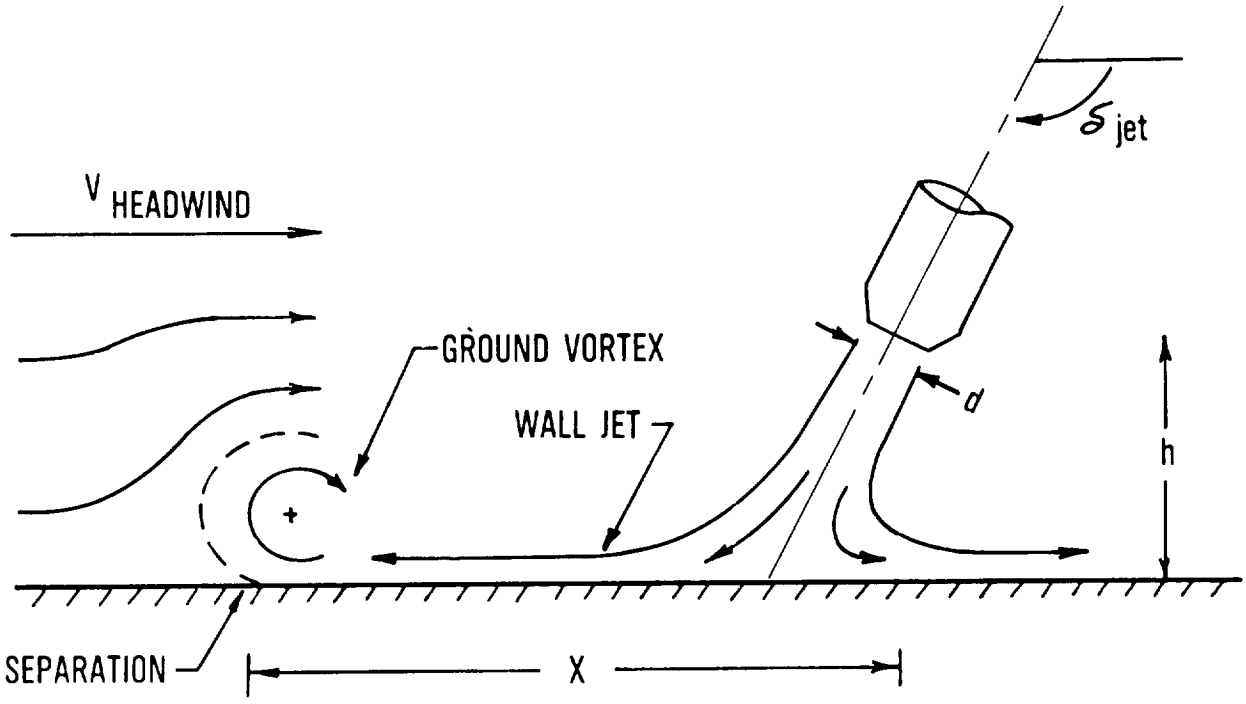

Figure 4. Formation of the Ground Vortex.

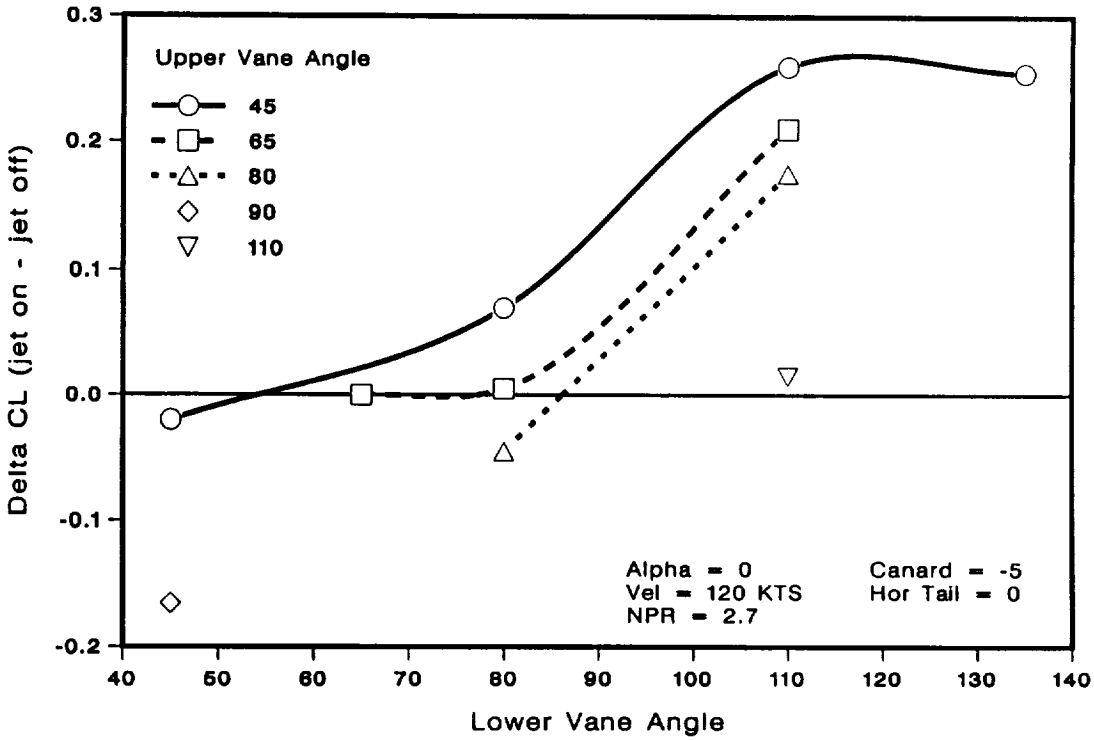

Figure 5. Lift Coefficient Increment as a Function of Upper and Lower Vane Angle. Free Air.

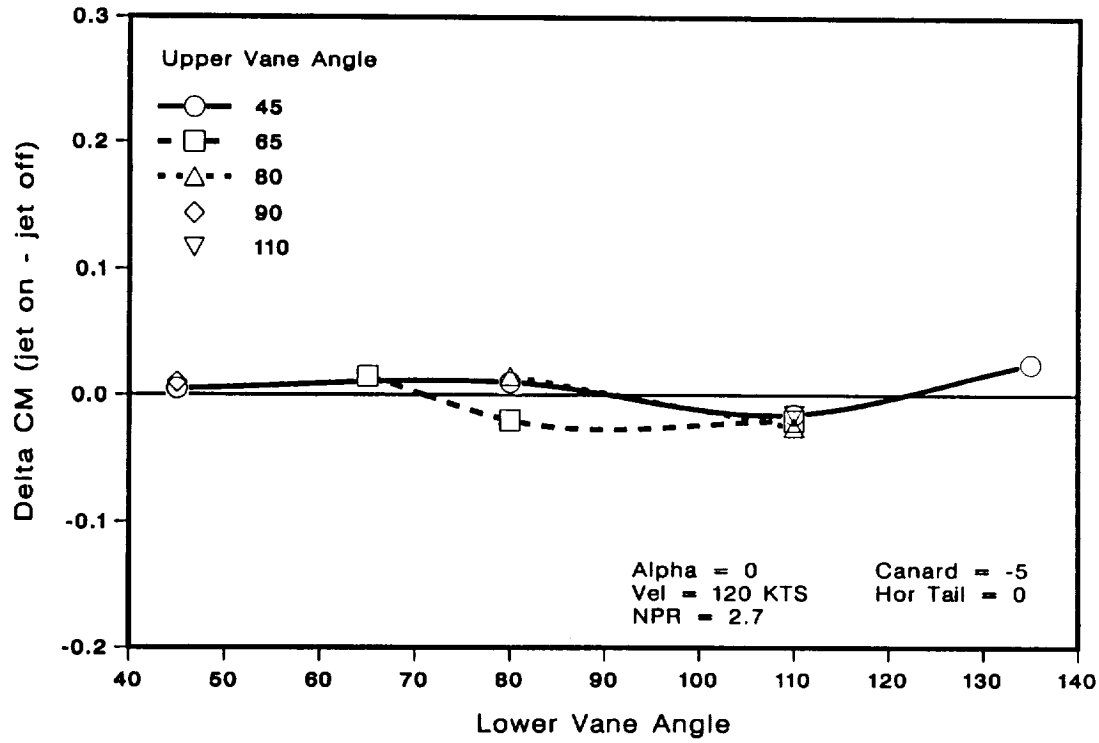

Figure 6. Pitching Moment Coefficient Increment as a Function of Upper and Lower Vane Angle. Free Air.

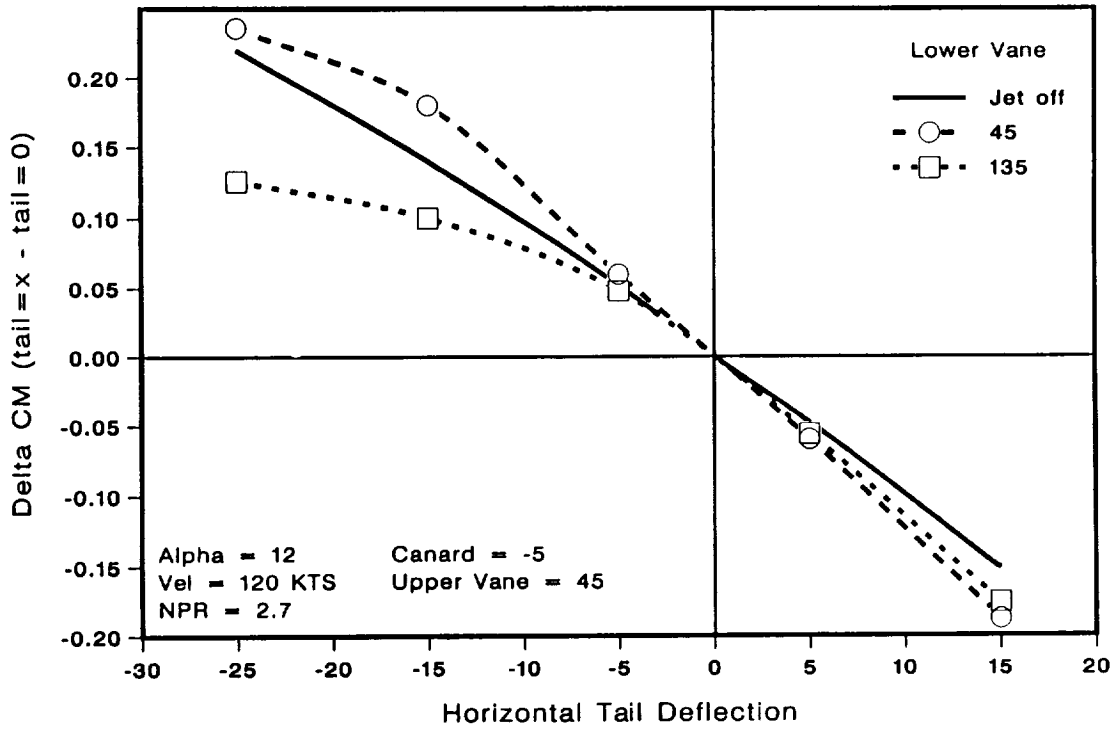

Figure 7. Increment in Pitching Moment Coefficient due to Horizontal Tail Deflection. Free Air.

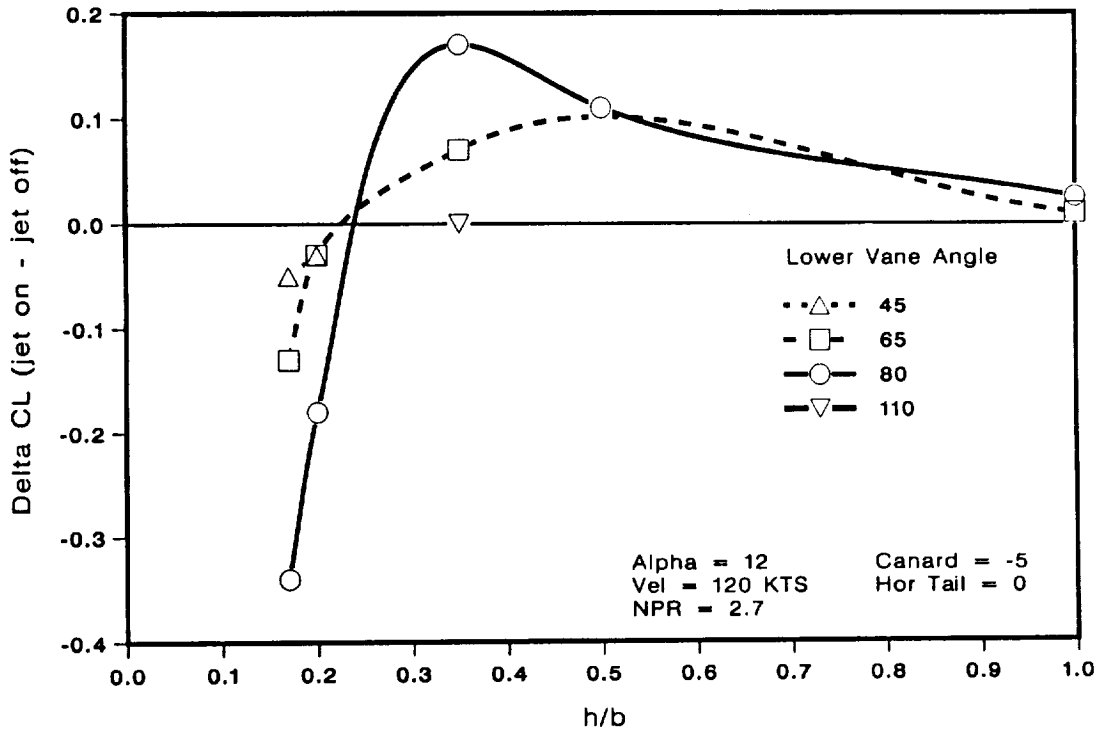

Figure 8. Lift Coefficient Increment as a Function of Lower Vane Angle. Height Transition.

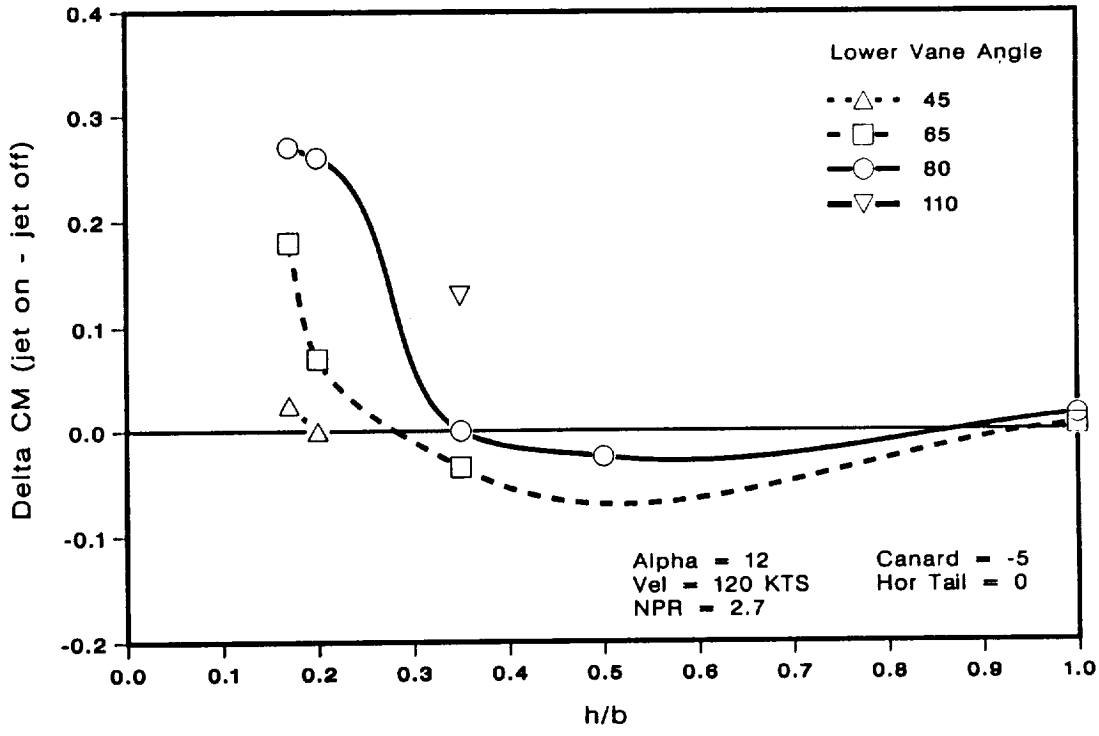

Figure 9. Pitching Moment Coefficient Increment as a Function of Lower Vane Angle. Height Transition.

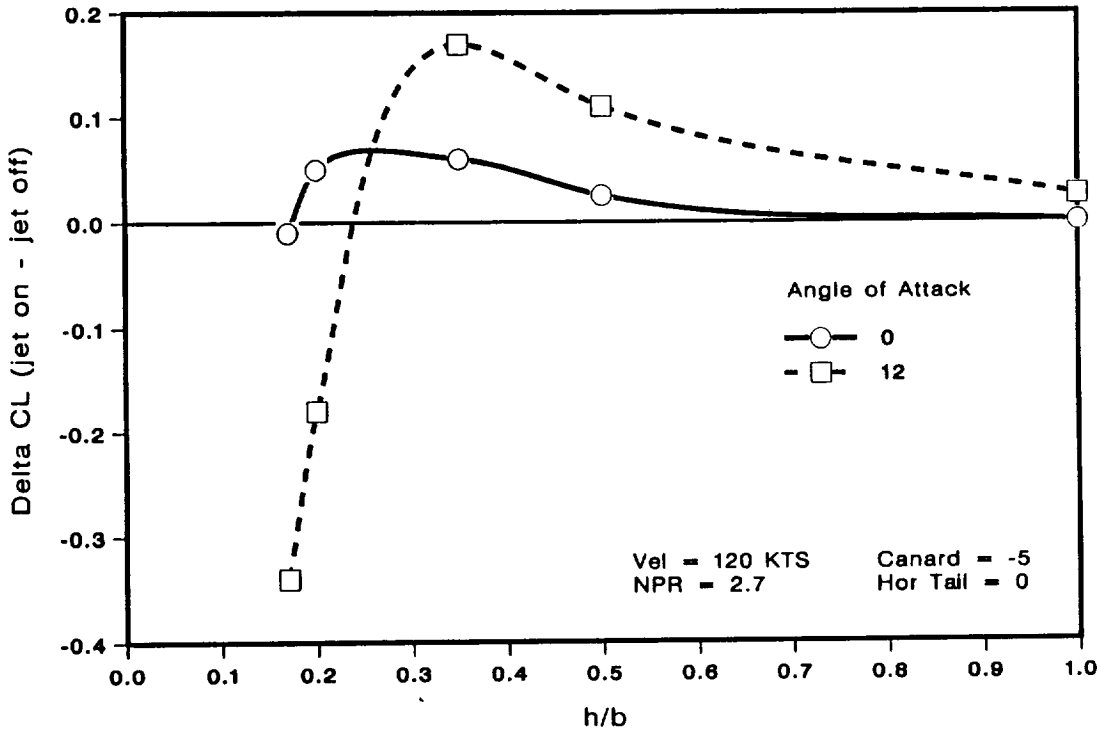

Figure 10. Lift Coefficient as a Function of Angle of Attack. Height Transition.

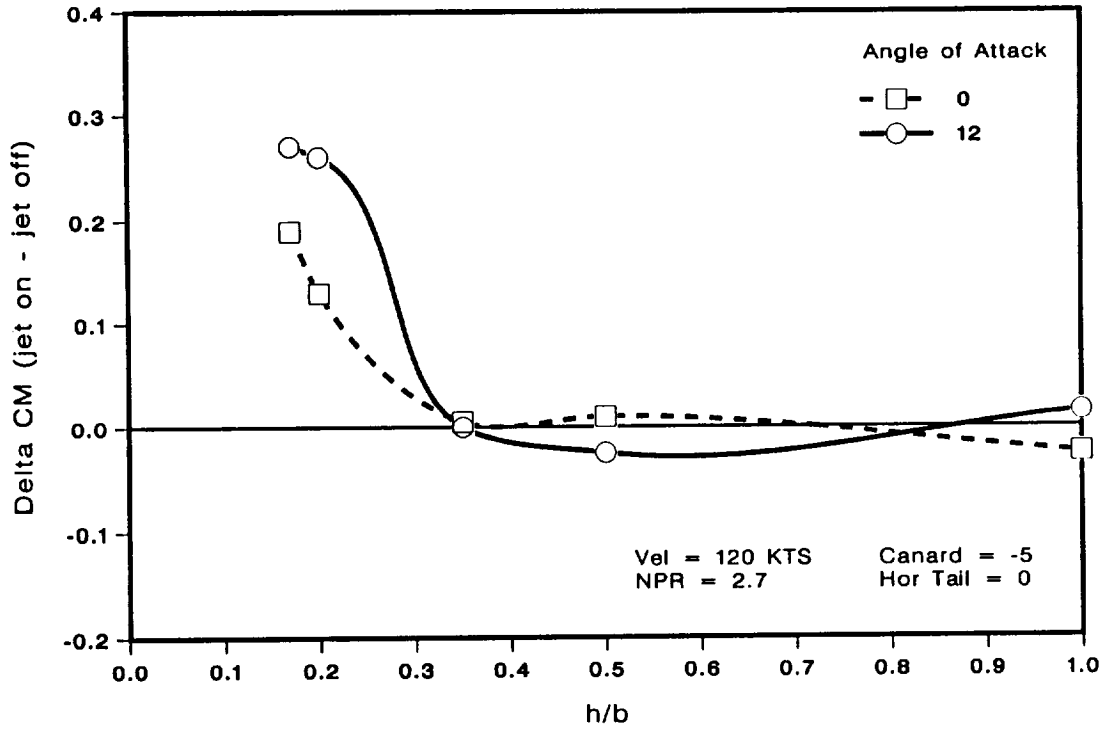

Figure 11. Pitching Moment Coefficient Increment as a Function of Angle of Attack. Height Transition.

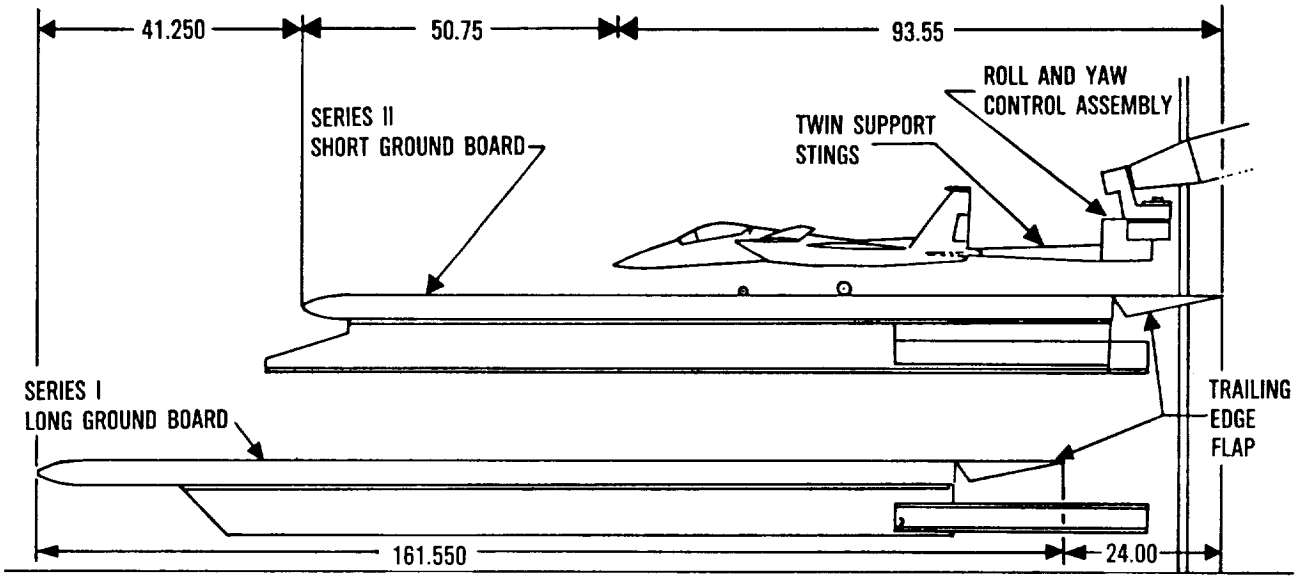

Figure 12. Comparison of Ground Board Installations.

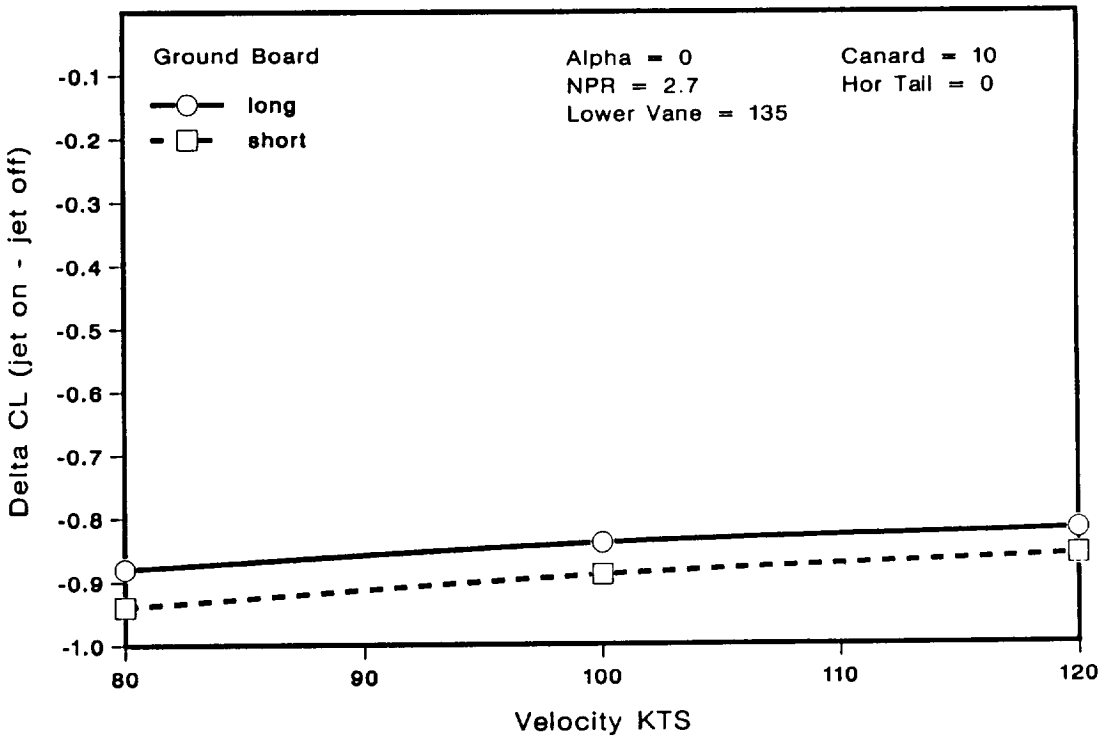

Figure 13. Effect of Ground Board Length on the Reverser Induced Lift Coefficient Increment. Landing Gear Height.

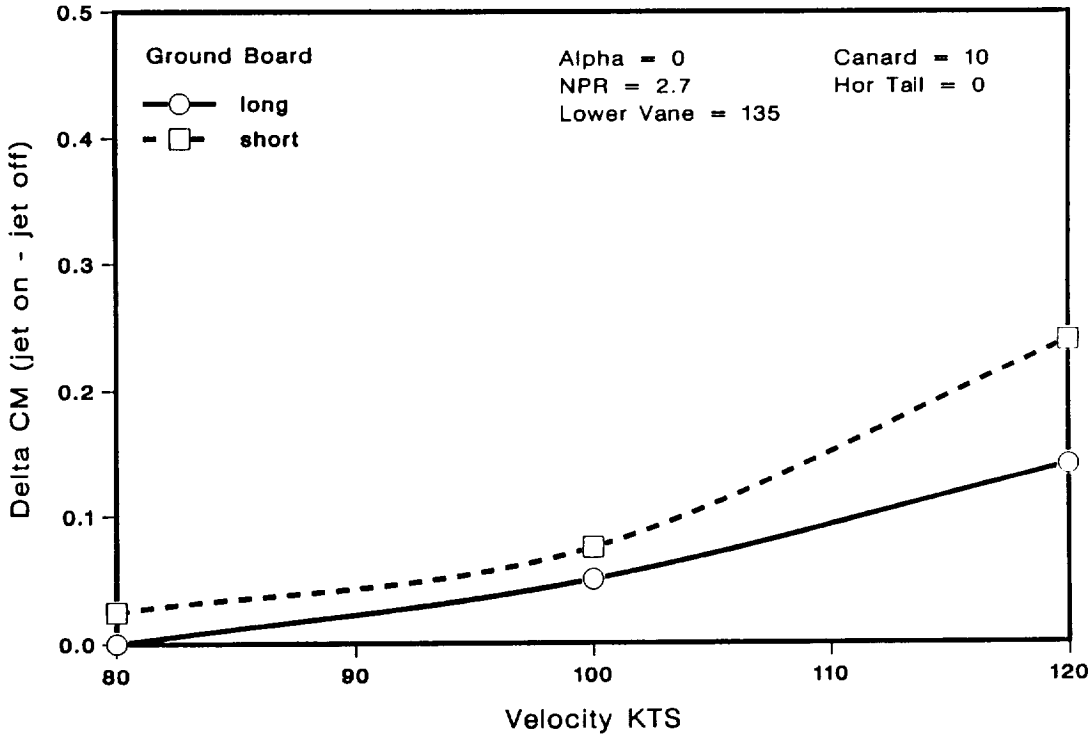

Figure 14. Effect of Ground Board Length on the Reverser Induced Pitching Moment Coefficient Increment. Landing Gear Height.

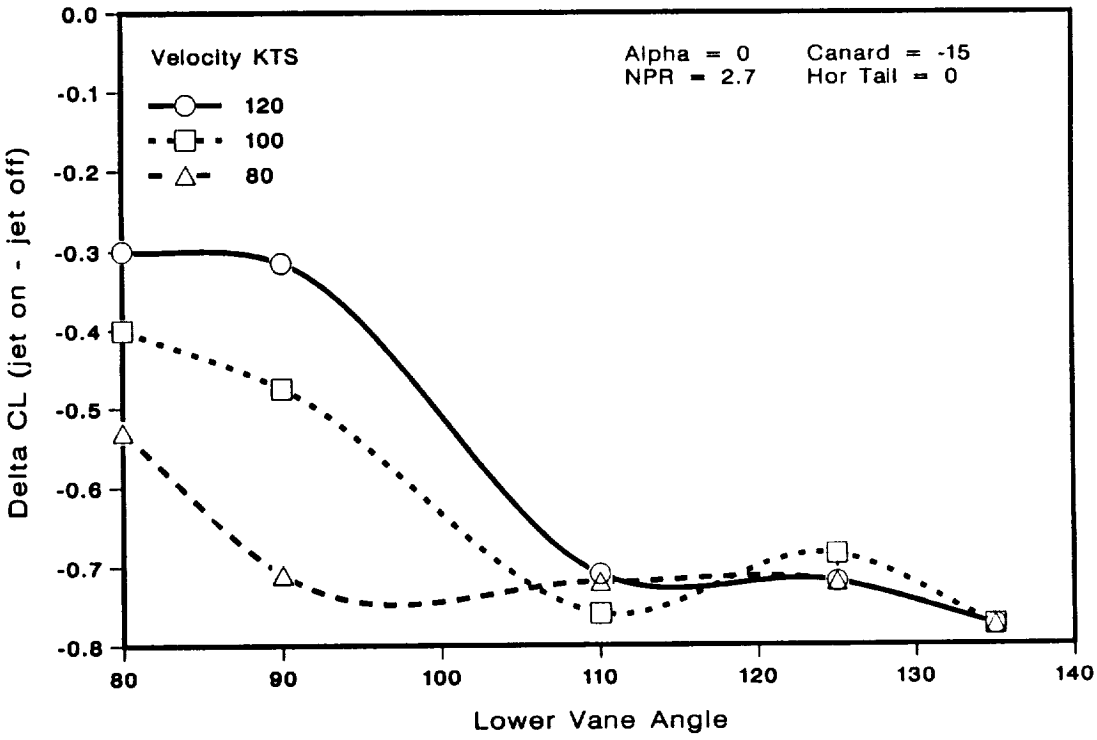

Figure 15. Effect of Free Stream Velocity and Lower Vane Angle on the Reverser Induced Lift Coefficient Increment. Landing Gear Height.

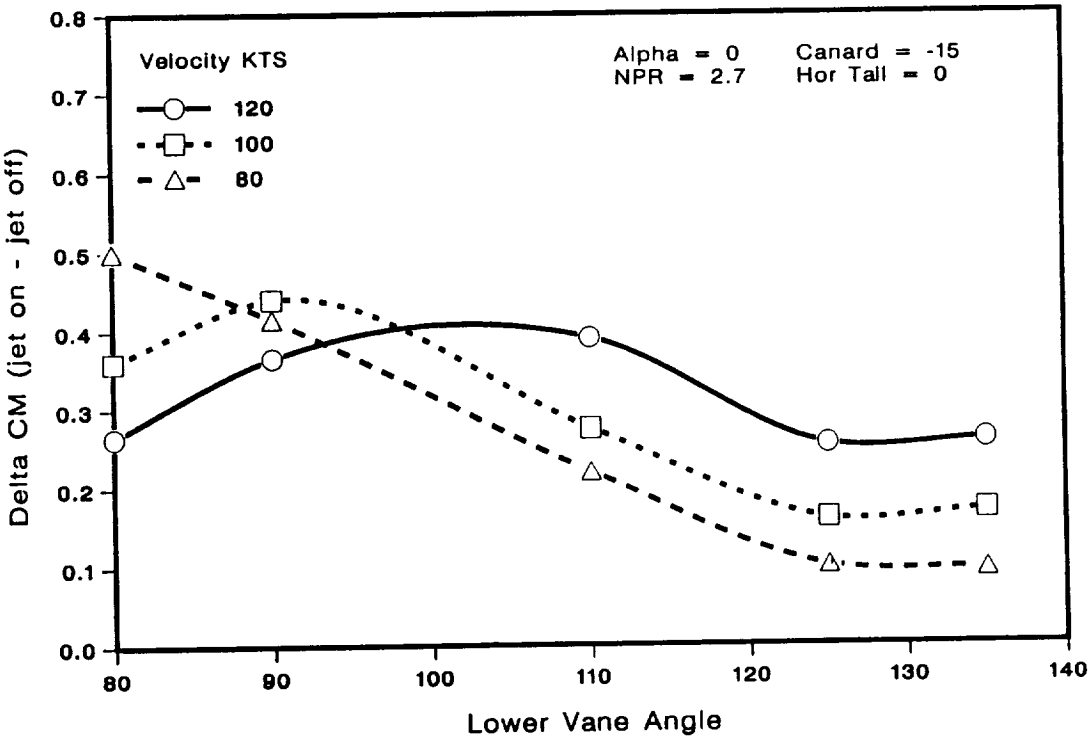

Figure 16. Effect of Free Stream Velocity and Lower Vane Angle on the Reverser Induced Pitching Moment Coefficient Increment. Landing Gear Height.

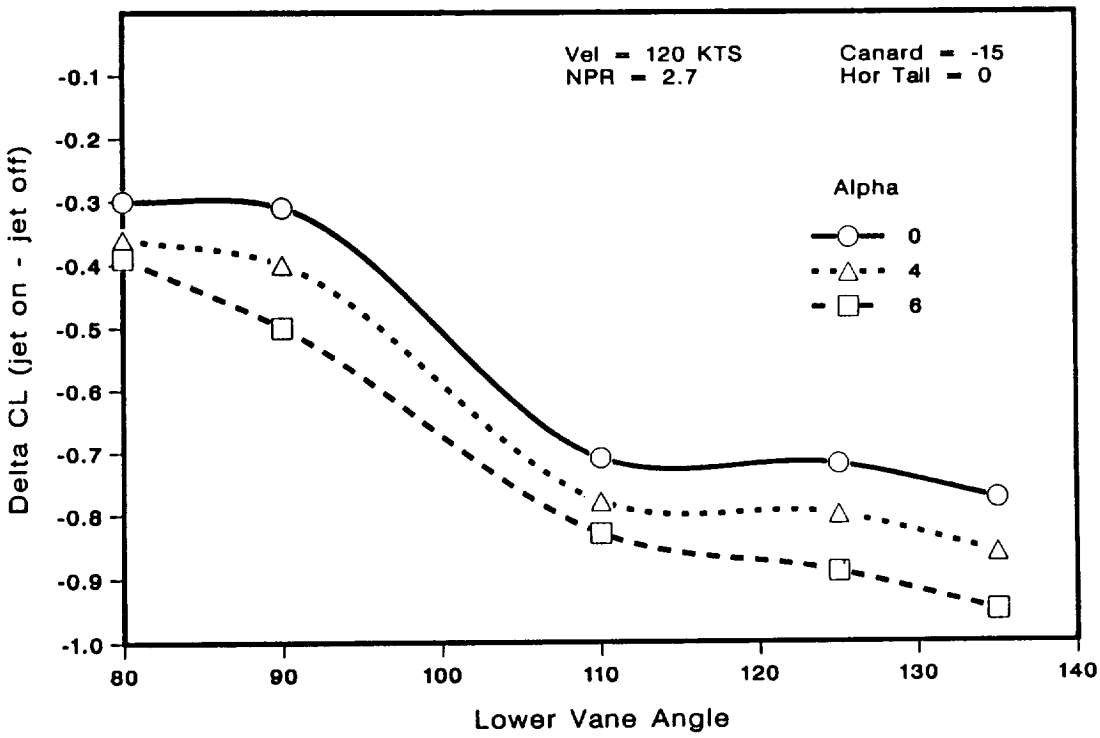

Figure 17. Effect of Angle of Attack and Lower Vane Angle on the Reverser Induced Lift Coefficient Increment. Landing Gear Height.

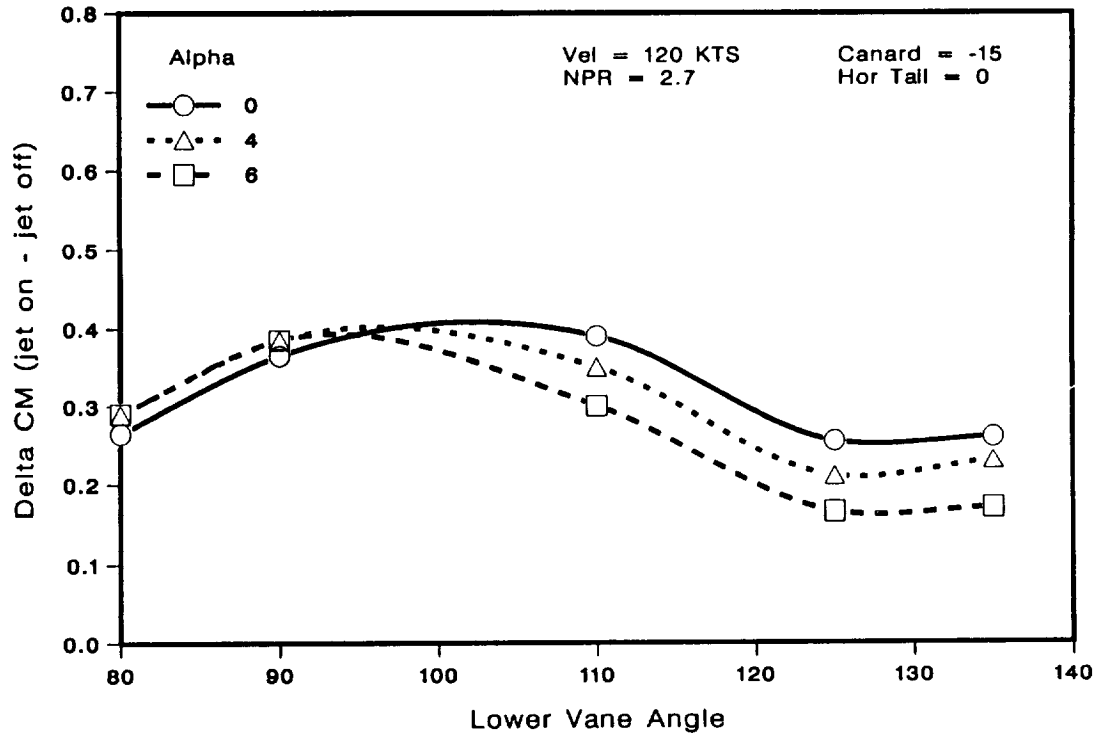

Figure 18. Effect of Angle of Attack and Lower Vane Angle on the Reverser Induced Pitching Moment Coefficient Increment. Landing Gear Height.

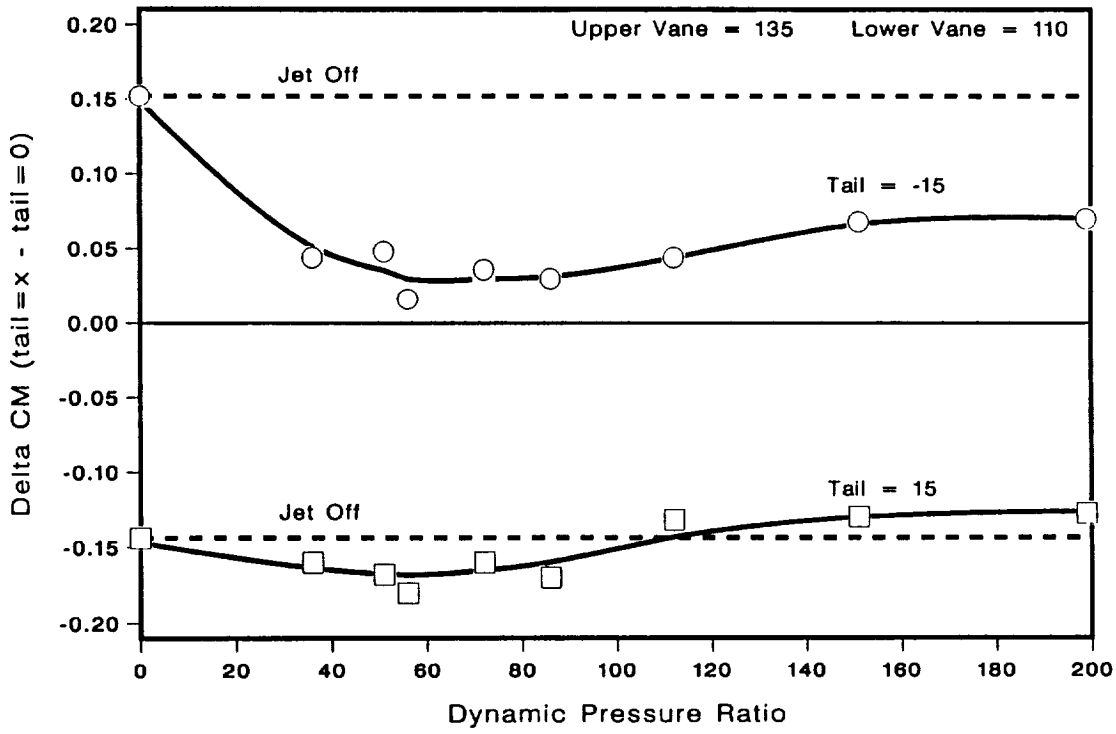

Fig 19. Pitching Moment Coefficient Increment due to Tail Deflection as a Function of the Reverser to Free Stream Dynamic Pressure Ratio. Landing Gear Height.

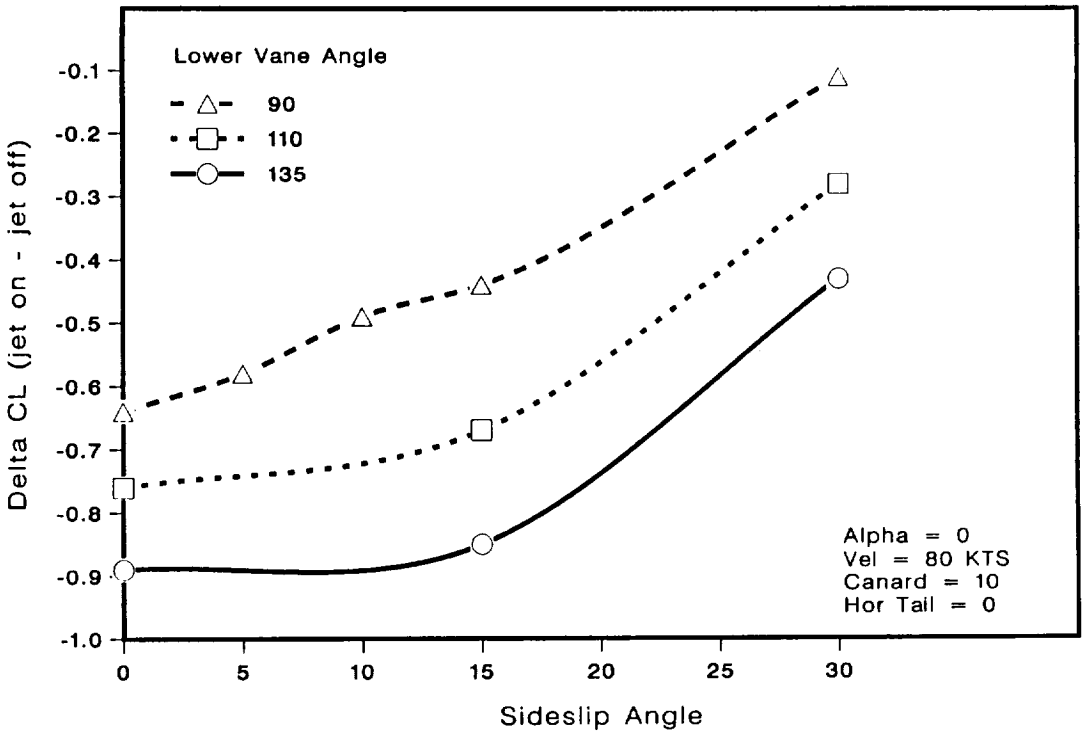

Figure 20. Effect of Sideslip Angle on the Reverser Induced Lift Coefficient Increment. Landing Gear Height.

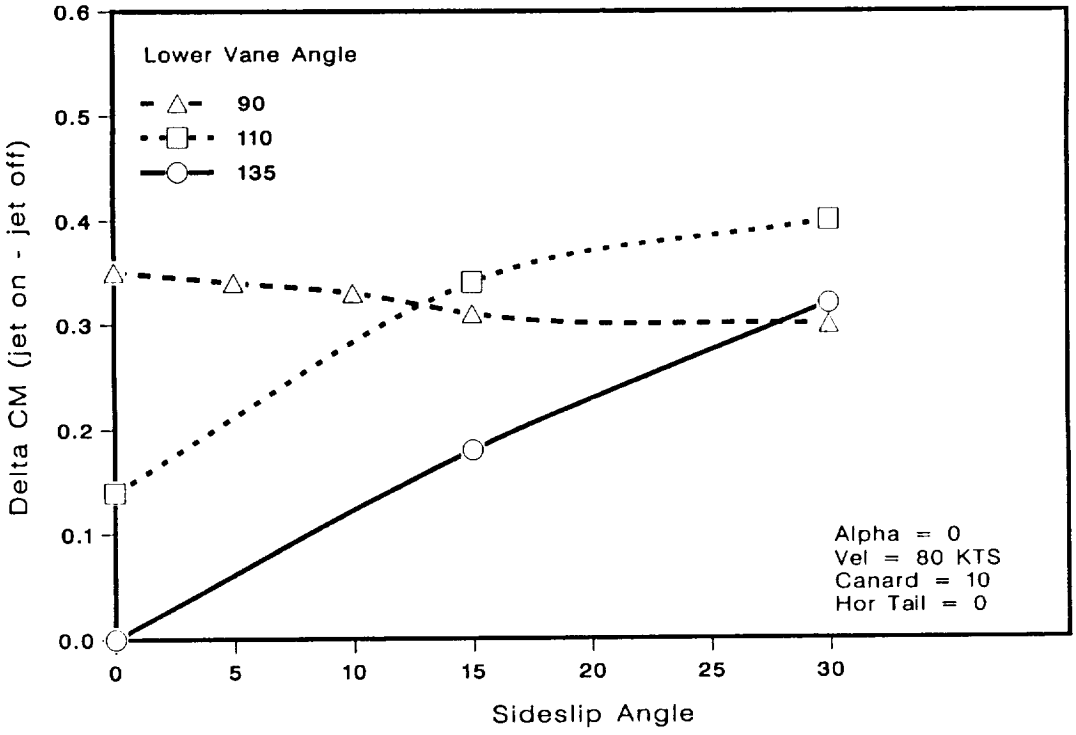

Figure 21. Effect of Sideslip Angle on the Induced Pitching Moment Coefficient Increment. Landing Gear Height.

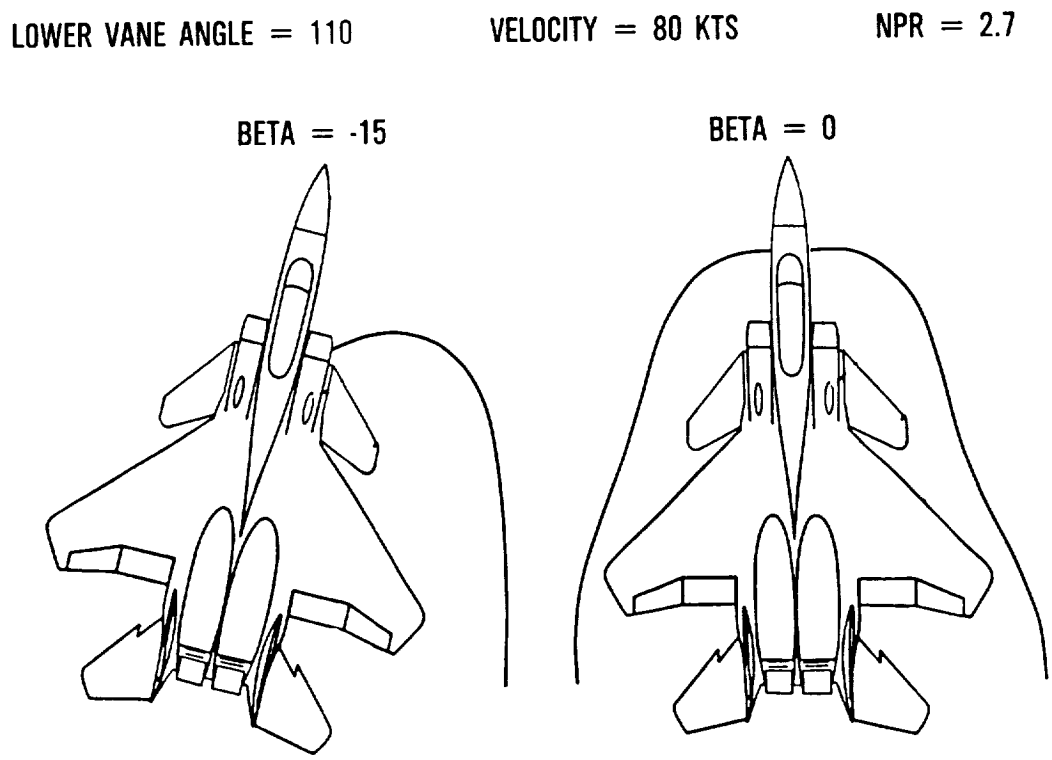

Figure 22. Ground Stagnation Line at Zero and Negative Sideslip.

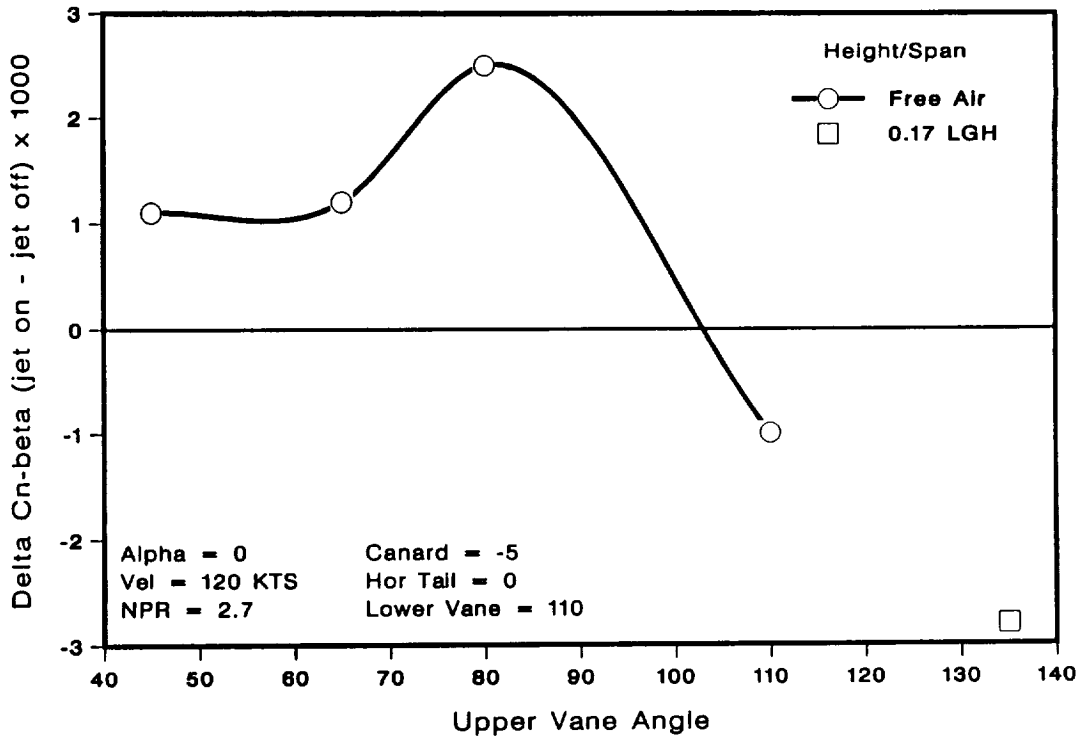

Figure 23. Increment in Directional Stability as a Function of Upper Vane Angle. Free Air.

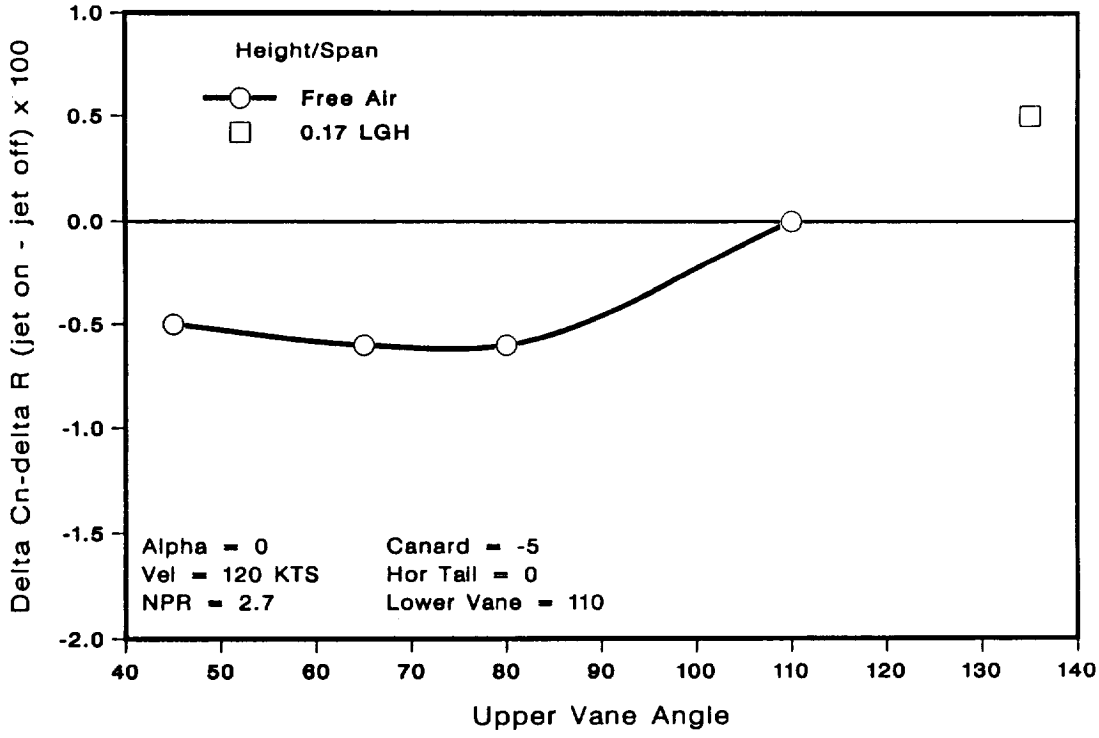

Figure 24. Increment in Rudder Effectiveness as a Function of Upper Vane Angle. Free Air.

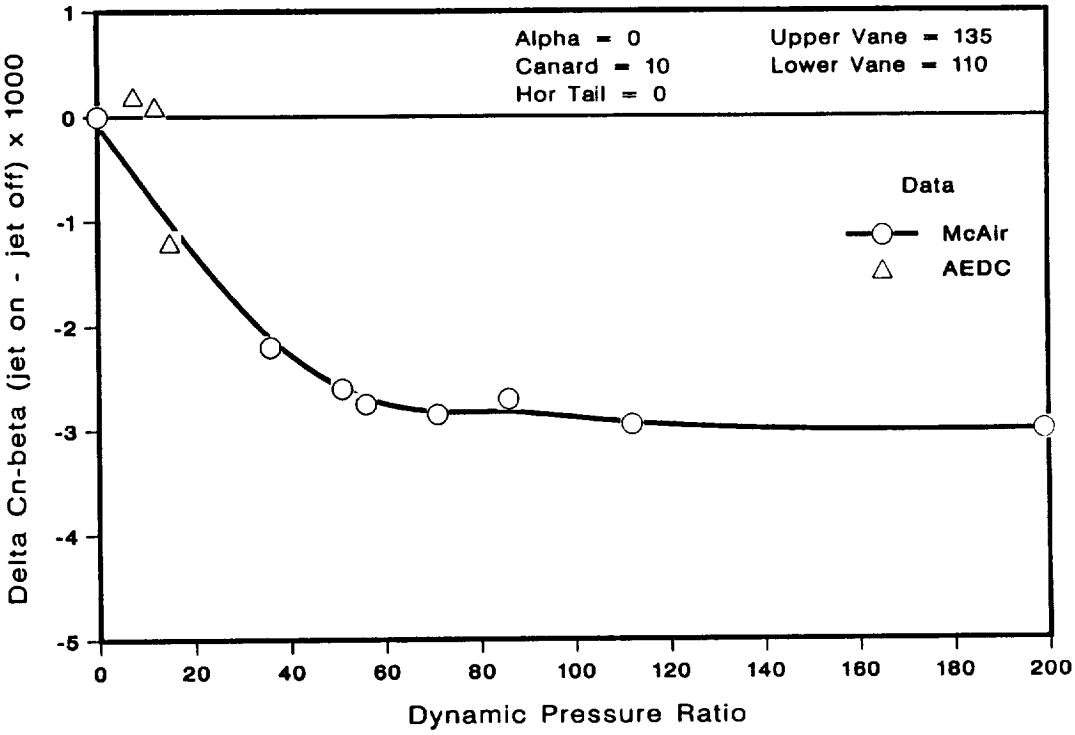

Figure 25. Increment in Directional Stability as a Function of the Reverser to Free Stream Dynamic Pressure Ratio. Landing Gear Height.

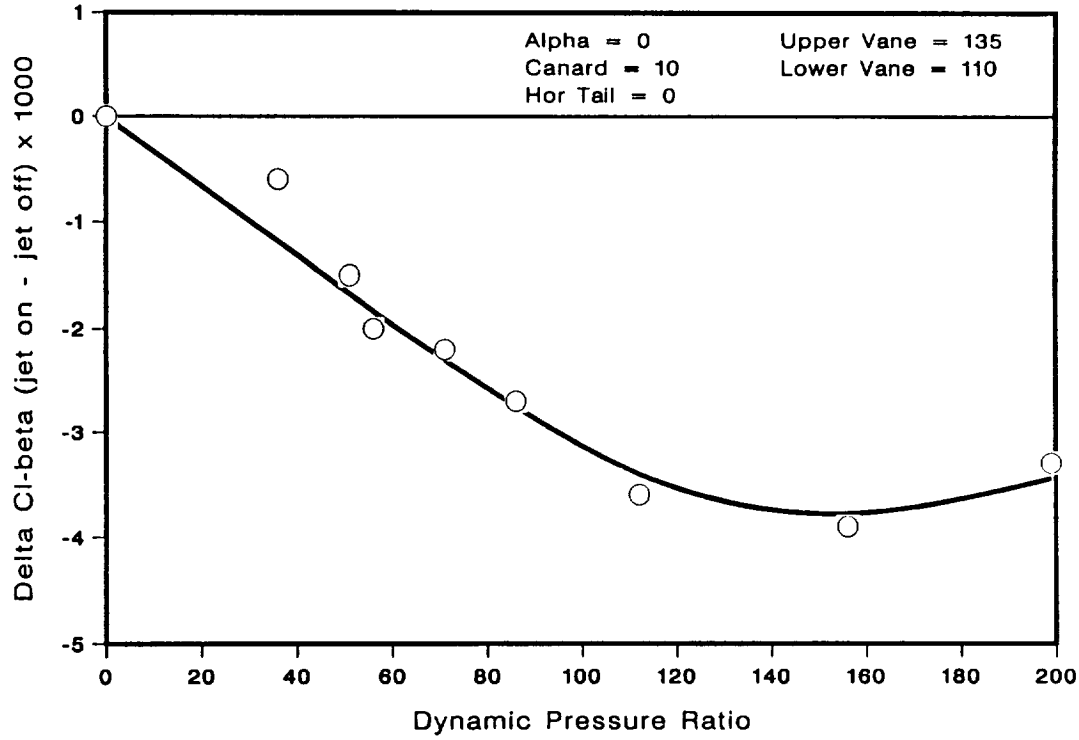

Figure 26. Increment in Lateral Stability as a Function of the Reverser to Free Stream Dynamic Pressure Ratio. Landing Gear Height.

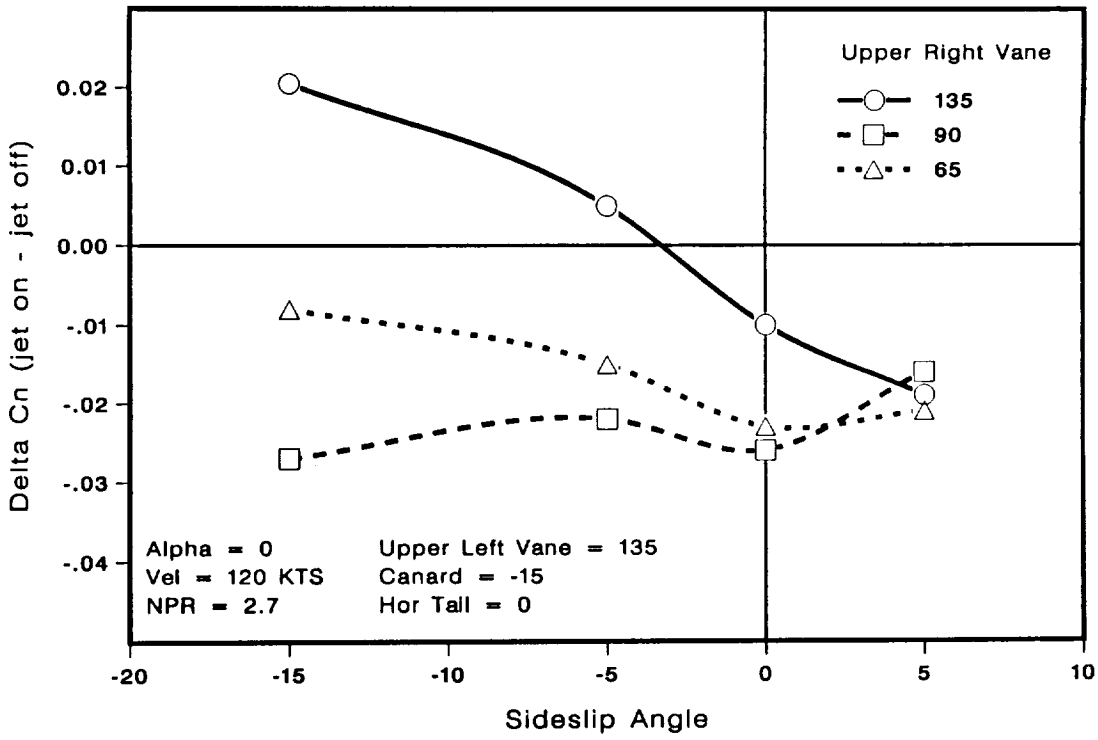

Figure 27. Yawing Moment Coefficient Increment as a Function of Upper Right Vane Angle. Landing Gear Height.

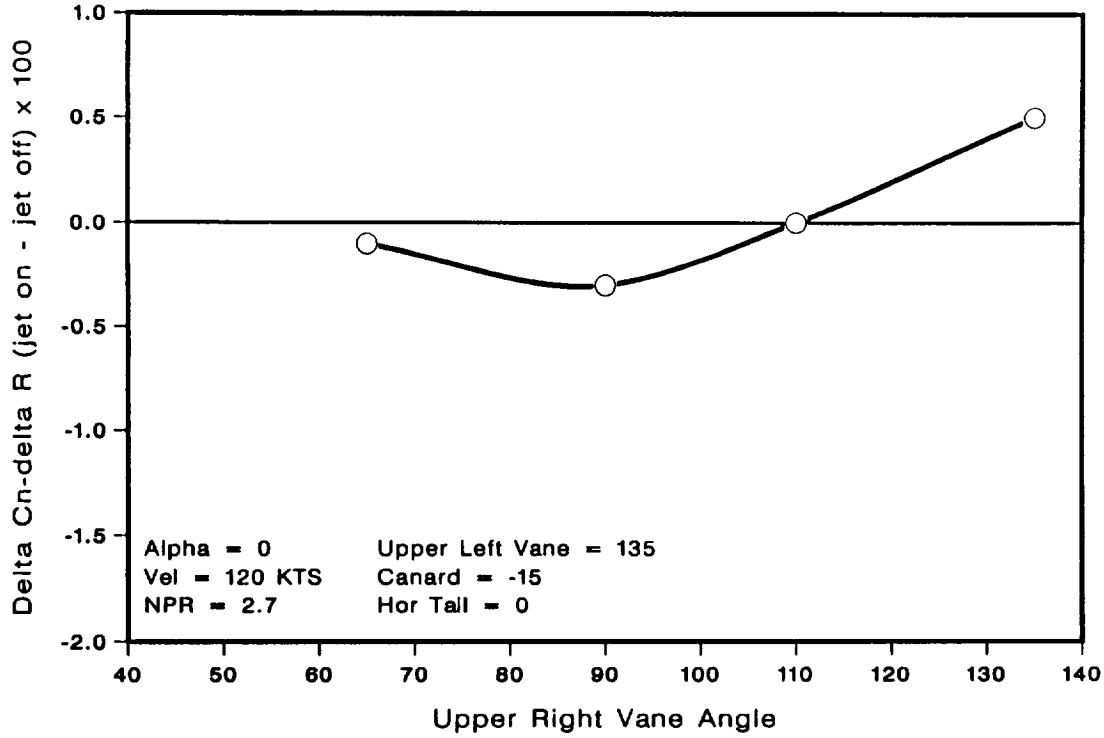

Figure 28. Increment in Rudder Effectiveness as a Function of Upper Right Vane Angle. Landing Gear Height.

AN ASSESSMENT OF GROUND EFFECTS DETERMINED BY STATIC AND DYNAMIC TESTING TECHNIQUES

John W. Paulson, Jr.

Guy T. Kemmerly

NASA Langley Research Center
Hampton, Virginia 23665

INTRODUCTION

Historically, aircraft ground effects have been determined by placing a model configuration in the wind tunnel, obtaining data at various heights above a ground plane and analyzing the results as a function of height. This approach yields time averaged static aerodynamic data as a function of height above the ground plane for use in analyzing aircraft performance during approach and landing. In actual flight testing ground effects can be determined in two ways: constant altitude flight above the ground, or descending flight toward the ground (final approach and landing)-both conducted at constant air speed and angle-of-attack. Results obtained with the constant altitude flight method and conventional wind tunnel ground effects tests are generally in good agreement (refs. 1-3). That is, lift increases, drag decreases and pitching moment changes indicated in static wind tunnel data are found to be present in flight results. However, if the flight test is conducted as a landing approach, where aircraft height varies with time as a function of rate of descent, then the flight test and wind tunnel results are not always in agreement (refs. 4-5). In particular, the increase in lift coefficient as the ground plane is approached seems to be lower when the aircraft has a rate-of-descent as compared to the case where rate-of-descent is zero or to static wind tunnel results. This variation in results appears to be caused by differences in the interactions that occur between the trailing vortex/wake system and ground plane (fig. 1) during descending flight ($\gamma < 0°$) and during level flight or static wind-tunnel tests ($\gamma = 0°$). These results have led to the hypothesis that rate-of-descent could be an important parameter in determining ground effects. The effects of sink rate might be particularly pronounced if vectored or reversed exhaust flows are involved,

which greatly amplifies the interactions of the exhaust, freestream, and the ground plane. In the past, the aircraft rate-of-descent has been simulated during wind-tunnel testing by moving the model vertically in the wind tunnel toward a ground plane. This method, described in references 6-7, was developed at Kansas University. Research conducted using the technique showed that a configuration with a rate-of-descent of up to about 3 ft/sec experienced less increase in lift in ground effect compared to static wind tunnel results at constant heights. However, this method is somewhat limited in maximum rate-of-descent because of the accelerations and vertical velocities possible within the confines of closed wind-tunnel test sections.

The present study was undertaken to evaluate the use of a new dynamic ground effects testing technique wherein a model is moved horizontally over an inclined ground plane. The evaluation was conducted at the Langley Research Center utilizing the Langley Vortex Research Facility (VRF). During the tests, the model is carried horizontally by a motorized cart down a towing tank at velocities up to 100 ft/sec and approaches a 4° inclined ground board producing effective descent rates of up to about 7 ft/sec. The VRF facility provides extensive data acquisition and support equipment, including compressed air for exhaust flow simulations. The study included the development of the dynamic test technique in the VRF and conventional ground effects tests in the Langley Research Center 14- by 22-Foot Subsonic Tunnel. These tests, using the same models and sting support hardware, allowed for a direct comparison between static and dynamic procedures to assess the effect of rate-of-descent on ground effect testing results. A description of the testing techniques and sample results are the subjects of this paper.

SYMBOLS

b	wing span, ft.
C_L	lift coefficient, Lift/ $q_\infty S$
ΔC_L	percent change in lift coefficient $(C_{L_{IGE}} - C_{L_{OGE}})/C_{L_{OGE}}$
d/dt	derivative with respect to time
g	acceleration due to gravity, 32.2 ft/sec^2
h	height above ground plane, ft.
$\dot{h}$	rate-of-descent, dh/dt, ft/sec.
NPR	nozzle total pressure ratio, P_t/P
P_t	nozzle total pressure, lbf/ft^2
P	static pressure, lbf/ft^2
q_∞	dynamic pressure, $1/2\ \rho V^2$, lbf/ft^2
S	wing area, ft^2
t	time, sec.
V	velocity, ft/sec.
α	angle-of-attack, deg.
γ	flight path angle, deg.
δ	deflection angle, deg.
θ	pitch attitude, deg.
ρ	density, $slugs/ft^3$

Subscripts:

IGE	in ground effect
OGE	out of ground effect
∞	freestream conditions
j	exhaust jet conditions

TEST TECHNIQUES AND MODEL HARDWARE

To produce a rate-of-descent in a ground based facility the model must effectively move toward a simulated ground plane. In the Vortex Research Facility (VRF) this was accomplished by moving the model horizontally over a ground board inclined toward the model path as shown in figures 2 and 3. In this procedure, the combination of forward velocity and ground board angle produced a rate-of-descent ($\dot{h}$) equal to $V_\infty \tan 4^\circ$ where V_∞ was varied up to 100 ft/sec, resulting in values of $\dot{h}$ up to 7 ft/sec.

In the VRF the sting-mounted models were attached to a vertical blade support system suspended below a powered cart which travels on rails above the test section (fig. 4). The cart was powered by a high-performance automobile engine and included electrical, mechanical and high-pressure air systems which provided data acquisition, control of test conditions and model/cart safety. Prior to a typical run, angle-of-attack and minimum ground height were preset using the support hardware. The cart accelerated up to the desired test velocity, which was maintained by a normal automobile cruise control system. The 14-foot high by 17-foot wide by 600-foot long test section shielded the model from the bow wave created by the moving cart. Before the test section was entered, air valves opened which allowed time for the exhaust flow to be stabilized at a desired nozzle pressure ratio before the model approached the ground board. As the model passed over the 100-foot long ramp section of the ground board, the height of the model over the ground board decreased to a minimum h/b which then remained constant over the 50 foot long flat portion of the ground board. Thus, during a single data run both dynamic (time varying height) and steady state (constant height) data were obtained. The data obtained consisted of aerodynamic forces and moments measured on a 6-component

balance, high pressure air data for exhaust flow characteristics, and cart velocity for test conditions. In addition, model and sting accelerations were recorded in order to remove inertial loads from the balance output. At the test section exit, the cart engine was shutdown and brakes were applied which brought the cart to rest with a 2-g decelaration. Because of this deceleration, the model had to be kept as light as possible (i.e. less than 25 lb.) to prevent the balance size from becoming so large that the low aerodynamic forces could not be measured accurately.

The models used in this investigation were the flat plate 60° delta wing (b = 3 ft.) shown in figure 5, and the 7-percent scale F-18 configuration shown in figure 6. Both models were equipped with non-metric reversed-thrust nozzles: The 60° delta wing used simple convergent pipes bent to 45° and the F-18 used a modification of a reverse nozzle/plenum box from a previous generic thrust reverser program (ref. 8). Both models were tested at various forward velocities (and hence rates-of-descent), minimum ground heights, nozzle pressure ratios and angles-of-attack in the VRF, and the resulting dynamic- and steady-state ground effects were determined for the unpowered and reverse thrust cases. After the VRF tests were completed, the same model/sting/airline configurations were installed in the 14- by 22-Foot Subsonic Tunnel and the static ground effects were determined with and without the moving belt ground plane. In this wind tunnel, the tunnel floor boundary layer is always removed during ground effects testing by a vacuum system located at the test section entrance. This ensures that with or without the moving belt, there is initially no boundary layer on the test section floor. The models had been designed and fabricated to allow the same sting support to

be used in both facilities to minimize support interference and to permit the direct comparison of the differences between static, steady state and dynamic ground effects.

DISCUSSIONS

The following discussion presents the effect of the moving ground belt on static wind-tunnel ground effects for both unpowered and reversed thrust cases with the 60° delta wing. The static ground effect results are then compared with the dynamic and steady state results from the VRF for both the 60° delta and the F-18 configuration. Finally the dynamic results for the unpowered 60° delta wing are analyzed as a function of rate-of-descent.

Effect of Moving Belt. For years it has been known that the wind-tunnel floor boundary layer can affect the results obtained from static wind-tunnel ground effects testing. Twenty years ago, studies showed that moving the tunnel floor at the freestream velocity could eliminate this floor boundary layer and improve ground effect results. The research reported in reference 9 presented a boundary of C_L versus h/b which defined the need for using the moving belt during ground effects testing. Because of the high values of C_L and relatively low low values of h/b required before the moving belt was needed, it was assumed that conventional powered fighter configurations would not require the belt for testing. However, since current fighter concepts may utilize reverse thrust on approach, it was felt that during this dynamic ground effect study an examination should be made of the influence of the moving belt on ground effects.

As expected, the effect of the moving belt on the static ground effects of the unpowered 60° delta wing was essentially nill (fig. 7). However, when the

thrust reversers were employed for the delta wing (fig. 8) the moving belt influenced the static ground effects. Since the reversed flow was penetrating against relatively high-energy freestream air (rather than a boundary layer) when the belt was moving, it did not flow as far forward and produced a lower loss in lift at low ground heights as compared to the fixed floor results. This trend was consistent for all configurations tested, and led to the conclusion that the moving belt may be required for wind tunnel ground effects testing of thrust-reversing configurations.

Comparison of Dynamic and Static Ground Effects. Since the magnitude of the lift increase in ground effect for the unpowered 60° delta wing was small, the comparison of static and dynamic ground effects is presented in figure 9 in terms of percent change in lift rather than lift coefficient. For a test condition of V_∞ = 70 ft/sec, α = 10° and a sink rate of 4.9 ft/sec, the percent increase in lift as the ground plane is approached was lower than that produced from the static ground effects. As mentioned earlier, the change due to sink rate is probably caused by differences in the interactions of the model wake with the ground plane in dynamic and static conditions. Note that the solid data point in figure 9 represents the steady state results from the VRF where the model was traveling over the 50 foot long flat portion of the ground board. These steady-state results compare well with those obtained during the static tests in the wind tunnel.

The comparison between dynamic and static ground effect was more dramatic when thrust reversers were employed on the 60° delta wing as shown in figure 10. These data indicate that the well-known loss in lift as the ground plane was approached statically was not present at all in the dynamic case. In fact, the model exhibited an increase in lift in the dynamic test. This result was caused by the model effectively "running away" from the reversed

thrust plume. However, once the model passed over the flat ground board the reversed flow field had time to establish steady state conditions and the result was close to the static wind-tunnel ground effects. The test condition was set to simulate a jet to freestream dynamic pressure ratio of approximately 100 which is representative of normal approach power setting for a fighter aircraft. If the dynamic pressure ratio were increased (i.e. the throttle setting advanced or the approach velocity reduced), then the reverse flow plume would be expected to penetrate farther forward and the ground effects would probably be different than the NPR = 1.6 case. The data shown in figure 11 for NPR = 1.8 indicate that the effect of the belt was reduced, and that the lift loss present in the static results was beginning to occur in the dynamic results as the reverse flow plume penetrated farther below and ahead of the model to interact with the ground plane at a greater distance than the lower NPR case. In effect, at this higher dynamic pressure ratio the model could not "escape" from the exhaust plume as the ground plane was approached. Once again, the steady state result was close to the static results.

Similar trends are shown for the F-18 configuration in figure 12 for a typical landing dynamic pressure ratio. It should be noted that the expected lift loss in the static data was of lower magnitude than the loss for the 60° delta wing. The F-18 exhaust nozzles were not located near the wing, but rather at the aft end of the fuselage and, therefore, have less effect on the wing flow field. However, this loss in lift was not indicated in the dynamic data and the steady state results matched the static results. As an assessment of on the effect of dynamic pressure ratio, the NPR was increased to 2.5 which yielded a dynamic pressure ratio much greater than a normal

approach condition. In this case, the plume should have been blown quite far ahead of and below the model. The data of figure 13 showed that the dynamic, static and steady state results were all similar indicating that the plume was in front of the model for all testing techniques.

Effect of Rate-of-Descent. In the VRF tests rate-of-descent could be varied by changing the cart velocity; unfortunately, this also changed test Reynolds number and dynamic pressure ratio. Since the 60° delta wing had a sharp leading edge, it was anticipated that Reynolds number effects would be small and that if the model was unpowered, a consistent set of data could be obtained at various rates-of-descent. Results presented in figure 14 show that increasing the rate-of-descent reduced the effect of the ground plane, resulting in reduced increases in lift at higher $\dot{h}$. This trend seems reasonable since at very high $\dot{h}$ an aircraft would be on the ground before the effect would be established.

CONCLUDING REMARKS

A new testing technique has been developed wherein rate of descent can be included as a parameter in ground effects investigations. This technique simulates rate of descent by horizontal motion of a model over an inclined ground board in the Langley Vortex Research Facility. During initial evaluations of the technique, dynamic ground effects data were obtained over the inclined ground board, steady state ground effects data were obtained over a flat portion of the ground board, and the results have been compared to conventional static wind tunnel ground effect data both with and without a moving belt ground plane simulation. Initial testing and analysis have led to the following conclusions:

1.) The moving belt ground plane had little effect on static ground effects for the configurations tested unless thrust reversers were employed. When thrust reversers were simulated, the moving belt yielded reduced lift losses in ground effect as the reversed nozzle flow could not penetrate against freestream flow as well as against the tunnel boundary layer.

2.) The inclusion of rate-of-descent in ground effects testing can have a significant effect on the results. In general, rate-of-descent reduced ground effects, compared to static or steady state results, to the point that for reversed thrust cases, an expected loss of lift due to ground effects was eliminated at approach conditions.

3.) In general, the the steady state results from the VRF matched static results obtained from the wind tunnel once the flow field stabilized over the flat portion of the ground board.

REFERENCES

1. Pelagatti, C.; Pilon, J. C.; and Bardaud, J.: Analyse Critique des Comparaisons des Resultats de Vol aux Previsions de Soufflerie pour des Avions de Transport Subsonique et Supersonique. Paper 23, AGARD CP-187, Flight Ground Testing Facilities Correlation, 1975.

2. O'Leary, C. O.: Flight Measurements of Ground Effect on the List and Pitching Moment of a Large Transport Aircraft (Coment 3B) and Comparison with Wind Tunnel and Other Data. British ARC R&M 3611, June 1968.

3. Rolls, L. S.; and Koenig, D. G.: Flight-Measured Ground Effect on a Low-Aspect-Ratio Ogee Wing Including a Comparison with Wind-Tunnel Results. NASA TN D-3431, 1966.

4. Baker, P. A.; Schweikhard, W. G.; and Young, W. R.: Flight Evaluation of Ground Effect on Several Low-Aspect-Ratio Airplanes. NASA TN D-6053, October 1970.

5. Thomas, J. L.; Hassell, J. L.; and Nguyen, L. T.: Aerodynamic Characteristics in Ground Proximaty. Powered-Lift, Aerodynamics and Acoustics, Session I, Paper No. 9, Pg. 145, NASA SP-406, May 1976.

6. Chang, R. C.: An Experimental Investigation of Dynamic Ground Effect. KU-FRL-410-1, , Flight Research Laborartory, University of Kansas Center for Research, Incorporated, April 1985.

7. Lee, P. H.; Lan, C. E.; and Muirhead, V. U.: An Experimental Investigation of Dynamic Ground Effect. Prepared under NASA Grant NAG1-616, CRINC-FRL-717-1, Flight Research Laborartory, University of Kansas Center for Research, Incorporated, January 1987.

8. Joshi, P. B.: Generic Thrust Reverser Technology for Near Term Application. Volume 1-4, AFWAL-TR-84-3094, February 1985.

9. Turner, T. R.: A Moving-Belt Ground Plane for Wind-Tunnel Ground Simulation and Results for Two Jet-Flap Configurations. NASA TN D-4228, November 1967.

10. Turner, T. R.: Ground Influence on a Model Airfoil with a Jet-Augmented Flap as Determined by Two Techniques. NASA TN D-658, February 1961.

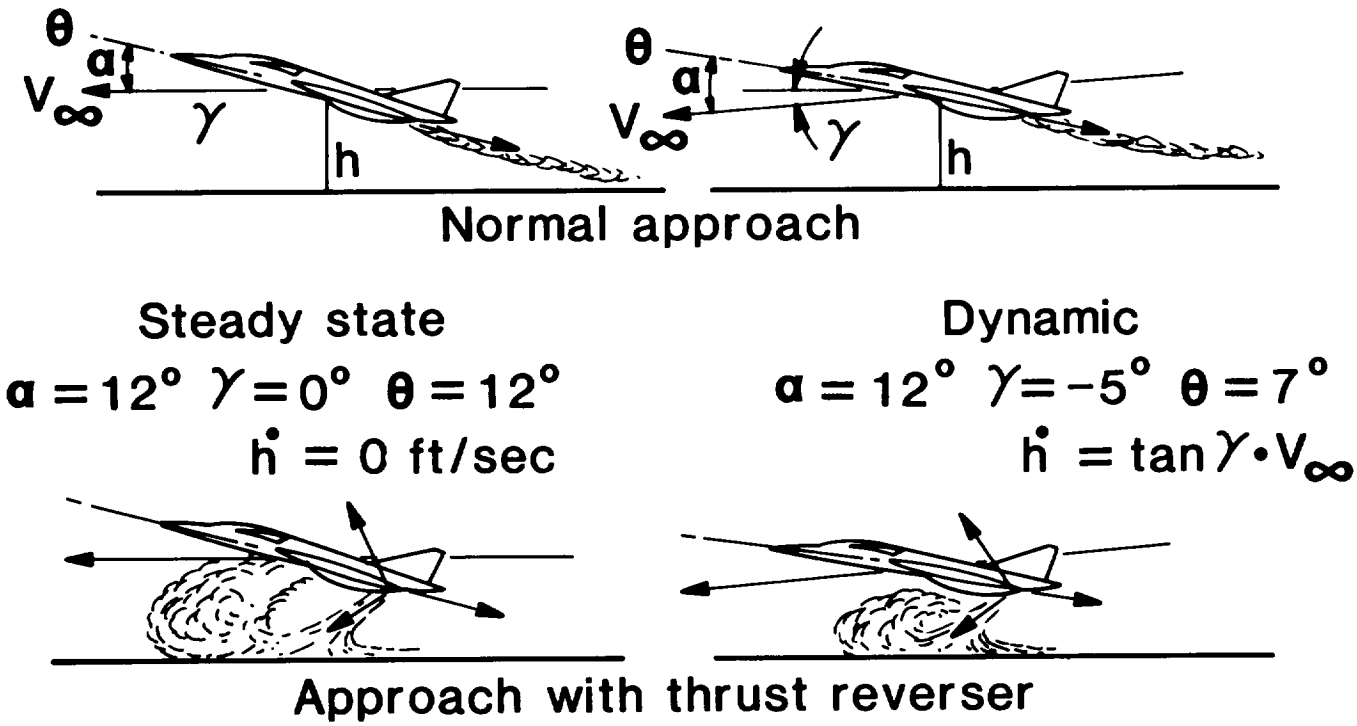

Figure 1. - Schematic of dynamic and steady state ground effects.

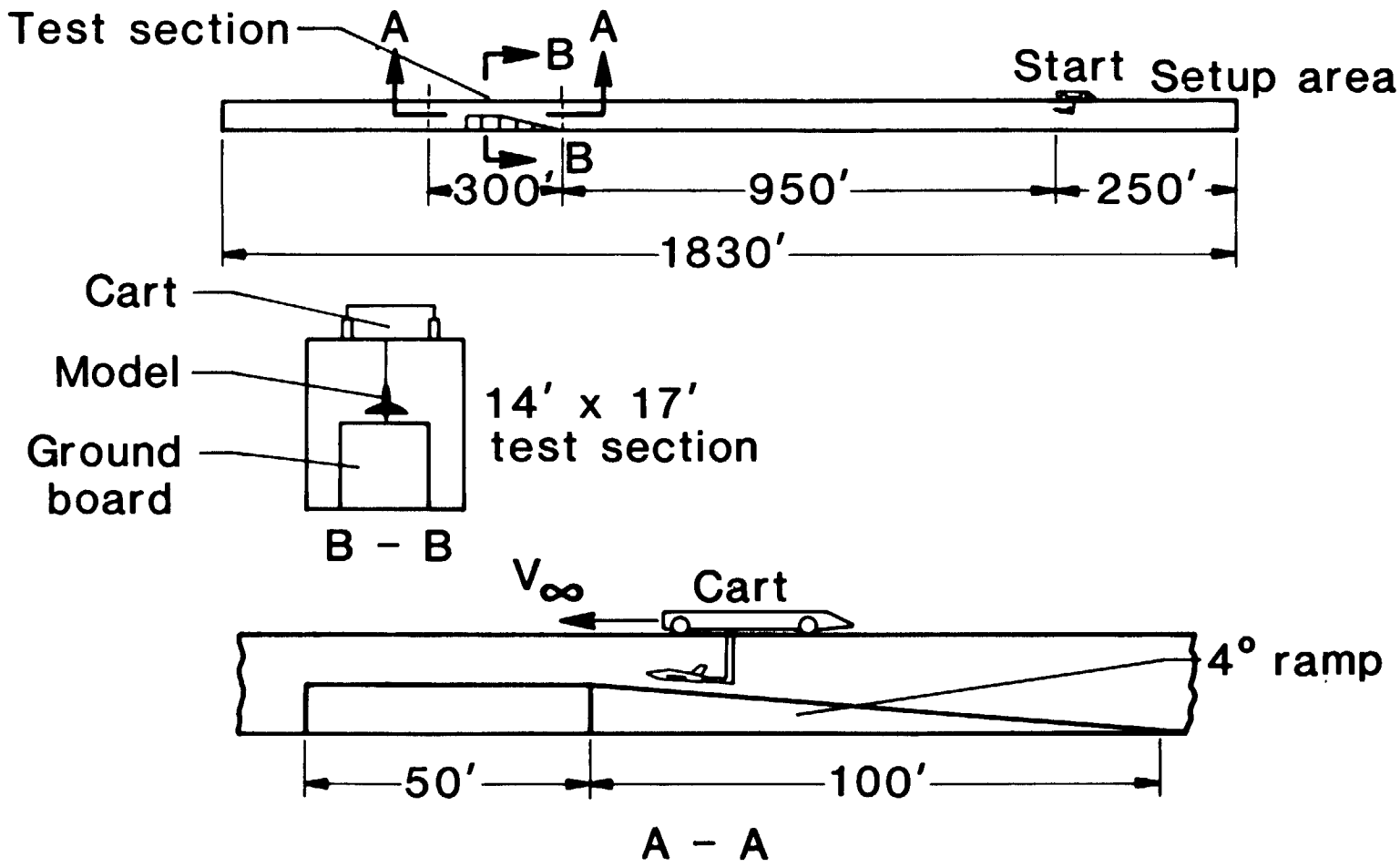

Figure 2. - Sketch of setup for dynamic ground effects testing in the Vortex Research Facility.

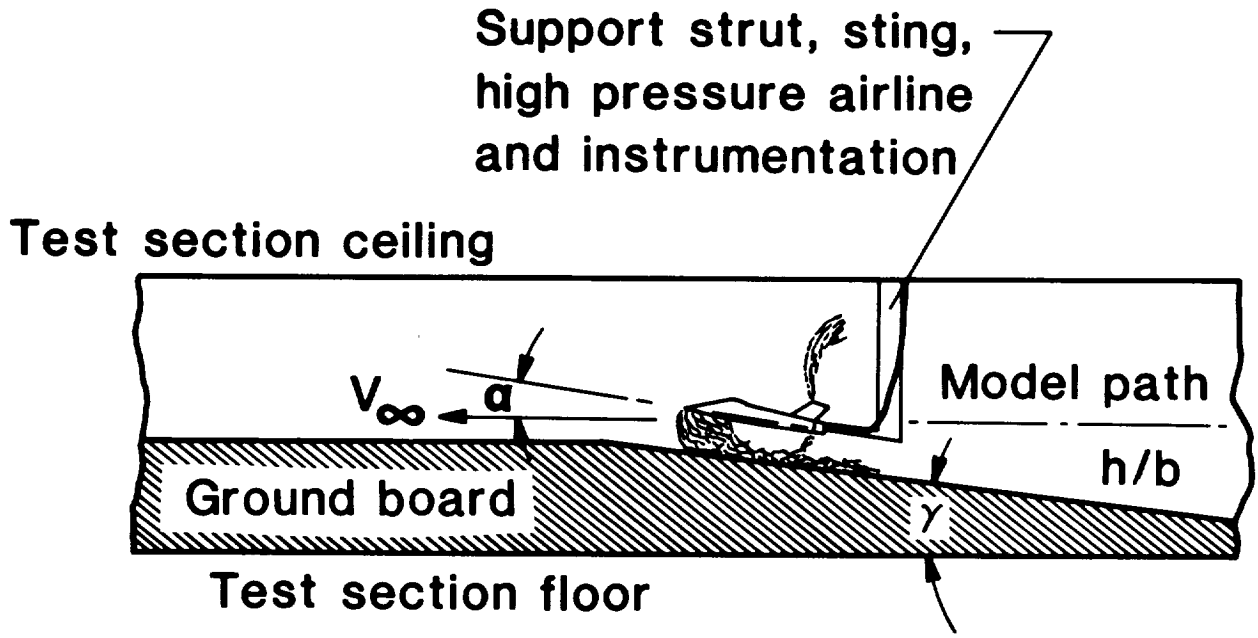

Figure 3. - Experimental concept in the Vortex Research Facility.

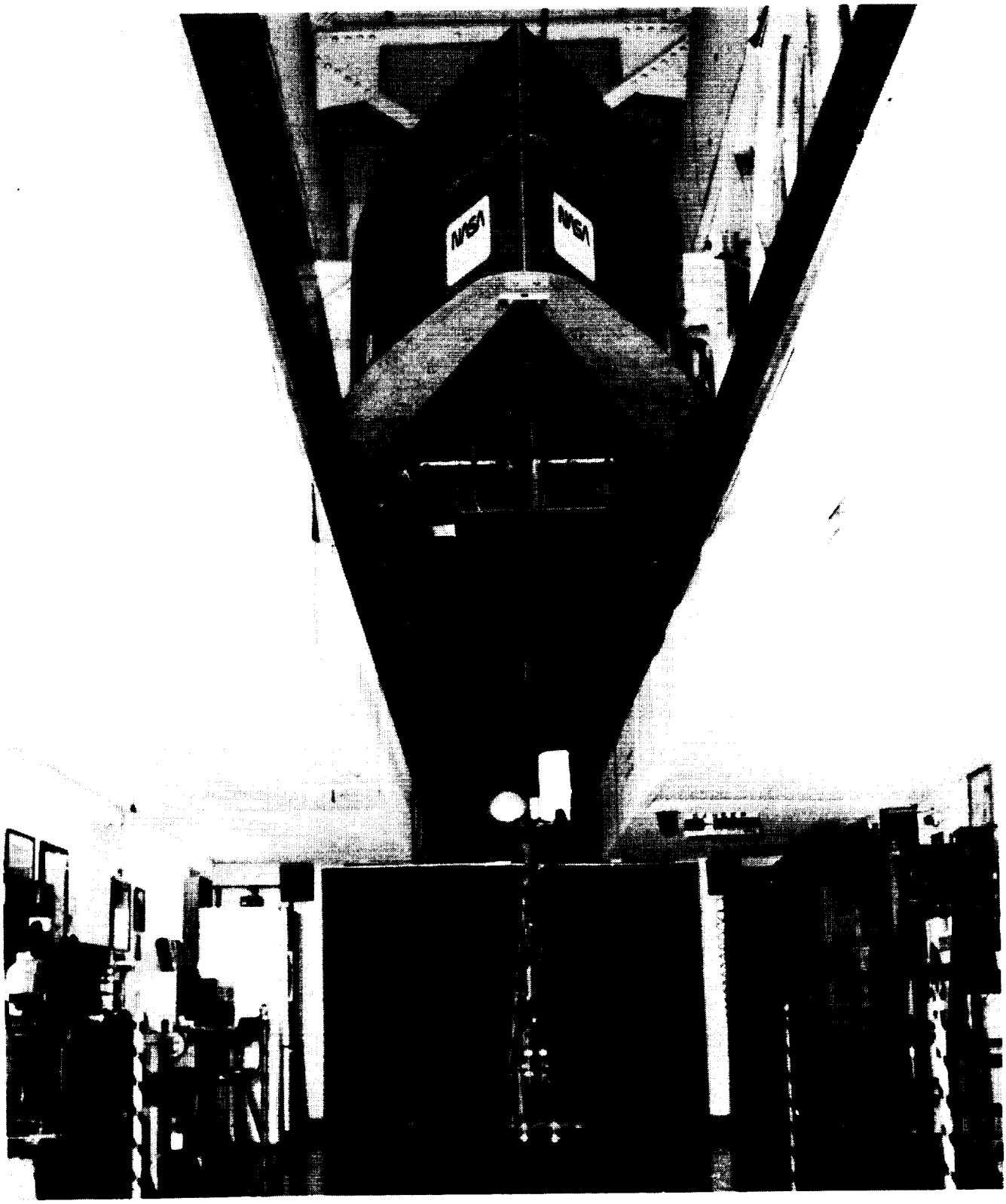

Figure 4. - Photograph of experimental setup in the Vortex Research Facility.

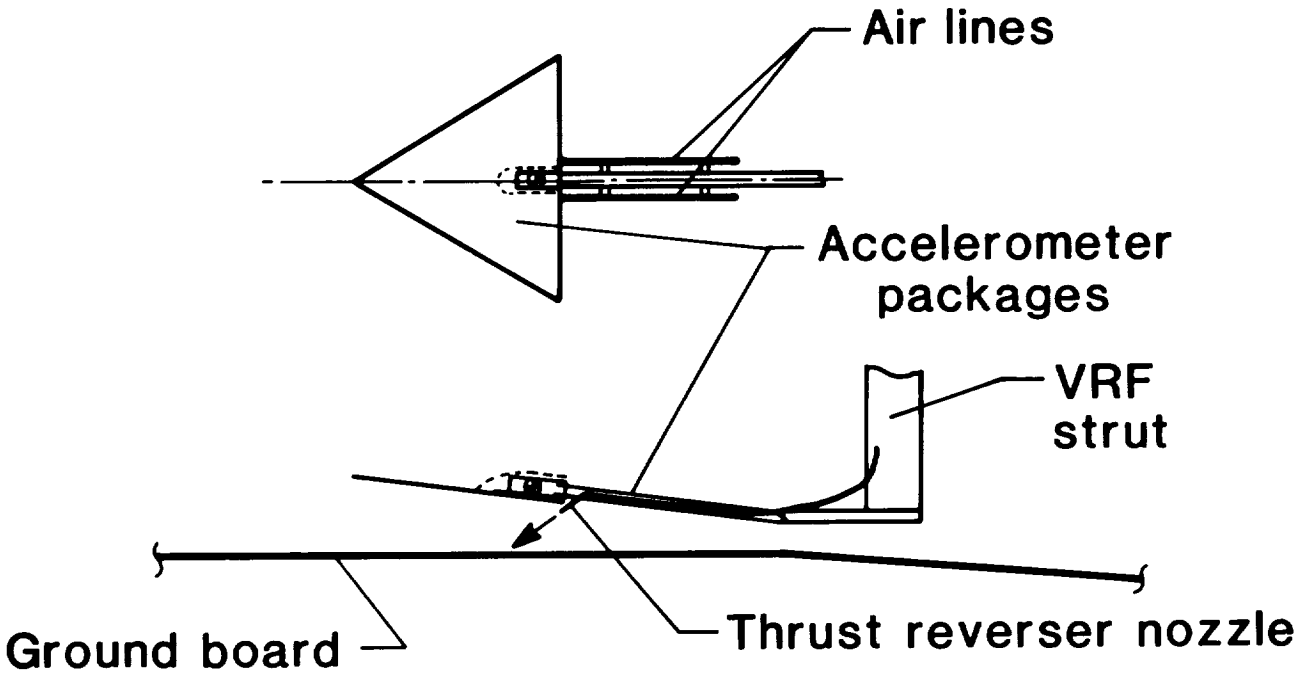

Figure 5. - Sketch of 60° delta wing model.

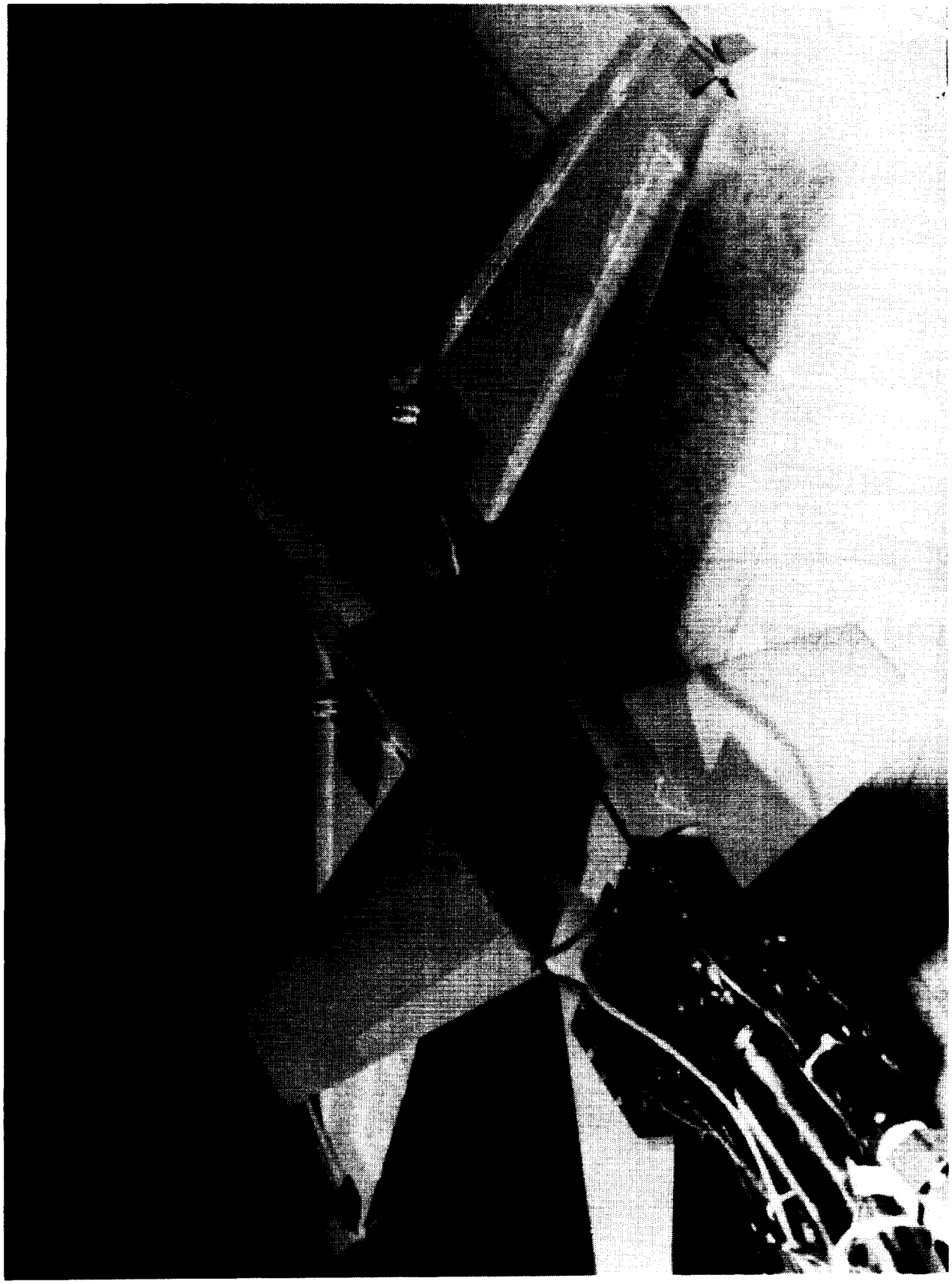

Figure 6. - Photograph of F-18 model.

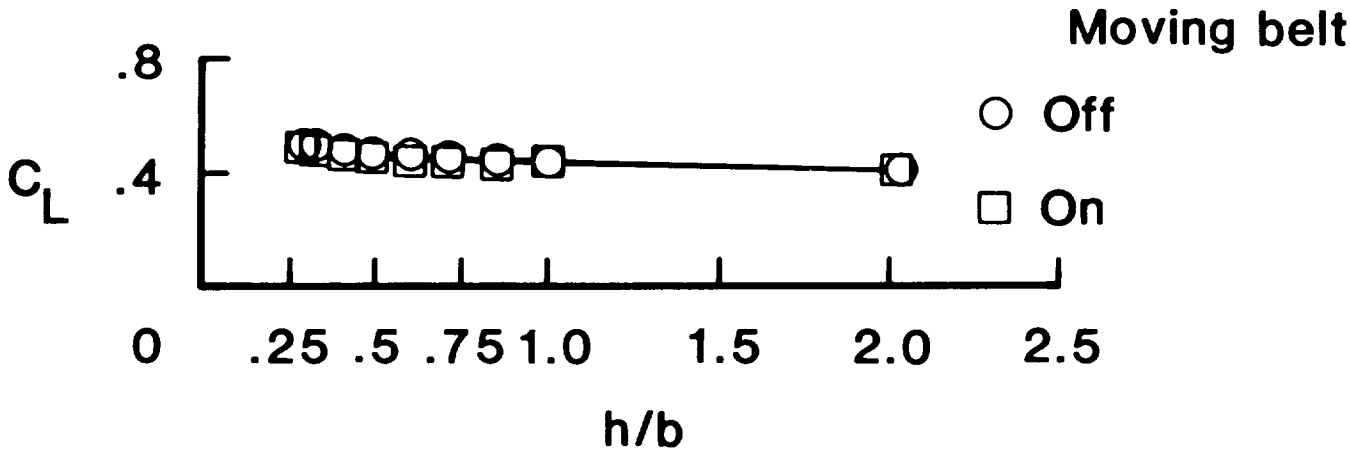

Figure 7. - Effect of moving belt ground plane on static ground effects of the 60° delta wing. α = 10 , NPR = 1.0, V_∞ = 70 ft/sec and h = 0.

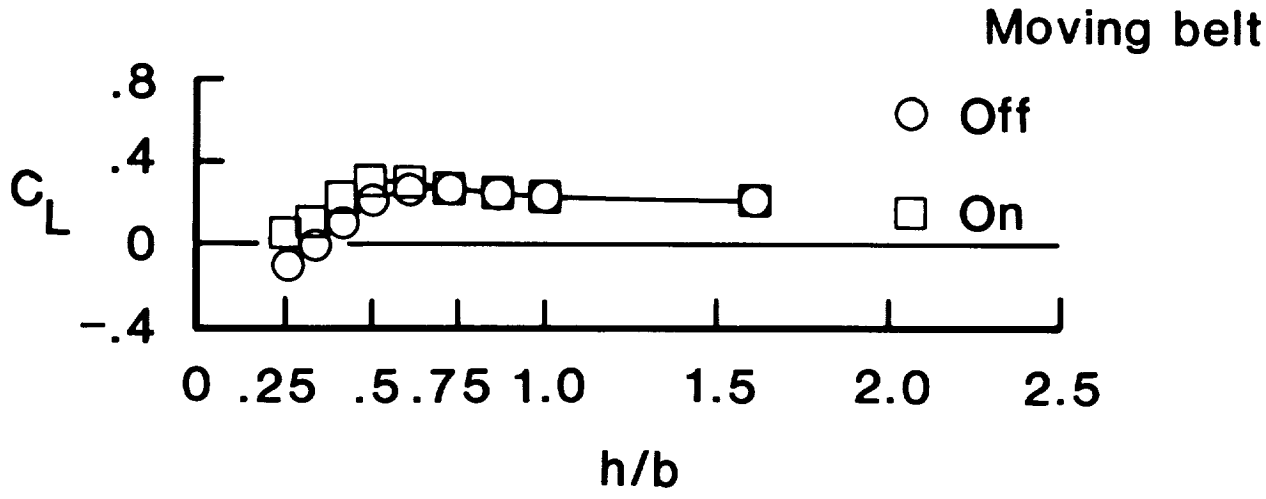

Figure 8. - Effect of moving belt ground plane on static ground effects of the 60° delta wing. α = 6.4°, NPR = 1.6, V_∞ = 70 ft/sec and $\dot{h}$ = 0.

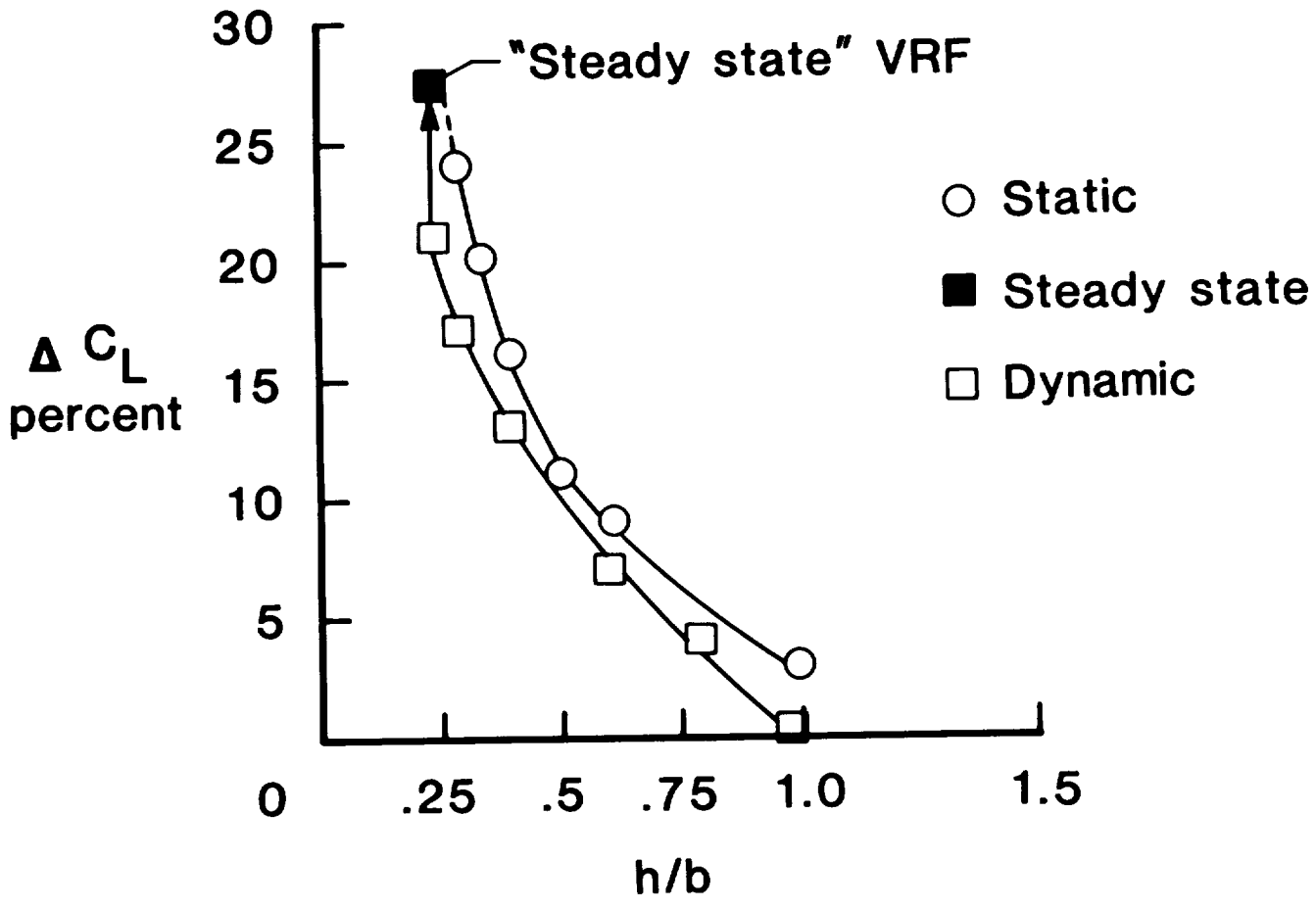

Figure 9. - Comparison of static and dynamic ground effects of the 60° delta wing. α = 10°, NPR = 1.0, V_∞ = 70 ft/sec, and $\dot{h}$ = 4.9 ft/sec.

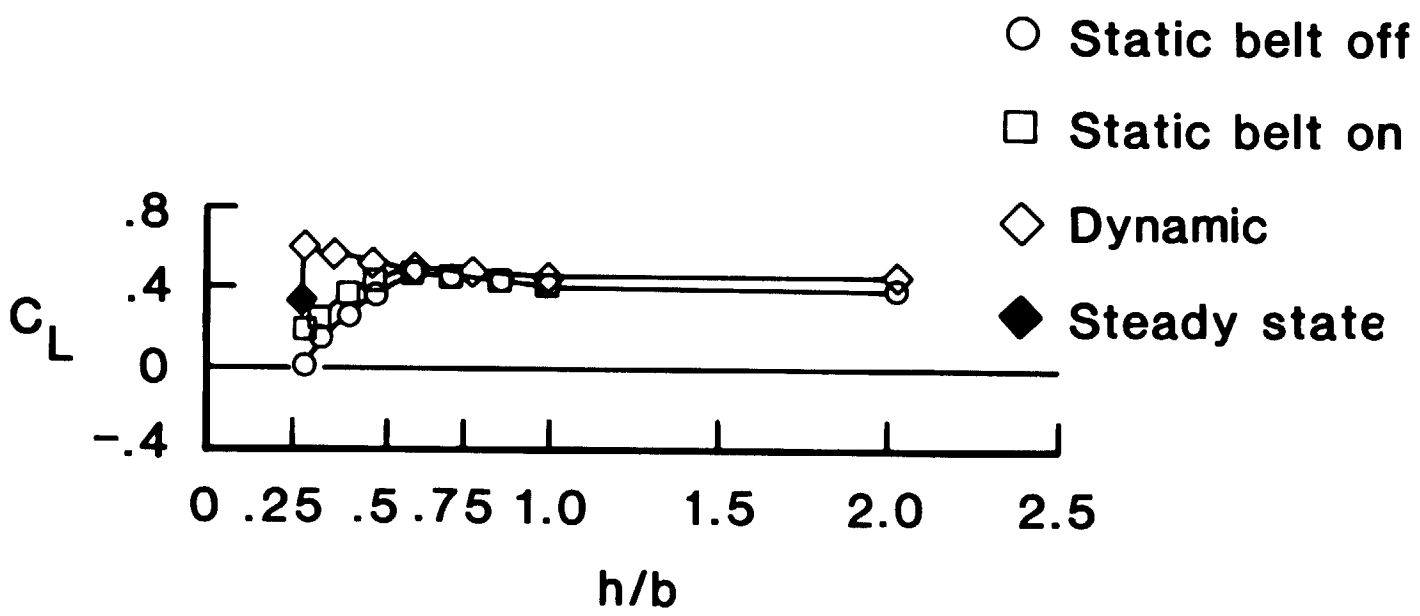

Figure 10. - Comparison of static and dynamic ground effects of the 60° delta wing.

α = 10°, NPR = 1.6, V_∞ = 90 ft/sec, and $\dot{h}$ = 6.3 ft/sec.

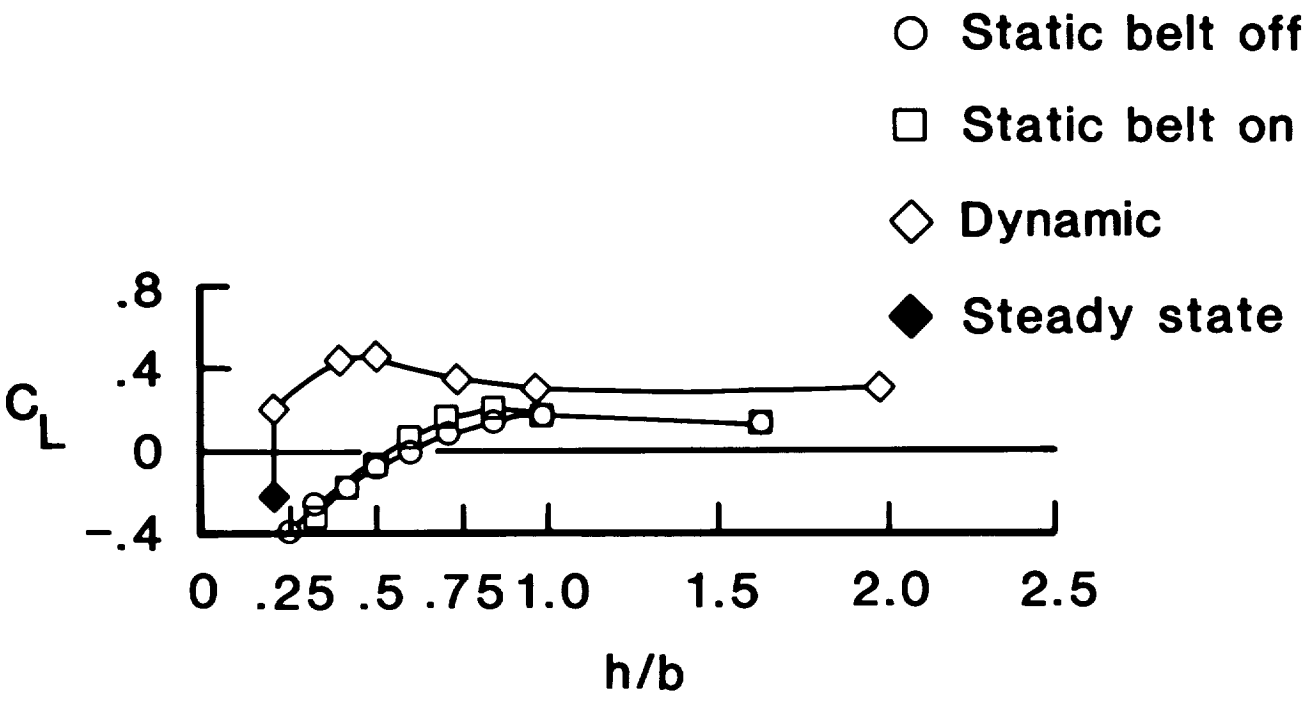

Figure 11. - Comparison of static and dynamic ground effects of the 60° delta wing. α = 6.4, NPR = 1.8, V_∞ = 70 ft/sec and $\dot{h}$ = 4.9 ft/sec.

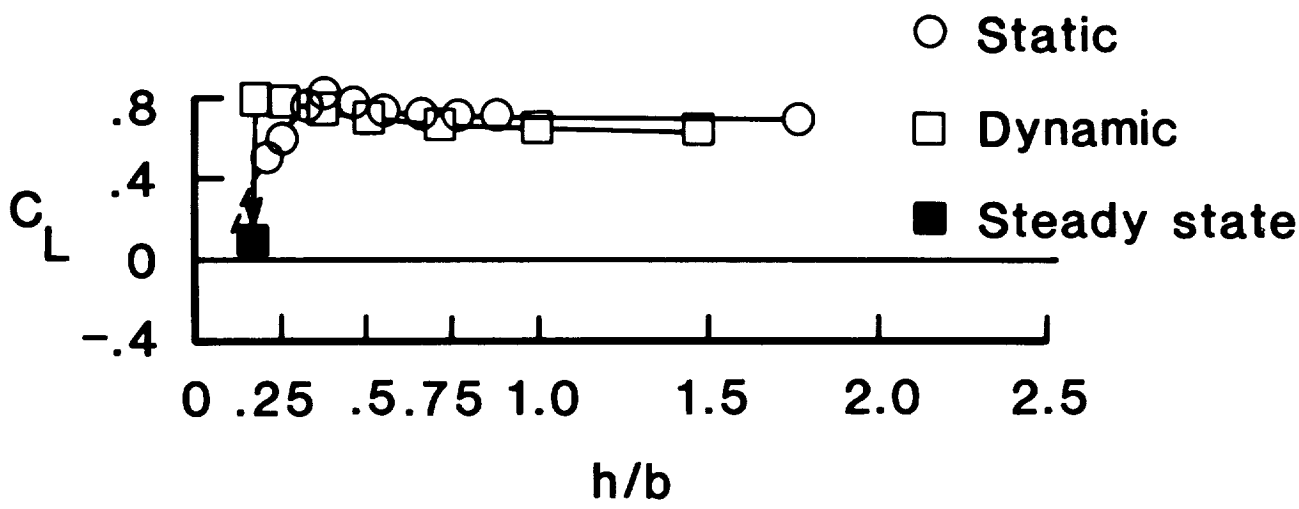

Figure 12. - Comparison of static and dynamic ground effects of the F-18 configuration.

α = 8.4°, NPR = 1.5, δ_f = 25°/20°/-10°, Noz = 45°/0°

V_∞ = 99 ft/sec and $\dot{h}$ = 6.9 ft/sec.

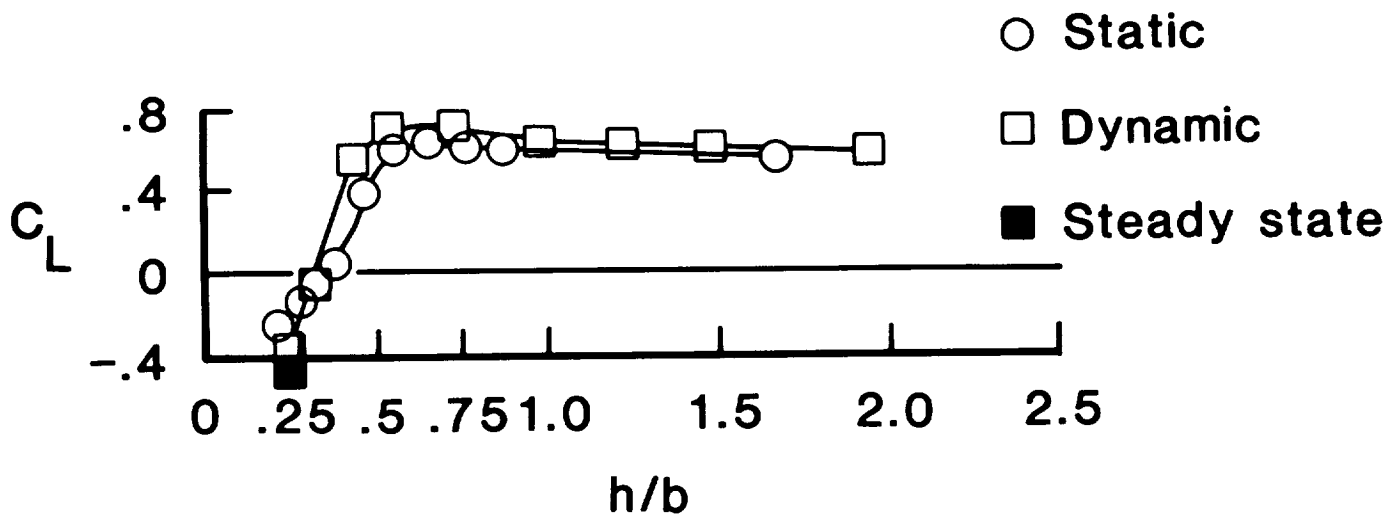

Figure 13. - Comparison of static and dynamic ground effects of the F-18 configuration. α = 8.4°, NPR = 2.5, δ_f = 25°/20°/-10°, Noz = 45°/0°, V_∞ = 98 ft/sec and $\dot{h}$ = 6.9 ft/sec.

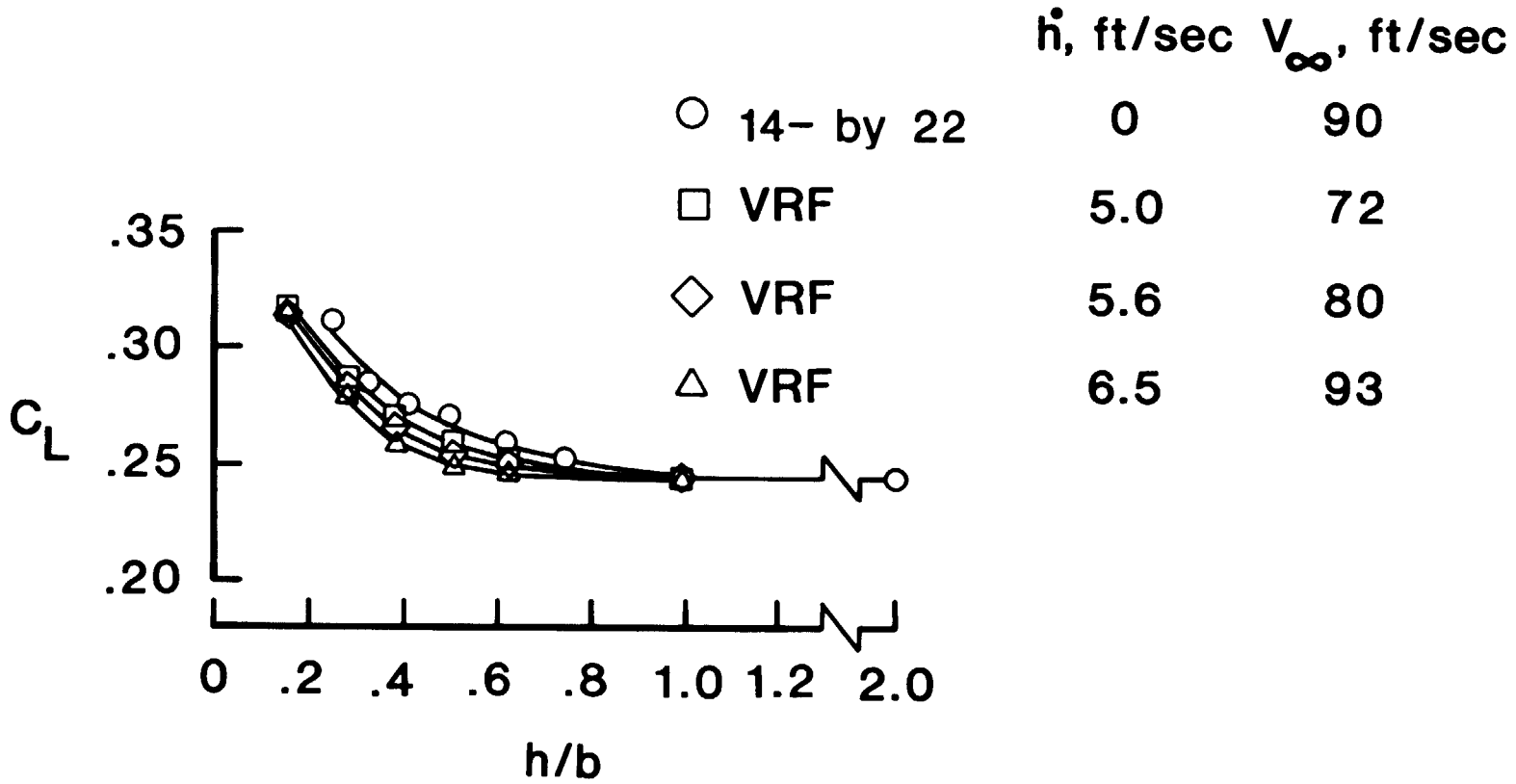

Figure 14. - Effect of rate-of-descent on dynamic ground effects of the 60° delta wing.

α = 6° and NPR = 1.0.

EFFECTS OF A GROUND VORTEX ON THE AERODYNAMICS OF AN AIRFOIL

by

A. Krothapalli
Fluid Mechanics Research Laboratory
The Florida State University
Tallahassee, FL

and

D. Leopold
Department of Aeronautics & Astronautics
Stanford University, Stanford, CA

ABSTRACT

An experimental investigation was carried out to study the aerodynamics of an airfoil with a rectangular jet exiting from its lower surface at fifty percent of the chord. The airfoil was tested with and without the influence of a ground plane. Surface static pressures were measured on the airfoil at jet to free stream velocity ratios ranging from 0 to 9. From these pressures, the variation of C_L with velocity ratio was easily determined.

The measurements indicated significant positive and negative pressure regions on the lower surface of the airfoil ahead of and after the nozzle exit respectively. The presence of a ground plane enhanced these pressure regions at low velocity ratios but at a particular ratio for each plate location, a recirculation zone or a vortex formed ahead of the jet resulting in decreased pressures and a drop in C_L.

INTRODUCTION

During the past several years there has been increased interest in V/STOL aircraft configurations which utilize lift jets and thrust augmentors mounted in the wings and/or the fuselage. One such configuration of interest uses a high lift system consisting of a wing with a long rectangular jet along the span issuing from below. Such a jet could be produced by installing two dimensional ejectors along the span of the wing. While these configurations usually exhibit improved lift characteristics, the interaction of the jet and the free stream can result in undesirable aerodynamic loading characteristics influencing the aircraft performance. For example, in hovering entrainment of the surrounding air by the jet induces a suction pressure on the lower surface of the wing causing a downward or suck-down force. During the transition from hovering to conventional forward flight this interaction produces a region of positive pressures upstream of the jet and a region of negative pressures downstream of the jet resulting, under certain conditions, in a net loss of lift and a nose-up moment. When the aircraft is operating in STOL mode, all the induced effects discussed above are present but modified by the presence of the ground. Close to the ground, the jet impinges on the ground and forms a wall jet that flows outward from the impingement region. The wall jet formed upstream of the jet exit, rolls up forming what is commonly known as a "ground vortex". This is a result of the interaction of the wall jet with the oncoming free stream. The location of this ground vortex and its induced effects on the

nearby lifting surfaces is of importance in predicting the performance of the STOL aircraft.

Various aspects of the jet induced effects on wings and fuselages have been the subject of many studies; and most of these have been experimental investigations. Currently, in most V/STOL aircraft designs, a semi-empirical approach guided by experimental data is followed to model the specific jet-induced flow field. Several researchers, over the years, have surveyed and described these jet-induced or propulsive effects (Margason[1], Skifstad[2]). More recently Kuhn[3] gave a comprehensive account of the induced aerodynamics of jet and fan powered aircraft. And recent advances in prediction methods for these effects on V/STOL aircraft were described by Agarwal[4]. Since these reviews are quite extensive, no attempt is made here to discuss the previous work on jet induced aerodynamics.

The problem addressed here is the determination of the various aerodynamic forces of the airfoil resulting from a jet issuing normal to its chord line into a uniform cross flow and in the presence of a ground plane, as shown in Figure 1. The interaction between the jet and the cross flow in the presence of an airfoil is characterized by the following parameters: the geometry of the airfoil, angle of attack of the airfoil, free stream Mach number, free stream Reynolds number based on the chord of the airfoil, the geometric parameters of the nozzle, location and orientation of the nozzle with respect to the airfoil, Mach number of the jet, the location of the ground plane with respect to the airfoil and the nature of the conditions at

the nozzle exit and the free stream.

The airfoil used was the NACA 0018. A rectangular nozzle of aspect ratio 87 was selected for the nozzle and the nozzle was oriented lengthwise along the span. The nozzle was located at 50 percent of the chord. The exit section of the nozzle was designed such that the jet exits normal to the chord. The free stream velocity was varied from 20m/sec to 60m/sec. The corresponding Reynolds number $R_e = U_\infty C/\nu_\infty$, varied from 2×10^5 to 6×10^5. The mean velocity at the nozzle exit was varied from 20 m/sec to 250m/sec. The angle of attack of the airfoil was kept at zero degrees.

APPARATUS, INSTRUMENTATION AND PROCEDURES

The wind tunnel used in this experiment was subsonic closed circuit type. The test section has the dimensions of 90.2 x 45.7 x 45.7cm. The flow speed in the test section can be varied between 20m/sec and 65m/sec. The model was situated midway between the upper and lower walls of the test section.

A NACA 0018 symmetric airfoil was chosen for the experiment. The airfoil was made in several sections using aluminum and stainless steel. It has a 15cm chord and spans the entire 45.7cm width of the test section. The aspect ratio of the wing was therefore equal to about 3.05. A rectangular slot with its long dimension in spanwise direction was cut into the lower surface at midchord. The length and width of the nozzle exit were 25cm and 0.3cm respectively. Before air reaches the nozzle exit, it passes through a settling chamber placed inside the wing and

extends along the span of the wing. Compressed air was supplied to the settling chamber from both ends of the wing. To ensure a uniform flow at the nozzle exit, adjustable vanes were placed inside the settling chamber. The inlet section of the slot was designed in such a manner that the jet stream exhaust perpendicular to the chord of the airfoil. With the optimum position of the vanes, a uniform flow was obtained. The variation of the mean velocity along the span was within ten percent of the value at the center of the nozzle exit. The jet exit velocity was varied from 0m/sec to 240m/sec. For simulation of a ground plane, an aluminum plate of 45.7cm wide, 61cm long and 0.3cm thick was used. The leading edge of the plate was rounded into parabolic shape and a flap was attached at the trailing edge to insure a attached flow at the leading edge. A transition strip was placed 10cm from the leading edge. The distance between the ground plane and the airfoil chord was varied from 3.75cm to 15cm.

Surface pressure measurements were made at several velocity ratios (nozzle exit mean velocity/free stream mean velocity). To obtain the aerodynamic force coefficients, the surface pressure data was integrated around the airfoil at mid-span location. The lift due to the jet reaction is not included in most of the data presented.

A Cartesian coordinate system (x,y,z) was used with the x-axis oriented along the center line of the wing section and with the origin located at the leading edge as shown in figure 1.

For most of the measurements errors were estimated to be of

the order of five percent.

The testing of V/STOL models in wind tunnel presents many problems that are not encountered in the testing of the conventional airfoils, where the testing techniques are relatively well understood[5]. V/STOL models such as the one tested have a relatively large wake deflection angle which presents one of the most difficult problems that is encountered in wind tunnel testing. The primary work on wind tunnel wall effects and their corrections for V/STOL configurations was done by Heyson[6]. Studies covering the limits on the minimum speed in V/STOL wind tunnel test were done by Rae[7]. Recently Margason and Hoad[8] gave an account of V/STOL aircraft model wind tunnel testing from model design to data reduction. In most of the instances, the model used is a fan-in-wing configuration. Since these correction techniques are highly configuration dependent, and the present wing model is not representative of any flight vehicle, no attempt is made here to correct the data.

One particularly important aspect of V/STOL model testing is the need to describe a "jet-off reference configuration" for each jet-on configuration tested. These data are then used to provide a basis for determining the interference of the jets on aerodynamic characteristics. Such a procedure was used in this experiment.

Another factor to take into account is the flow impingement on the ground plane. In a wind tunnel with the air moving with respect to the model and to the ground plane, there is a boundary layer on the floor. The effect of this can be minimized by using

a moving belt ground plane. Several investigations have been carried out on this subject by Hackett et al[9]. In the experiments described here the ground plane was fixed and no attempts have been made to bleed the boundary layer.

RESULTS AND DISCUSSION

Typical variations of the surface pressure on both upper and lower surfaces of the free airfoil, at zero angle of attack with and without the jet, are shown in Figure 2. The pressures are plotted in the form of the pressure coefficient C_p given by

$$C_p = (p - p_\infty)/q_\infty$$

It is observed that without the jet, the pressure distribution on both sides of the airfoil are very nearly identical, confirming the symmetric property of the airfoil. For a velocity ratio (jet exit velocity/freestream velocity) of 6, the influence of the jet on the surface pressure is quite significant as shown in the figure. When comparing this distribution with the jet-off condition, the following observations are made: on the lower surface, in the region upstream of the jet, an increase in pressure occurs, while a decrease in pressure is noticed in the region behind the jet. The positive pressure ahead of the jet is a result of the blockage of the free stream by the jet. The effect of this is an increase in effective angle of attack of the airfoil, resulting in a relatively low pressure on the upper surface of the airfoil. At very low velocity ratios, the recirculation zone behind the jet is small and the flow reattaches to the lower surface. As

the jet strength is increased by increasing the exit velocity, the flow in the region between the jet and the trailing edge forms a recirculation region and it extends into the wake. The magnitude of the pressure coefficient in this region was observed to be fairly constant as depicted by its distribution in the region between the jet and the trailing edge in figure 2. The "Kutta Condition" requires that the pressure on both lower and upper surfaces at the trailing edge be equal. This being the case, the pressure on the upper surface near the trailing edge is fixed by its value in the recirculation region on the lower surface or vice-versa.. It is interesting to note that very little variation in the magnitude of C_p is observed on the upper surface for x/c greater than about 0.6, thus suggesting that only the pressure changes in the first half ($x/c < 0.5$) of the airfoil are mostly responsible for the generation of the induced lift. From these observations it may be suggested that the positive and negative pressure regions on the lower surface are essentially responsible for many changes in the gross aerodynamic characteristics of the airfoil to be noted later.

From the chordwise pressure distribution determined, the sectional lift was easily obtained by numerical integration of pressure over the span wise section. For each value of the velocity ratio in the range tested, a corresponding sectional lift coefficient C_L was obtained at mid span location. The reaction force due to the jet is not included in the definition of the lift. Figure 3 shows the variation of C_L with the velocity ratio. It can be seen from the figure that the C_L

increases monotonically up to a velocity ratio of about 5. This is a result of the pressure increasing rapidly in front of the jet on the lower surface. In the range of velocity ratios between 5 and 8, the pressure in the recirculation regions behind the jet decreases rapidly with increasing velocity ratio, thus resulting in a drop of C_L as shown in the figure. The detailed discussion of these regions and their effect on the aerodynamics of a free airfoil is given by Krothapalli and Leopold[10]. For velocity ratios greater than 8, an increase in C_L is observed, and this is attributed to the influence of the tunnel wall or ground effect.

At low velocity ratios, the influence of a ground plane on the flow around the airfoil seems to enhance the same general trends found for the free airfoil. The regions ahead of and behind the jet both increase and decrease respectively with increasing velocity ratio but the variations are more pronounced; the degree of which depends strongly on plate position. This phenomenon is shown in figure 4 where the pressure distribution for two plate locations are compared to the free airfoil distribution at a velocity ratio of 2. As this ratio is increased, the pressure in front of the jet drops dramatically resulting in a sharp decrease in C_L. The velocity ratio at which this occurs depends strongly on plate position.

The variation of lift coefficient throughout the velocity ratio range is shown in figure 5 for three plate locations and are compared with the free airfoil. These curves indicate a unique velocity ratio for each plate location where C_L reaches a

maximum. As the ratio increases further, the pressure in front of the jet on the lower surface decreases thus resulting in a reduced C_L. These unique points represent a boundary between favorable and unfavorable operating conditions which are shown in figure 6. In region 1, favorable conditions exist. The lift coefficient increases as the jet velocity increases. In region II, unfavorable conditions exist since the lift coefficient decreases as the jet velocity increases. The relation in figure 6 also indicates the beginning of a new type of flow structure in front of the jet; the influence of which on the overall aerodynamics of the airfoil increases as the velocity ratio increases. This complex flow is best visualized in figure 7 where case I corresponds to the flow condition occurring in region 1 of figure 6. For this case, the momentum of the jet is small enough for the jet stream to be bent by the oncoming free stream. The recirculation is confined to the region behind the jet therefore creating a low pressure zone behind the jet and a high pressure zone in front of the jet. In case II, the jet momentum reaches a high enough value that the jet impinges normal to the plate creating two recirculation regions. The region in front of the jet drops in pressure resulting in a decreased C_L. As the jet velocity increases, the recirculation zone in front of the jet increases in intensity and eventually forces C_L to a negative value. The recirculatory region in front of the jet is commonly known as the ground vortex.

CONCLUSIONS

From this preliminary experimental investigation, the following conclusions can be drawn. The static pressure distribution around the airfoil shows two distinct regions on the lower surface, which greatly influence the overall aerodynamics. First there is the positive pressure region upstream of the jet. This is attributed to the "blockage" of the freestream by the jet. The second is the region between the jet and the trailing edge, marked by the negative pressure coefficient, and the magnitude of the pressure coefficient in this region is found to be nearly constant. The pressure on the upper surface of the airfoil is also influenced by the presence of the jet, and the influence is such that only the pressure distribution for the leading half of the airfoil contributes to the lift coefficient. The presence of the ground plane, for moderate heights, and at low velocity ratios, improves the aerodynamic characteristics of the airfoil. However, a further increase in the velocity ratio for a fixed ground plane height, a large vortex develops in front of the jet, commonly known as "ground vortex", resulting in a sharp decrease in C_L.

ACKNOWLEDGMENTS

The work presented here has been supported by NASA Ames Research Center under grant numbers NAG2-111 and NAC2-198 and the work was carried out at Stanford University.

REFERENCES

1. Margason, R.J., "Review of Propulsion Induced Effects on Aerodynamics of Jet V/STOL Aircraft", NASA TN D - 5617, 1970.
2. Skifstad, J.G., "Aerodynamics of Jets Pertinent to V/STOL Aircraft", Journal of Aircraft, Vol. 7, No. 3, 1970.
3. Kuhn, R.E., "The Induced Aerodynamics of Jet and Fan Powered V/STOL Aircraft", Recent Advances in Aerodynamics, Edited by A. Krothapalli and C.A. Smith, Springer-Verlog, 1986.
4. Agarwal, R.K., "Recent Advances in Prediction Methods for Jet Induced Effects on V/STOL Aircraft", Recent Advances in Aerodynamics, Edited by A. Krothapalli and C.A. Smith, Springer-Verlog, 1986.
5. Pope, A. and Harper, J.J., "Low-Speed Wind Tunnel Testing", John Wiley & Sons Inc., 1966.
6. Heyson, H.H., "The Effect of Wind Tunnel Wall Interference on the Performance of a Fan-In-Wing VTOL mOdel", NASA TN D-7518, 1974.
7. Rae, W.H., "Limits on Minimum Speed V/STOL Wind Tunnel Tests", Journal of Aircraft, Vol. 4, No. 3, 1967.
8. Margason, R.J. and Hoad, D.R., "V/STOL Aircraft Model in Wind Tunnel Testing from Model Design to Data Reduction", Vol. 17, No. 3, 1980.
9. Hackett, E.J. and Bles, R.A., "Ground Interaction and Tunnel Blockage for a Jet-Flapped, Basic STOL Model Tested to a Very High Lift Coefficient", NASA CR - 137, 1976.
10. Krothapalli, A. and Leopold, D., "A Study of Flow Past an Airfoil with a Jet Issuing from its Lower Surface", Joint

Institute of Aeronautics and Acoustics TR-54, Stanford University, June 1984.

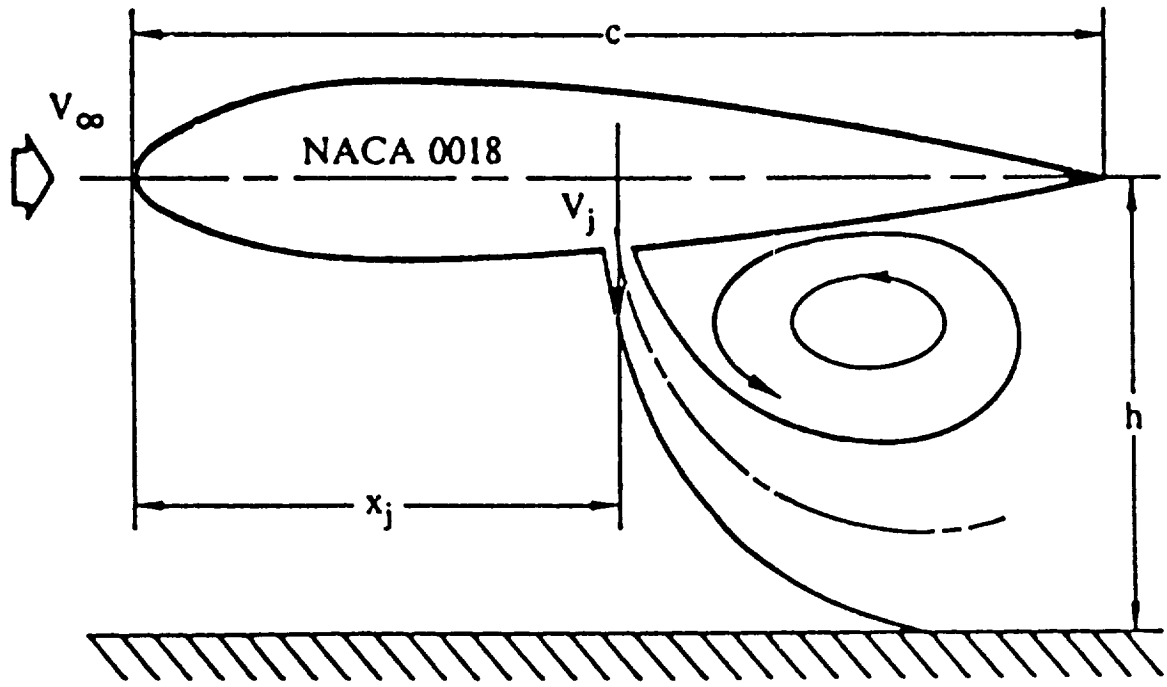

Figure 1. Schematic of the model and nomenclature.

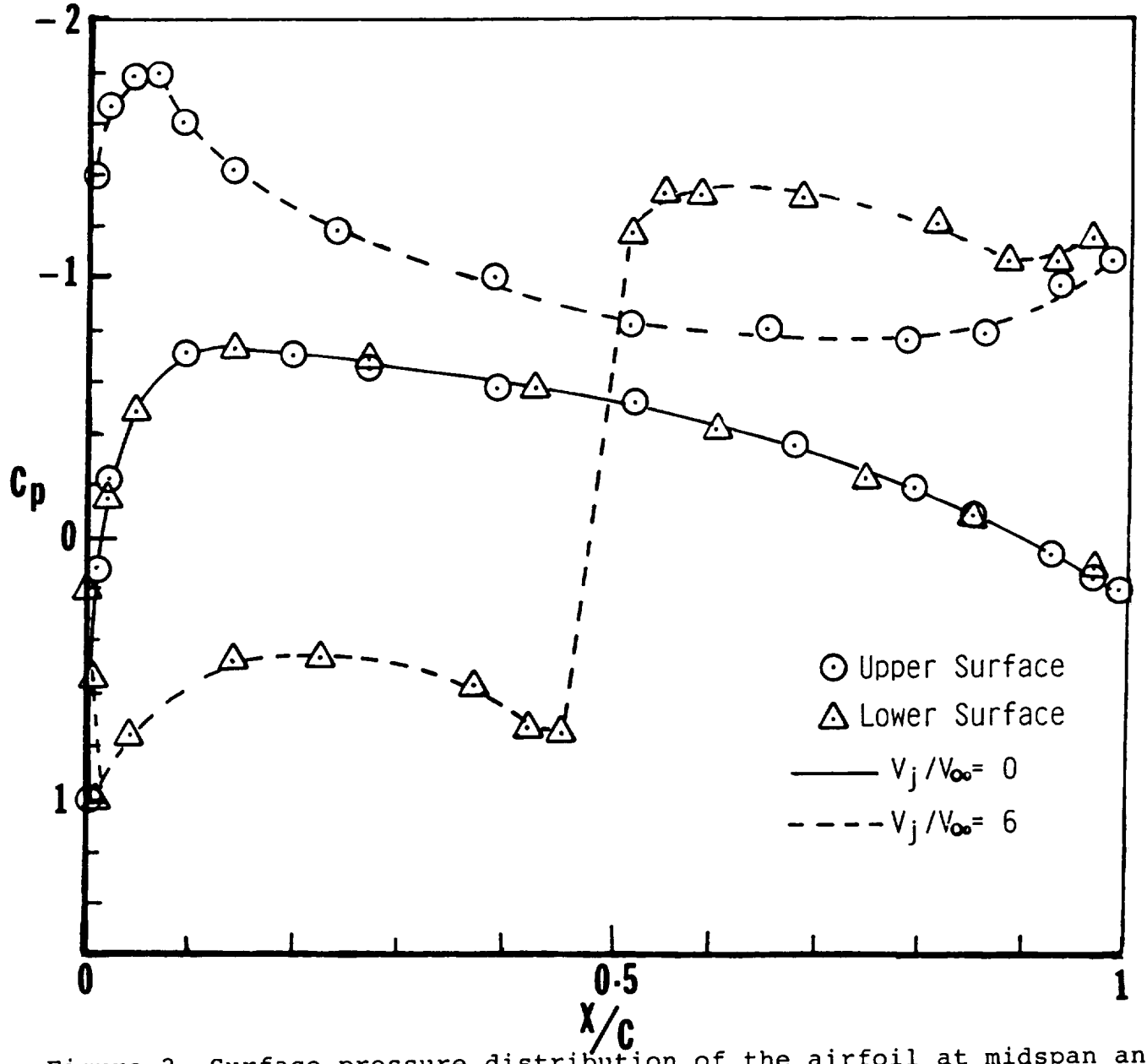

Figure 2. Surface pressure distribution of the airfoil at midspan and out of ground effect.

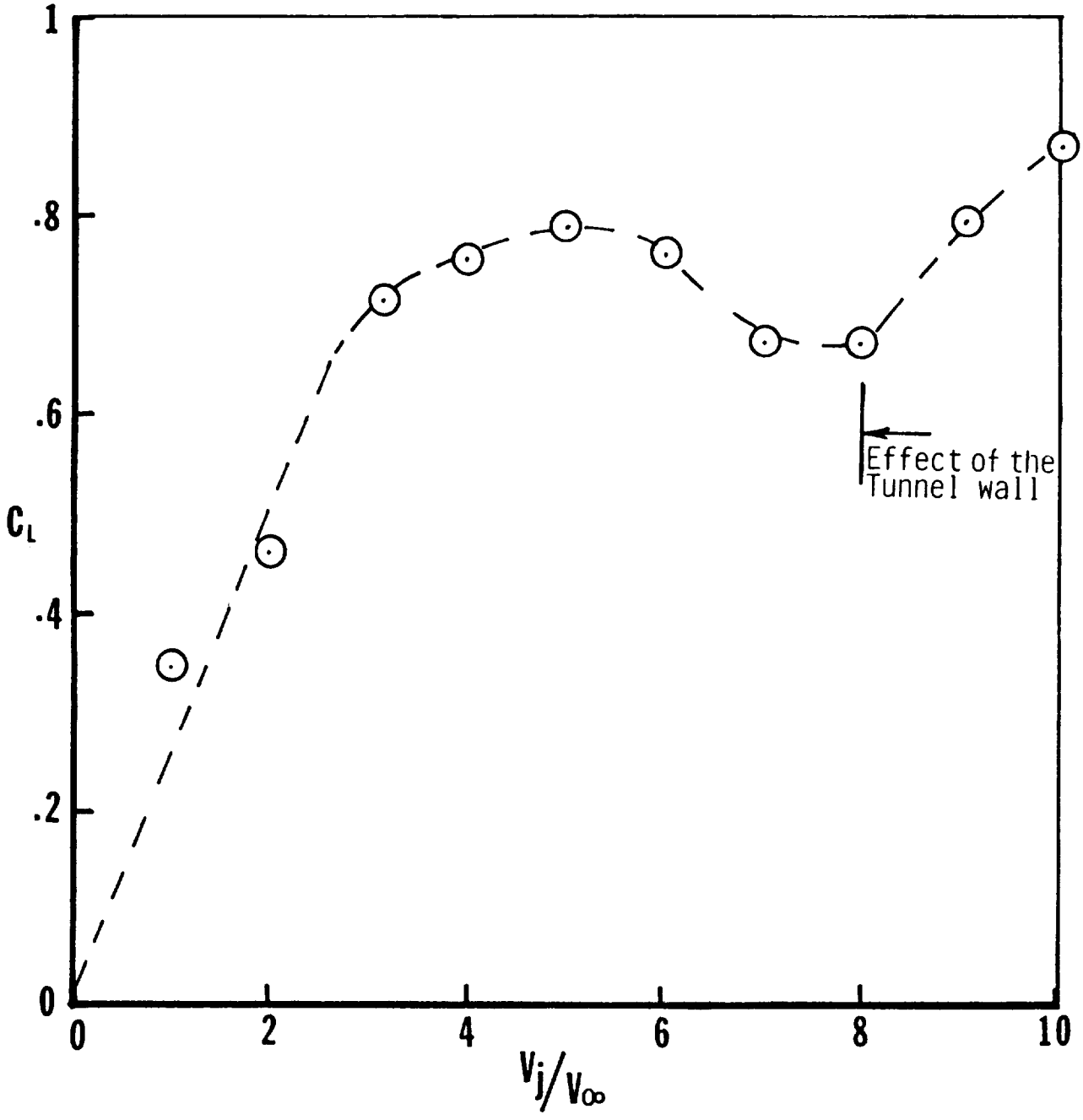

Figure 3. Variation of the sectional lift coefficient with velocity ratio for the case of the free airfoil.

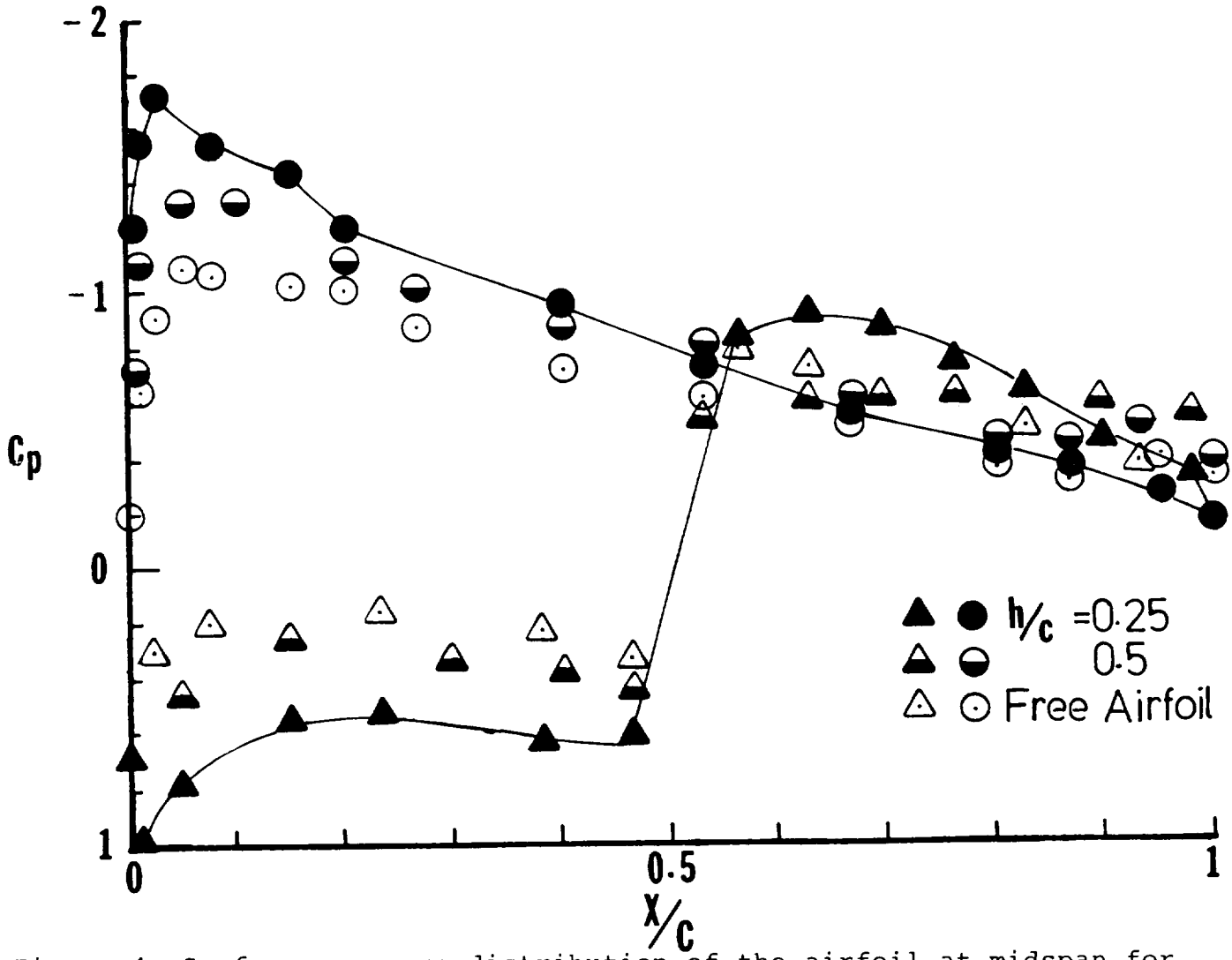

Figure 4. Surface pressure distribution of the airfoil at midspan for different ground plane locations; velocity ratio = 2.

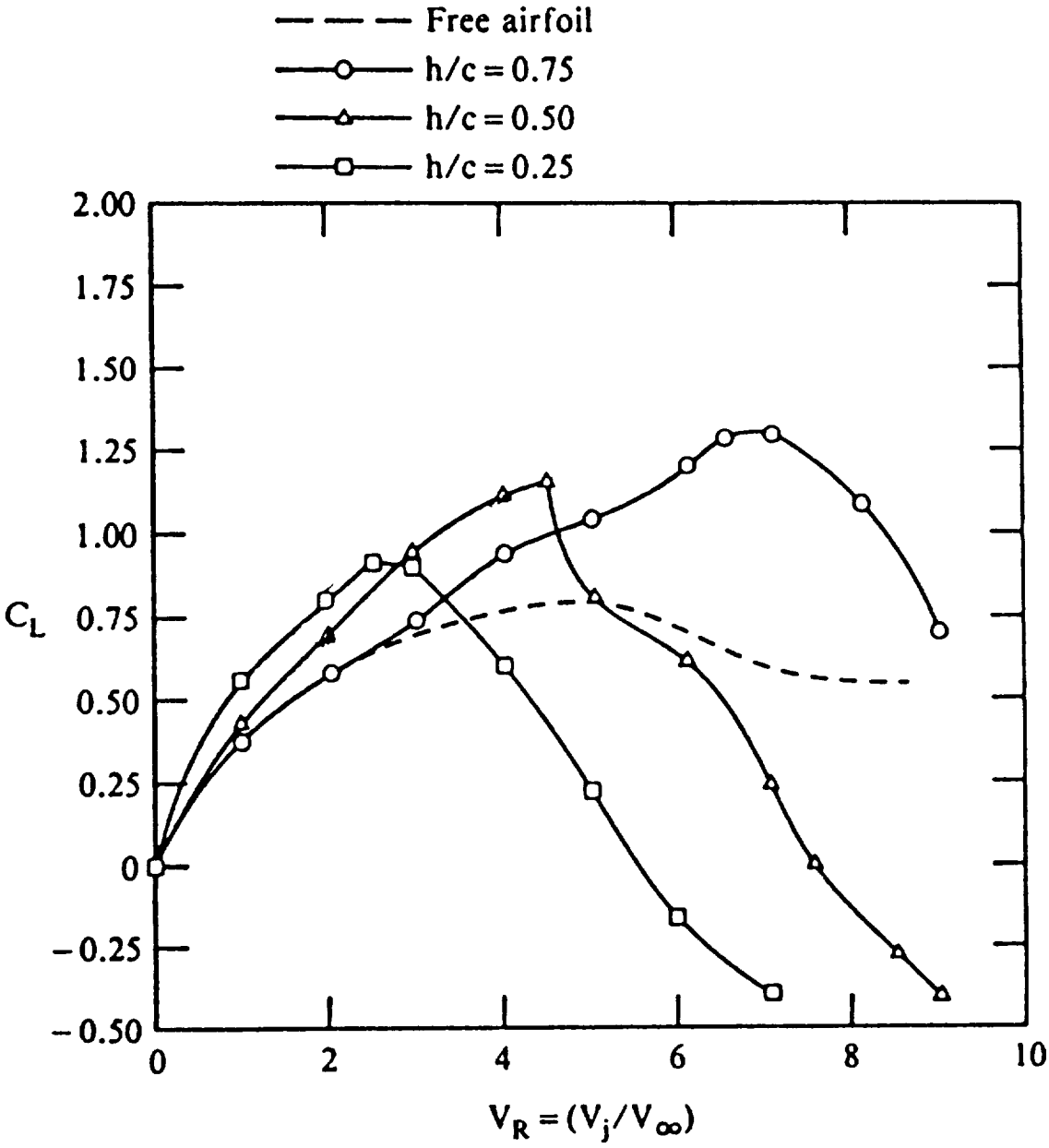

Figure 5. Variation of the jet induced sectional lift coefficient with velocity ratio for different ground plane locations.

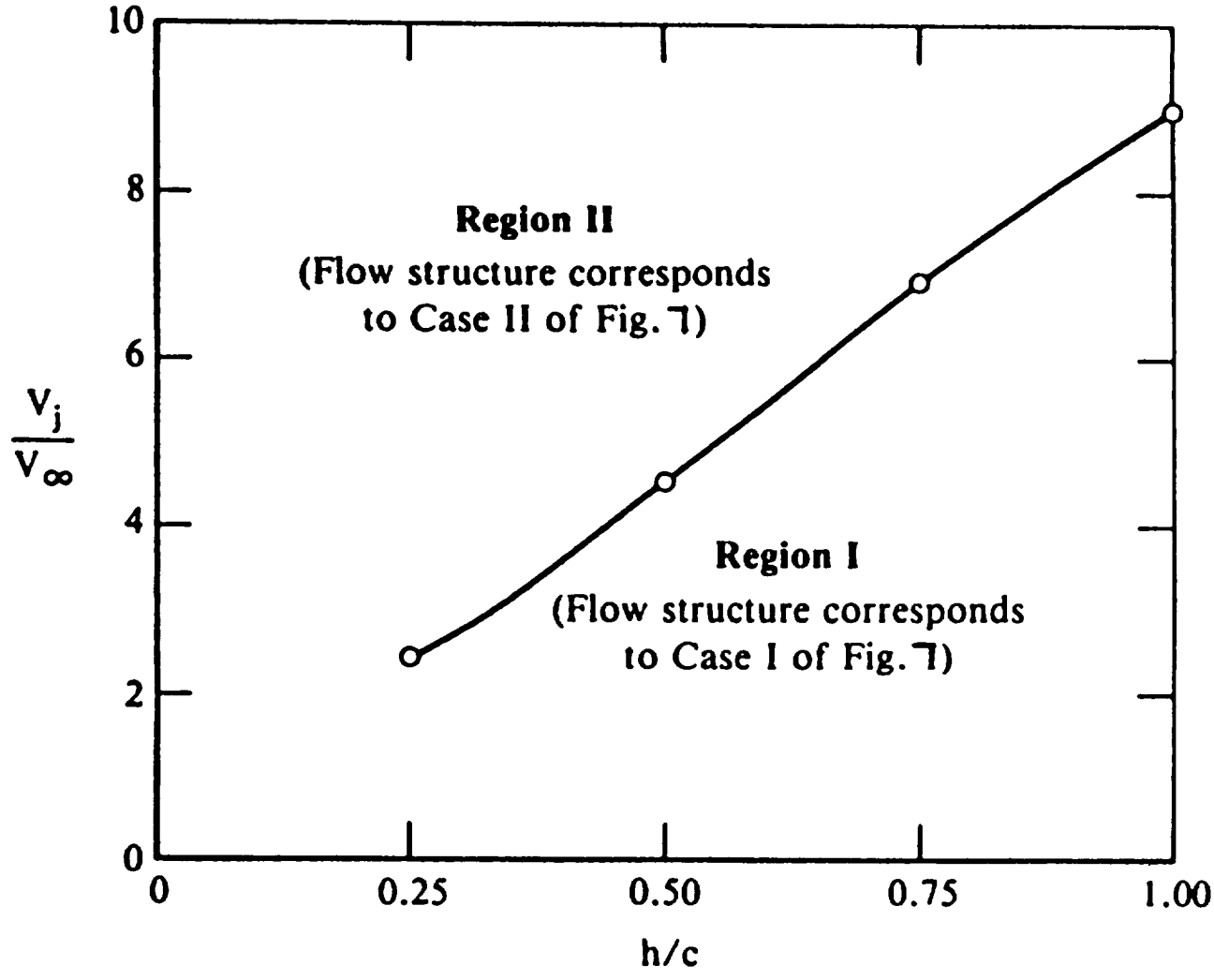

Figure 6. The loci of the maximum C_L for different ground plane locations.

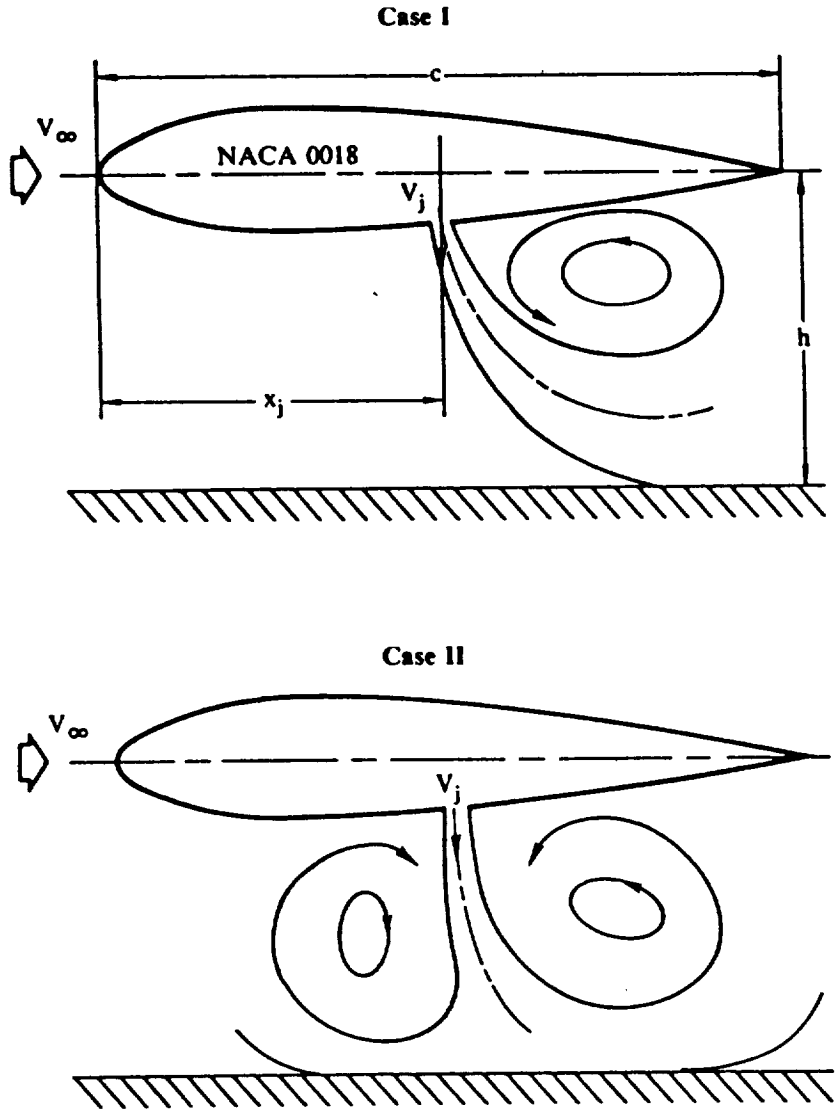

Figure 7. The flow structure corresponding to regions identified in figure 6.

NOISE OF THE HARRIER IN VERTICAL LANDING AND TAKEOFF

Paul T. Soderman
and
John D. Foster

NASA Ames Research Center, Moffett Field, CA 94035

Abstract

The noise of the Harrier AV8C aircraft in vertical takeoff and landing was measured 100 ft to the side of the aircraft where jet noise dominates. The noise levels were quite high - up to 125 dB overall sound level at 100 ft. The increased noise due to jet impingement on the ground is presented as a function of jet height to diameter ratio. The impingement noise with the aircraft close to the ground was 14 to 17 dB greater than noise from a free jet. Results are compared with small-scale jet impingement data acquired elsewhere. The agreement between small-scale and full-scale noise-increase in ground effect is fairly good except with the jet close to the ground. It is proposed that differences in the jet Reynolds numbers and resultant character of the jets may be partially responsible for the disparity in the full-scale and small-scale jet impingement noise. The difference between single-jet impingement and multiple-jet impingement may also have been responsible for the small-scale and full-scale disagreement.

Introduction

This report describes an experimental study of the noise of a V/STOL aircraft operating near the ground - specifically, the noise of the Harrier AV8C in vertical landing and takeoff. The apparent acoustic amplification of jets impinging on the ground has been the subject of several small-scale studies, but there is a lack of information in the literature on full-scale jet ground effects. The ground vortex itself, the main subject of this workshop, may affect the propagation of that noise; but this study was conducted without wind, so a true ground vortex was not present.

Historically, it would appear that military fighter aircraft noise has not been addressed because of the possible performance penalties from sound control equipment. However, there is now a concern among aircraft manufacturers and the military that the noise of high-powered STOVL-type aircraft may be sufficiently high, during vertical landing in particular, to a) damage the aircraft or stores due to acoustically induced vibrations. b) interfere with the pilot's communication and complicate his workload, and c) cause ear damage or interfere with the work of the ground crews assigned to launch and capture the aircraft. Those problems are all serious, but items (b) and (c) could conceivably be dealt with using improved ear protectors and communication equipment. Item (a) is more difficult. For example, damage to an air-to-air missile during landing for refueling could lead to loss of the aircraft in subsequent combat. It should be noted that current designs give a STOVL aircraft much more power than the Harrier, particularly designs aimed at supersonic flight, and therefore they will have much more capacity for noise generation.

The approach in this study was to measure the noise of the Harrier AV8C in vertical landing and takeoff with ground level microphones placed 100 ft from the aircraft. The results are then compared with data from small-scale studies (ref. 1 and NASA Contract NAS3-23708) done elsewhere to see if the small-scale data show ground effects similar to those measured with the Harrier. Some of the small-scale data indicate very high levels of acoustic tones when jets impinge perpendicularly on a simulated ground plane. Those tones are generated by an aeroacoustic feedback mechanism involving vortex rings in the jet, ground impingement, and acoustic radiation back to the nozzle. Since those studies have been done at a very small scale, their applicability to full-scale jet noise must be proven. The Harrier flight test did not confirm the presence of such a feedback mechanism.

Harrier AV8C Aircraft

The Harrier aircraft, a swept-wing transonic fighter, utilizes four vectored nozzles for thrust and lift. It is capable of STOL or VTOL operation. Figures 1(a) and (b) are photographs of the NASA AV8C Harrier aircraft. Figure 1(a) shows the nozzle deployment in a vertical landing and the small dams on the underside of the fuselage that are designed to block the flow of the jet upwash along the fuselage.

Figure 2 is a schematic of the turbofan Pegasus engine used in the aircraft. The fan bypass air is exhausted out the two front nozzles, and the turbine exhaust gas is exhausted out the two rear nozzles as shown. Typical temperatures and jet speeds are noted. The rear jet Mach number was nominally 0.93 based on sound speed in the jet. The front and rear nozzle dimensions are given in figure 3(a). The nozzles are rectangular and cut parallel to the corner vanes shown in figure 2. That is, the exhaust area is not perpendicular to the duct axis. This is also illustrated is figure 3(b), which is a photograph of a forward nozzle. The effective diameter of each nozzle, defined as the diameter of a duct with the same cross-sectional area as the rectangular nozzles (measured perpendicular to the duct axis), is approximately 1.5 ft.

Other sources of noise on the aircraft are the inlet fan and reaction-control jets. The inlet fan noise was avoided in this study by positioning the microphones to the side of the aircraft. The reaction jet noise was not identified in the data.

Test Procedure

The aircraft was landed on a concrete apron with the microphones positioned to the right side of the aircraft as shown in figure 4. That is a direction where the noise of the jets dominates the engine fan noise. The pilot approached the landing site, hovered at 100 ft altitude, and descended vertically at a uniform rate of around 2.5 ft/sec with a minimum of throttle adjustments. However, it is standard procedure to increase the throttle setting just before touchdown, followed by a sudden throttle cut before the wheels hit the ground. The throttle settings were not recorded, but by plotting the data as a function of altitude it is possible to separate throttle effects from ground effects on the noise. After a cool-down, the aircraft took off vertically to the same altitude, hovered for several seconds, and descended uniformly again. Most of the data are presented from the second

descent. Recordings were also made ahead of the aircraft while it was on the ground to document the fan tone noise. During the flight test, the atmospheric conditions were as follows:

Temperature	69° F
Relative Humidity	18%
Barometric pressure	30 in Hg
Wind	3 knots maximum

The primary data microphone was 100 ft to the side of the landing center point. Actually, two microphones were used side by side at that location, one laid on the ground and one on a 4 ft tripod. As expected, the elevated microphone data show non-uniform ground reflections in the acoustic spectra, so that data is not presented. The ground microphone, on the other hand, had a uniform ground reflection of 6 dB across the spectrum, which was subtracted from the data. This is one of the procedures recommended by the S.A.E. for measuring jet noise.[2] A hand held sound level meter was used 300 ft from the aircraft in the same direction as the 100 ft microphone.

During the aircraft descents and ascents, the pilot announced his altitude readings using the aircraft radar altimeter. The radio transmissions were then noted on the acoustic data tape voice channel. Unfortunately, many of those radio transmissions were not heard in the instrumentation van because of the high noise from the aircraft. Therefore, it was necessary to interpolate between known aircraft altitudes assuming uniform descent or ascent rates. We also noted the time used to descend from or ascend to a known altitude. No time code system was available. The result of this is that the aircraft position was known only approximately. Plots of noise versus altitude show scatter caused by this uncertainty. However, the trends are readily apparent. It is clear that the flight test data cannot be considered as accurate as laboratory-quality data. On the other hand, the data represent results from a flight aircraft and, therefore, contain no errors resulting from scale effects or imperfect simulations.

Instrumentation

Figure 5 shows the acoustic instrumentation. The primary data microphone was a B&K 4133, 1/2-in. condenser microphone powered by a portable power supply/amplifier. The signal was transmitted 200 ft by coaxial cable to the instrumentation van and recorded on a Nagra tape recorder. The system was calibrated in the field with a single-tone piston phone. After the flight test, the data were processed in an HP 5423 FFT spectrum analyzer controlled by an HP 87 computer system.

Data Reduction

Ideally, ground effects are best measured by keeping the aircraft and instrumentation fixed while moving the ground plane. In the flight test, however, the ground and microphone were fixed and the noise source was moved. Thus, the distance from the noise source to the microphone (and subsequent noise levels) was constantly changing irrespective of the ground effect. Furthermore, free jet noise is directional so that, as the aircraft ascended or descended, the angle between the jet axis and the microphone changed, and the noise levels at the microphone changed irrespective of the

ground effect. Both the distance and directivity effects had to be removed from the data to isolate the ground effect on the noise. The distance effect was removed by normalizing the data to the source/microphone distance with the aircraft at 100 ft altitude using free field decay rate (6 dB per double distance). The free-jet directivity effect was removed by normalizing the data to the exhaust nozzle/microphone angle at 100 ft altitude, which was 135° relative to the engine axis looking forward. Since jet noise 135° from the axis is louder than the noise 90° from the axis, for example, a correction factor was added to the noise at 90° equal to the difference in radiated jet noise at 135° and 90°. From ref. 2, it was estimated that the maximum correction factor was 15.5 dB at 400 Hz and 90°. The correction factor reduces for larger angles and higher frequencies as listed below. The jet directivities from ref. 2 are typical of isolated jet engines; but without actual directivity data from the Harrier (which is affected by the fuselage and wing) the directivity corrections must be considered as approximations. The corrections do not account for changes in directivity caused by jet impingement because that is an effect we did not want to remove from the data. The complete corrections are as follows:

$$L_{pn}(f) = L_{po}(f) + \Delta dB_1 + \Delta dB_2 + \Delta dB_3 \qquad \text{dB re } 2 \times 10^{-5} \text{ Pa} \quad (1)$$

where

$L_{pn}(f)$ = sound pressure level corrected to source at H = 100 ft
$L_{po}(f)$ = sound pressure level measured flush with the ground
f = frequency, Hz
ΔdB_1 = 20 log (d/141.4) distance correction
d = distance from microphone to aircraft center, ft (141.4 is distance to aircraft center at H = 100 ft)
ΔdB_2 = -6 ground reflection correction
ΔdB_3 = directivity correction from following table (selected frequencies listed)
θ = angle at jet exhaust between jet axis looking upstream and line to microphone

	ΔdB_3		
θ, deg	400 Hz	1000 Hz	8000 Hz
90-95	15.5	10.5	7.5
95-100	13.0	9.0	5.5
100-110	10.0	6.5	4.5
110-120	6.5	2.5	1.5
120-130	1.0	1.5	1.5
130-135	0	0	0

Where appropriate, the overall sound levels without distance and angle corrections are noted on the figures to represent the noise that would actually be heard at that aircraft position and operating condition.

The data corrections were applied to the constant bandwidth spectral plots before plotting. To get the overall sound levels, the spectral plots were integrated assuming incoherent addition of acoustic energy from band to band. The spectral analyses were made from 0 to 12.8 kHz using an effective

bandwith of 37.5 Hz. Because of the aircraft motion, only two samples of data were averaged at any one altitude, each sample representing a 40 ms time window. The aircraft movement during the sampling time was small. However, due to the random nature of jet noise, the short sample times resulted in spectral plots with an apparent spread of ±3 to 4 dB. The noise level at any frequency was taken to be the middle point of that data spread. All data are labeled with the nondimensional altitude, H/D (where H is the aircraft nozzle altitude in feet, and D is the effective diameter of one nozzle, 1.5 ft). When the Harrier is on the ground, the value of H/D is approximately 3. (The center of the forward nozzle exhaust is 5 ft above the ground, and the center of the aft nozzle exhaust is 4 ft above the ground, for an average height of 4.5 ft.)

Results and Discussion

Flight Test Data

Figure 6 shows Harrier acoustic spectra measured during takeoff for nozzle-height-to-diameter ratios (H/D) of 3 and 70; i.e., in- and out-of-ground effect. The spectra are typical of broadband jet noise and do not contain visible tones. Because of the short, 2-sec sample time and the narrow bandwith, the scatter in these spectra is around ±4 dB. The noise increase due to the ground appears to range from 10 to 20 dB. However, time records to be shown indicate that the noise increases near the ground were inflated by a high throttle setting used for the rapid takeoff. Thus, the ground effects on the noise in figure 6 are exaggerated. The landing data, however, were taken with a much more uniform throttle setting that was similar to the setting at hover. Figures 7(a)-(b) show similar spectral data measured during landing at values of H/D of 3 and 20 compared to the out-of-ground effect data at H/D = 70. The Harrier noise during landing at H/D = 3, the lowest altitude, was louder by 5 to 15 dB than the out-of-ground noise. At H/D = 20, the ground amplification was 4 to 13 dB. Because of the random fluctuations in jet noise and the short average times used, the data scatter makes it difficult to get accurate differences in the two curves. There is further uncertainty because of possible errors in aircraft position discussed above. These uncertainties can be reduced by plotting continuous time records of the Harrier noise using wider filters. Before leaving the narrow band data, it is important to note that the compressor tones measured ahead of the aircraft during cool-down with low engine speed, shown in the spectrum of figure 8, are not visible in the ground-effect data measured to the side of the aircraft where jet noise dominates.

Figures 9(a)-(c) show time records of the takeoff and landing noise measured in 400, 1000, and 8000 third-octave bands. These data were also digitized with 2-sec average times. But with wide bandwidths, the data scatter is considerably reduced compared to the narrow band data. Two curves are shown, one with raw data, the other with data corrected for ground reflection, source-microphone distance, and jet directivity variations as discussed above. At approximately 2 sec on the time scale, the aircraft engine speed was increased. Takeoff occurred at around 8 sec, which was the highest throttle condition and maximum noise condition. The aircraft ascended vertically to 100 ft by approximately 14 sec and hovered briefly, then descended vertically with a uniform throttle setting. Touchdown occurred at around 58 sec. Although the results show some scatter, a fairly uniform increase in noise is evident during descent. Comparing the noise levels at hover with the

noise at other altitudes during descent, the difference is assumed to be due to the jet/ground interaction. The takeoff phase of the flight is ignored because of the higher throttle settings required to climb.

Figure 10 shows the increases in landing noise relative to the noise at H/D = 70 taken from figures 9 (a)-(c). At touchdown, the amplification of the sound was 14-17 dB. The amplification decreased more or less uniformly to zero with increases in H/D from 0 to approximately 60.

At this point it is not clear how much of the noise was amplified by the ground and how much was simply reflected and redistributed. For example, a random noise (like jet noise) will reflect off a hard surface, such as concrete, and increase the average noise above the surface by 3 dB (6 dB for a flush mounted microphone). With a wing and fuselage above the source, sound parallel to the ground would go up more than 3 dB because, as the wing-to-ground distance is decreased, the acoustic energy would be forced outward to the side. This directivity effect is complicated by the hot exhaust upwash, which can refract sound waves. On the other hand, Preisser and Block[1] showed large increases from a small, cold jet impinging on a ground plane even without a wing present, indicating that other phenomena besides reflections and refractions are important.

Comparison With Small-Scale Test Results

Figure 11 shows the experimental setup from two small-scale studies of jet impingement noise. The left sketch shows an experiment currently being conducted by K. Ahuja and associates at Lockheed-Georgia (NASA Contract NAS3-23708). A 0.264-in. diameter nozzle projecting from a simulated fuselage is being used to study jet impingement on a metal plate. The nozzle/plate separation distance is adjustable. Acoustic, aerodynamic, and flow visualization measurements are made using heated and unheated jets. The right sketch shows a similar experiment using a 2.5-in. diameter nozzle used by Preisser and Block at NASA Langley.[1] Preisser and Block measured the acoustic radiation and the unsteady pressures on the ground plane.

Figures 12(a) and (b) are preliminary results from the Lockheed-Georgia study (NASA Contract NAS3-23708) showing acoustic spectra with and without the ground plane installed. Figure 12(a) shows very large noise increases due to ground impingement at H/D = 2 (around 20 dB broadband noise increase, plus the appearance of very loud tones another 20 dB above the broadband noise). Even at H/D = 20, the noise increase due to the jet/ground interaction was over 10 dB as shown in figure 12(b). Using flow visualization, Ahuja traced the tone generation to a feedback loop mechanism illustrated in figure 13. At certain values of H/D and acoustic frequencies, sound from the jet impingement radiates to the jet nozzle and excites a flow instability which coalesces into a series of ring vortices in the jet. The ring vortices strike the ground and radiate sound back to the nozzle to excite further vortex rings to create a resonant, coherent flow structure and subsequent strong tone radiation. This feedback phenomenon has been described by others such as Krothapalli,[3] who demonstrated the same coherent flow and tone radiation from narrow rectangular jets impinging on a ground plane.

Preisser and Block[1] at NASA Langley also found large increases in jet overall sound levels (OASPL) due to ground impingement as illustrated in

figure 14. However, they found no distinct tones and make no mention of resonant flow conditions. (Note that they show zero impingement noise on the ground, which contradicts the Harrier flight test data.) They attribute the noise increase above the ground to increased turbulence and unsteady pressures on the ground and in the jet due to impingement. The location of the strongest noise sources was at the outer portion of the impingement region, between 1 and 3 jet diameters from the center of the jet stagnation point on the wall. The primary difference between the two small-scale studies is the jet diameter. The nozzle used at NASA Langley[1] had a diameter about 9 times that of the nozzle used at Lockheed-Georgia. The jet speeds were similar, and both jets were cold. Thus, the Reynold's number of the Langley experiment based on diameter ($Rn = 7.8 \times 10^5$) was 9 times that of the Lockheed-Georgia experiment ($Rn = 8.8 \times 10^4$) for the data shown here. This suggests that the tones and resonant flow conditions found by Ahuja and associates may have been a low Reynolds number phenomenon that does not exist at higher Reynolds number. Certainly, no significant tones were found in the Harrier flight test ($Rn = 1.2 \times 10^7$), though the existence of multiple jets may have obliterated resonant flow in the jets in any case. Other resonant flow fields such as vortex street shedding are known to be Reynolds number sensitive. This is not to say that coherent flow structure cannot be found in jets. On the contrary, other researchers[4] have used conditional sampling techniques to document the presence of a large-scale structure in what would seem to be randomly turbulent jets. Neuwerth[5] found ordered turbulence structure in a jet operated at a Reynolds number of 1×10^6, which caused large noise increases including tones, when impinged on a flap system. (The feedback tones were generated for $H/D < 6$.) Nontheless, Reynolds number and, consequently, scale effects are very important to jet/ground impingement studies both acoustically and aerodynamically. It is probable that as Reynolds number is increased, the role of coherent structure and resonant tone generation becomes weaker relative to the unsteady pressures and noise from random turbulence. A careful study of Reynolds number and scale effects on jet impingement aerodynamics and acoustics should be made before results of small-scale studies can be used with confidence.

A comparison of the full-scale Harrier flight test results and the two small-scale experiment results are made in figure 15. Admittedly, a comparison of multiple-jet impingement noise and single-jet impingement noise may be unfair, but the trends are of interest. The noise increase due to the ground effect is plotted versus H/D. The Ames 400 Hz third-octave band data is compared with the Langley[1] overall noise measured 55° from the horizon and with the Lockheed-Georgia data measured at 27.2 kHz. (Note that the 27.2 kHz data is not the strong tone in figure 12(a); that tone would be 45 dB above the out-of-ground data.) The Ames Harrier data was dominated by low frequencies, so the 400 Hz data should show the same ground effects as overall noise. At the same time, the 400 Hz Harrier data will scale to the Lockheed-Georgia 27.2 kHz small-scale data (assuming that the jet noise scales with Strouhal number based on jet diameter). The comparison of the full-scale and small-scale data is fairly good with two exceptions; the Lockheed-Georgia data show much greater ground effect at low values of H/D, and the Langley data show faster decay of ground effect with increase of H/D. With so few small-scale data points, it is not clear if the differences between the Ames and Langley data are due to data scatter or actual trends. Similarly, it is not clear if the differences between the Ames and Lockheed-Georgia data is due to Reynolds number effects or due to multiple-jet interactions which affected

the flow field and subsequent impingement noise. In any case, the lack of agreement indicates that more work is required to resolve the differences between full-scale and small-scale jet/ground impingement studies.

Concluding Remarks

The short flight test of the Harrier AV8C in vertical landing and takeoff showed that the noise levels to the side of the aircraft are quite high - up to 125 dB overall noise level. The sound levels were amplified and redirected by the ground such that the noise levels over a large frequency range increased 14-17 dB relative to the free jet noise during landing. It is not clear how much of the increase was due to redirection of the sound and how much was due to amplification caused by impingement. The noise increase due to ground effect became weaker as the jet height was increased and became small above a jet height-to-diameter ratio (H/D) of 60. There is some uncertainty in the actual levels versus height because of a) uncertainties in aircraft location, b) short data sample times, and c) assumptions about jet directivity irrespective of ground effect.

Comparisons of the ground effects on jet noise with small-scale data acquired elsewhere indicated that jet impingement aerodynamics and acoustics may be Reynolds number sensitive. One small-scale experiment resulted in the generation of strong tones, while the other small-scale experiment did not, presumably because of the higher Reynolds number flow in the second case. No significant tones were found in the Harrier flight test data. The Harrier full-scale data and published small-scale data showed the same trend; that is, jet impingement noise increases as the jet approaches the ground. However, the magnitudes of the impingement noise and the decay rate with jet height were different when comparing full-scale and small-scale data. It is not known if Reynolds number effects or the multiple-jet interactions accounted for the differences. Though coherent flow structure can exist in almost any jet, it is proposed that the role of coherent structure and subsequent tone generation will become weaker (relative to that of random turbulence and noise) if jet Reynolds numbers are increased or if multiple jets interact to break up the coherent structure. Finally, it appears that a careful study of jet impingement noise at different scales is required to resolve questions about the accuracy of small-scale simulations and resulting correlation with full-scale jet impingement.

References

1. Preisser, J.S.; and Block, P.J.W.: An Experimental Study of the Aeroacoustics of a Subsonic Jet Impinging Normal to a Large Rigid Surface. AIAA Paper 76-520, 3rd AIAA Aero-Acoustics Conf., Palo Alto, CA, July 1976.

2. SAE Committee A-21: Practical Methods to Obtain Free-Field Sound Pressure Levels from Acoustical Measurements Over Ground Surfaces. SAE Aerospace Information Report 1672B, June 1983 (See Appendix D).

3. Krothapalli, A.: Discrete Tones Generated by an Impinging Underexpanded Rectangular Jet. AIAA J., Dec. 1985, pp. 1910-1915.

4. Crow, S.C.; and Champagne, F.H.: Orderly Structure in Jet Turbulence. Boeing Sci. Res. Lab. Doc. D1-82-0991, 1970.

5. Neuwerth, G.: Flowfield and Noise Sources of Jet Impingement on Flaps and Ground Surface. AGARD CP-308, Proceedings of Conf. on Fluid Dynamics of Jets with Applications to V/STOL, 1981, pp. 13.1-13.7.

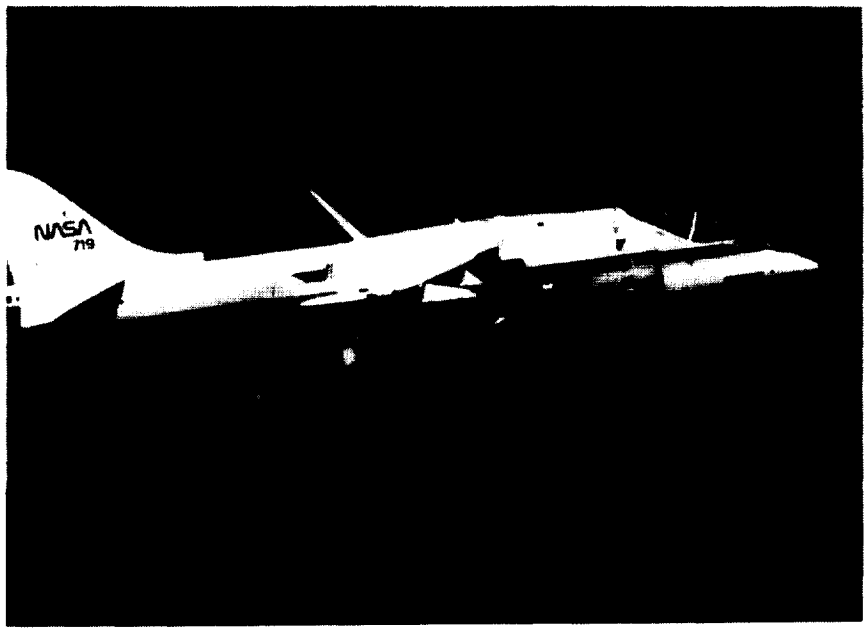

(a) SIDE VIEW DURING HOVER

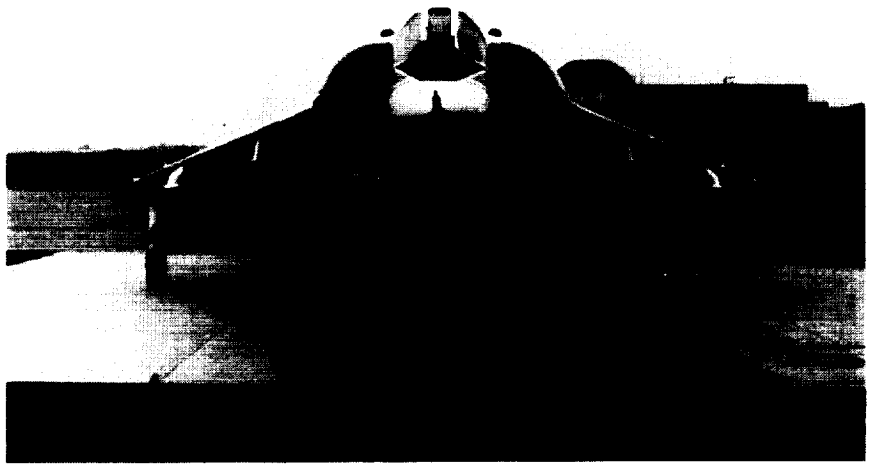

(b) FRONT VIEW ON GROUND

Figure 1 - Harrier AV8C aircraft.

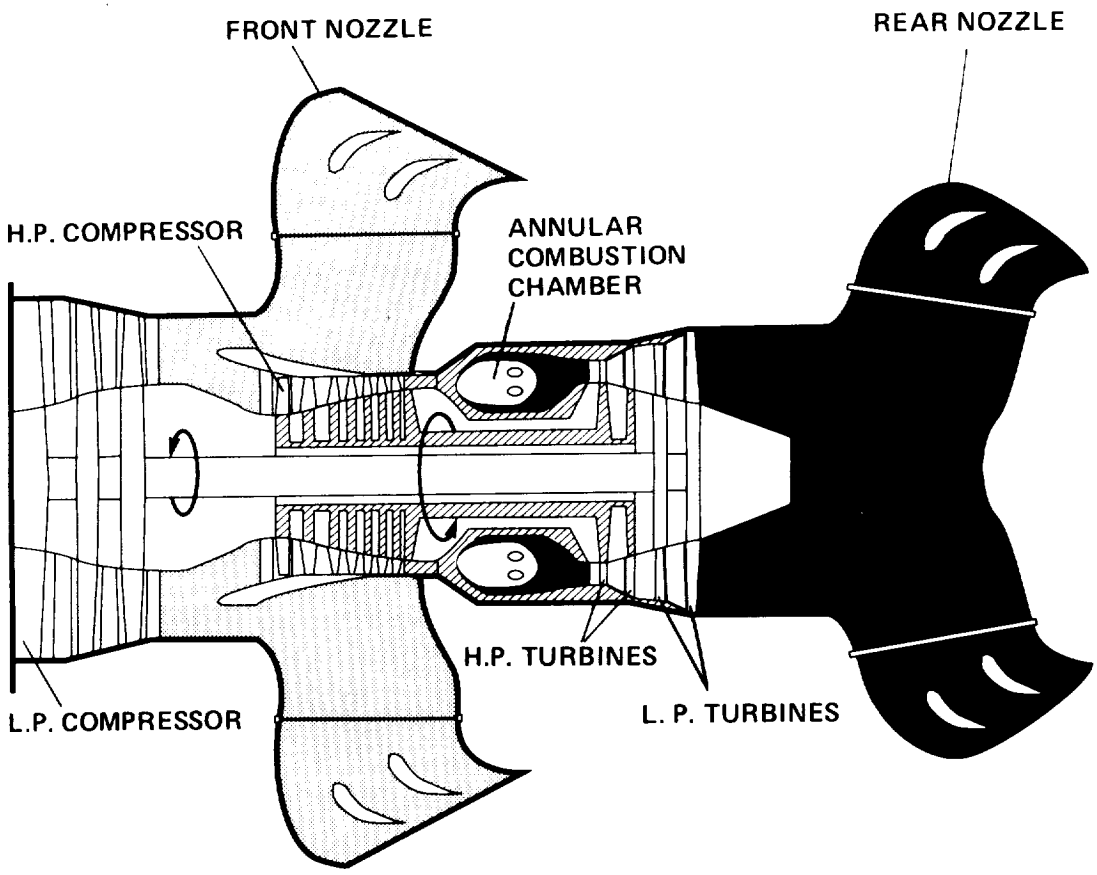

Figure 2 - Pegasus engine and exhaust ducting. Velocities and temperatures are for nominal V/STOL operation.

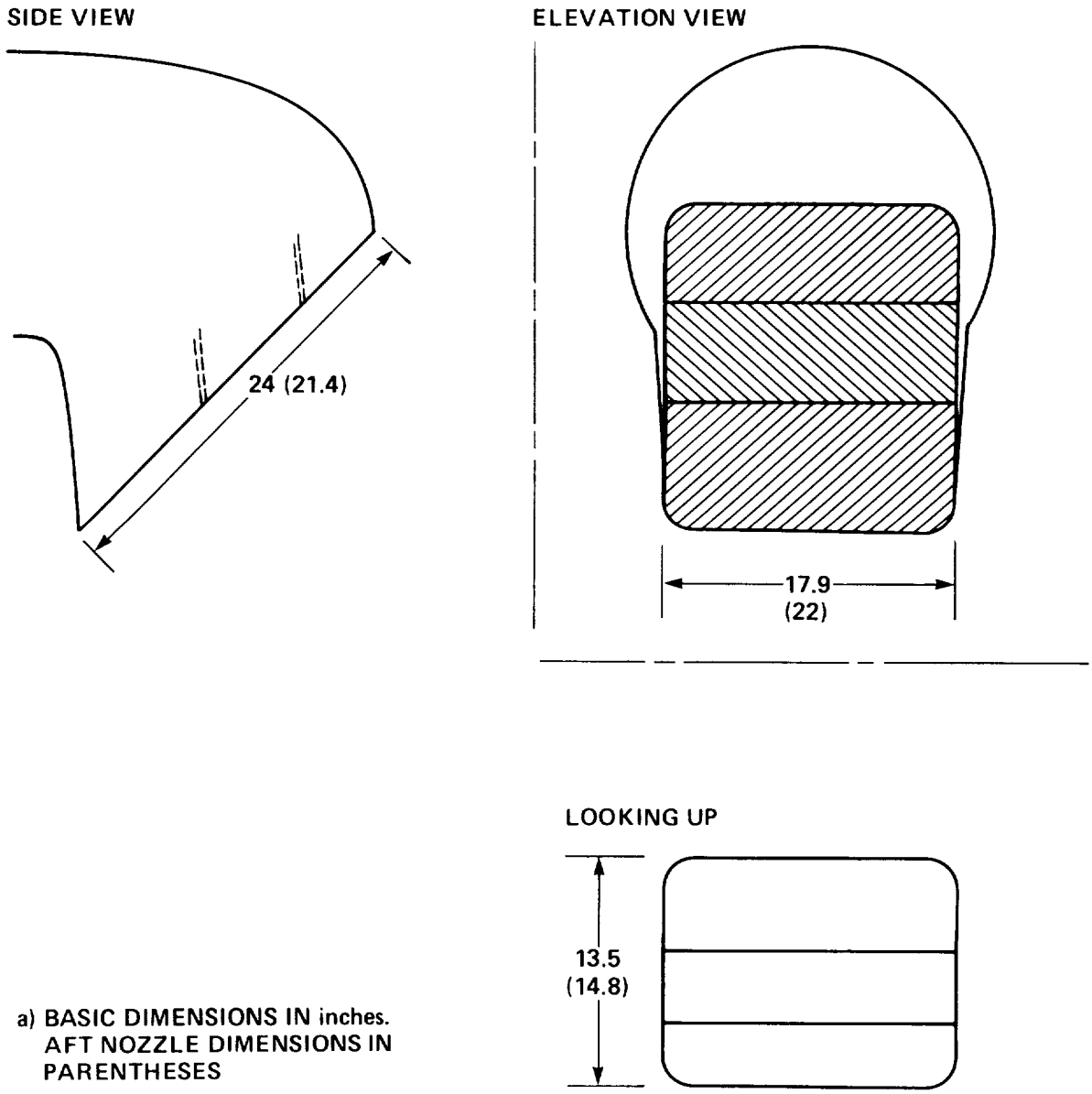

Figure 3 - Exhaust nozzle geometry and dimensions.

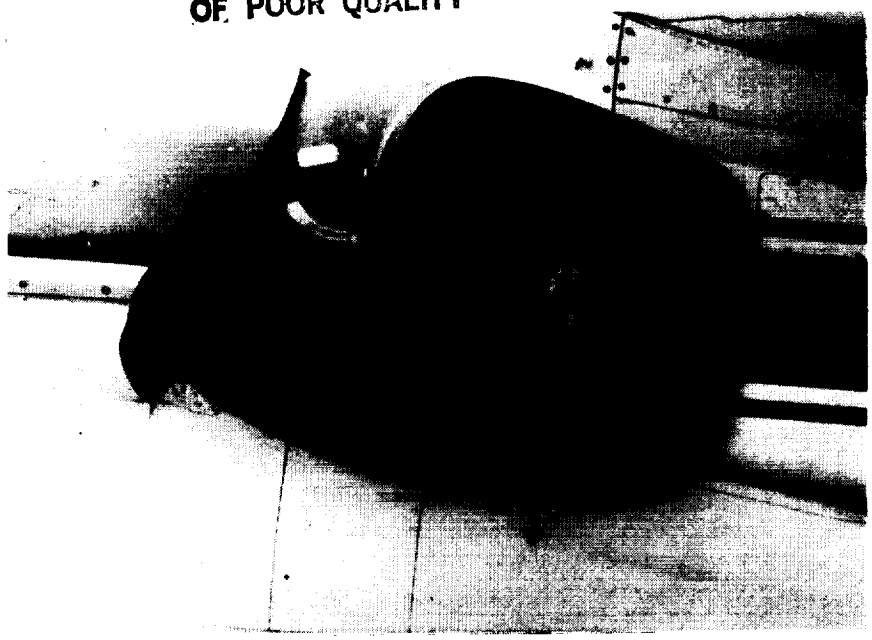

(b) FORWARD NOZZLE IN CRUISE ORIENTATION

Figure 3 - Concluded.

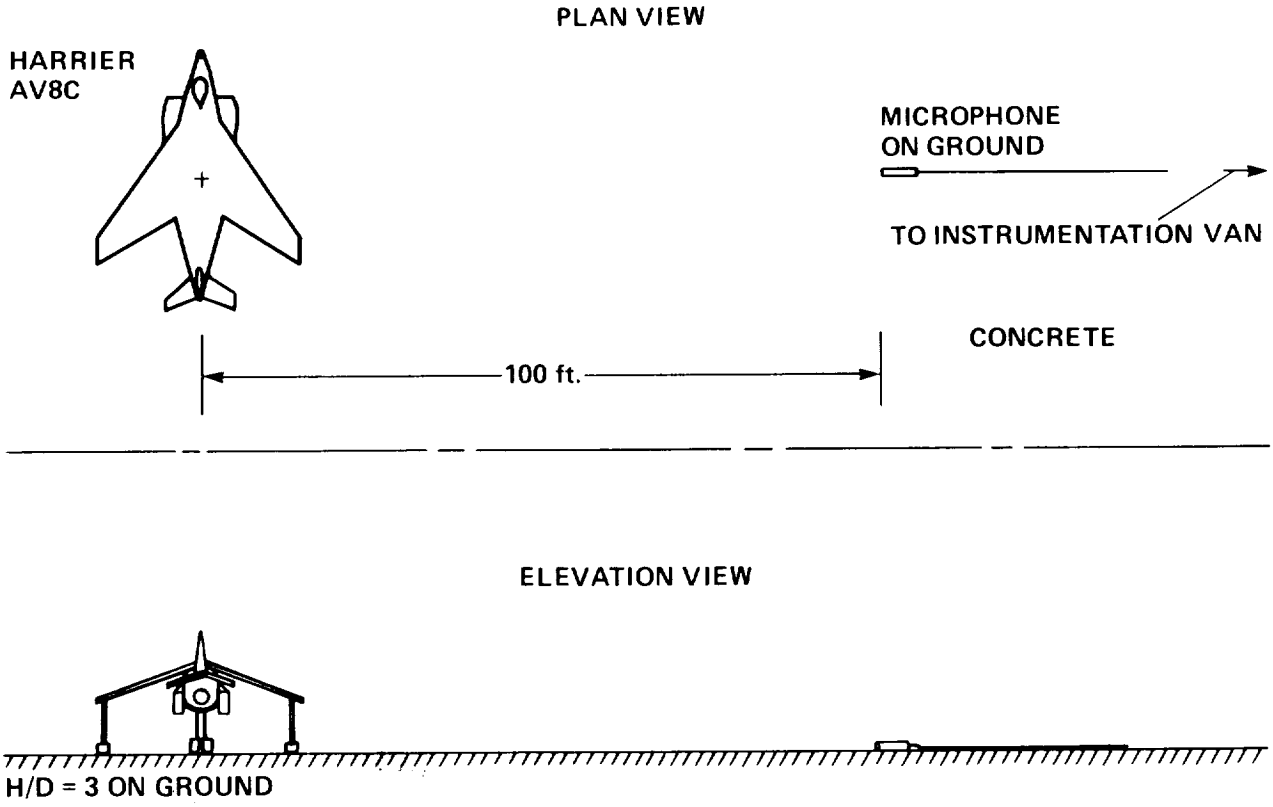

Figure 4 - Flight test setup showing microphone location relative to aircraft at touchdown. Instrumentation van was 300 ft from aircraft.

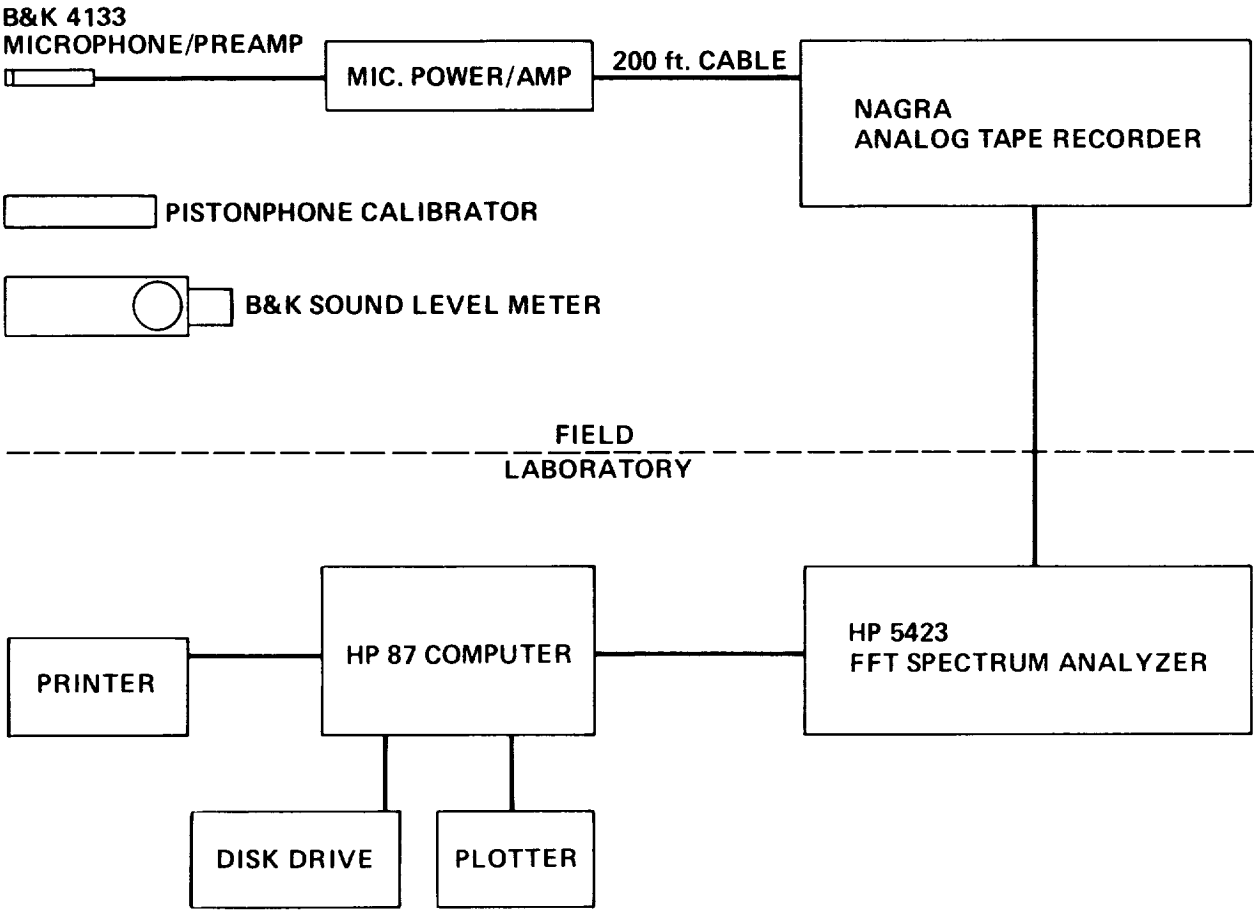

Figure 5 - Acoustic data acquisition and reduction instrumentation.

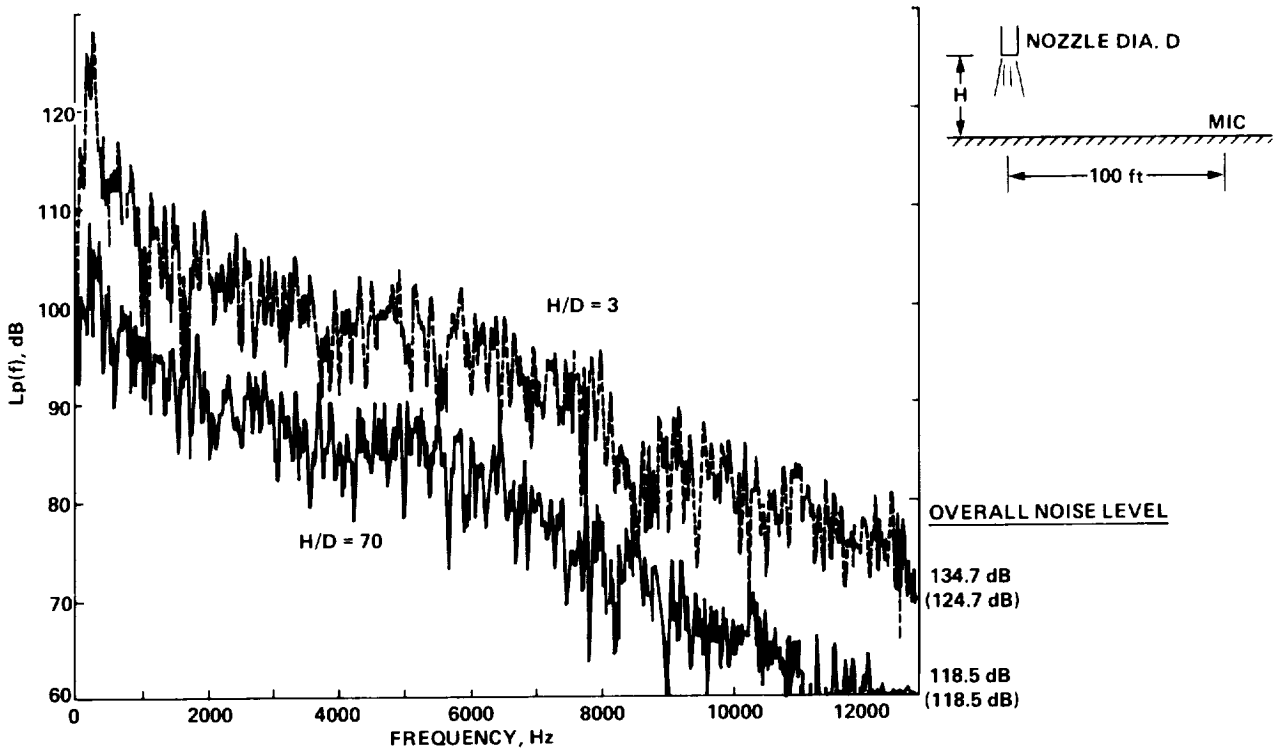

Figure 6 - Takeoff noise at H/D = 3 and 70. Acoustic differences caused by distance and jet directivity have been removed from spectra and overall noise levels except for numbers in parentheses.

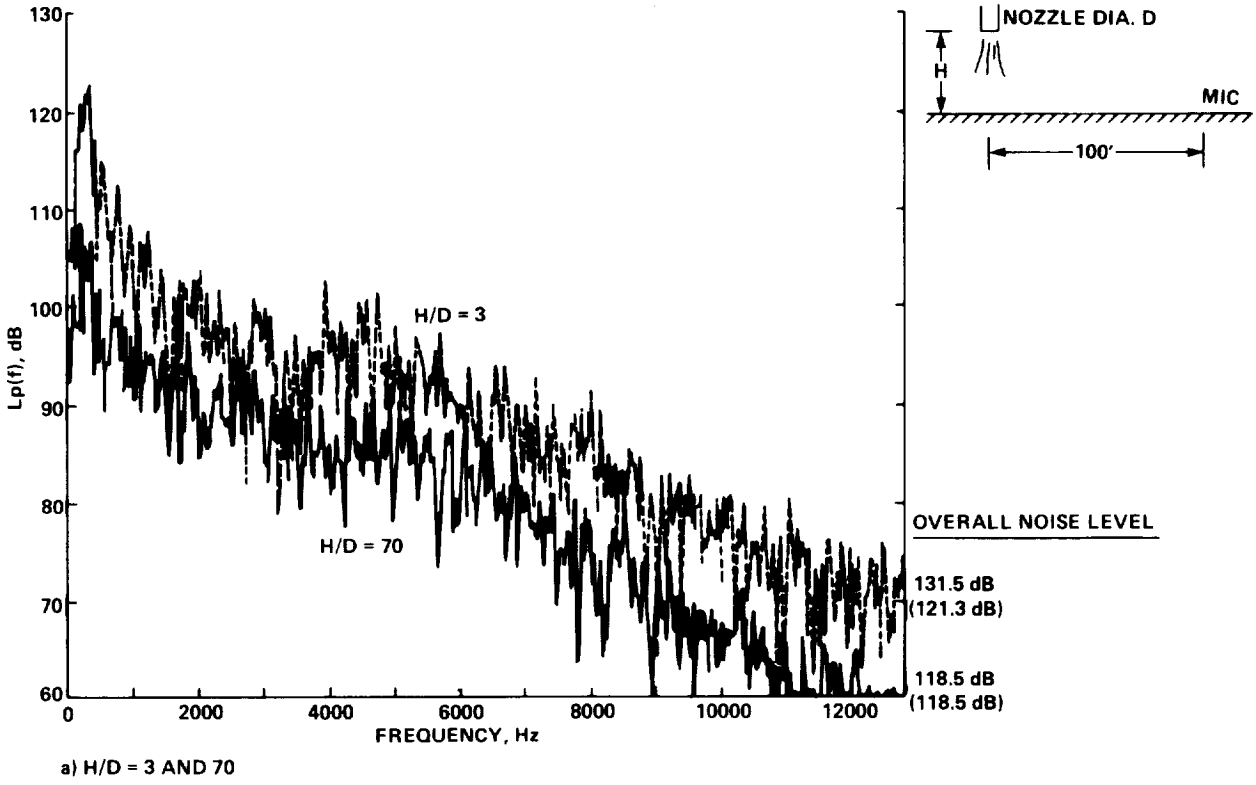

a) H/D = 3 AND 70

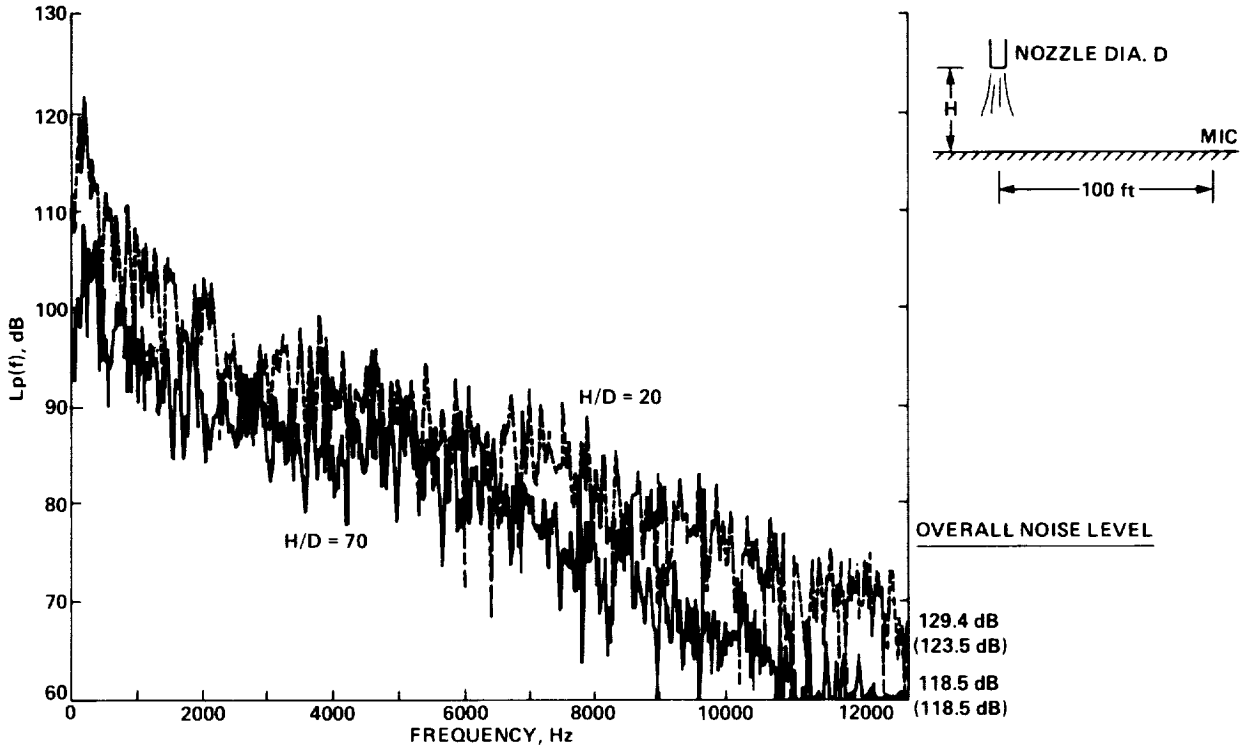

b) H/D = 20 AND 70

Figure 7 - Landing noise at three values of H/D. Acoustic differences caused by distance and jet directivity have been removed from spectra and overall noise levels except for numbers in parentheses.

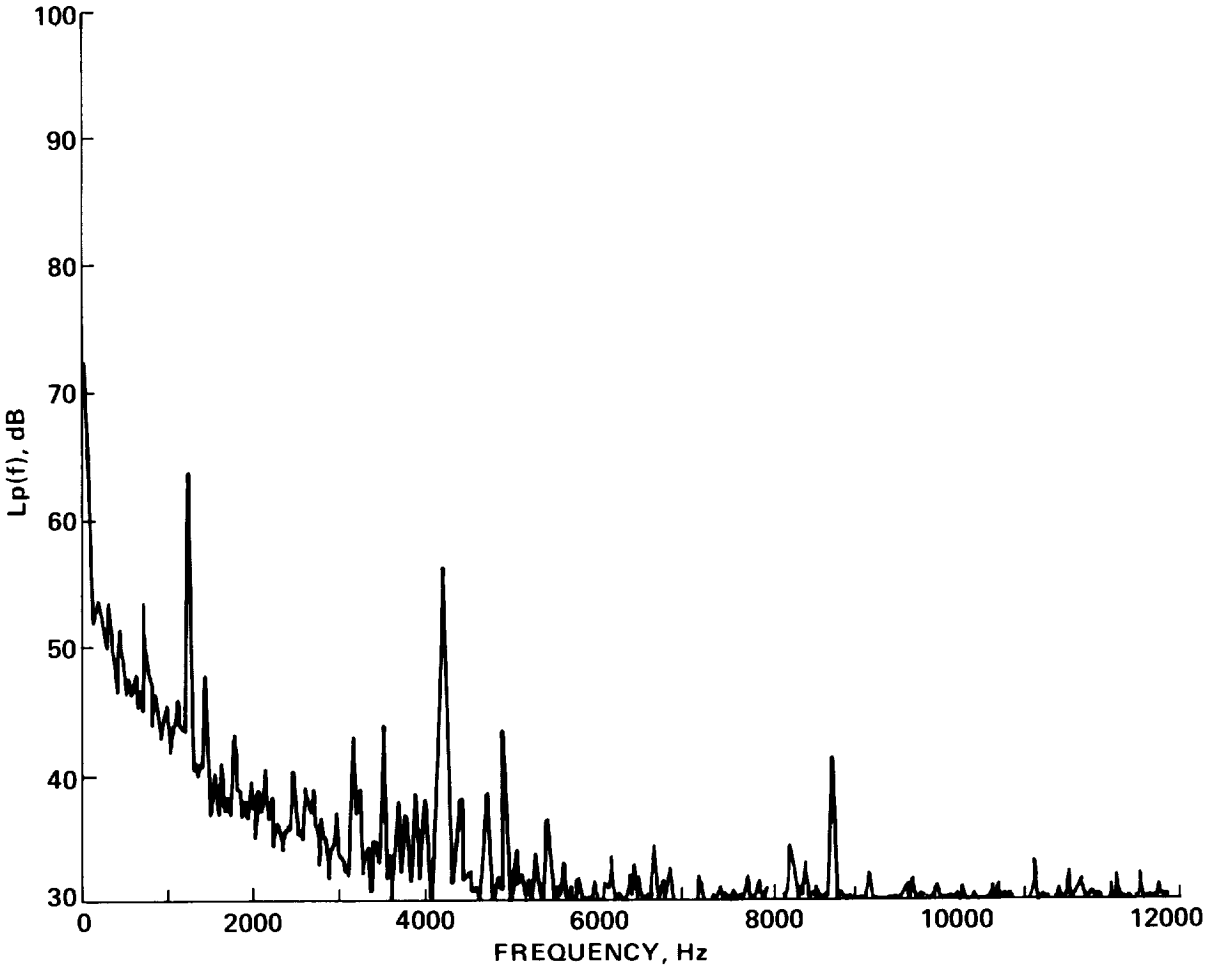

Figure 8 - Noise spectrum ahead of the aircraft while operating on the ground. Compressor tones are visible.

C - 3

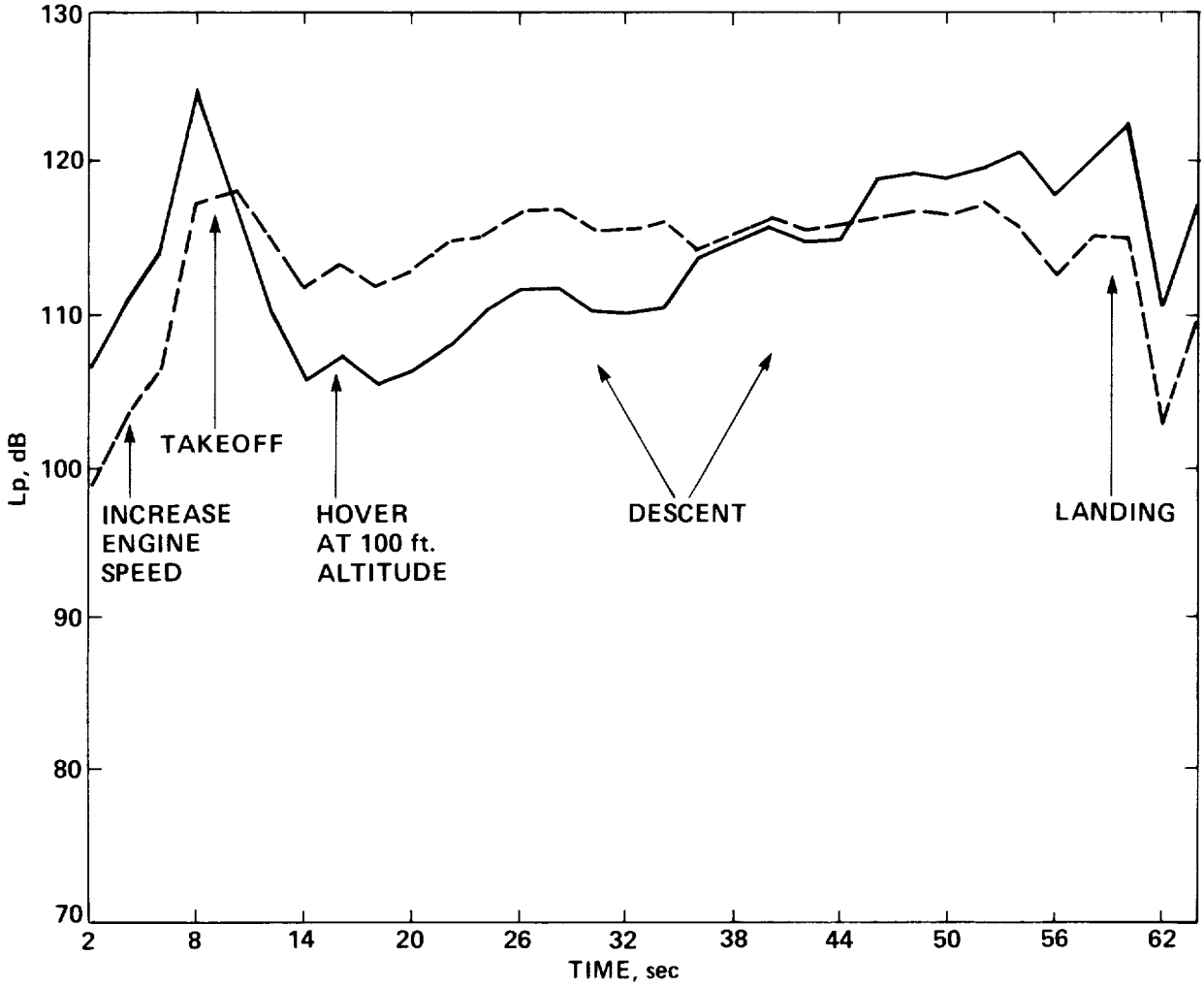

a) 400 Hz THIRD OCTAVE BAND

Figure 9 - Time record of Harrier noise during vertical takeoff, climb, hover and descent to landing; noise measured in third-octave bands for 2 sec averaging times. The dash line is uncorrected data; the solid line is data corrected for ground reflection, aircraft distance, and jet directivity effects.

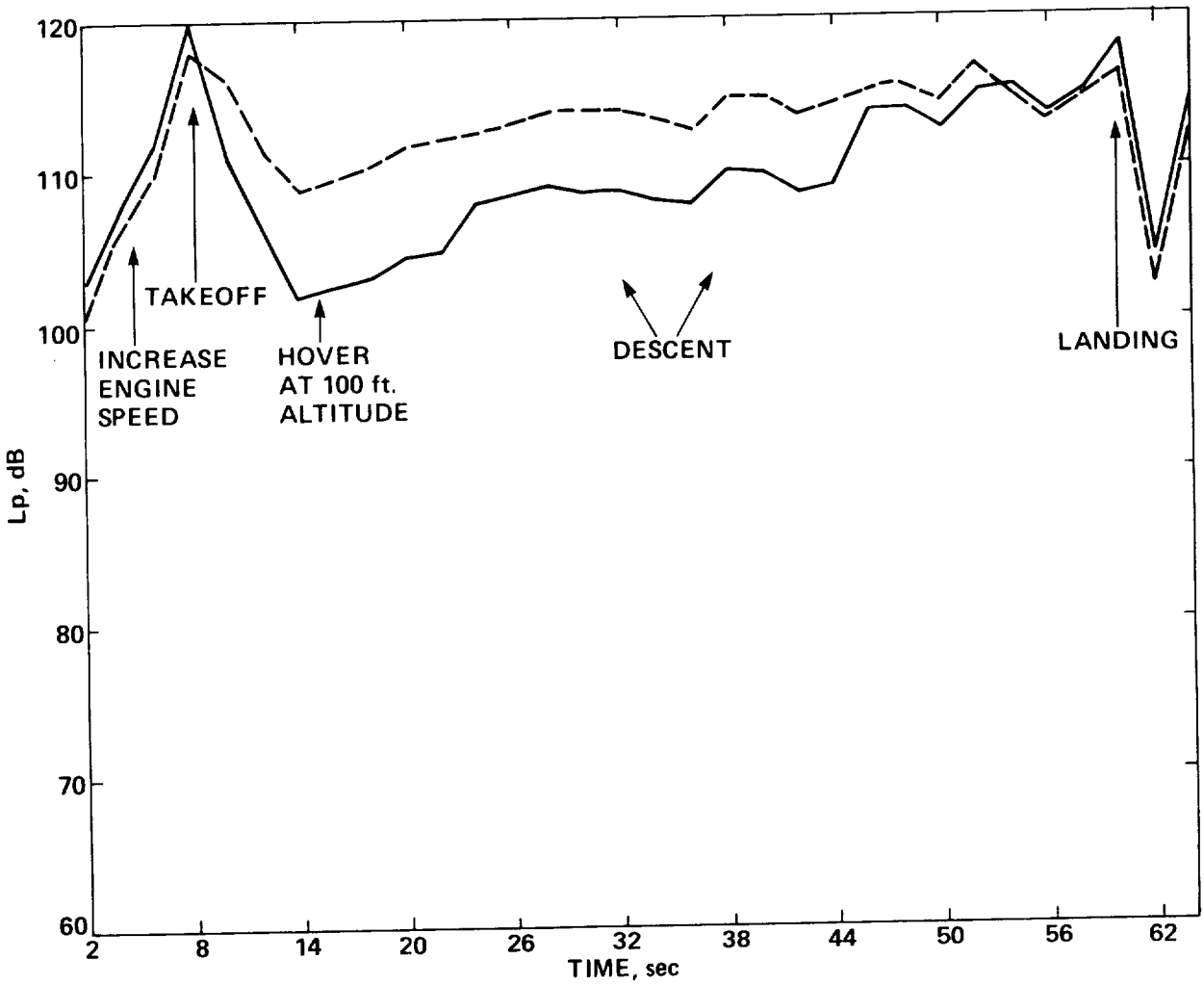

b) 1000 Hz THIRD OCTAVE BAND

Figure 9 - Continued.

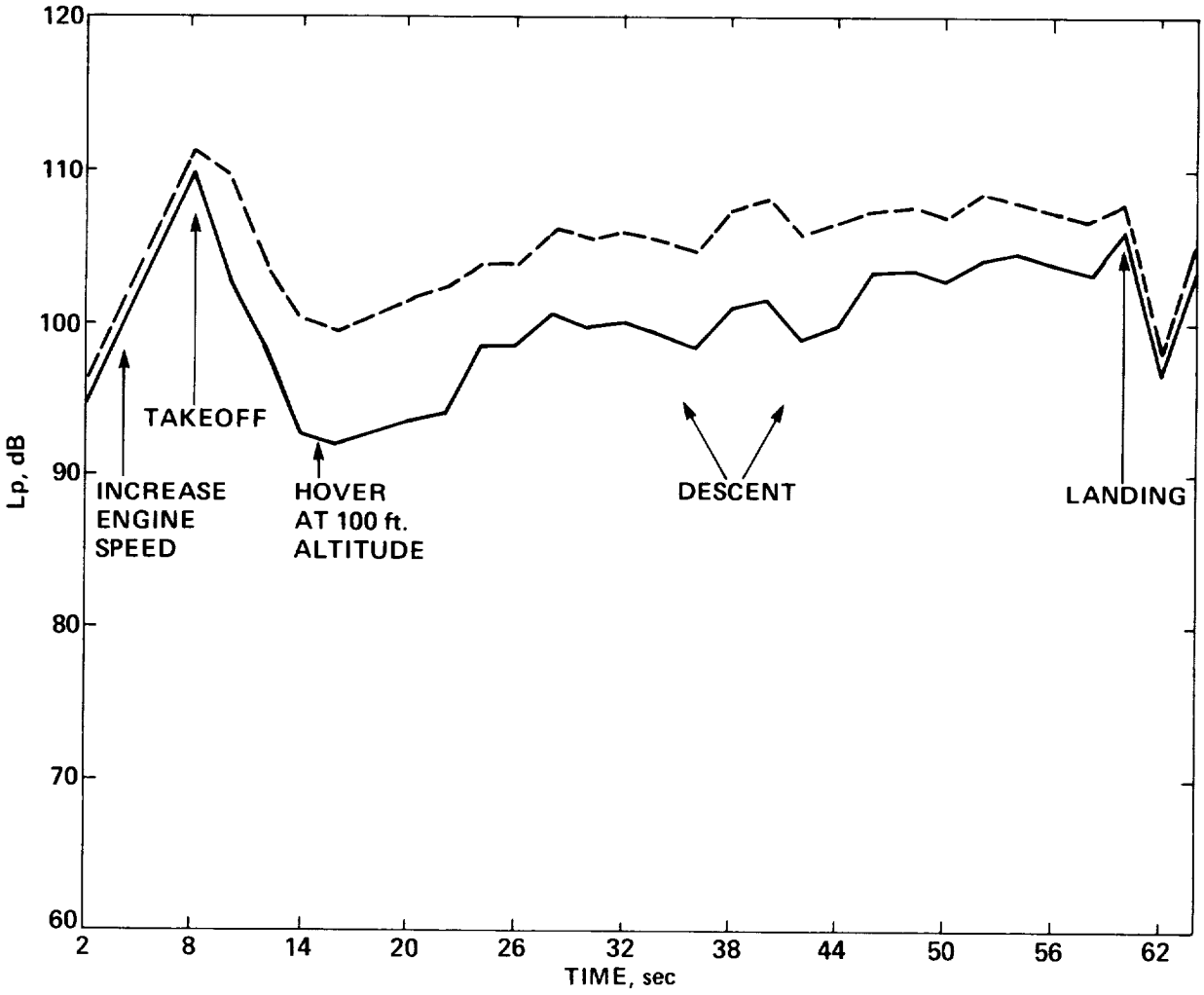

c) 8000 Hz THIRD OCTAVE BAND

Figure 9 - Concluded.

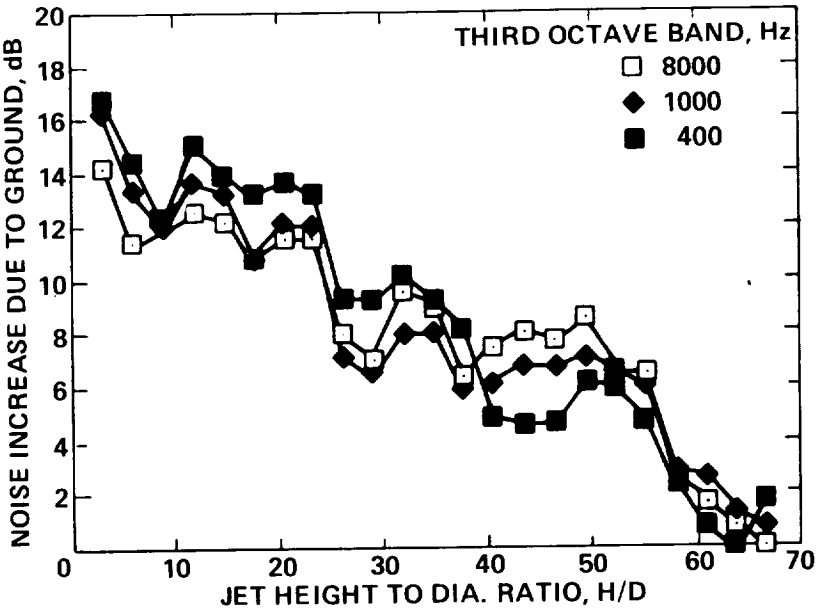

Figure 10 - Summary plot of landing noise relative to noise at H/D = 70 from data in figures 9(a)-(c).

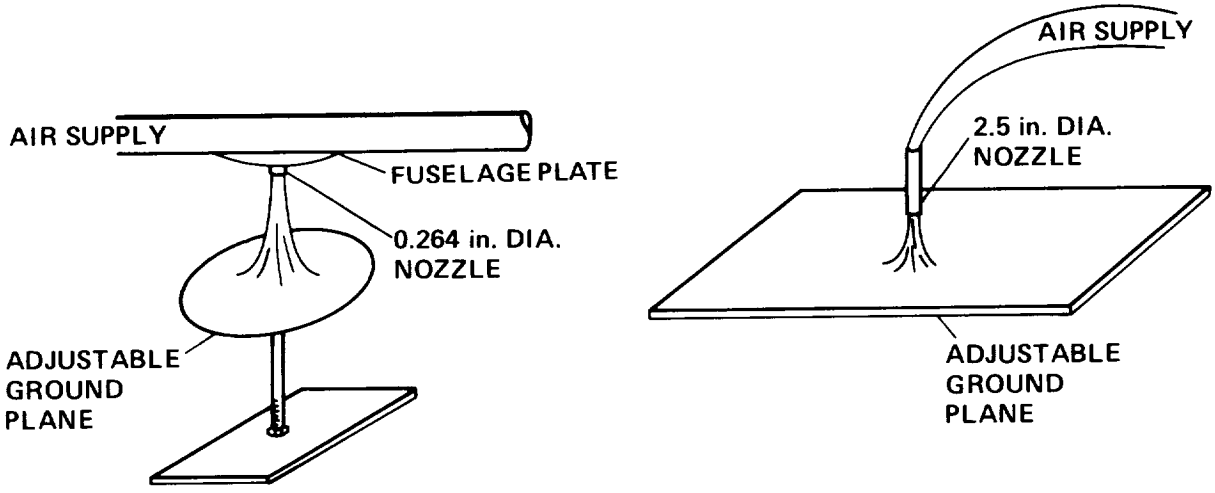

LOCKHEED-GEORGIA
NASA CONTRACT NAS3-23708
K.AHUJA et al.

NASA LANGLEY
AIAA PAPER 76-520
PREISSER AND BLOCK (ref. 1)

Figure 11 - Experimental setup for two small-scale studies of jet impingement on simulated ground planes.

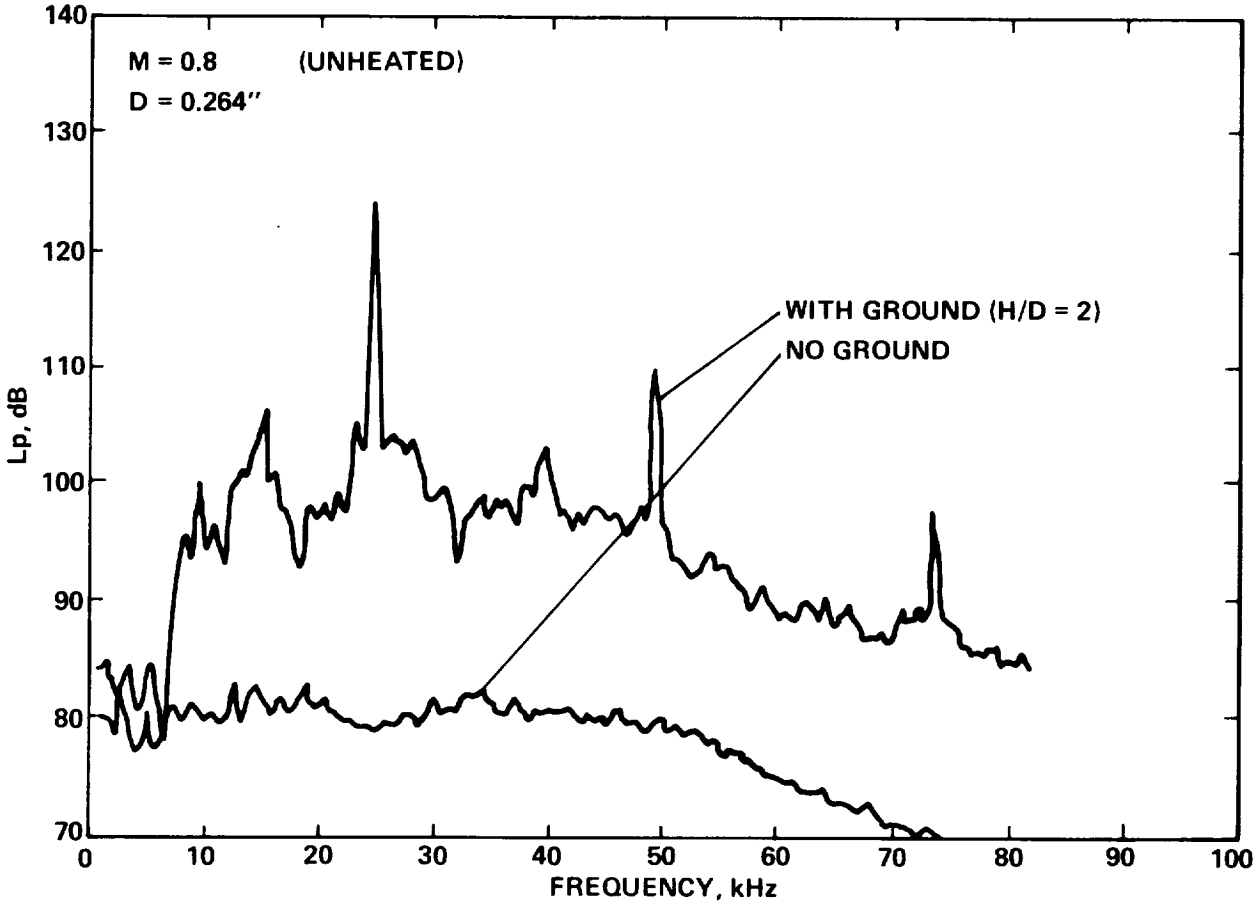

a) H/D = 2

Figure 12 - Ground effect on jet noise from Lockheed-Georgia study by K. Ahuja and associates.

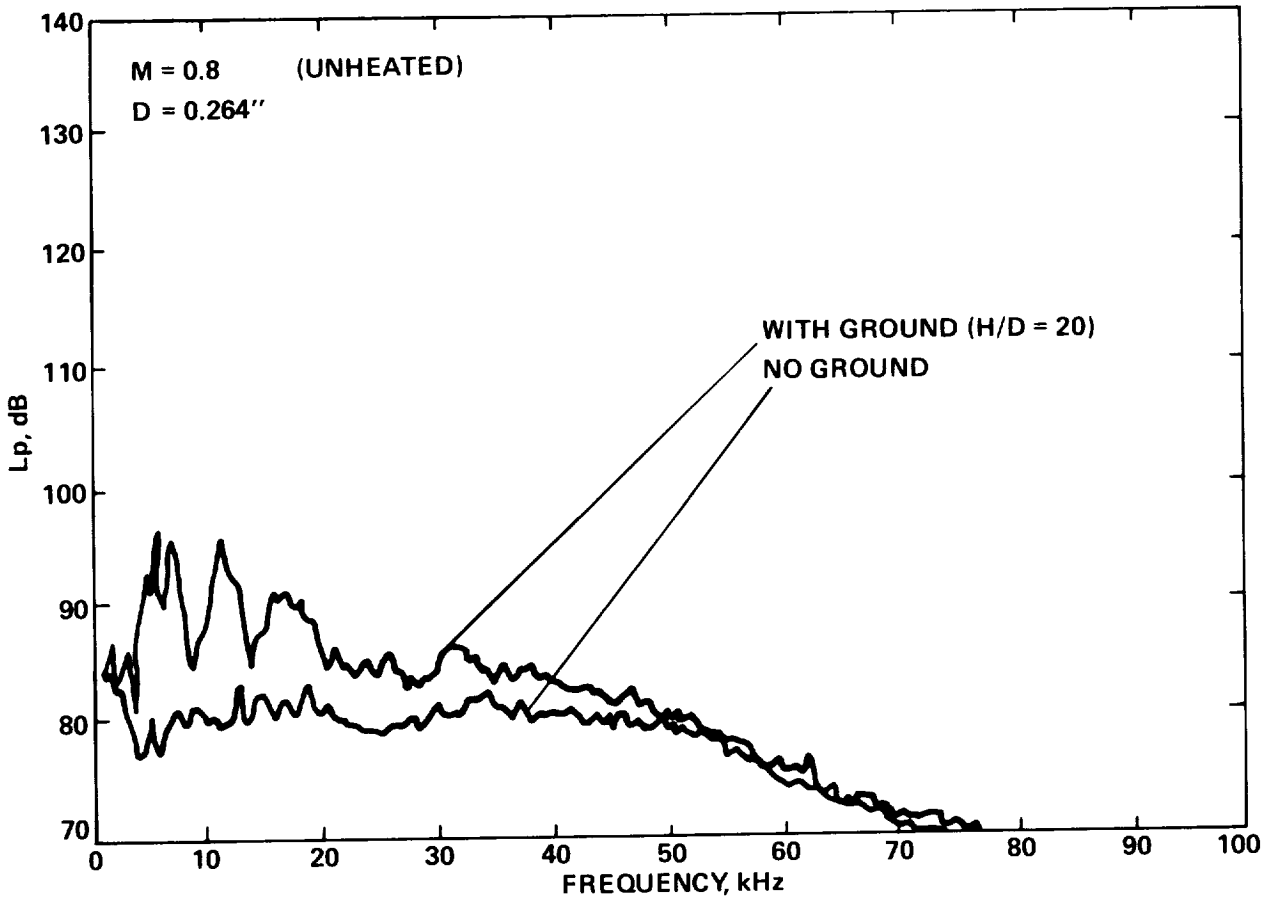

(b) H/D = 20

Figure 12 - Concluded.

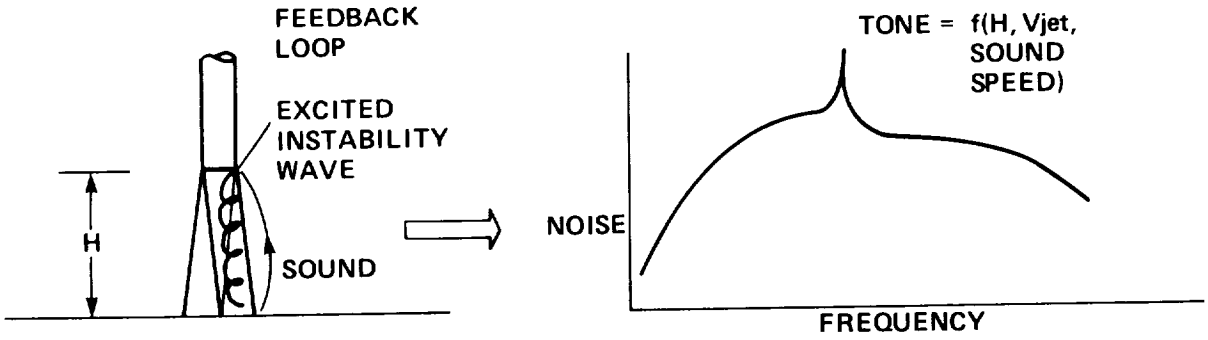

Figure 13 - Illustration of probable aeroacoustic feedback loop responsible for jet impingement tones shown in figure 12.

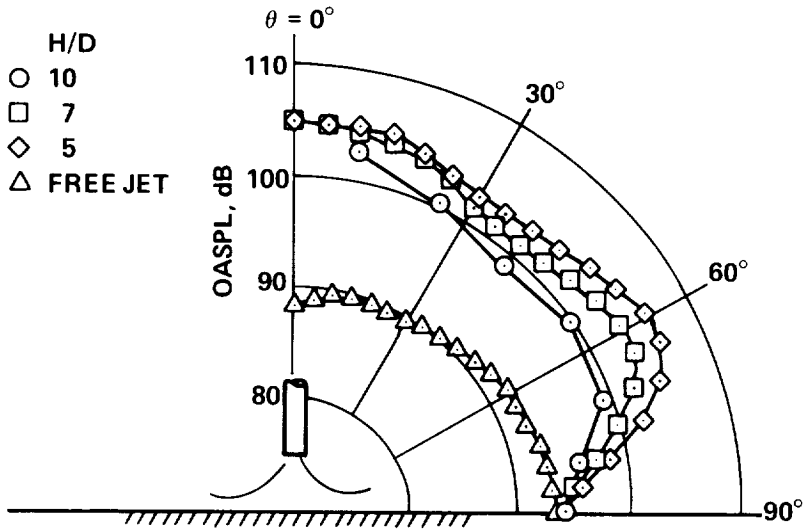

Figure 14 - Ground effect on jet noise from Preisser and Block (ref. 1). Mj = 7; r/D = 48 (r/D = mic distance from stagnation point/jet dia).

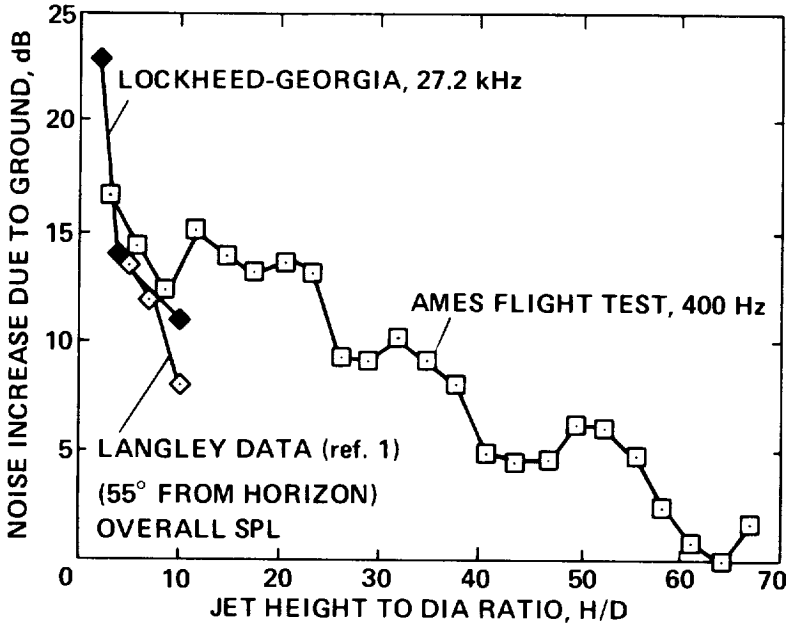

Figure 15 - Comparison of full-scale Harrier ground-effect data with small-scale results. The difference between sound levels measured in- and out-of-ground effect at various values of H/D are plotted.

NUMERICAL INVESTIGATION OF A JET IN GROUND EFFECT USING THE FORTIFIED NAVIER-STOKES SCHEME

William R. Van Dalsem and Joseph L. Steger
NASA Ames Research Center, Moffett Field, CA.

SUMMARY

One of the flows inherent in VSTOL operations, the jet in ground effect with a crossflow, is studied using the Fortified Navier-Stokes (FNS) scheme. Through comparison of the simulation results and the experimental data, and through the variation of the flow parameters (in the simulation) a number of interesting characteristics of the flow have been observed. For example, it appears that the forward penetration of the ground vortex is a strong inverse function of the level of mixing in the ground vortex. Also, an effort has been made to isolate issues which require additional work in order to improve the numerical simulation of the jet in ground effect flow. The FNS approach simplifies the simulation of a single jet in ground effect, but will be even more effective in applications to more complex topologies.

FLOW TOPOLOGY

Most VSTOL aircraft use propulsive thrust to supply control and lift forces near a landing surface at low forward speeds. In many cases, these forces are created by a jet issuing at an angle to the line of flight and impinging on a solid surface. Therefore, the jet in ground effect flow, shown in figure 1a, has been the subject of considerable experimental work (e.g., refs. 1-6). This flow contains many of the basic fluid dynamics phenomena which are important in VSTOL flows, yet does not involve complex geometry or grid generation. Therefore, its study is a good "first step" in the application of CFD to the VSTOL area. Specifically, in the present work an effort has been made to computationally simulate the experimental setup of Stewart, Kuhn, and Walters (refs. 1-2).

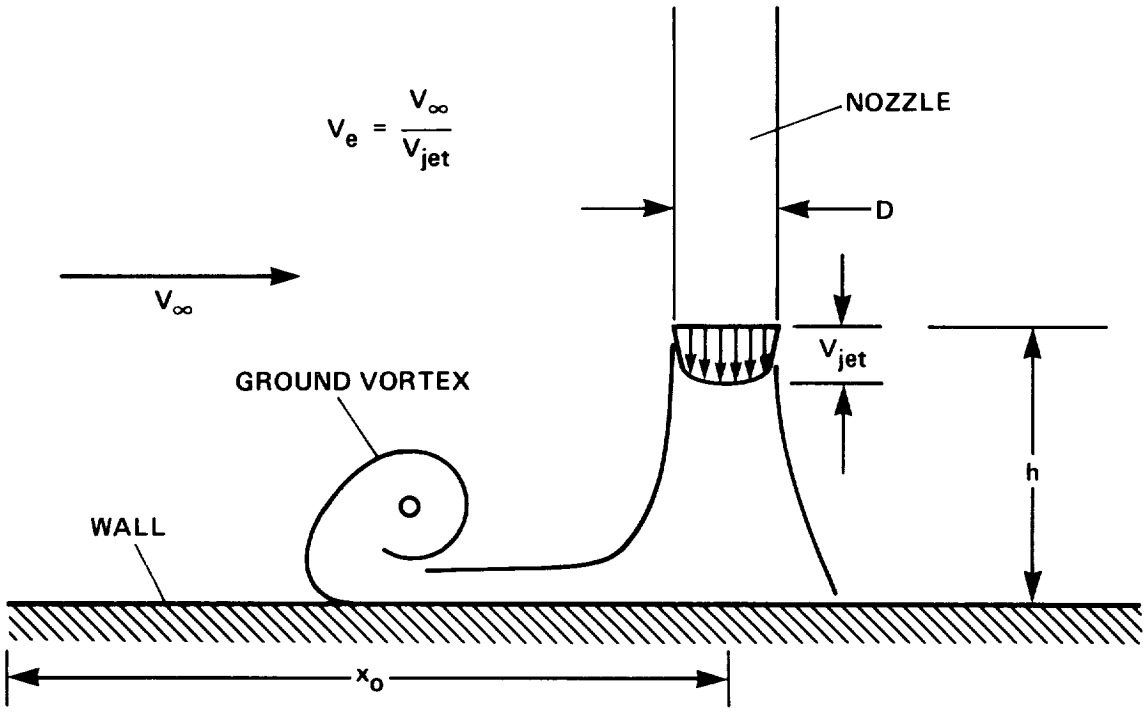

Figure 1a.- Jet in ground effect with a crossflow.

NUMERICAL APPROACH AND GRID TOPOLOGY

This flow was simulated by solving the Reynolds-averaged, Navier-Stokes equations using an implicit, partially flux-split, two-factor algorithm (ref. 7). To account for the viscous stresses normal to the wall (ζ-direction) and normal to the nozzle body (ξ-direction) the thin-layer viscous terms in both these directions have been included. At this point, the viscous cross terms have not been included as they should be important only at isolated corners of the grid. Also, only the ζ direction viscous terms are treated implicitly, which significantly simplifies the algorithm.

The FNS scheme (refs. 8-10) was originally envisioned as a simple way to couple various numerical algorithms and formulations. For example, in references 8-9, three-dimensional boundary-layer and Euler/Navier-Stokes algorithms are coupled using the FNS scheme. It was shown that a significant improvement in the performance (i.e., computer time required to obtain a solution of a given accuracy) of the Navier-Stokes algorithm could be obtained. However, it has since been recognized that the FNS scheme can also be used to patch, overset, or enrich grid systems. Furthermore, it is useful in imposing conditions within a computational domain. These last two capabilities are useful in simplifying the grid-interfacing and generation problems. It is the ability to impose conditions within the computational domain that is used in the work presented here.

In the FNS scheme a simple numerically stabilizing source term is implicitly added to the numerical algorithm in any region in which a "solution" is known from another predictive scheme. For example, the FNS scheme is added to the partially flux-split, two-factor algorithm by including the underlined terms

$$\begin{aligned}
&\left[I + \underline{h\chi I} + h\delta_\xi^b(\widehat{A}^+)^n + h\delta_\zeta \widehat{C}^n - hRe^{-1}\bar{\delta}_\zeta J^{-1}\widehat{M}^n J - D_i|_\zeta\right] \\
&\times \left(I + \underline{h\chi I}\right)^{-1} \\
&\times \left[I + \underline{h\chi I} + h\delta_\xi^f(\widehat{A}^-)^n + h\delta_\eta \widehat{B}^n - D_i|_\eta\right] \Delta\widehat{Q}^n = \\
&- \Delta t\{\delta_\xi^b[(\widehat{F}^+)^n - \widehat{F}_\infty^+] + \delta_\xi^f[(\widehat{F}^-)^n - \widehat{F}_\infty^-] + \delta_\eta(\widehat{G}^n - \widehat{G}_\infty) \\
&+ \delta_\zeta(\widehat{H}^n - \widehat{H}_\infty) - Re^{-1}\bar{\delta}_\xi(\widehat{S}_\xi^n - \widehat{S}_{\xi\infty}) - Re^{-1}\bar{\delta}_\zeta(\widehat{S}_\zeta^n - \widehat{S}_{\zeta\infty})\} \\
&- (D_e|_\eta + D_e|_\zeta)(\widehat{Q}^n - \widehat{Q}_\infty) + \underline{h\chi(\widehat{Q}_f - \widehat{Q}^n)}
\end{aligned}$$

where $\widehat{Q}$ is the solution vector and $\widehat{Q}_f$ is the forcing solution vector obtained from another source. (The reader is referred to ref. 7 for a detailed description of the base algorithm.) When $\chi = 0$, the original algorithm is recovered. However, as χ becomes very large, the algorithm reduces to

$$h\chi\Delta\widehat{Q}^n = h\chi(\widehat{Q}_f - \widehat{Q}^n)$$

or simply

$$\widehat{Q}^{n+1} = \widehat{Q}_f$$

Therefore, in any region where an accurate (or known) solution can be obtained, it can be built into the Navier-Stokes scheme. For example, $\widehat{Q}_f$ could be obtained from a specialized solver (e.g., a boundary-layer algorithm (refs. 8 and 9)), another grid zone (useful for grid patching or overlapping), or a known condition (such as at the face of an actuator disk). It is important to emphasize that χ is only a blending or switching function, and that it is not a "fudge factor." In regions where it is not desired to force the Navier-Stokes algorithm χ is simply set to zero, whereas χ is set to some large value (e.g., 1000 or 10,000) in regions where and when forcing is desired.

An important attribute of the FNS scheme is that in regions where the solution vector $\widehat{Q}_f$ is specified and χ is large, a large diagonal term is added to the implicit matrix operators, which increases the diagonal dominance of the matrices and (as shown in ref. 8) improves the convergence rate of the algorithm. From this point of view, it could be said that the solution vector $\widehat{Q}_f$ is used to condition the inversion matrices. A great deal of flexibility is available as χ can be a function of ξ, η, ζ, $\widehat{Q}$, $\widehat{Q}_f$, time, or even a positive definite operator. For example, in the grid oversetting application, in which multiple solutions are available in the overlap regions, χ could be varied to produce a smooth blending of the solutions.

In the current work the FNS scheme is used only to simplify the grid topology needed to simulate the nozzle/jet/ground geometry shown in figure 1b. A cylindrical coordinate system is used because it allows a natural clustering of the points to the shear layers created by both the nozzle body and the jet. A disadvantage of the cylindrical

coordinate system is that it introduces an axis boundary condition at the center of the jet. Using the FNS capability, the nozzle body no-slip conditions are imposed within the grid along a portion of a constant ξ plane. Similarly, the jet conditions are imposed on a subset of a constant ζ plane. The ability to insert conditions internal to the boundaries of the computational domain (e.g., the nozzle body and face) allows this geometry to be easily modeled with a single, simple, stretched-cylindrical-coordinate system. Without the FNS approach, multiple grid zones would have been required.

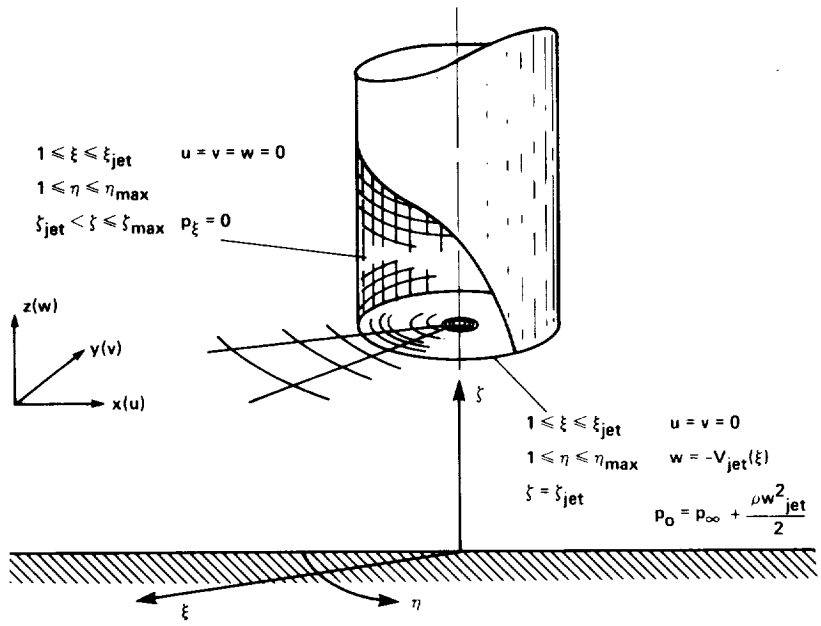

Figure 1b.- Jet and nozzle treatment.

RESULTS

The jet-in-ground-effect flow for $V_e = 0.223$, $h/D = 3$, and $x_0/D = 30$ was studied extensively. The experimentally measured jet profile was inserted at the nozzle exit. Also, in general it was assumed that the boundary-layer transitions to turbulent very near the leading edge of the plate.

Grid Refinement

Initially, the flow was computed assuming that the entire flow was completely turbulent using the Baldwin-Lomax turbulence model (ref. 11), including the modifications suggested by Schiff and Degani (ref. 12). The simulated oil-flow pattern presented in figure 2 shows jet impingement and the characteristic horseshoe vortex pattern observed experimentally. However, comparison with the experimental C_p distribution (measured along the jet centerline) shown in figure 3a indicates that the C_p minimum (corresponding to the location of the ground vortex) is too far forward. These computations were first performed on a 49 (radial) x 35 (circumferential) x 49 (normal to the

wall) grid. After studying the flow as resolved on this grid, it appeared that the grid was not fine enough in the radial direction to resolve the radial gradients in the ground-vortex region. Therefore, the grid was increased from 49 x 35 x 49 (84,035 points) to 82 x 35 x 49 (140,063 points), with most of the additional points clustered to the ground-vortex region. As shown in figure 3a, grid refinement did not affect the ground-vortex location, but did allow the resolution of higher gradients within the ground vortex. It is somewhat reassuring that the pressure gradients within the ground vortex resolved on the finer mesh are roughly the same as those observed experimentally.

Ground-Vortex Upstream Penetration and Turbulence Modeling

This initial simulation captured all the basic flow phenomena (specifically, the jet impingement and the ground vortex), but failed to accurately predict the location of the ground vortex. In an attempt to understand the ground-vortex flow a number of the flow field parameters were varied. For example, the initial jet profile was varied from that observed experimentally to an ideal slug flow. Also, the Reynolds number of the flow was varied over two-orders of magnitude. Various far-field boundary conditions were also studied. In general, it was found that the ground-vortex location was relatively insensitive to all of these variations.

It was observed that the ground-vortex location is very sensitive to the level of mixing in the boundary layer produced by the jet which moves upstream and forms the ground vortex. For example, if it is assumed that the flow is entirely laminar, then the ground vortex moves far upstream (figs. 3b and 4a). Similar results are obtained when the oncoming flow is retained as turbulent and only the wall flow moving upstream is assumed laminar (i.e., the ground-vortex region). Conversely, if it is assumed that the turbulence intensity in the boundary layer formed by the jet is underpredicted and should be greater, then the ground vortex moves back past the location that was observed experimentally (figs. 3b and 4b). Specifically, if the turbulent viscosity in the boundary layer emanating from the jet impingement point and moving upstream is increased by a factor of 10, the ground vortex moves back and sits just in front of the jet. A further increase of the turbulent viscosity in the jet footprint does not significantly change the ground-vortex location (fig. 3c). It appears that this reduced sensitivity to the turbulence intensity (at high turbulence levels) is due to the fact that the ground vortex is already "sitting" on the front of the jet, and further downstream motion is not possible.

From the numerical experimentation just described, it appears that the extent of forward penetration of the ground vortex is a strong function of the level of turbulent mixing in the ground-vortex region. In particular, to achieve agreement with the experimentally observed ground-vortex location it is necessary to increase the amount of turbulent mixing (predicted by the Baldwin-Lomax turbulence model) in the ground vortex. At this point we returned to experimental observations for guidance.

Kuhn, DelFrate, and Eshleman (ref. 13) prepared a video recording of a recent jet-in-ground-effect study made at the NASA Ames/Dryden Research Center Flow Visualization Facility. From viewing this video tape it is clear that there is intense large scale mixing in the ground-vortex region. Furthermore, some of this mixing is of such a large scale that it appears that we should be resolving it, while we must still supply an appropriate model for the turbulent mixing below our grid resolution.

Because the Baldwin-Lomax model was developed for thin boundary-layer flows, it is very likely that it is not adequate for this ground-vortex region.

The Baldwin-Lomax model represents one of two basic approaches to turbulence modeling. This model assumes that none of the turbulent mixing is resolved, and attempts to model all effects of turbulence. Another approach is to attempt to resolve the larger turbulent structures and only model the small scale turbulent mixing using a Sub-Grid-Scale (SGS) model. The advantage of this approach is that there is reason to believe that models for the small-scale turbulent mixing may be more universal. This concept has a long history. One of the first references to this concept appeared in 1932 and is due to G. I. Taylor (ref. 14). The concept has since been used in weather prediction (e.g., Smagorinsky's work (ref. 15)) and Large-Eddy-Simulation (e.g., ref. 16), and has recently been applied to the jet-upwash problem by, for example, Childs and Nixon (ref. 17), and Rizk (ref. 18).

One of the simpler SGS models, used for example by Childs and Nixon (ref. 17), is:

$$\mu_{SGS} \doteq c_1 \Delta z^2 |w|$$

where Δz is a representative grid-spacing length scale. This model is in contrast to the general character of the Baldwin-Lomax model which we can roughly represent in the following form:

$$\mu_{BL-INNER} \doteq c_2 z^2 |w|$$
$$\mu_{BL-OUTER} \doteq c_3 z_{max}^2 |w|_{max} F_{KLEB}$$

where z is the distance normal from the surface and the max subscript indicates the values of z and $|w|$ at which $z|w|[1 - exp(-y^+/A^+)]$ is maximum (c_1, c_2, and c_3 are simple numerical constants). Among the interesting differences between these models is that as the grid is refined (and more of the turbulent mixing is captured) the SGS model inserts less eddy viscosity, while the Baldwin-Lomax model is not grid dependent and is inconsistent in the limit of a very fine mesh.

If both these models are applied to the ground-vortex flow (figs. 5a and b) drastically different eddy viscosity levels are predicted. It appears that the Baldwin-Lomax model predicts high turbulence levels near the wall, but misses entirely the outer vortex region. On the other hand, the SGS model does not predict the correct near-wall behavior, but seems to model the large amount of turbulent mixing in the ground-vortex region which is observed in the video tapes of the experiment. This must be accounted for if the numerical simulation is to predict the ground-vortex location observed experimentally.

One approach is to use the SGS model throughout the bulk of the flow, but to return to the Baldwin-Lomax model near the wall. This results in the C_p distribution denoted as "modified SGS" in figure 5c. In this case, without ad hoc variation of the turbulence coefficients one obtains the ground vortex in roughly the correct location. Unfortunately, the shape of the C_p distribution is not correct. Indicating that overall we may have made some progress, but that more work is required.

It is apparent that the turbulent mixing in the ground-vortex region strongly influences the ground-vortex location; however, it is not clear what the mechanism

is that makes the ground-vortex flow so unsteady and results in the large amount of mixing. Some of the recent flow visualizations of Billet (ref. 19) indicate that a train of vortices is created by the shearing action between the jet and the freestream and that these vortices move up into the ground vortex and then "burst." Also, the recent work of Kuhn, DelFrate, and Eshleman (ref. 13) indicated that the resulting flow is not a strong function of the turbulent levels of the jet. These two points indicate that the large mixing in the ground vortex is due to unsteadiness inherent in the flow, and is not due to variations in the jet. On the other hand, recent work by Rizk (ref. 18) indicates that axisymmetric or azimuthal pulsing of the jet can create much different spreading rates in the resulting upwash flows. Perhaps, this flow is "self-exciting" and jet unsteadiness is not required to generate the large mixing, but may enhance it. For example, the moderate variations in the forward extent of the ground vortex indicated in figure 2 of the paper in this proceedings by Kuhn, DelFrate, and Eshleman may be due in part to variations in the nature of the jet flow.

Observed Jet Deformation

The front and side views of the traces of the particles released from the jet face, shown in figures 6 and 9a respectively, indicate a flow feature which may be difficult to observe experimentally. From the front view it appears that the jet is expanding rapidly as it leaves the nozzle, while the side view shows that the jet is contracting. This follows if one considers the pressures induced on the surface of the jet by the freestream flow (similar to those induced on a cylinder in crossflow). It appears that the high pressures on the front and back of the jet, and the low pressures on the sides of the jet are acting to deform the jet into an oval with the major axis normal to the freestream. Then shear stresses act to tear the ends off this oval (fig. 7), and create the swirling flow structure behind the jet.

From these observations it appears that a jet of elliptical cross-section with the major axis aligned with the flow would be more resistant to the break-up caused by the interaction with the freestream. Furthermore, such a jet nozzle would be more streamline than a round jet nozzle. Indeed, the jet nozzles on the Harrier aircraft are roughly of elliptical cross-section with the major axis parallel with the direction of forward flight.

h/D Variation

This flow was also computed at an $h/D = 6$. From the traces of particles released from the nozzle face (fig. 8), it appears that under these conditions the jet impinges upon the wall, but that a ground vortex does not form. According to reference 1, jet impingement may begin at $h/D = 10$ (for this V_e), and definitely occurs by $h/D = 6$; while the ground vortex does not form until $h/D = 4$. Hence, the numerical results at $h/D = 3$ (jet impingement and ground-vortex formation) and at $h/D = 6$ (jet impingement and no ground-vortex formation) correlate with experimental observation.

Nozzle vs. Actuator Disk Jet Sources

The difference between the jet issuing from a nozzle (a mass source) typically studied experimentally and the jet created by a rotor or jet engine (which are momentum but not mass sources) was also studied. In the latter case, nearby flow is entrained into the jet, which can be modeled as an actuator disk. Figures 9a-b show the particle

traces created by these two types of flow. Overall the flows are fairly similar, but the differences are great enough that caution should be used in studying one flow to understand the other. For example, in the nozzle case the forward extent of the ground vortex is greater, the vortex is flatter, and there is less defined structure behind the jet than in the actuator disk case.

CONCLUSIONS

A Fortified Navier-Stokes (FNS) algorithm has been applied to the jet-in-ground-effect flow and the results have been compared and contrasted with experimental data. From this work it appears that:

1. The FNS approach simplifies the simulation of the single jet in ground effect, but will be even more critical for the more complex topologies.
2. At least 140,000 points are required to resolve the numerous high-gradient regions (e.g., ground boundary layer, jet/freestream shear layer, and the ground vortex) in this flow.
3. The forward penetration of the ground vortex is a strong function of the turbulent mixing in the ground-vortex region, and more effort is required to either resolve or model the mixing in this region.
4. The numerical simulation predicts the characteristic jet footprint observed experimentally, and allows additional insight into the deformation of the jet by the freestream.
5. By varying h/D in the numerical simulation, it is possible to correlate with the experimental observations on jet impingement and ground-vortex formation as a function of h/D.
6. Nozzle jet flows (mass/momentum source) may produce a ground vortex which penetrates farther upstream and is of a smaller vertical extent than the ground vortex created by a jet engine installation (momentum source).

REFERENCES

1. Stewart, V. R.; Kuhn, R. E.; and Walters, M. M.: Characteristics of the Ground Vortex Developed by Various V/STOL Jets at Forward Speed. AIAA Paper No. 83-2494, Oct., 1983.
2. Stewart, V. R.; and Kuhn, R. E.: A Method for Estimating the Propulsion Induced Aerodynamic Characteristics of STOL Aircraft in Ground Effect. NADC 80226-60, Aug., 1983.
3. Colin, P. E.; and Olivari, D.: The Impingement of a Circular Jet Normal to a Flat Surface with and without Cross Flow. Report AD688953 von Karman Institute for Fluid Dynamics, Rhode-St., Genese, Belgium, Jan., 1969.
4. Abbott, W. A.: Studies of Flow Fields Created by Vertical and Inclined Jets when Stationary or Moving over a Horizontal Surface. ACR CP No. 911, 1967.
5. Schwantes, E.: The Recirculation Flow Field of a VTOL Lifting Engine, NASA TT F-14912, 1973.

6. Weber, H. A.; and Gay, A.: VTOL Reingestion Model Testing of Fountain Control and Wind Effects. Prediction Methods for V/STOL Propulsion Aerodynamics, vol. 1, Naval Air Systems Command, 1975, pp. 358-380.
7. Steger, J. L.; Ying, S. X.; and Schiff, L.B.: A Partially Flux-Split Algorithm for Numerical Simulation of Compressible Inviscid and Viscous Flow. Proceedings of a Workshop on Computational Fluid Dynamics held by the Institute of Nonlinear Sciences at the University of California at Davis, 1986.
8. Van Dalsem, W. R; and Steger, J. L.: The Fortified Navier-Stokes Approach. Proceedings of a Workshop on Computational Fluid Dynamics held by the Institute of Nonlinear Sciences at the University of California at Davis 1986.
9. Van Dalsem, W. R.; and Steger, J. L.: Using the Boundary-Layer Equations in Three-Dimensional Viscous Flow Simulation. Proceedings of the 58th Fluid Dynamics Panel Symposium on the Applications of Computational Fluid Dynamics in Aeronautics, paper 24, CP 412, Aix-en-Provence, France, 1986.
10. Steger, J. L.; and Van Dalsem, W. R.: Developments in the Simulation of Separated Flows Using Finite-Difference Methods. Proceedings of the Third Symposium on Numerical and Physical Aspects of Aerodynamic Flows, California State University, Long Beach, 1985.
11. Baldwin, B. S.; and Lomax, H.: Thin Layer Approximation and Algebraic Model for Separated Turbulent Flow. AIAA Paper No. 78-257, Jan., 1978.
12. Degani, D.; and Schiff, L. B.: Computation of Supersonic Viscous Flows Around Pointed Bodies at Large Incidence. AIAA Paper No. 83-0034, Jan., 1983.
13. Kuhn, R. E.; DelFrate, J. H.; and Eshleman, J. E.: Ground-Vortex Flow Field Investigation. Proceedings of the Ground-Vortex Workshop, NASA-Ames Research Center, April 22-23, 1987.
14. Taylor, G. I.: The Transport of Vorticity and Heat through Fluid in Turbulent Motion. Proc. Roy. Soc., vol. A., no. 135, pp. 685-703.
15. Smagorinsky, J.: General Circulation Experiments with the Primitive Equations, I, The Basic Experiment. Mon. Wea. Rev., vol. 91, pp. 99-165.
16. Rogallo, R. S.; and Moin, P.: Numerical Simulation of Turbulent Flows. Ann. Rev. Fluid Mech., vol. 16, 1984, pp. 99-137.
17. Childs, R. E.; and Nixon, D.: Unsteady Three-Dimensional Simulations of a VTOL Upwash Fountain. AIAA Paper No. 86-0212, Jan., 1986.
18. Rizk, M.; and Menon, S.: Large Eddy Numerical Simulation of an Array of Three-Dimensional Impinging Jets. Flow Research Report No. 403, May, 1987.
19. Billet, B.: Summary of an Experimental Investigation of the Ground Vortex. Proceedings of the Ground-Vortex Workshop, NASA-Ames Research Center, April 22-23, 1987.

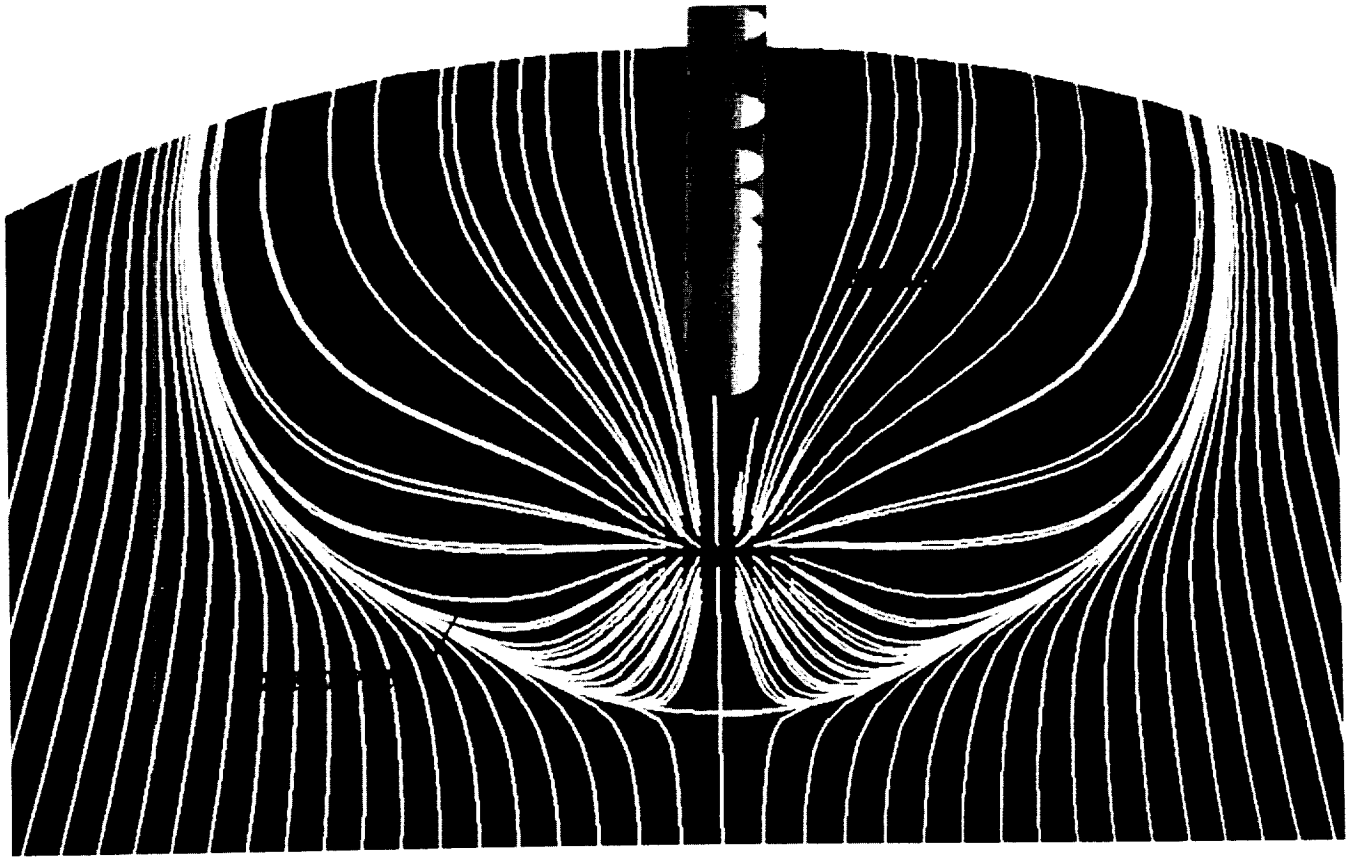

Figure 2.- Simulated oil-flow pattern showing jet footprint for a turbulent jet with $V_e = 0.223$ and $h/D = 3$ (front view).

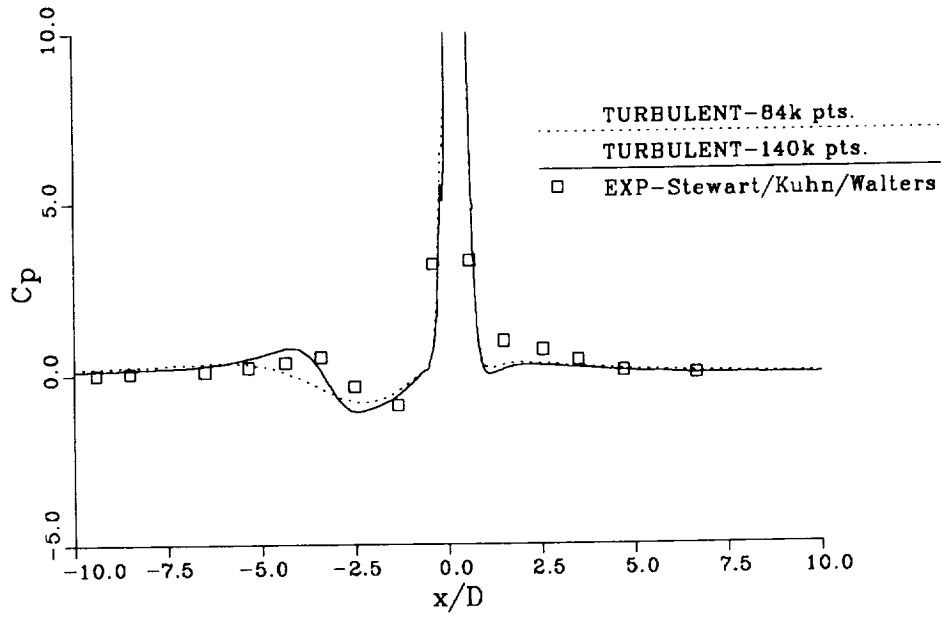

Figure 3a.- Impact of grid resolution on centerline C_p distributions for a turbulent jet with $V_e = 0.223$ and $h/D = 3$.

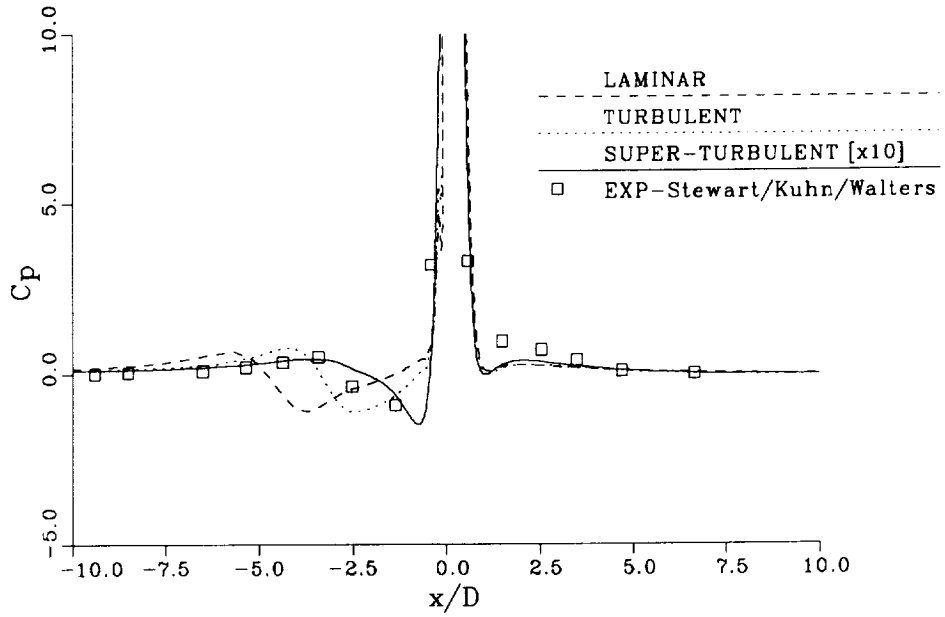

Figure 3b.- Impact of jet turbulence level on location of ground vortex, as shown by centerline C_p distributions for a jet with $V_e = 0.223$ and $h/D = 3$.

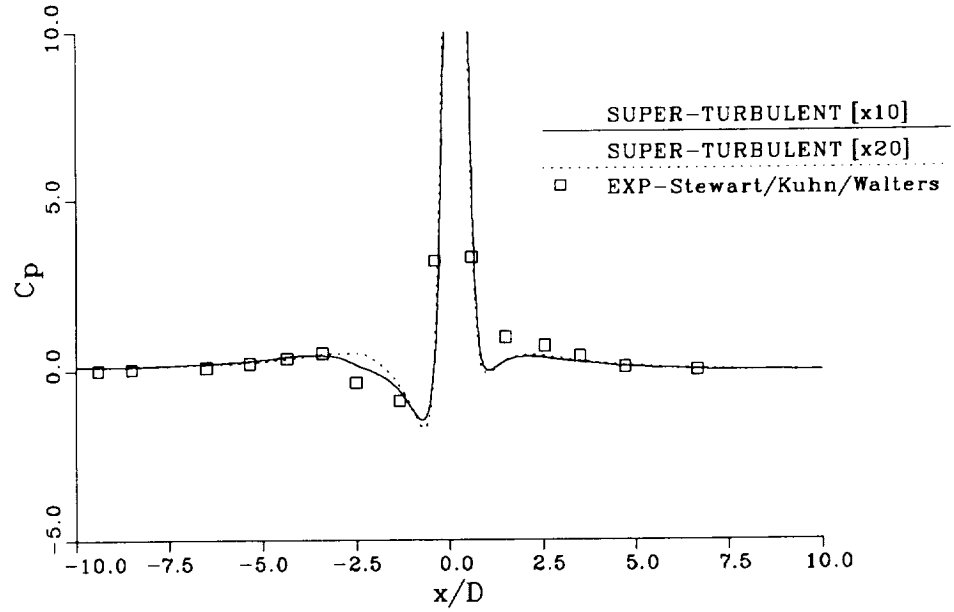

Figure 3c.- Relative insensitivity of centerline C_p distribution for a jet with $V_e = 0.223$ and $h/D = 3$ on jet turbulence level once a high turbulence level has been reached.

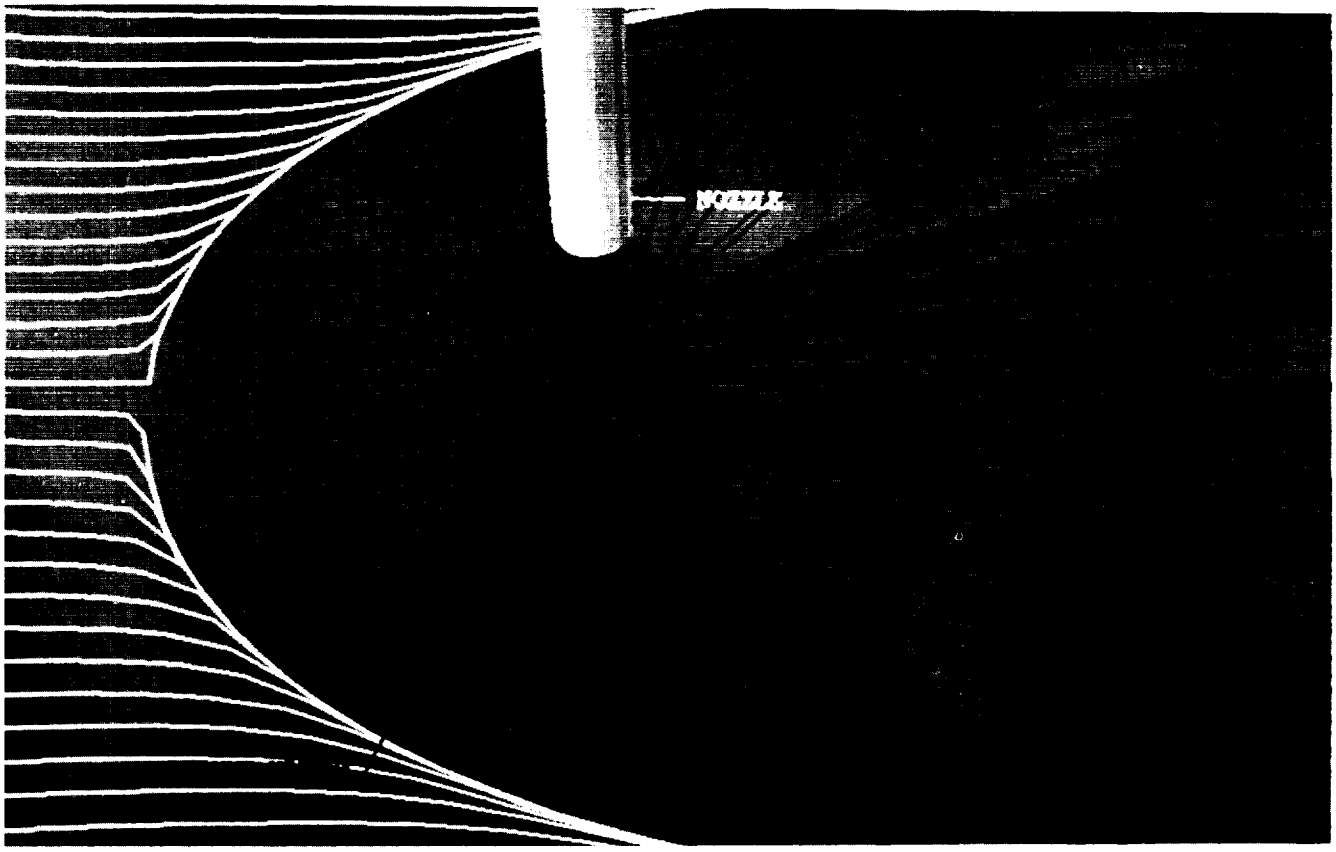

Figure 4a.- Particle traces for a laminar jet with $V_e = 0.223$ and $h/D = 3$ (top view).

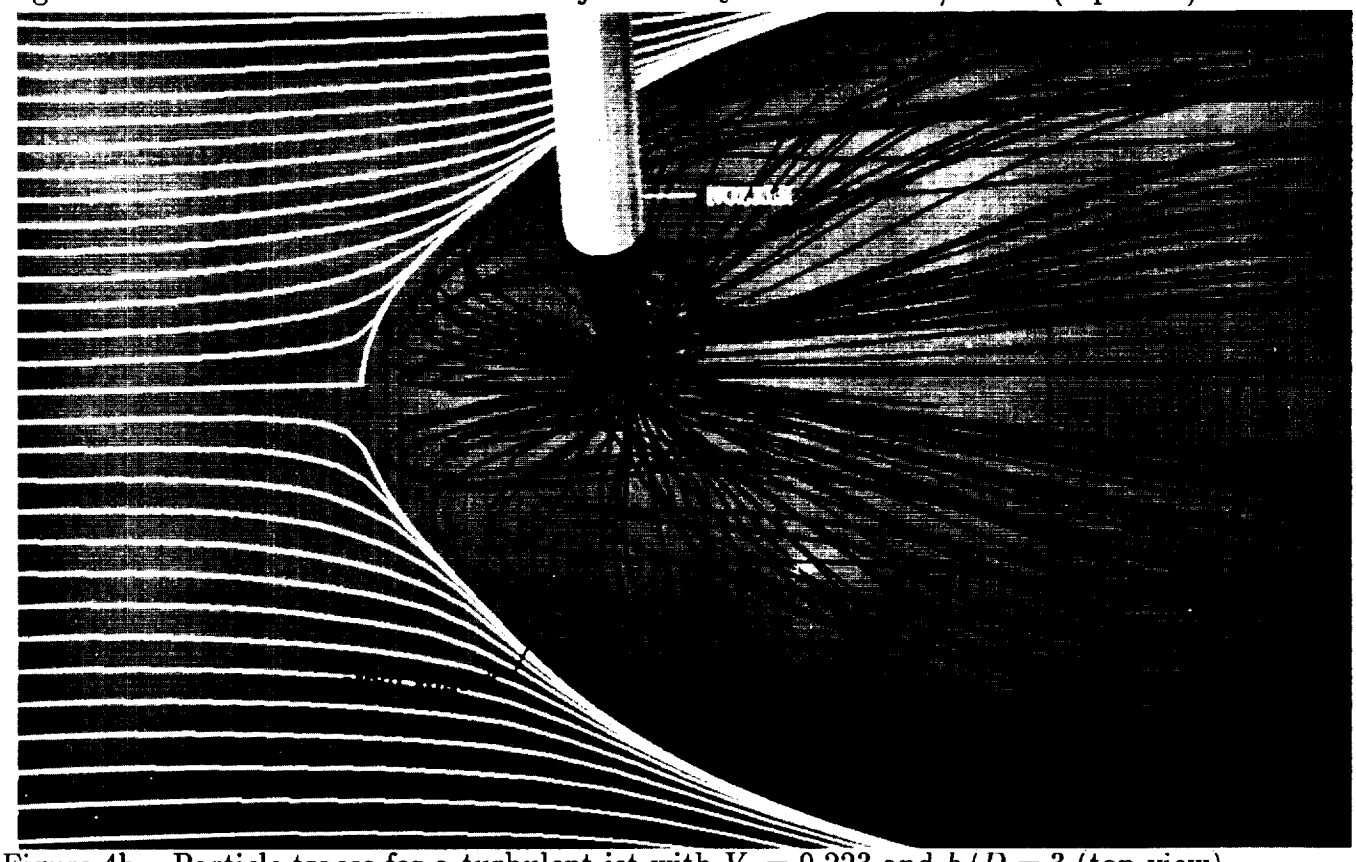

Figure 4b.- Particle traces for a turbulent jet with $V_e = 0.223$ and $h/D = 3$ (top view).

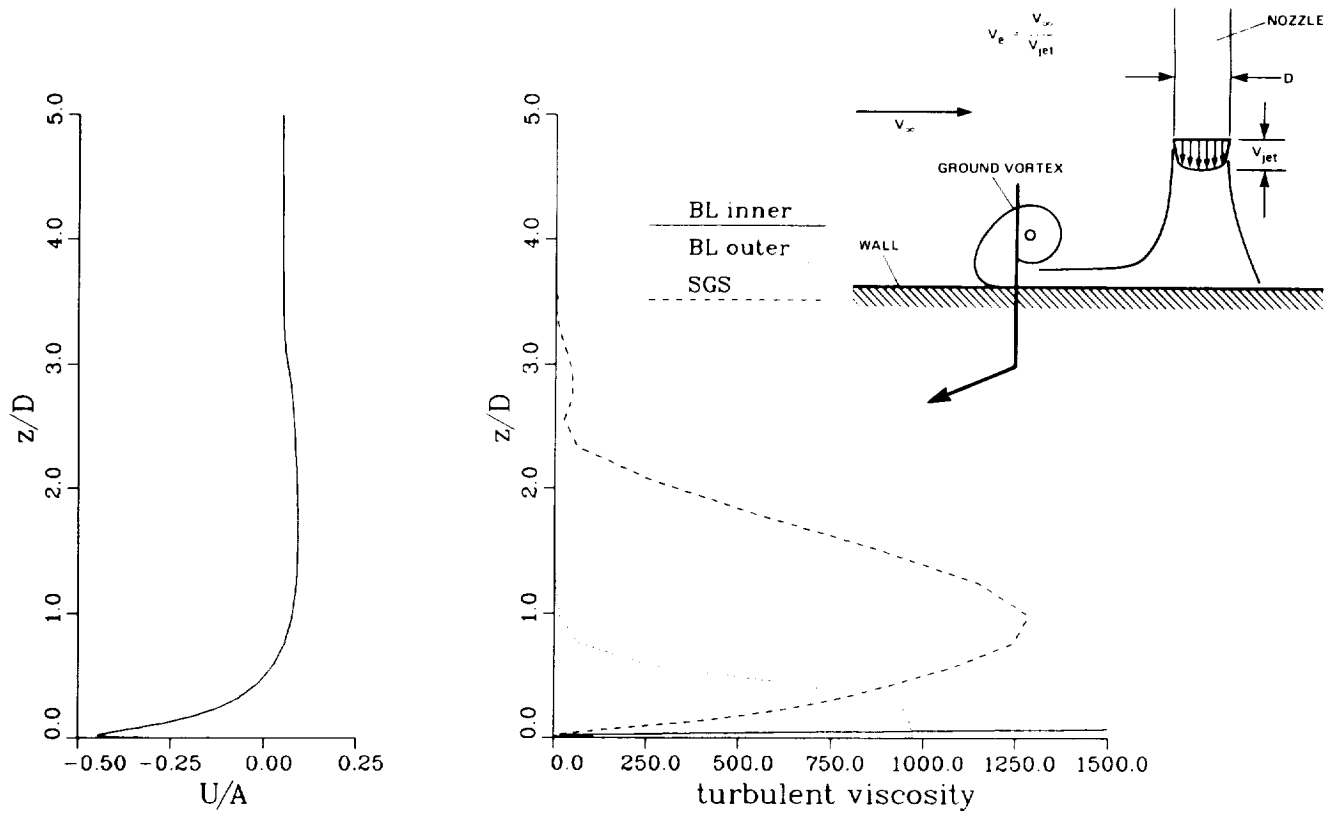

Figure 5a-b.- Streamwise velocity and turbulent viscosity (nondimensionalized by the molecular viscosity) profiles within the ground vortex.

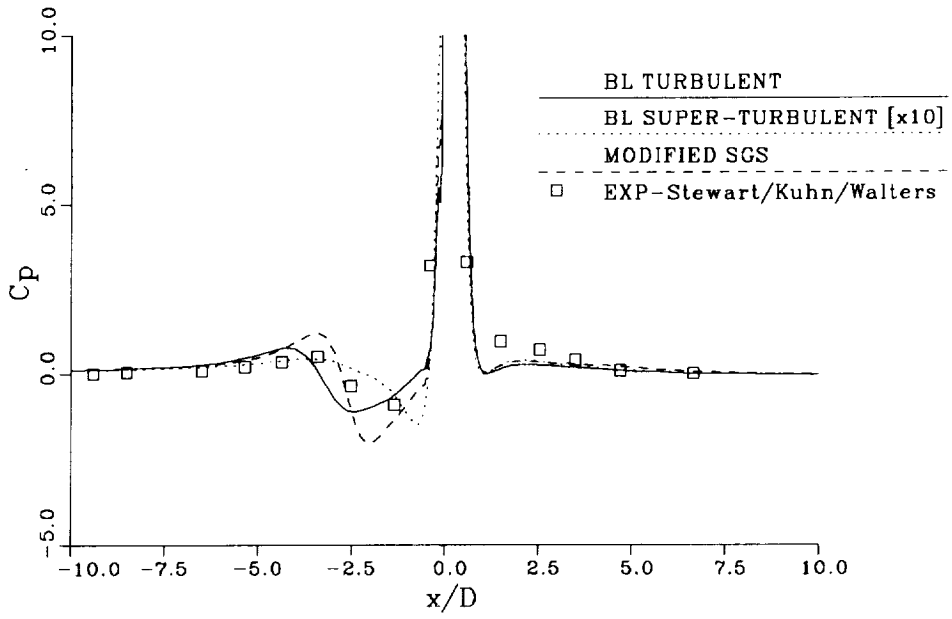

Figure 5c.- Impact of turbulence modeling on centerline C_p distribution for a jet with $V_e = 0.223$, and $h/D = 3$.

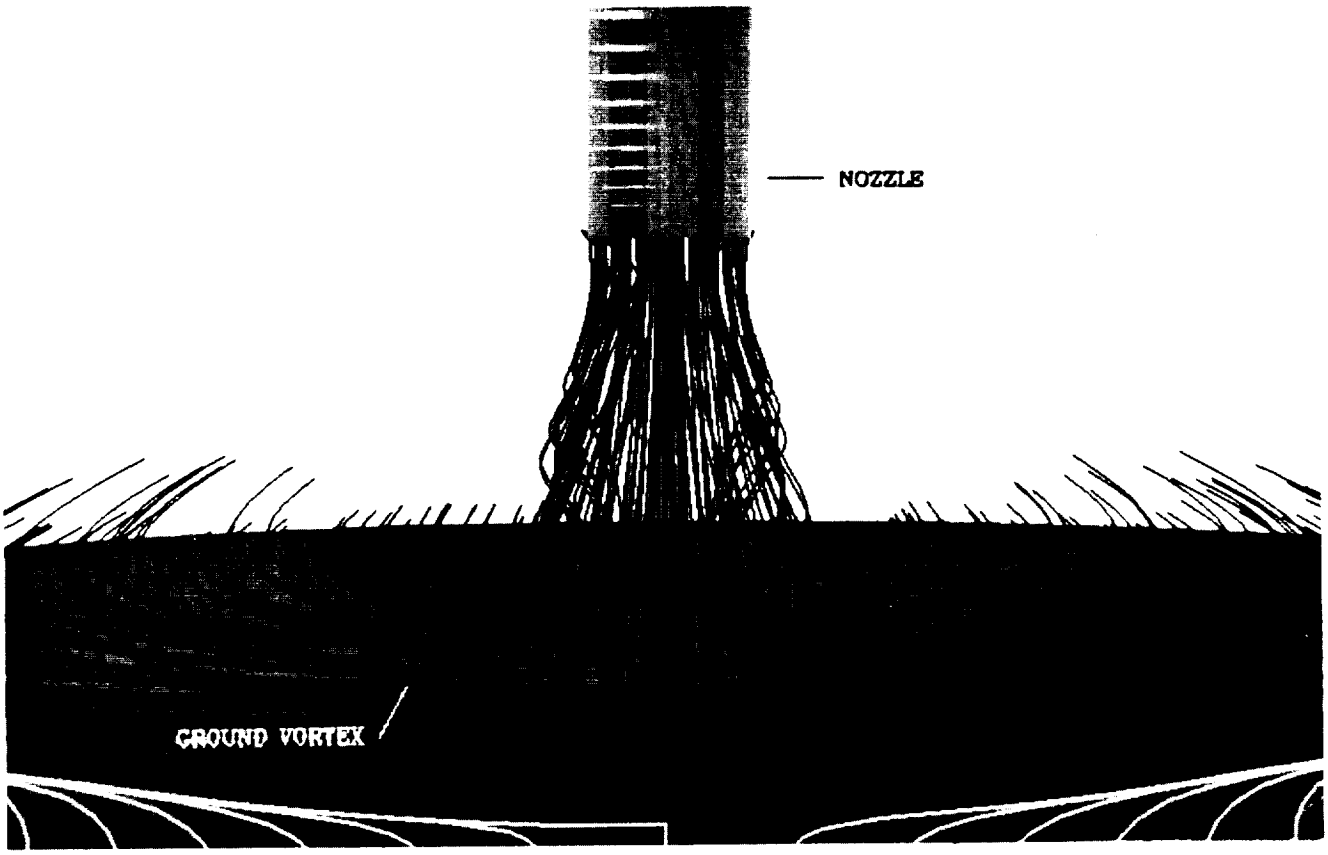

Figure 6.- Particle traces for a turbulent jet with $V_e = 0.223$ and $h/D = 3$ (front view).

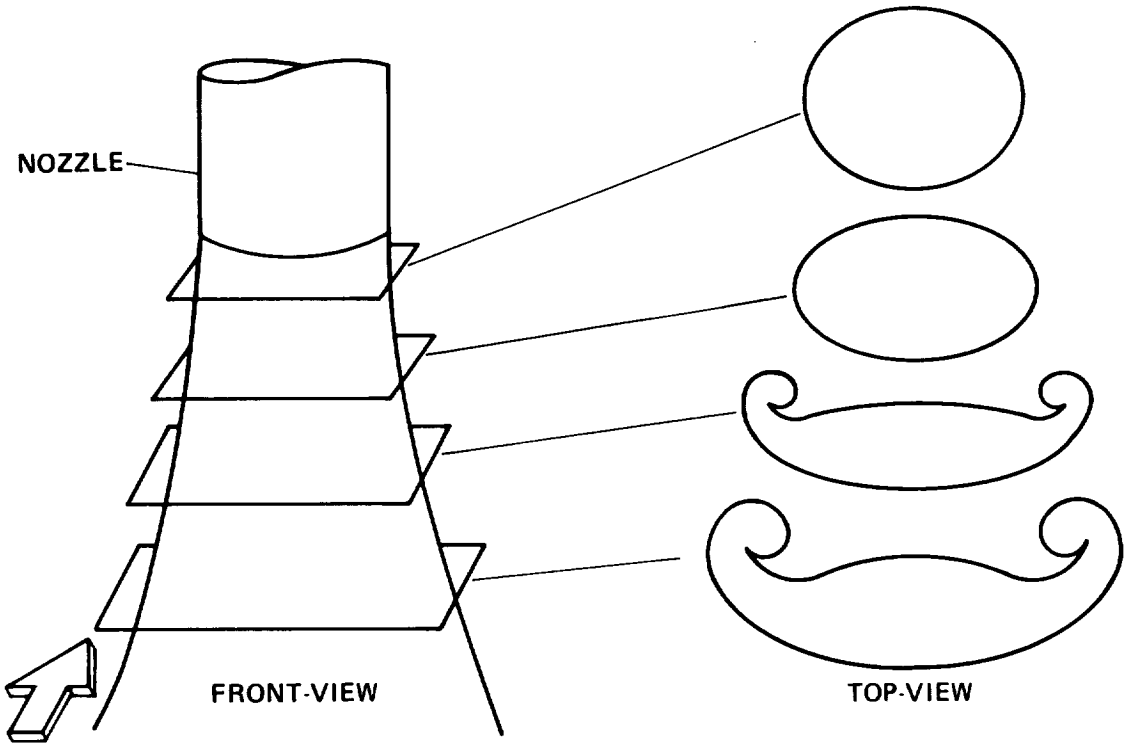

Figure 7.- Observed deformation of jet caused by pressures induced by freestream flow.

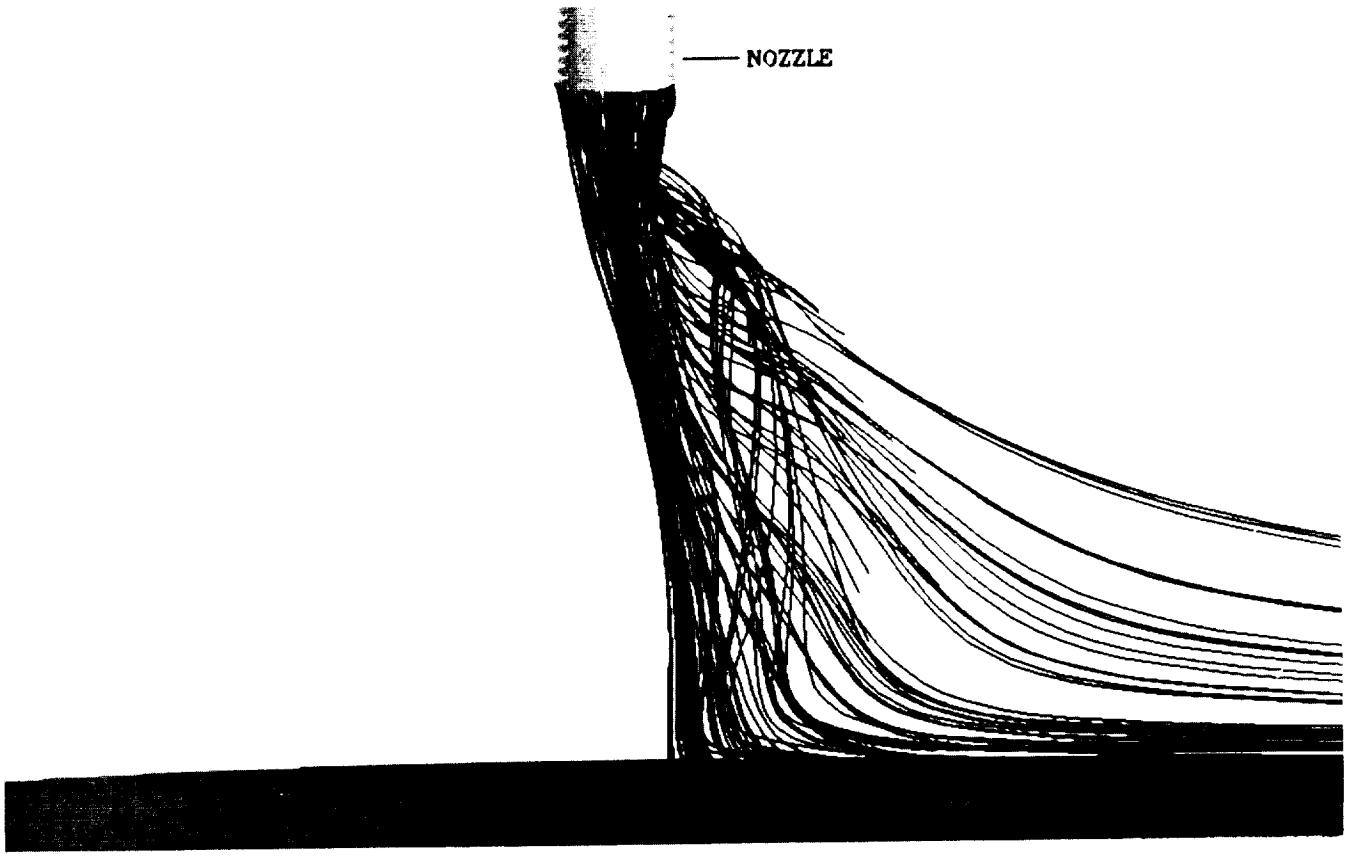

Figure 8.- Particle traces for a turbulent jet with $V_e = 0.223$ and $h/D = 6$ (side view).

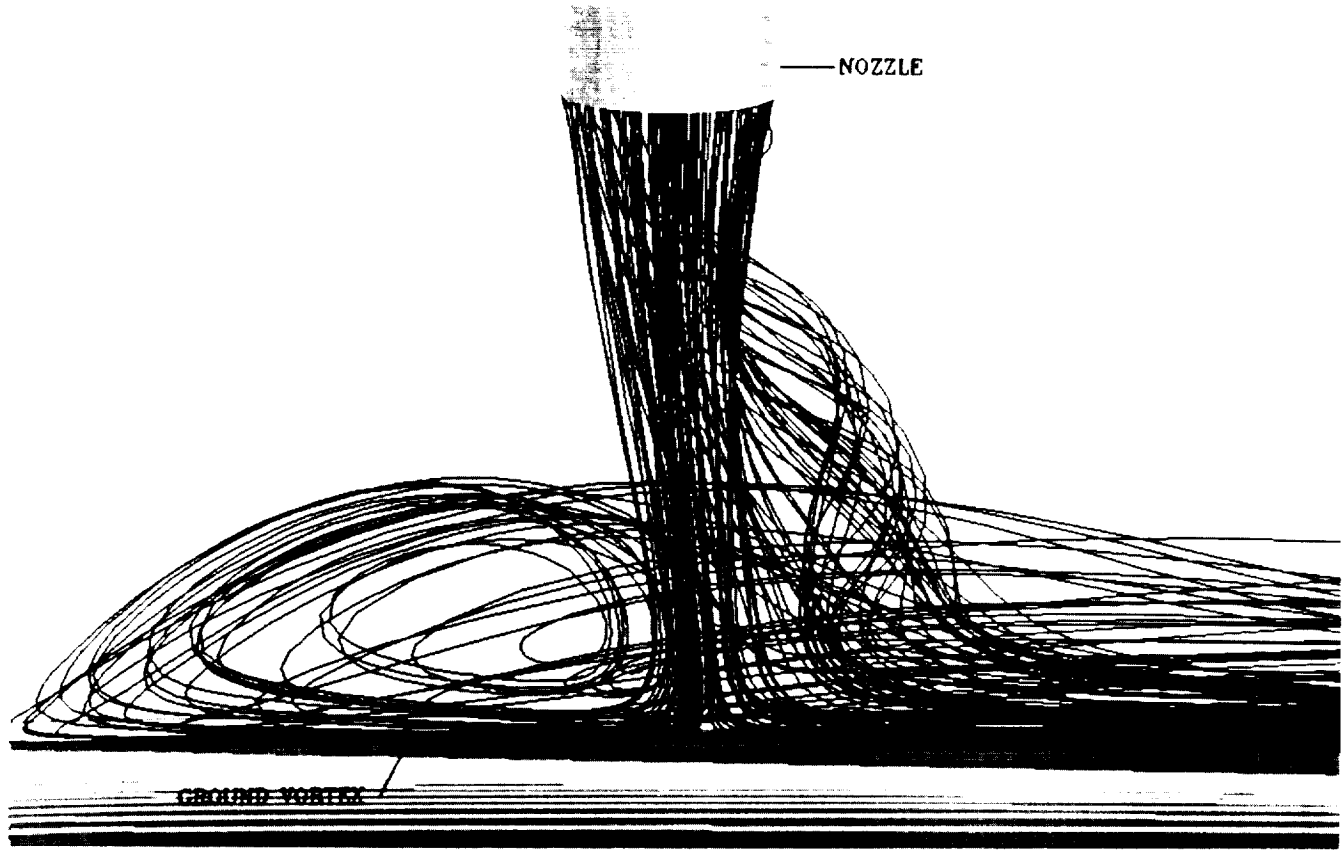

Figure 9a.- Particle traces for a turbulent jet exiting from a nozzle with $V_e = 0.223$ and $h/D = 3$ (side view).

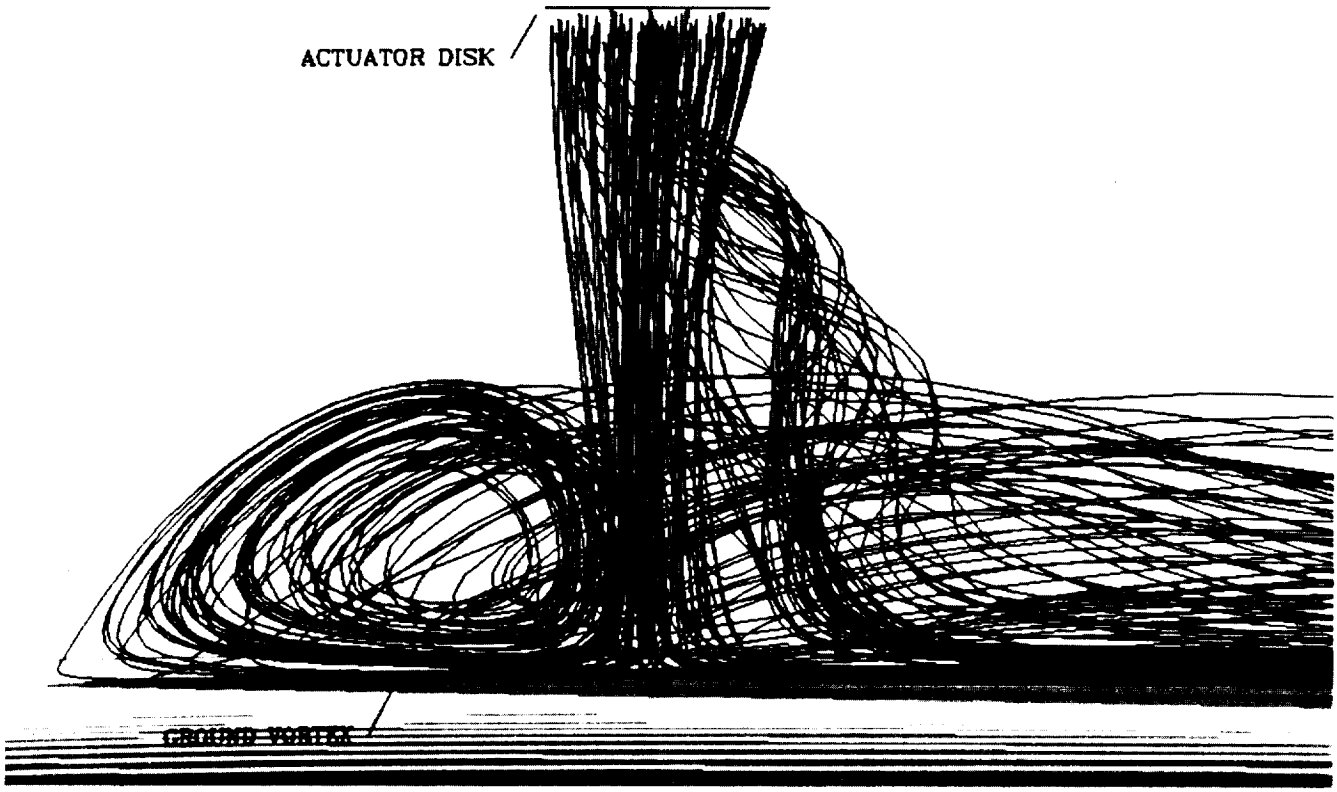

Figure 9b.- Particle traces for a turbulent jet exiting from an actuator disk with $V_e = 0.223$ and $h/D = 3$ (side view).

PANEL DISCUSSION

Summarized by R. E. Kuhn

The panel discussion took place on the morning of April 23, 1987. Mr. Richard J. Margason was moderator and the panelists were the speakers who presented the papers on the previous day. They were:

Vearl R. Stewart
Michael L. Billet
Richard E. Kuhn
William B. Blake
John W. Paulson, Jr.
A. Krothapalli
Paul T. Soderman
William R. Van Dalsem
Robert Childs

In addition to the panel members there were about 20 in the audience, many of whom took part in the discussion.

Prior to the discussion there were two presentations illustrating the broad nature of the ground vortex phenomena. Dr. Fred Schmitz presented a movie of the ground vortex generated by the downwash from a helicopter operating in ground effect. The problem being demonstrated concerned the loss of directional control encountered by the UH-1 helicopter hovering in a quartering tail wind. Under certain conditions the ground vortex could engulf the tail rotor and because the direction of rotation of the tail rotor and the ground vortex were the same tail rotor thrust would be decreased and directional control would be lost.

Mr. Margason showed slides illustrating the ground vortex type flow fields experienced by tilt wing, jet flap and jet V/STOL configurations in STOL operation and pointing out the lift loss, control problems and ingestion problems encountered under certain operating conditions. The presentations of the previous day had concentrated on the ground vortex flow fields generated by jet impingement, however these presentations showed that the phenomena was independent of disk loading and occurred at all scales.

The early part of the discussion concentrated on the fluid mechanics aspects of the flow field and the highly unsteady nature of the flow. Possible origins of the unsteadiness, the effects of noise, and the possibility of a feed back from the flow field on the ground to the flow exiting the nozzle were discussed. Much of the discussion was directed at what we need to know to provide a basis for successful CFD calculations. Significant progress is being made in developing CFD methods to calculate these types of flows and these efforts should be accelerated. Obtaining a clearer understanding of the physical mechanisms involved is key to the development of improved CFD methods.

It was clear that the vortices developed in the shear layer of an open jet issuing into free air, and the spreading of these vortices when the jet impinges on the ground play a role, and that under some conditions there is a feedback between the effects of these vortices and the turbulence of the jet. However the importance of the turbulence of the jet as it issues from the nozzles, relative to the turbulence generated by impingement and in the wall jet is not known. Nor is it clear that it is necessary to include feedback between the turbulence generated on the ground and the flow issuing form the nozzle to calculate the flow developed. Similarly it is clear that the impingement of the jet on the ground increases the noise of the jet but whether or not a feedback mechanism is necessary to explain this increase in noise or how it affects the development of the ground vortex flow field is unknown. The reduced forward projection of the ground vortex flow field with a moving ground plane (rather than a fixed ground board, as in conventional wind tunnel tests) has been shown but the extent to which this effect is due to the elimination of the free stream boundary layer, the additional scrubbing action of the ground moving aft under the wall jet or whether other mechanisms are also involved is not clear. Additional carefully structured tests, as well as CFD analysis, will be needed to answer all of these questions.

The effects of the ground vortex on the aerodynamics of an aircraft in ground effect was the next area discussed. Here it was pointed out that the different assumptions with regard to how the flow field develops and how it may be calculated may not be significant with respect to the effects on the aircraft. The data available demonstrates that, on a time averaged basis, the flow field is steady and its effects on the aircraft will be repeatable. What is needed with respect to the effects on the aircraft is the development of broadly based CFD methods for predicting the effects of the ground vortex flow field as well as a systematic data base to provide design guidelines and data for verification of the CFD methods. Carefully structured general research investigations are needed to develop this data base. In addition when tests of specific configurations are undertaken they should be structured to emphasize configuration build up so that the effects of the ground vortex on various components can be identified.

The ground vortex flow field is one of the mechanisms involved in the ingestion of hot gases and debris. Here the time averaged flow field will probably give a good indication of the average inlet temperature rise and thrust loss that may be encountered but not the temperature spikes which could cause surge. More work is needed to define the average flow field and resultant ingestion and also to define the extremes of the unsteadiness that will determine the operational limits for the configuration.

The third major area discussed was the effects of rate of descent on the development of the flow field and the resultant effects on the configuration. While it was pointed out that none of the many V/STOL test beds that have been flown have had any problems in landing that could be traced to the effects of rate of sink. It was also pointed out that most of these aircraft were depending primarily on the propulsion system rather than the wing for lift and

they did not include thrust reverser configurations which are subjected to a more intense ground vortex flow field. The need to develop equipment, similar to that already available in Europe, for wind tunnel investigations of the effect of rate of sink and rate of climb was identified. Also the need to keep the moving model facility at Langley operational until the more versatile wind tunnel equipment comes on line was stressed.

SUMMARY AND RECOMMENDATIONS

In summary the discussion identified 4 thrusts for future work on the ground vortex phenomena.

1. Basic fluid mechanics aspects: What is going on in the nozzle, the free jet, during impingement, in the wall jet, in the roll back caused by the free stream and in the free stream itself; what are the feed back mechanisms and how important are they; is noise a cause or effect; and what do we need to know to calculate the flow field. This will require the type of investigation conducted at Penn State and extensions to include the effects of controlled turbulence in the jet, measurements of the turbulence and space-time correlations of the unsteady pressures in the flow field and correlation with similar measurements on the flow fields generated by full scale jet engines.

2. Effects on the aircraft: The ground vortex can induce large lift losses, pitching moments and rolling moments on aircraft configurations. In addition it is one of the primary mechanisms in hot gas ingestion. The CFD methods for calculating the ground vortex flow field should be extended to predicting these effects on the aircraft. A systematic data base on the effects of jet arrangement, aircraft configuration variables, etc. needs to be developed to provide design guidelines as well as to provide data for validation of these CFD methods.

3. Effects of rate of descent and rate of climb: The work started in the moving model facility at Langley has shown that there are time dependent aspects to the development of the flow field and to the forces and moments experienced by configurations (particularly thrust reverser equipped configurations) entering ground effect. This work should be continued and equipment for making these types of investigations in wind tunnels should be developed. The moving model facility at Langley should be kept operational at least until comparable capability is developed for wind tunnel investigations.

4. Flight tests: Available aircraft (presently the QSRA and the YAV-8B Harrier) should be used to provide full scale flight data for verification of both wind tunnel data and computational methods. Flight test data should be reviewed and programs set up to obtain ground vortex flow field data as well as data on the effects of the ground vortex flow field on the aircraft. Related wind tunnel tests and computations should follow these flight programs so that the configurations, variables and operating conditions can be faithfully matched.

REFERENCES

During the discussion reports of several investigations pertinent to the ground vortex problem were mentioned. Each panelist was asked to supply citations of these and other references that illustrate and amplify the points made and provide additional information on the ground vortex problem. The following are the references supplied.

1. Binion, T. W. Jr.; "Investigation of the Recirculation Region of a Flow Field Caused by a Jet in Ground Effect With Crossflow". AEDC-TR-70-192, September 1970.

2. Childs, R. E., and Nixon, D.; "Unsteady Three-Dimensional Simulation of a VTOL Upwash Fountain". AIAA-86-0212, January 1986.

3. Childs, R. E., Nixon, D., Kuhn, G. D. and Perkins, S. C.; "Further Studies of Impinging Jet Phenomena". AIAA-87-0017, January 1987.

4. Ho, C. M. and Nossier, N. S.; "Dynamics of an Impinging Jet, Part 1: The Feedback Phenomenon". Journal of Fluid Mechanics, Vol. 105, 1981, pp. 119-142.

5. Nossier, N. S. and Ho, C. M.; "Dynamics of an Impinging Jet, Part 2: The Noise Generation". Journal of Fluid Mechanics, Col. 116, 1982, pp. 379-391.

6. Neuwerth, G.; "Flow Field and Noise Sources of Jet Impingement on Flaps and Ground Surfaces". AGARD CPP-308, 1981, pp. 13.1-13.7.

7. Marsh, H. A.; "Noise Measurements Around a Subsonic Air Jet Impinging on a Plane Ground Surface". Journal of Acoustical Society of America, Vol. 33, 1961, pp. 1065-1066.

8. Wagner, R. F.; "The Sound and Flow Field of an Axially Symmetric Free Jet Upon Impact on a Wall". NASA TTF-13942, 1971.

9. Krothapalli, A.; "Discrete Tones Generated by an Impinging Underexpanded Rectangular Jet". AIAA Journal, Vol. 23, No. 12, December 1985, pp. 1910-1915.

NASA National Aeronautics and Space Administration

Report Documentation Page

1. Report No.	2. Government Accession No.	3. Recipient's Catalog No.
NASA CP-10008		

4. Title and Subtitle	5. Report Date
1987 Ground Vortex Workshop	February 1988
	6. Performing Organization Code

7. Author(s)	8. Performing Organization Report No.
Richard J. Margason, Editor	A-88008
	10. Work Unit No. 505-61-71

9. Performing Organization Name and Address	11. Contract or Grant No.
Ames Research Center Moffett Field, CA 94035	
	13. Type of Report and Period Covered
12. Sponsoring Agency Name and Address	Conference Publication
National Aeronautics and Space Administration Washington, DC 20546-0001	14. Sponsoring Agency Code

15. Supplementary Notes

Point of Contact: Michael R. Dudley, Ames Research Center, MS 247-2
Moffett Field, CA 94035 (415) 694-5046 or FTS 464-5046
Proceedings of a meeting held at Ames Research Center on April 22-23, 1987.

16. Abstract

A Ground Vortex Workshop was held at NASA Ames Research Center on April 22-23, 1987, and was sponsored by the Center's Powered-Lift Group of the Fixed Wing Aerodynamics Branch. The purpose of the workshop was to discuss the current understanding of the ground vortex phenomena and their effects on aircraft, and to establish directions for further research on advanced, high-performance aircraft designs, particularly those concepts utilizing powered-lift systems; e.g., V/STOL, ASTOVL, and STOL aircraft. A total of 9 papers covering a survey of early work on the ground vortex, recent experimental and theoretical studies, and the effect of the ground vortex flow field on the aircraft were presented on the first day. This publication presents 8 of the 9 papers given at the workshop. These papers are printed from photo-ready originals supplied by the authors, who are responsible for the content and the technical accuracy of their respective papers. A panel discussion was held on the morning of the second day to summarize the papers presented and to discuss the direction that future work should take. A synopsis of that discussion is presented at the end of this publication.

17. Key Words (Suggested by Author(s))	18. Distribution Statement
Ground vortex Ground effects V/STOL Powered lift	Unclassified-Unlimited Subject Category - 02

19. Security Classif. (of this report)	20. Security Classif. (of this page)	21. No. of pages	22. Price
Unclassified	Unclassified	218	A10

For sale by the National Technical Information Service, Springfield, Virginia 22161